Technische Universität München
TUM School of Natural Sciences

Enhancing gene editors and their delivery to target cells for gene therapy and bioengineering

Wolf Julian Geilenkeuser

Vollständiger Abdruck der von der TUM School of Natural Sciences der Technischen Universität München zur Erlangung eines

Doktors der Naturwissenschaften (Dr. rer. nat.)

genehmigten Dissertation.

Vorsitz: Prof. Dr. Matthias Feige

Prüfende der Dissertation:

1. Prof. Dr. Gil G. Westmeyer
2. Prof. Dr. Alessandra Moretti
3. Assoc. Prof. Benjamin P. Kleinstiver, Ph.D.

Die Dissertation wurde am 29.07.2025 bei der Technischen Universität München eingereicht und durch die TUM School of Natural Sciences am 06.02.2026 angenommen.

Acknowledgements

First I want to thank the prime enablers of this thesis: Professor Gil Westmeyer for all the experienced advice and providing me the opportunity and autonomy to pursue my research interests; Jeffery Truong for sparking my curiosity, guiding me the way, having a sound answer to every question and calling me out on my mistakes; and Niklas Armbrust for 10 years and counting of collaborative studying, researching, (occasionally vivid) discussion and friendship.
I want to express my gratitude also towards my other co-authors and especially all undergraduate students among them, as without your enormous effort and commitment this would not have been possible. I want to thank Anja Ammer and all other colleagues and students at the Westmeyer Lab for your support and the lighthearted and productive environment you helped to create and maintain. My special thanks go to Davide Bertoldo for your mentorship and perspective, and to Gabriele Loiudice for productive writing and gaming sessions.
I am grateful to my university fellows Christoph, Nicola, Caro, Luisa, Valentin, Janice, Gerald and Laurin for your lasting friendship. My heartfelt gratitude also goes to my parents and family for always backing me up, even if the distance and workload sometimes affected how much you would hear from me in return. Lastly, thank you Andrea for your love and patience, despite working even harder yourself and often the opposite hours.

~ Kaum macht man's richtig, schon funktioniert's ~

Zusammenfassung

Die Entdeckung von CRISPR/Cas9 hat das Gebiet der Gentechnik und Genom-Editierung revolutioniert und zu einer bis heute andauernden Welle an Innovationen in therapeutischen Anwendungen und solchen der synthetischen Biologie geführt. Dies betrifft sowohl die Erfindung neuer Techniken für Bildgebung, Mutagenese-Screens und Aufzeichnung zellulärer Aktivitäten, als auch die Entwicklung neuartiger und Verbesserung existierender Werkzeuge für Genom-Editierung. Dies zeigt sich insbesondere an der Evolution von CRISPR Nukleasen zu 'base editors' und 'prime editors', welche wiederum viele weitere Verbesserungen erfahren haben um ihre Präzision und Effektivität auch für kompliziertere Genomveränderungen weiter zu steigern. Die Arbeit innerhalb dieser Dissertation hat zu diesem Prozess durch die Entwicklung eines mit einer Exonuklease ausgestatteten 'prime editors' beigetragen, mit welchem die Effektivität und Präzision größerer Insertionen wie Rekombinations-Sequenzen oder Affinitäts-und Fluoreszenz-Komplementationspeptide weiter gesteigert werden konnte, zur Anwendung in der synthetischen Biologie und biologischen Grundlagenforschung.

Während CRISPR in der Beschleunigung und Ermöglichung wissenschaftlicher Entdeckungen verschiedenster Techniken zur Genmanipulation überaus erfolgreich war, wurde die therapeutische Anwendung in der Behandlung und Heilung genetischer Erkrankungen durch verschiedenste Hindernisse verzögert oder sogar gänzlich verhindert. Dies liegt einerseits begründet in der Schwierigkeit das Zielgewebe in hinreichendem Ausmaß zu erreichen, und andererseits in der Präzision, also Begrenzung jeglicher genetischer Modifikationen auf die einzig beabsichtigte im ausgewählten Gen-Lokus und Zielgewebe. Dies kann durch lokale Applikation, der Auswahl des Editierungs-Strategie und dem gezielten Engineering beteiligter Proteine bereits teilweise adressiert werden, doch ein Großteil dieser Herausforderung hängt auch mit der Auswahl des Transportvektors zusammen. Dieser bestimmt über die Gewebe-Spezifität und Aufnahme-Effektivität des Gen-Editors, und dadurch letztlich über seine effektive Konzentration in der Zielzelle.

Virale Vektoren wurden als erste für diesen Zweck verwendet, da sie von Natur aus zum gerichteten Transfer genetischen Materials hervorragend geeignet sind. Zunächst wurden die Geneditoren dabei auf DNA-Genomen von Adeno-assoziierten Viren (AAV) oder RNA-Genomen von Lentiviren (LV) kodiert, welche anschließend in das Genom der Zielzelle integrieren. Um allerdings den Anforderungen an die Präzision im therapeutischen Kontext gerecht zu werden, wurden Systeme entwickelt welche die lediglich kurzfristige Expression von Geneditoren in der Zielzelle ermöglichen. Tatsächlich ist ein Umschwenken hin zu nicht-viralen Vektoren wie Lipid-Nanopartikeln (LNP) und virusartigen Partikeln (VLP) zu beobachten, welche die vorübergehende Einbringung von Geneditoren in Form von mRNA-Transkripten oder bereits assemblierten Ribonukleoproteinen (RNP) erlauben. Obwohl sich die Herstellungsprozesse von LNP und VLP fundamental unterscheiden, ist die aktuelle Forschung in beiden Bereichen auf ähnliche Engpässe gerichtet, von der Kompatibilität zu verschiedenen Arten von genetischer „Fracht" über ihre effiziente Verpackung bis hin zu zielgerichtetem Transport. VLPs haben dabei eine hohe Effizienz im Transport von RNP-Material gezeigt, welches in den meisten VLP-Systemen durch die Fusion des Geneditor-Proteins an Virus-Kapsid-Proteine erreicht wurde. Dieser Ansatz ist allerdings in seiner Modularität bezüglich der Verpackung verschiedener Geneditor-Proteine eingeschränkt, und

es lässt die komplexe Kinetik unberücksichtigt mit welcher RNP-Komplexe gebildet und degradiert werden.
Um derartige Limitierungen zu überwinden, wurde in dieser Arbeit eine VLP-Technologie entwickelt welche mittels Aptameren prä-assemblierte RNP-Komplexe aktiv aus dem Nukleus rekrutiert, wodurch sich die RNP-Stabilität erhöht und außerdem eine hohe Modularität ermöglicht wird. Während die Spezifität von LNPs durch ihre Lipid-Komposition moduliert werden kann, erben VLPs die Fähigkeit zur Transduktion bestimmter Zelltypen von den Glykoproteinen ihrer viralen Vorgänger, welche an spezifische Rezeptoren auf der Zellmembran-Oberfläche der Zielzelle andocken. VLP-basierte Technologien profitieren daher nicht nur von Jahrzenten der Forschung auf dem Gebiet lentiviraler Transduktionssysteme, sondern haben auch das wissenschaftliche Interesse an Glykoprotein-Engineering neu entfacht um weitere Gewebetypen zu erschließen und mit höherer Spezifität zu erreichen.

Das Forschungsfeld der Gen-und Zelltherapie als Ganzes über das letzte Jahrzehnt betrachtet, zeigt sich eine Verschiebung: Bald nach der Erfindung verschiedenster Geneditierungs-Werkzeuge mit therapeutischem Potenzial wurden auch Transport-Vehikel der nächsten Generation entwickelt, und der Zelltyp-spezifische Transport in komplexe Gewebe als das aktuell größte Hindernis scheint nun zur Entwicklung neuartiger Glykoprotein-Systeme zu führen. Um VLP-Technologien für den Geneditor-Transport nun auch erfolgreich in die Klinik zu bringen und ihre konzeptuellen Vorteile gegenüber anderen Transportmethoden auszuspielen, ist weitere Forschung im Bereich der GMP-konformen Produktion sowie Formulierung und Verträglichkeit unerlässlich.

Abstract

The discovery of CRISPR/Cas9 has revolutionized the field of gene editing and genome engineering, leading to a sudden burst of innovation in therapeutic and synthetic biology applications which continues still today. This concerns both the conception of innovative techniques for imaging, mutational screens and molecular recording, as well as the development of novel editing tools and optimization of existing ones, also highlighted by the progression from CRISPR nucleases to base editors and prime editors. Base and prime editing in particular have received many further tailored enhancements to increase editing fidelity or increase the efficacy of specific, more complex edits. We have contributed to this progress through the development of a exonuclease-enhanced prime editor, which improves the efficacy and precision of larger insertions such as recombination sites, affinity tags or fluorescence complementation peptides, promoting basic research and synthetic biology applications.

While the promise of CRISPR to supercharge scientific discovery and enable the development of novel genetic engineering technologies is being delivered on continuously, its therapeutic aspect of treating and curing genetically inherited diseases has faced various additional challenges and roadblocks, slowing down or even preventing its clinical implementation. Of particular concern are on one side reaching the target tissue with sufficient efficacy to facilitate the desired edit, and on the other side editing precision, i.e. limiting editing activity only to the intended edit, at the intended locus, and in the intended tissue. Editing precision can be partially addressed by local administration, the choice of gene editing strategy, and further engineering of the gene editor itself; but a large part of this challenge is also related to the mode of delivery, i.e. how the gene editor is packaged. The delivery vector also determines tissue specificity and delivery efficacy, and consequently the effective gene editor abundance in the target cell.
With their proficiency for targeted transfer of genetic material, viral systems were the first to be utilized as delivery agents, with gene editors initially just encoded on DNA genomes such as with adeno-associated viruses (AAVs) or on RNA genomes with subsequent stable integration into the host cell genome via lentiviruses (LVs). But owing to the requirement of high precision and low off-target editing in a therapeutic context, systems were conceived that allowed for controlled and short-term gene editor expression. In this regard, a shift has occurred towards non-viral delivery agents, such as lipid nanoparticles (LNPs) and virus-like particles (VLPs) among others, that enable the transient delivery of gene editor components as mRNA transcripts or even pre-assembled ribonucleoproteins (RNPs). While the assembly and production process of LNPs and VLPs is fundamentally different, current research in each field is focused on similar bottlenecks, such as the applicability of different cargo types, the efficiency of cargo packaging, and tissue tropism and specificity. VLPs have shown high proficiency for RNP delivery, which has mainly been achieved through fusion of gene editors to their respective capsid proteins. However, this approach is limited in its modularity to package different types of editors, and it generally does not account for the complex assembly and degradation kinetics of gene editor RNPs.
To overcome these bottlenecks, we have developed a VLP technology that actively recruits fully assembled gene editor RNPs from the nucleus, provides additional stability to the RNP complex, and is also highly modular via its aptamer-based mode of recruitment. While LNPs utilize specific lipid compositions to generate tissue tropism, VLPs inherit the ability from their enveloped origin viruses to display glycoproteins on their surface to access specific receptors

on the target cell membrane. VLP-based technologies therefore not only profit from decades of research on lentiviral delivery techniques, but have also re-ignited the fields interest in glycoprotein engineering platforms to access more tissue types with higher specificity.

Looking at the development of the gene and cell therapy research field over the last decade, there seems to be a shift of focus: Soon after the conception of various novel CRISPR-based gene editing tools with therapeutic potential, next-generation delivery technologies were developed, and the currently biggest bottleneck seems to be the targeting efficacy and specificity in complex tissues, giving rise to a variety of new glycoprotein engineering approaches. To successfully translate VLP-mediated gene editor delivery into the clinic and leverage conceptual advantages over other transient delivery methods, further research regarding GMP-compliant manufacturing, formulation and tolerability is now imperative.

Table of contents

Publication record

This cumulative dissertation is based on the following peer-reviewed first-author publications:

1. Truong, D.-J.J*., **Geilenkeuser, J.***, Wendel, S.V., Wilming, J.C.H., Armbrust, N., Binder, E.M.H., Santl, T.H., Siebenhaar, A., Gruber, C., Phlairaharn, T., et al. (2024). Exonuclease-enhanced prime editors. Nat. Methods. https://doi.org/10.1038/s41592-023-02162-w.

2. **Geilenkeuser, J*.**, Armbrust, N.*, Steinmaßl, E., Du, S.W., Schmidt, S., Binder, E.M.H., Li, Y., Warsing, N.W., Wendel, S.V., von der Linde, F., et al. (2025). Engineered nucleocytosolic vehicles for loading of programmable editors. Cell *188*, 2637-2655.e31. https://doi.org/10.1016/j.cell.2025.03.015.

Further contributions as co-author to peer-reviewed publications or pre-prints:

1. Armbrust, N., **Geilenkeuser, J.**, Grosshauser, M., Stroppel, L., Schmidt, S., Panne, T., Steinmaßl, E., Widenmeyer, F., Warsing, N., Berezin, O., et al. (2024). Non-destructive transcriptomics via vesicular export. bioRxiv. https://doi.org/10.1101/2024.11.11.622832.

2. Truong, D.-J.J., Armbrust, N., **Geilenkeuser, J.**, Lederer, E.-M., Santl, T.H., Beyer, M., Ittermann, S., Steinmaßl, E., Dyka, M., Raffl, G., et al. (2022). Intron-encoded cistronic transcripts for minimally invasive monitoring of coding and non-coding RNAs. Nat. Cell Biol. *24*, 1666–1676. https://doi.org/10.1038/s41556-022-00998-6.

3. Ma, R., Santino, L.M., Chobola, T., Armbrust, N., **Geilenkeuser, J**., Sukumaran, S., Jing, Z., Levkina, A., Ridderbeek, K., Peng, T., et al. (2025). A telescopic microscope equipped with a quanta image sensor for live-cell bioluminescence imaging. Nat. Methods *22*, 1321–1330. https://doi.org/10.1038/s41592-025-02694-3.

4. Wurst, W., Schuhmacher, M., Gruber, C., Lang, C., Ruijpers, R., Mazneykova, L., Krus, A., Tremmel, B., Reinhardt, F., Kadletz, K., […] **Geilenkeuser, J.**, […] et al. (2024). Creating bottom-up RNA transfer vehicles from synthetic protein assemblies. Research Square. https://doi.org/10.21203/rs.3.rs-5123765/v1.

Introduction

Gene editing

Gene and genome editing describes the process of making defined, programmed changes to DNA. This is in distinction to chemical or radiation mutagenesis widely applied in crop breeding, which lead to the acquisition of random mutations across the genome, albeit with a bias towards certain types of mutations depending on the mutagenesis method. With the introduction of gene editing tools like zinc finger nucleases (ZFNs) and transcription activator-like effector nucleases (TALENs), it was possible to alter DNA in a site-specific manner by directing a nuclease towards a defined location in the genome. This massively catalyzed scientific discovery and genetic engineering, but also opened up the possibility of therapeutic gene correction.

While TALENs and ZFNs were cumbersome to customize and often lacked specificity and efficacy, the advent of CRISPR/Cas9 revolutionized the field with its high efficacy and customizability, together with many CRISPR homologs that were subsequently discovered[1]. In their fundamental conformation, Cas nucleases are directed to a target site through an engineered guide RNA (gRNA) as a ribonucleoprotein complex to facilitate a double strand break in a highly specific fashion, dependent on a spacer sequence within the gRNA that is complementary to the target sequence. Restoration of the target site through cellular repair mechanisms such as homology-directed repair (HDR) and non-homologous end joining (NHEJ) is followed by continuous re-targeting until eventually an insertion or deletion (InDel) event occurs, usually causing a frameshift mutation and consequently a functional knock-out of the respective gene.
The capability of a cell to carry out HDR can also be harnessed to introduce a novel piece of DNA from an exogenous donor vector for the integration of transgenes or intact copies of defective endogenous genes. This was possible even before the discovery of targeted nucleases, but it became site-specific and more efficient in combination with targeted DNA disruption. And with CRISPR/Cas9 specifically, the execution of large-scale knockout studies or knock-ins of exogenous donor DNA then got much easier and faster. Critically though, Cas9 could also be transformed into a mere targeting mechanism, by inactivating its two nicking domains HNH and RuvC, to guide a plethora of associated effectors to a target site. Two major examples are CRISPR interference, which utilizes the fusion of specific transcription factors to alter gene expression, and CRISPR imaging, where fluorescent proteins fused to the Cas domain can visualize genomic organization.
This customizability of Cas9 with various effectors also led to the development of new editing techniques, the major developments being first base editing (BE)[2–4] and then prime editing (PE)[5], which allowed for defined genome modifications without causing a double strand break (DSB), greatly increasing editing precision. While base editing utilizes Cas9 nickase (nCas9) fusions with nucleotide deaminases to mediate specific transitions or transversions proximal to a target site, prime editing removed almost any restrictions to what kind of edit could be performed, from single nucleotide substitutions to large insertions or deletions.

Prime editing and its expanded toolbox

Prime editing utilizes a reverse transcriptase (RT) domain fused to nCas9 in combination with a prime editing gRNA (pegRNA), which is constructed like a gRNA but also encodes the desired edit within a 3'-extension. After spacer annealing and DNA unwinding, a primer binding site (PBS) on the 3' end of the pegRNA binds to the freed-up ssDNA flap proximal to the nick, upon which the RT prolongs the flap through reverse transcription with the pegRNA as template. The newly synthesized 3' flap then enters a competition with the existing 5' flap for incorporation into the locus during DNA repair. In a final step, the edit is either propagated into the complementary DNA strand, or eliminated by cellular DNA repair to reconstitute the original sequence[6].

Naturally for such a complex, multistep, multi-component process, many different parameters have been identified that can be optimized or modulated for beneficial effect in terms of editing efficacy, precision, and feasible edit types. Since its inception, prime editing research has primarily focused on **editing strategies**, **pegRNA design and stability** and **prime editor protein engineering**. The multi-step editing process also involves a variety of **cellular determinants**, which are involved in DNA repair, flap degradation, ligation and DNA damage tolerance[7,8], only partially overlapping with known pathways for base editing[9] and DSB repair[10]. These factors interact with each other and have also been tailored individually or in combination towards specific edit types, such as **larger insertions**.

Next-generation prime editing strategies

Suffering from low efficacy initially due its complexity, many further advances and innovations were made to better understand and optimize the prime editing process and expand its utility[11,12]. The foundational publication already provides the first iteration called "PE3", in which a nick is introduced into the other DNA strand using a separate gRNA[6], shifting the equilibrium towards edit incorporation during DNA repair. To prevent unproductive nicking events by the nicking gRNA (ngRNA), a "PE3b" strategy was also proposed in which the ngRNA could only bind the target sequence after the novel 3' flap was already introduced.
To stabilize the endogenous DNA flap that serves as template for reverse transcription, Song *et al.* added the DNA-binding domain RAD51 to the PE complex[13].
Hypothesizing that PE was influenced by specific endogenous DNA repair mechanisms, multiple groups used genetic screens to identify mismatch repair (MMR) as a relevant pathway[8,14]. Chen *et al.* observed increased prime editing efficacy when addig the dominant negative variant of the MMR component MLH (MLHdn) to the PE complex, and termed it "PE4". They also found that the beneficial effects of PE4 and PE3 were additive in certain instances, and termed the combination of both strategies PE5[8].
To improve chromatin accessibility for PE, a second, non-cutting Cas9 complex was directed to a proximal site via a truncated sgRNA[15]. For the same purpose, another study utilized different mechanisms to recruit the transcription factor P65 to the target site[16].

To expand on the possible range of edits and potentially access other pathways of DNA integration and repair, some groups coupled the RT domain with an active nuclease again[17–19], a strategy now conventionally termed "PEn". The presence of a DSB enabled larger re-arrangements[18], and integration of the reverse-transcribed flap could now also be mediated

through NHEJ without any homology area between the RT template of the pegRNA and the endogenous site[19]. To address the increased prevalence of unintended InDel events associated with the resolution of DSBs, various end joining inhibitors were deployed[19,20] which had shown benefit for nuclease-mediated donor integration before[21,22], although a more recent publication also advises some level of caution[23]. Eventually, those repair-modulating proteins and compounds were applied to conventional nicking PE strategies as well[24,25].

Some groups re-evaluated the necessity of a reverse transcriptase for PE, and turned to DNA-dependent polymerases (DDPs) instead. In one instance from Liu *et al.*[26], DNA-dependent PE was utilized to benefit from the higher fidelity and dNTP affinity of DDPs, requiring the synthesis of a DNA-RNA chimera as separate DNA template. This template was then recruited via an RNA aptamer-binding protein fused to the DDP, which itself is not tethered to Cas9 anymore[26]. In another technique termed “click editing”, a DNA template for the DDP is completely separated from the gRNA and recruited through covalent tethering to a Cas9-fused HUH endonuclease, enabling high-throughput screening of optimal DNA templates[27].

pegRNA design

For standard PE, there were only two parameters one could finetune beyond spacer selection, which are the length of the PBS and the length of the RT template (RTT).
The PBS is constrained in length on one side by the nick, and in the other direction by the extent of ssDNA being made accessible the complementary spacer. With SpCas9 and a spacer length of 20 nt, this defines the maximum PBS length to be 17 nt. While this length is rarely required to reach the optimal PBS melting temperature (based on the GC composition of the target sequence), it was still recognized that there is a possibility even with shorter PBS lengths to bind to its complementary spacer sequence, rendering the pegRNA inactive. To alleviate this issue of pegRNA misfolding and auto-inhibition, strategies were developed that prevent the pegRNA to fold in on itself, for instance through selected silent mutations or protective RNA motifs[28–31]. The complementarity between PBS and spacer was also eliminated on a conceptual level with reverse/inverse PE strategies, where the PBS binds on the same strand as the spacer[32,33].
The RTT includes both the edit and the homology sequence, also often referred to as overhang. The design of the edit sequence is in large part pre-determined by the type of edit that needs to be carried out, but there is some potential for optimization. Studies on the role of cellular MMR have shown that it mostly recognizes smaller mismatches in DNA. Similar to MMR inhibition with PE4, MMR can therefore be evaded by increasing the edit window through additional synonymous mutations[8,34].
By definition, the RT overhang starts behind the last changed nucleotide (i.e. the edit) and is therefore not modifiable in sequence but only in length. After reverse transcription, the generated 3’ overhang is sequence-identical to the endogenous 5’ flap and mediates the incorporation of the edit into the endogenous site. Early experiments have shown that its optimal length can be as short as 9 nt[5,35], but this is highly dependent on other parameters such as edit type and target sequence. A commonly known issue is RT readthrough into the pegRNA scaffold, and subsequent partial incorporation of the scaffold into the target site facilitated by minor homology extensions between target site and the pegRNA scaffold. While this effect could be reduced by mindful overhang design to a certain degree, Antoniou *et al.*

also developed a chemically modified pegRNA scaffold that prevents RT readthrough at the scaffold – overhang border altogether[36].

To deal with the increased complexity of pegRNA design, a number of tools were developed which automate the design process and enable the construction of large-scale experiments for a variety of edit types and editing strategies available at the time[37–39]. But it was also apparent that predicting the impact of a respective design choice was not straightforward. Beyond the variety of sequence-dependent parameters such as the appropriate spacer and the PBS melting temperature, cell type and epigenetics are also interconnected factors which are even more difficult to predict. In that regard, two parallel studies report that low dNTP abundance in certain cell types restricts RT activity and therefore PE efficacy, suggesting the inhibition of a dNTP-depleting factor via the lentiviral protein Vpx[40,41]. Another study even found that altering the epigenetic state of a target locus can modulate prime editing efficiency, with the suggestion to condition a target locus with CRISPR activation to increase editing rates[42].
Accounting for the multitude of interacting parameters that influence pegRNA activity, multiple prediction algorithms combined experimental data generated from large pegRNA libraries with deep learning to guide the choice of appropriate spacer, PBS and RTT sequences[43–45]. More recent iterations incorporate different editing strategies, complex edits such as larger insertions[46,47], and also consider the state of locus-specific chromatin features[47]. But given that the PE toolbox is continuously expanding, prediction algorithms likely need to be updated iteratively or even tailored towards a specific innovation or modification to yield accurate results.

pegRNA stability

The 3’ poly-uridine stretch used for polymerase-III-dependent transcription termination is already widely known as a destabilizing factor[48]. Beyond that, multiple studies have focused on the additional need for stabilization of pegRNAs in particular, recognizing that their exposed 3’ end makes them even more susceptible to exonuclease-mediated degradation[35]. Just like gRNAs[49], pegRNAs could be chemically modified to increase their stability[8,35]. But to protect the pegRNA 3’ end specifically in a genetically encoded fashion, stable RNA hairpins such as RNA aptamers[31] or pseudoknot motifs[35,50] were screened for their ability to provide resistance against exonuclease degradation, and the identified candidates now find widespread use. “epegRNAs” were even shown to be compatible with chemical synthesis and modification, to due the small size of the utilized tevopreQ1 motif[35].
Similar to the development of PE4, screening for cellular determinants of PE also led to the discovery of the exonuclease protection factor La, which binds to the polyuridine stretch at the pegRNA 3’ end when co-expressed in target cells[51]. This modification termed ”PE7” demonstrated compatibility with all conventional previous PE strategies and even with epegRNAs to some extent[51].
It was also shown in two independent studies that the PBS-RTT section could be separated from the pegRNA and circularized using self-cleaving ribozymes to increase stability of both the resulting circular template and the remaining gRNA[31,52].

Engineering of prime editor proteins

Alongside the development of new PE strategies and pegRNA optimizations, the prime editor protein component was continuously refined and adapted as well. PE2 as the very first modification of prime editing actually constituted a codon optimization of the RT domain together with five activity-enhancing mutations, coining it as the foundational PE strategy[6]. Soon after, a protein called “PEmax” was generated through systematic optimization of nuclear localization sequences (NLS), addition of activity-enhancing Cas9 mutations, and overall optimized codon usage[8]. As the latest iteration from the Liu lab, editors were tailored through phage-assisted evolution towards specific edit types, yielding a set of editors termed “PE6” a-g[53].
In the meantime, others sought to expand the target space of prime editors by adapting other Cas nucleases to prime editing, such as SaCas9[54], Cas12a[55] and engineered Cas9 variants with relaxed PAM requirements[56].
Some effort was put towards fitting the quite large PE protein into AAV vectors to make PE suitable for *in vivo* studies. While this could be achieved through inteins[57] or minimized/truncated PE protein variants[58], a number of studies also just separated the RT domain from the Cas protein and either left it untethered without any additional modifications[59], recruited it via coiled-coil interactions[60] or complemented it with a split-pegRNA approach as referenced above[52,55], including an aptamer recruiting the RT domain to the edit site.

Larger insertions with prime editing

Prime editing for the first time enabled insertion-type edits without DSBs, but they remain a particularly challenging edit type, and this challenge only ever increases with insertion length. Already shown to be feasible in the foundational publication, it also displayed a drastic decrease in efficacy as soon as the length of the inserted sequence entered the double digits. Only PE3 was able to substantially increase the efficacy again[6], which could originate from (staggered) DSBs, created by the additional nick, being particularly beneficial for larger edits. In the same sense, the capability of PEn to handle large insertions[61] might also originate from the presence of a DSB. On the protein engineering end, phage-assisted evolution yielded variants with an increased propensity for insertion-type edits, specifically PE6c and PE6d[53].

Along the notion of staggered DSBs, an entire group of strategies was being developed in parallel which were tailored towards insertions, deletions or large rearrangements. All of them featured the common principle of two pegRNAs spanning a target site, and are collectively referred to as dual-pegRNA approaches[62–68]. Being demonstrated in plants initially[62], the difference between them mostly concerns aspects of pegRNA design, dependent on their respective primary use case such as mid-size insertions[66] or even genomic deletions on the kilobase scale[65].
A strategy termed template jumping PE (TJ-PE) followed a slightly different approach: With a single (very long) pegRNA carrying both RT overhangs, it only uses an additional nicking gRNA to enable insertion of the novel strand on the opposing end, mimicking the template-primed reverse transcription (TPRT) mechanism of retrotransposons[69]. To enable chemical modification, the pegRNA was subsequently split into gRNA and a circular template RNA, as shown previously[52].

Based on the ability of PE to introduce mid-size insertions, a strategy was conceived to follow up on the insertion of a recombination site “landing pad” with a corresponding integrase and a DNA donor sequence[70,71], bursting previous limits on insertion size at the cost of a 2-step process. In one strategy called “PASTE”, a Bxb1 integrase is fused to the prime editor protein, constituting an “all-in-one” complex together with a pegRNA and the DNA donor template[70]. Another independent study opted for twinPE-mediated integration of the landing pad and simultaneous or successive delivery of evolved Bxb1 integrases, reportedly surpassing PASTE by an order of magnitude in terms of integration efficiency[71].
In a very recent strategy termed “prime assembly”, the dual-pegRNA approach twinPE was combined with either an ssDNA donor or a dsDNA donor with 3’ overhangs to facilitate large insertions in the kilobase range, akin to a Gibson assembly in molecular cloning[72,73]. Lastly, the EXPERT system used a pegRNA variant where the PBS binds upstream of the spacer, enabled by the addition of a nicking gRNA to unwind the target locus[74]. Because the additional nicking gRNA nicks the same strand as the pegRNA, there is no formation of a staggered DSB.

It appears that in general, the facilitation of larger insertions required a (staggered) DSB to be reasonably efficient, often incurring a penalty on editing precision. Within this niche, we developed exonuclease-enhanced prime editors to improve insertion-type edits without a secondary nick to maintain precision.

Delivery of gene editors

The term “delivery” pertains to the means and process to actively transfer an substance, usually a biomolecule, into a target cell. In the context of genome engineering, this can mean any combination of DNA, RNA and proteins with the ability to make genetic or epigenetic changes. With powerful genome editing tools available, efficient delivery of those tools is the next major challenge for therapeutic genome editing[75]. Physical methods like electroporation or microinjection can be highly efficient in cell culture settings, but are mostly not applicable to complex models, highlighting the need for sophisticated biocompatible vehicles.
The choice of a suitable vector depends on multiple characteristics, such as packaging efficiency for a respective cargo molecule, the capability to protect the cargo during transit, tolerability for the target organism, and its potency and specificity for target cell entry. Depending on the cellular uptake mechanism, there is also the additional hurdle of endosomal escape that needs to be cleared to gain access to the target cell cytoplasm or nucleus.

Viruses were the first choice for the engineered, targeted delivery of genetic material *in vivo*, since this is what they naturally evolved to excel at. Viral vectors such as LVs and AAVs, which stably integrate their cargo DNA/RNA into the host cell genome or persist long-term episomally, have seen widespread use to deliver entire genes, even resulting in approved therapies like CAR-T cells[76] or gene replacement[77,78]. Naturally, they were also the first vectors to be used for the delivery of gene editors, which has also seen some use in clinical studies[79]. But it is now being recognized that the long-term expression associated with stable integration is not compatible with gene editing strategies, having raised concerns about increased off-target editing[80,81], immunogenicity[82], and oncogenic potential through insertional mutagenesis and unintended vector integration[83–86]. While BE and PE are safer editing tools than nucleases in those aspects, some genotoxicity issues remain[87]. Viral vectors are therefore not ideal for gene editing applications, despite their efficacy and tissue specificity.

Non-viral delivery technologies

To avoid the complications of long-term expression, a lot of research interest has shifted towards methods that can deliver editors in a transient fashion, an approach that is often referred to as “hit-and-run”: Gene editors are delivered to target cells as mRNA or RNP, where they execute their purpose and are subsequently degraded. For gene editors, the delivery as RNPs is particularly advantageous because they are immediately active, and gRNAs are better protected from premature degradation[88].
Because of the enormous variety of non-viral RNP delivery methods[88], those without demonstrated potential for *in vivo* therapy will not be discussed here in detail. For instance, “non-viral” includes physical methods by definition, and those find use in ex vivo therapy (such as RNP electroporation in combination with viral vectors), but they are not suitable for *in vivo* settings. Another concept that has shown promise *in vitro* are cell penetrating peptides (CPPs), which can facilitate the naked delivery of gene editors based on charge or receptor engagement[89–91], although facing challenges regarding endosomal escape[92,93]. One study investigated editor RNP delivery with CPPs, but its effectiveness remained limited compared to other vectors[94]. Certain peptides have also been conjugated with lipids to promote self-assembly into “nanosomes”, which could also deliver Cas9 RNPs in vitro[95].

Synthetic nanoparticles

The assembly of molecules into nanostructures that incorporate cargo is the common characteristic of synthetic nanoparticles, which have been studied extensively for CRISPR RNP delivery[88]. They are usually chemically synthesized and subsequently formulated together with respective cargo molecules. Lipid-based approaches have seen the most traction, but there are also formulations based on various polymers[96–99] and occasionally inorganic substances[100,101]. Yet, aside from lipid-based nanoparticles, they currently lack substantial demonstration of *in vivo* efficacy and tolerability.

A notable recent addition to the nanoparticle spectrum are protein nanoparticles: Neither chemical nor cell-derived but recombinantly expressed, they evade this conventional classification scheme. In a technology called ENTER, elastin-like polypeptides are combined with endosomal escape peptides to deliver a variety of cargo types[102]. The potential for genome engineering is highlighted by the delivery of Cre recombinase, as well as Cas9 nuclease and base editor RNPs, although currently without any mechanism for targeted delivery[102].

Lipid nanoparticles (LNPs)

LNPs canonically consist of four components: an ionizable lipid, cholesterol, a helper lipid, and a PEG-lipid conjugate. This is in distinction to other lipid-based nanoparticles such as lipoplexes and liposomes: Lipoplexes only contain permanently cationic lipids and find widespread use as lipofection reagent in cell culture even for CRISPR RNPs[103]. While there are examples of local application[104], lipoplexes are generally considered less suitable for *in vivo* therapy due to their high toxicity[105]. Liposomes enclose cargo in an aqueous core with a phospholipid bilayer, which also be functionalized for targeted delivery. In that regard, they resemble cell-derived vesicles[106], which will be discussed in greater detail. Just like with lipoplexes, there is plenty of research around liposome-mediated *in vitro* delivery of CRISPR components[107], but no successful *in vivo* study to date.

The LNP formulation and cargo encapsulation process usually involves ethanol and acidic buffers. The choice of respective lipids is vast, and the specific composition determines size, shape and charge of the resulting particle, which also has a major influence on cargo encapsulation. The preferred cargo type for LNPs is RNA, because the protonated ionizable cationic lipids can interact with the negatively charged nucleotide backbone. The LNP composition further affects its stability, biodistribution and biocompatibility, which are important metrics for an *in vivo* application. Having risen to the occasion as potent mRNA vaccine carriers during the coronavirus pandemic[108], LNPs have been intensify studied as delivery vector for the therapeutic application of gene editors[109], with a lot of traction towards clinical translation. LNPs are known to accumulate in the liver, and were consequently used for liver targeting or applied locally when delivering gene editors *in vivo*[110–113].

LNPs have also been adapted to PE[114], but the predominant co-delivery of Cas9 effector mRNA with a “naked” gRNA is presumably not optimal: The large size of Cas9 effector mRNAs can limit the efficacy of LNP-mediated delivery[115], and the stability of unbound gRNAs would benefit from complexation into an RNP even when chemically modified[49]. Recent research on LNP-mediated editor delivery has therefore aimed at packaging RNP cargos as well, which is more challenging due to electrostatic repulsion between lipids and cargo protein[116], as well as the risk of protein denaturation/degradation during LNP formulation at acidic pH[117]. This was addressed by adding a permanently cationic lipids to the composition, enabling cargo

encapsulation at neutral pH[117]. It was also suggested to add highly negatively charged protein domains to facilitate protein encapsulation by LNPs[118,119]. In another instance, Cas9 RNPs were combined with single-stranded oligodeoxynucleotides (ssODNs) during formulation to facilitate HDR *in vivo*, with the interaction between RNPs and ssODNs apparently exerting a major influence on cargo loading efficiency[120]. Chen *et al.* tackled the denaturation issue of RNPs during LNP formulation by using a highly thermostable Cas9 variant[121]. Lastly, a very recent study successfully delivered BE and PE RNPs *in vivo*, but recognized that a highly specific composition of lipids is required that also has to be re-optimized for each different RNP[94].

Cell-derived vesicles

On the opposing end of synthesized nanoparticles stand cell-derived particles, which have equally seen a lot of use for gene editor delivery as extracellular vesicles (EVs) and virus-like particles (VLPs)[122]. They are generated from production cells that are usually (transiently or permanently) genetically engineered for this purpose. For gene editors, this would mean the stable integration or more commonly transfection of producer cells with constructs for cargo expression, particle formation and target cell entry. Key performance indicators for cell-derived vesicle systems are their rate of particle assembly and budding, cargo packaging efficacy, and efficacy/specificity of target cell entry. Cell-derived vesicles are enveloped, and as such usually taken up by a target cell through endocytosis. Therefore, an additional important metric is the capability of endosomal escape to release cargo into the target cell cytoplasm, which is mostly mediated through fusogenic glycoproteins.
Unlike with nanoparticles, there is no possibility to artificially stabilize any cargo component through chemical modification, which adds to the stability advantage of RNPs over other types of cargo molecules.

Extracellular vesicles (EVs)

EVs are a natural component of many cells with a variety of functions, one of them being the transfer surface proteins or genetic material between cells as means of communication[123]. This capability could be harnessed for the transfer of custom cargo[124]. A foundational study utilized the glycoprotein of the vesicular stomatitis virus (VSV-G) to generate EVs with enhanced particle formation, fusogenicity and endosomal escape[125]. These EVs termed “gesicles” were used to transfer a receptor protein to a target cell surface via endosomal membrane fusion. The potential for the delivery of cargo within the vesicle lumen was recognized, but not realized[125]. Another EV technology termed “VesiCas” was then one of the first to use gesicles for the delivery of Cas9 RNPs to target cells, yet still without active cargo recruitment[126]. That was later implemented via fusion of a cargo protein to the cytoplasmic domain of VSV-G, coupled with chemically-induced dimerization[127,128] or split-protein complementation[129]. Instead of VSV-G, others combined induced dimerization with other, engineered targeting domains displayed on the EV surface[130]. It was also shown that EVs could be loaded by just myristoylating the cargo protein[131] or one part of an induced dimerization system directly[132].
It was shown that EV formation could be promoted further by certain proteins that engage with the endogenous ESCRT machinery responsible for particle budding[133]. Chen *et al.* then fused Cas9 to an engineered variant of such a protein called ARRDC1 to generate RNP-loaded EVs[134].

Another technique for cargo recruitment into EVs is based on the observation that some proteins like CD63 and Hspa8 are naturally enriched in EVs, so-called EV markers or sorting proteins. This was actually already utilized in earlier studies, where fusions of those EV markers to aptamer-binding proteins like MCP from the MS2 phage were used to recruit and deliver mRNAs or miRNAs[135,136]. A study by Yao *et al.* then used this concept to package base editor RNPs into EVs via the com aptamer system, and combined it with VSV-G for endosomal escape[137]. To recruit assembled RNPs, the com aptamer was integrated into the gRNA scaffold.

Other studies focused on protein recruitment: Ye *et al.* fused GFP to the intracellular domain of CD63 and an anti-GFP nanobody to Cas9[138], Osteikoetxea *et al.* tested multiple induced protein dimerization systems in combination with a variety of EV markers to mediate Cas9 recruitment and release[139]. A very recently developed EV technology called VEDIC instead features an intein-mediated release mechanism from direct fusions of Cas9 to CD63[140], which they then expanded to other sorting proteins as well[141].
Showcasing an entirely different loading mechanism, Pan *et al.* harvested EVs from bone marrow and loaded them with Cas9 RNPs via electroporation to impede osteosarcoma progression[142].

Virus-like particles (VLPs)

Viruses have evolved to efficiently package their own genetic material and transfer it to other cells, making them the ideal framework for the targeted transfer of customized genetic material. The most commonly used frameworks for VLPs are lentiviruses (HIV-1) and retroviruses (MMLV), although there are other examples[143,144]. Broadly, both encode three major polyproteins for structural components (gag), replication (pol) and cell entry/fusogenicity (env). Gag contains domains responsible for membrane recruitment (MA), capsid assembly (CA), nucleocapsid assembly and RNA genome recruitment (NC) and budding (p6). Pol contains a protease (PR), reverse transcriptase (RT) and integrase (INT)[145]. Pol domains are contained within a gag-pol polyprotein, that is expressed at a lower rate than gag itself through a ribosomal frameshift (HIV-1) or stop codon readthrough mechanism (MMLV). After budding, viral particles undergo a protease-mediated maturation phase, in which all domains are proteolytically released.
Lentiviral vectors (LVs), based on HIV-1 and commonly used for stable integration of genetic cargo, can be considered a precursor to VLPs: The viral genes on the RNA genome are replaced by a custom transgene, and instead supplied to the production cell in *trans*. Thus, LVs are not replication-competent anymore, but still facilitate stable integration of the customized genetic payload. Integration-deficient lentiviruses (IDLVs) go one step further, as the integration of genetic cargo is prevented through a mutation in the viral integrase domain. This means that any transferred genetic cargo only persists episomally in the target cell short-term.
Env is usually replaced by other fusogenic glycoproteins such as VSV-G, a technique known as “pseudotyping”. This LV-inherited capability to straightforwardly modulate tissue tropism is a key advantage of VLPs over other non-viral delivery, and will be discussed in detail in a subsequent chapter.

Critical capabilities that determine the efficacy of VLP systems include, in chronological order: Cargo packaging/compatibility, particle assembly, budding, target cell entry, endosomal escape and cargo release.
The cargo recruitment mechanism is particularly important, because it determines which types of cargo (protein, RNA, RNP) can be packaged. While different recruitment mechanisms also find use in EVs, this choice is even more fundamental with VLPs because of other interrelated design choices regarding particle assembly and cargo release. Current VLP technologies for gene editor delivery can therefore be classified along two modes of cargo recruitment: Protein-focused or gRNA-focused.

Protein-focused cargo recruitment

Early designs were based on the direct fusion of a cargo protein to the gag-pol polyprotein of an LVs or IDLVs, with some variations. For instance, a cargo protein could be fused either to the N-terminus of gag-pol[146,147] (while retaining the myristoylation site required for membrane association), or the C-terminus[148]. In the latter example, the integrase domain could also be removed, since it is not required for protein delivery[148].
In both of those designs however, the cargo protein remained attached to gag, which could inhibit its function. The first designs that demonstrated gene editor protein delivery therefore included a cleavage site for the viral protease, releasing the cargo protein in the target cell after maturation[149,150]. Furthermore, the viral myristorylation signal was replaced with a pleckstrin homology domain to enhance gag recruitment to the membrane[151]. Complementing Cas9 protein delivery, the sgRNA was encoded on a lentiviral transfer vector to yield "all-in-one" particles[150].
Instead of direct fusions to the gag domain, it was also discovered that cargo proteins could be delivered by fusing them to lentivirus-associated proteins, which are incorporated into virions through non-covalent interaction with gag[152–154]. Based on this strategy, one study fused Cas9 to the lentiviral protein Vpr, again separated by a protease cleavage site[155]. Another study used Cyclophilin A (CypA) for this purpose[156], due to its ability to bind to lentiviral capsids[157]. As before, the gRNA was co-delivered on a lentiviral transfer vector.

While the protease domain facilitates cargo release in these designs, it is still possible to deliver proteins without it. In fact, the entire pol gene is not essential for particle formation either[145]. An early study by Kaczmarczyk *et al.* merged these concepts to deliver a cargo protein with retroviral VLPs only consisting of gag domains[158]. However, the absence of a cargo release mechanism likely limited its efficacy. In a similar fashion, the VesiCas study attempted Cas9 fusions to gag, but did not observe any advantage over their EV designs[126].
To enable cargo release again, Mangeot et al. supplemented MMLV-Gag-Cas9 fusions with integrase-deficient gag-pol as a "helper" protein[159]. With their "Nanoblade" particles, they were also the first to demonstrate RNP delivery, relying on gRNAs associating to Cas9 in the producer cell. Through polybrene-mediated complexation of nanoblade particles with ssDNA donor templates, they further constructed all-in-one particles for HDR[159].
Due to its efficacy and multitude of innovations, nanoblades had substantial impact in the field, and were utilized in several follow-up studies demonstrating efficacy in various cell types[160] and even organoids[161], or adaptation to other Cas variants[162]., Banskota *et al.* expanded on the nanoblade design with the development of "eVLPs", improving cargo release through optimized linker cleavage, stoichiometry of the integrase-deficient gag-pol helper, and

adaptation to the delivery of base editor RNPs[163]. Importantly, they also introduced a nuclear export sequence (NES) into gag, offsetting the NLS on Cas9 to optimize the localization of the gag-Cas9 fusion protein during particle assembly in the producer cell. eVLPs were also utilized in several other studies for organoid[164] and zygote[165] editing, and adapted to epigenome editing[166]. Directed evolution later yielded improved eVLPs specifically for base editing[167].
Both nanoblades and eVLPs were eventually adapted to PE with additional tweaks. While the adaptation to nanoblades termed "NanoScribes" utilizes intronic pegRNA transcription with Polymerase II promoters and also implements multiple NES to optimize localization, it sticks to the fusion-based approach[168]. "PE-eVLP" introduces the recruitment of the prime editor via coiled coil domains, and additionally utilizes a pegRNA-grafted aptamer to separately improve recruitment of pegRNAs via a modified gag-pol domain[169].

Alongside this continuous development of retroviral VLPs for gene editor delivery, the same process took place with lentiviral particles. Hamilton *et al.* used Gag-Cas9 fusions, also with protease-cleavable linker and wild-type gag-pol as helper, to construct Cas9-EDVs[170]. Utilizing the ability of the maturated lentiviral nucleocapsid to transfer a lentiviral transgene directly into the nucleus[171], Cas9-EDVs facilitated simultaneous gene knock-out and lentiviral integration. In one follow-up study mainly focused on immune cell-targeted pseudotyping, the Cas9-EDV design was further refined, implementing the localization optimization via NLS and NES motifs[172]. By substituting the HIV-1 protease cleavage site with a different one from tobacco etch virus (TEV), they also found that lentiviral maturation and nucleocapsid formation was not required for efficient RNP delivery into the target cell nucleus[172]. In a recent pre-print, the group then systematically assessed which components of Cas9-EDVs were actually essential, yielding a drastically minimized variant supplemented by an equally minimized helper domain[173]. Interestingly, this study also reported that proteolytic release was entirely expendable for Cas9 editing activity, indicating that gag-Cas9 fusions could facilitate editing with similar efficacy[173].
In an independent study, Haldrup *et al.* developed lentivirus-derived nanoparticles (LVNPs), which they used for nuclease editing, BE and also for the first time PE via VLPs[174], slightly ahead of PE-eVLPs. In the final LVNP3.0 configuration, the gene editor is fused to the C-terminus of gag-pol, retaining only the protease domain while eliminating RT and INT. This design utilizes the natural ribosomal frameshift mechanism of HIV-1 to modulate the stoichiometry of editor-fused and unmodified gag transcripts for ideal particle assembly. While this design is not dependent on a helper construct in principle, integrase-deficient gag-pol was still included during production. Unlike with other fusion-based designs[163,172], the NLS motifs attached to Cas9 were not compensated with NES motifs elsewhere to aid particle assembly.

gRNA-focused cargo recruitment

Lentiviruses and retroviruses already possess a mechanism for RNA delivery: The NC domain binds to a packaging signal on their RNA genome. This mechanism is also used for lentiviral transduction systems and IDLVs, and some early designs for Cas9 protein delivery still encode the gRNA on the lentiviral transfer vector[150,155]. It is even possible to recruit Cas9 proteins via a gRNA encoded on a transfer vector[156].
But the general mechanism of lentiviral RNA packaging, based on the interaction between an aptamer and an aptamer-binding protein, also inspired orthogonal techniques for mRNA delivery: Prel *et al.* tagged an mRNA transcript with multiple MS2 aptamers, and integrated the

corresponding MS2 coat protein (MCP) into the NC domain of gag, which was no longer needed for RNA recruitment[175]. This design was later adapted in multiple other studies to deliver Cas9 mRNA, combined with the gRNA on a lentiviral transfer vector[176,177]. Another group also tested MCP insertions into the MA domain, as well fusions to the lentiviral accessory proteins Vpr and NEF[178].

The first example of an aptamer-modified gRNA for recruitment into VLPs was published in 2018 by Knopp et *al.*, who co-delivered MS2-tagged Cas9 mRNA with an MS2-tagged gRNA[179]. This was achieved with MLV-derived VLPs in which the gag and pol frames were split into two separate plasmids, and NC was replaced with MCP. The same group later demonstrated gRNA delivery also with RSV-derived VLPs, testing multiple potential aptamer grafting positions within the gRNA scaffold[180].

Lyu *et al.* were the first to explicitly pursue RNP delivery, without the requirement for additional Cas9 mRNA packaging[181]. Further exploring this design, they then systematically assessed various aptamers and sgRNA grafting positions, also demonstrating the capability of multiplexing different RNPs with the same particle[182] and also the delivery of base editor RNPs[183]. Looking for improvements on their design, they eventually revisited mRNA co-delivery, and also recruitment of the lentiviral transfer vector via orthogonal aptamers[184].

The latest addition to aptamer-mediated RNP delivery was the RIDE system[185]. Based on a VLP design that the group had developed before for mRNA delivery[176,186], Cas9 nuclease and base editor RNPs are recruited via MS2-grafted gRNAs and N-terminal fusion of MCP to lentiviral gag-pol, supplemented with integrase-deficient gag-pol helper. While their VLP design did not feature any innovation compared to previous studies, they instead focused on the development novel glycoproteins for tissue-specific delivery, which will also be discussed in detail later on.

Publication: Exonuclease-enhanced prime editors

Prime editors mark a significant advancement in the gene editing toolkit, but while high efficacy could be achieved for substitution-type edits and small insertions and deletions, bigger edits remain challenging. In this work, an exonuclease domain from the T5 phage was utilized to enhance the efficacy of prime editing for insertions, specifically digesting the endogenous 5' flap to make space for the new 3' flap generated through reverse transcription from the pegRNA, alleviating the first bottleneck of flap competition. It was shown across multiple loci and cell types that Exo-PE enhances the insertion efficacy of a 30 nt affinity tag and a 54 nt recombination site, compared to the reference strategies PE2, PE3, PE4 and PE5. Contrary to the dual-nick strategies PE3 and PE5, Exo-PE maintained high editing precision.

The successful demonstration of the Exo-PE strategy relied on two key findings: Firstly, the localization of the exonuclease domain relative to the site of DNA unwinding is essential. While direct fusion of the exonuclease to either Cas9 terminus resulted in an at most minor increase in editing efficacy, recruitment via a pair of aptamer and aptamer-binding protein, with the aptamer inserted into the tetraloop of the pegRNA, yielded a significant increase. Secondly, the choice of exonuclease is critical, as we found that from a variety of 5' exonucleases tested, only two led to an increase in editing efficacy. Intriguingly, both of these also show 5' flap endonuclease activity.

During the development of Exo-PE, we generated an enhanced traffic-light reporter (eTLR) as a multimodal, digital flow cytometry-compatible high-throughput readout tool. Initially developed to screen for HDR-enhancing compounds, eTLR simultaneously detects HDR and InDel events in all forward reading frames and successfully validated the mutagenic end-joining inhibitors i53 and AZD7648 (a DNA-PK inhibitor). It can further be applied to measure base editing efficacy, and in the context of Exo-PE development it was used to measure the efficacy of a 54 nt insertion via prime editing, restoring a truncated red fluorescent protein. Utilizing eTLR, we also generated an improved prime editor (iPE) featuring an optimized nuclear localization sequence. iPE displayed a consistent increase in editing performance for this type of edit.

My contribution to this study includes the co-generation of all constructs, co-conduction of all cell and biochemical experiments and the co-analysis of all data related to prime editing. Specifically, I led efforts to further characterize Exo-PE after its initial conception, and designed and executed all benchmarking experiments on endogenous sites as well as the exploratory study on endogenous cell tagging via fluorescence complementation. I carried out the entire statistical analysis and led the writing of the revised manuscript.

The article is published in *Nature Methods*, licensed under a CC BY 4.0 license and available at https://doi.org/10.1038/s41592-023-02162-w.

nature methods

Article

https://doi.org/10.1038/s41592-023-02162-w

Exonuclease-enhanced prime editors

Received: 13 January 2022

Accepted: 19 December 2023

Published online: 1 February 2024

Check for updates

Dong-Jiunn Jeffery Truong[1,2,4], Julian Geilenkeuser[1,2,4], Stephanie Victoria Wendel[1,2], Julius Clemens Heinrich Wilming[1,2], Niklas Armbrust[1,2], Eva Maria Hildegard Binder[1,2], Tobias Heinrich Santl[1,2], Annika Siebenhaar[1,2], Christoph Gruber[3], Teeradon Phlairaharn[1,2], Milica Živanić[1,2] & Gil Gregor Westmeyer[1,2]

Prime editing (PE) is a powerful gene-editing technique based on targeted gRNA-templated reverse transcription and integration of the de novo synthesized single-stranded DNA. To circumvent one of the main bottlenecks of the method, the competition of the reverse-transcribed 3′ flap with the original 5′ flap DNA, we generated an enhanced fluorescence-activated cell sorting reporter cell line to develop an exonuclease-enhanced PE strategy ('Exo-PE') composed of an improved PE complex and an aptamer-recruited DNA-exonuclease to remove the 5′ original DNA flap. Exo-PE achieved better overall editing efficacy than the reference PE2 strategy for insertions ≥30 base pairs in several endogenous loci and cell lines while maintaining the high editing precision of PE2. By enabling the precise incorporation of larger insertions, Exo-PE complements the growing palette of different PE tools and spurs additional refinements of the PE machinery.

PE entails the reverse transcription of a Cas9-bound RNA template at a targeted DNA site, successful insertion of the generated 3′ flap and repair of the DNA locus. The initial demonstration of PE by Anzalone et al.[1] was a remarkable achievement given the complex spatial arrangement and orchestration of the different molecular functions, the delicate ratio of affinities between self-complementary PE gRNA (pegRNA) and primer-binding site (PBS), and the downstream cellular processes resulting in the incorporation of the intended edit.

One of the critical bottlenecks emphasized in the original publication[1] is the need for the de novo synthesized 3′ DNA flap to outcompete the original 5′ end, which is, in particular, disfavored for longer stretches.

The DNA repair machinery has to subsequently maintain the desired edit in lieu of the original sequence. The PE3 strategy attempts to bias the outcome towards the desired edit by causing a secondary nick on the unedited strand, flagging it for repair. However, this strategy carries the risk of an increased rate of insertions and deletions (indels). The PE4 strategy inhibits DNA mismatch repair (MMR), although it seems to be less effective for longer edits[2]. PE5 combines both of these strategies simultaneously.

Furthermore, alternative PE strategies use paired pegRNAs to generate two de novo 3′ DNA flaps that anneal together to replace the original segment. These 'paired PE' strategies have been customized for different types of edits (short substitutions, insertions or large deletions)[3]. However, using a secondary nick in the paired PE strategy still poses the danger of unintentionally creating a staggered double-strand break (DSB).

Here, we describe developing and optimizing a complementary PE strategy called Exo-PE, which involves recruiting a 5′–3′ exonuclease to the editing site. This active recruitment generates an engineered gap for the invasion of the de novo synthesized 3′ flap, thereby relieving the bottleneck of flap competition and thus enabling also larger inserts without a secondary nick.

Results

Fluorescent reporter line for gene-editing events

To improve the precision and throughput of our gene-editing studies, we first developed a fluorescence-activated cell sorting (FACS) screening system that comprehensively captures both successful PE- or homology-directed repair (HDR)-mediated

[1]Institute for Synthetic Biomedicine, Helmholtz Munich, Neuherberg, Germany. [2]Department of Bioscience, TUM School of Natural Sciences and TUM School of Medicine,Technical University of Munich, Munich, Germany. [3]Institute of Developmental Genetics, Helmholtz Munich, Neuherberg, Germany. [4]These authors contributed equally: Dong-Jiunn Jeffery Truong, Julian Geilenkeuser. e-mail: gil.westmeyer@tum.de

https://doi.org/10.1038/s41592-023-02162-w

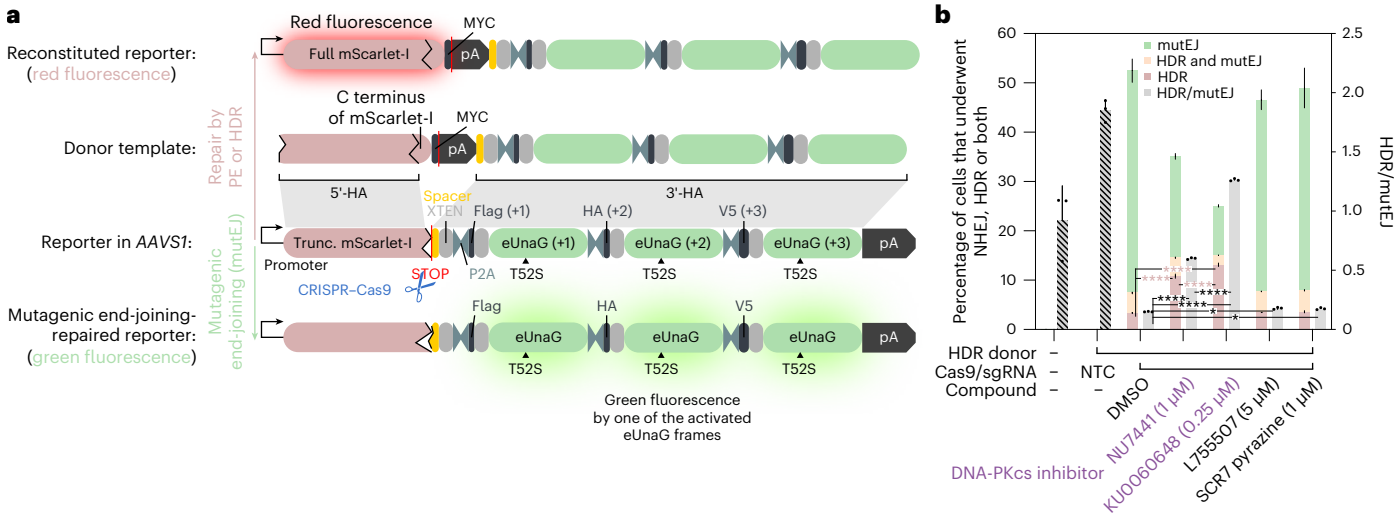

Fig. 1 | Development of an eTLR to monitor all editing events. a, eTLR is based on C-terminally truncated (Trunc.) mScarlet-I followed by a stop codon and a concatenation via P2A sites of three different frames coding for the green fluorescent protein eUnaG$_{T52S}$. Out-of-frame ATGs were removed to prevent unintended translation initiation. Disruption of the stop codon via, for example, NHEJ/MMEJ/SSA results in readthrough and the activation of one of the eUnaG frames (eUnaG (+1/2/3)) (green fluorescence). Instead, successful repair via PE or HDR results in full-length mScarlet-I (red fluorescence). Cells with a biallelic integration of eTLR were analyzed via FACS, where red fluorescence reports successful HDR or PE, while green fluorescence indicates a mutagenic end-joining event. A signal on both the red and green channels (shown in orange) indicates that both events have occurred, each on a separate allele. **b**, HEK293 cells carrying biallelic copies of the eTLR system in *AAVS1* were transfected with a promoterless repair template for mScarlet-I and an all-in-one CRISPR–Cas9 plasmid targeting eTLR. At 16 h after transfection, the indicated compounds were added to the cells. At 3 days after transfection, cells were analyzed for red and green fluorescence by flow cytometry to quantify the effect of the compounds on the repair outcome. Colored bars quantify the fraction of cells with green, red, or both (orange) signals representing the different editing outcomes (left *y* axis), whereas the gray bars (right *y* axis) display the ratio of HDR over mutagenic end-joining events as a measure of editing precision. Selected results of a Bonferroni MCT after one-way ANOVA were shown for the HDR events as well as editing precision (HDR/mutEJ) and are indicated by asterisks; $^{*}P < 0.05$, $^{****}P < 0.0001$. Bars, mean ± s.d. ($n = 3$ biological replicates). Please note that only very few red or green events were recorded by FACS for the condition without donor and Cas9, and the non-targeting control (NTC) such that the corresponding HDR/mutEJ ratios are not informative (shaded bars).

outcomes as well as mutagenic end-joining (mutEJ) events leading to indels (Fig. 1).

In distinction to previous systems that could only report approximately one-third of unintended edits[4], our enhanced traffic light reporter (eTLR) system reports all frameshifts resulting from indels at the target site. Specifically, the reporter design allows the C-terminally truncated red fluorescent mScarlet to be restored by PE or HDR, whereas any indels occurring in any of the frames are detected via the expression of the small green fluorescent protein enhanced UnaG (eUnaG)[5] enabled by translational readthrough into one of the frames (Fig. 1a). We removed all out-of-frame stop codons by synonymous codon replacements, except for M51-T52 (ATG–ACN), where neither methionine nor threonine could be synonymously substituted to remove the +2 frame *opal* stop codon. Therefore, T52S had to be introduced into eUnaG to remove this out-of-frame stop codon. Moreover, to minimize leaky background fluorescence, we removed all out-of-frame start codons (ATG) to prevent translation initiation by cryptic promoters (Extended Data Fig. 1a,b). If desired, it would also be possible to decode the exact frame by immunofluorescence against the frame-specific epitope tags (Flag, HA, V5).

We first confirmed the functionality of the three reading frames by creating −1/−2/−3 nucleotide deletions to simulate mutagenic end-joining events at the target site, which led to visible green fluorescence (Extended Data Fig. 1c).

To validate that the degree of green or red fluorescence of eTLR reflect the different genome editing outcomes, we used CRISPR–Cas9-driven HDR of the truncated mScarlet-I, whose efficiency was modulated by established pharmacological compounds. We transfected a clonal cell line carrying biallelic copies of the eTLR system, with CRISPR–Cas9 components directed against the editing site together with a promoterless HDR template containing the 54 nucleotide missing C terminus of mScarlet-I and a new polyadenylation site (Fig. 1b and Extended Data Fig. 1d).

The biallelic eTLR cell line can thus distinguish three different outcomes: red fluorescent cells indicate successful homologous recombination, and green cells indicate mutagenic end-joining events. Detection of both red and green fluorescence for one cell in FACS analysis (Methods) indicates that one allele was repaired via PE (or HDR), whereas the second reporter copy on the other allele was repaired by mutagenic end-joining (mutEJ), such as nonhomologous end-joining. The fraction of red fluorescent cells was used to determine the desired editing efficacy, and the ratio of total red to green cells was used to measure editing precision[4].

Optimization of the PE enzyme and its nuclear localization

First, we used the eTLR system to generate an improved PE (iPE) by optimizing the protein component (Fig. 2). Specifically, we incorporated an enhanced nuclear localization sequence (NLS) motif (superNLS) (Fig. 2a,b) and a codon-optimized reverse transcriptase (RT). Moreover, we removed several potential splice sites contained in the original unoptimized prime editor[1], which may lead to mRNA mis-splicing[6] and nuclear retention by splice factors (Fig. 2a, marked in red). We also re-examined which terminus of the Cas9 nickase (nCas9) is optimal for the RT fusion, comparing a version with RT fused C-terminally (iPE-C), and one with RT fused N-terminally (iPE-N) (Fig. 2a).

We then benchmarked iPE-N/C against PEmax[2], which contains a C-terminally-fused codon-optimized RT domain, additional mutations to nCas9 (R221K + N394K)[7], and improved nuclear localization. iPE-N and iPE-C showed an increased editing efficacy over PEmax in a PE3 setting using an engineered pegRNA (epegRNA) with a 3′-protection motif (tevopreQ1)[2] (Fig. 2c).

https://doi.org/10.1038/s41592-023-02162-w

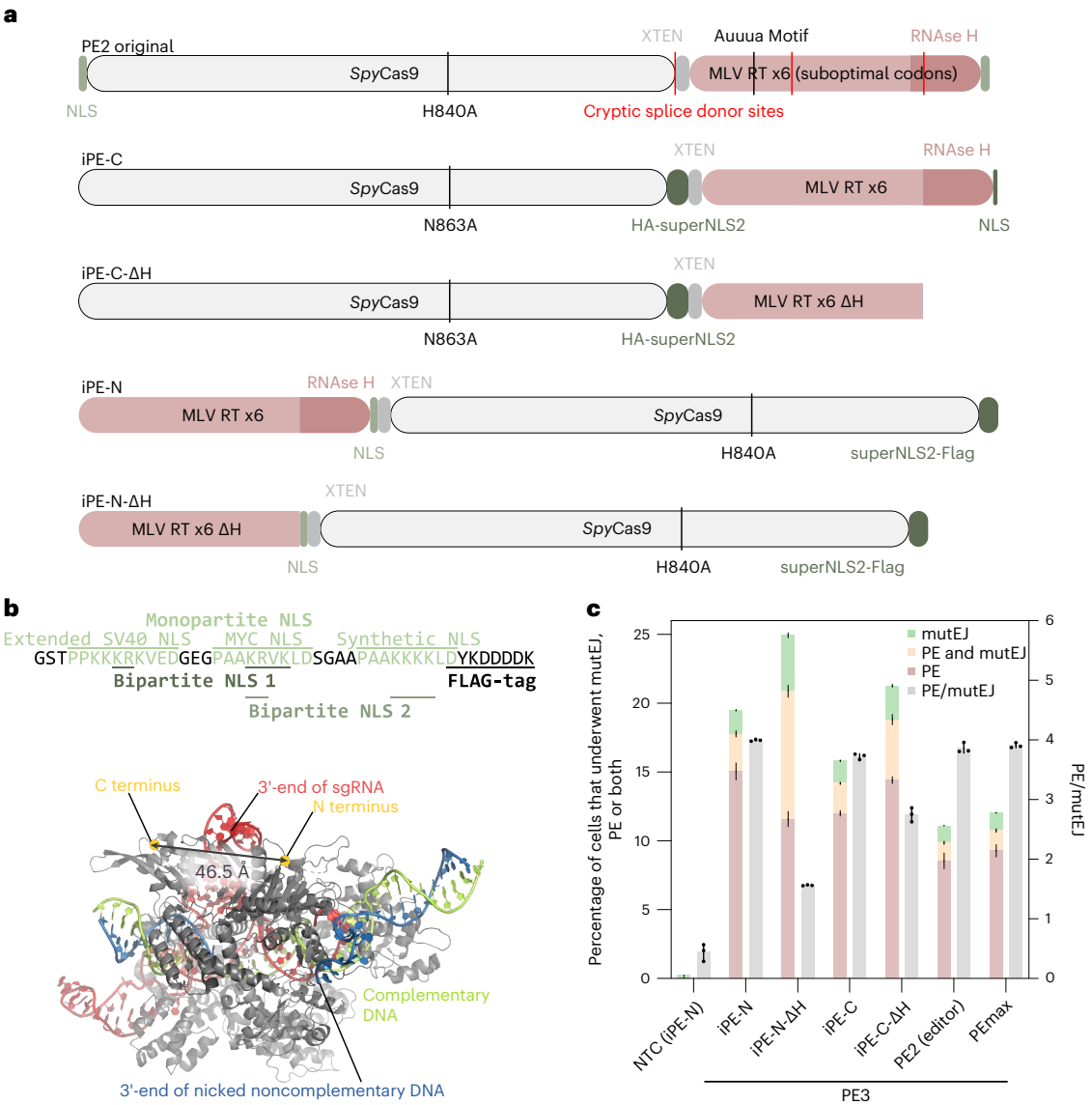

Fig. 2 | Development of an iPE in combination with engineered/protected pegRNA containing an RNA aptamer. a, Schematic representation of the original PE construct from ref. 1 (top) and optimized PE constructs. Cryptic splice donor sites were detected using NetGene2 (ref. 6). **b**, Top, depiction of the superNLS, harboring three mono- and two bipartite NLS sequences. Bottom, structure of the ternary Cas9–sgRNA–DNA complex with nicked nontargeting DNA (PDB, 6VPC). **c**, Comparison of the original PE2 editor and the optimized PEmax[2] with iPE with RT fused N-terminally or C-terminally (iPE-N and iPE-C) and its ΔRNAse H variants, combined with a 3′-tevopreQ1-modified pegRNA, in a PE3 setup. Bars represent mean ± s.d. ($n = 3$ biological replicates).

In the eTLR system, we also found that deleting the RNAse H domain of RT (iPE-N/C-ΔH) increased the indel frequency and thus reduced the precision for the N-terminal configuration, whereas the same deletion had only an attenuated effect in the C-terminal fusion (Fig. 2c).

The original PE2 enzyme[1] was not significantly worse than PEmax when combined with engineered pegRNAs (Fig. 2c). However, when pegRNAs without tevopreQ1 were used, the original PE2 enzyme performed much worse compared with iPE-N in both the PE2 and PE3 strategy (Extended Data Fig. 2a; PE2, $P = 0.0007$; PE3, $P < 0.0001$; two-tailed unpaired t-test), indicating optimized enzymes can compensate for suboptimal pegRNAs.

When further comparing iPE-N and iPE-C on eTLR, we found that iPE-N had a slightly higher editing efficacy for the PE3 and paired PE strategy than the C-terminal fusion (iPE-C; Extended Data Fig. 2b; red bars, $P = 0.0222$; one-way analysis of variance (ANOVA) with Bonferroni multiple comparison test (MCT)) also when the RT was exchanged with MarathonRT (Extended Data Fig. 2c; $P < 0.0001$; two-tailed unpaired t-test).

We have thus identified optimal iPE proteins with an N- or C-terminal fusion of RT to nCas9 (iPE-N or iPE-C) featuring an improved NLS, linker length, and codon usage.

Recruiting an exonuclease to the PE complex

We next assessed whether installing a 5′-exonuclease directly on iPE could more efficiently free up space for inserting the de novo synthesized 3′ flap, comprising the desired edit and the invasion/homology region. We searched for highly active 5′-DNA-exonucleases/flap endonucleases and identified T5-bacteriophage and T5-like 5′–3′-DNA -exonucleases[8,9], which also possess flap endonuclease activity as potential candidates for creating engineered gaps at the primary PE site. Since both termini of *Streptococcus pyogenes* Cas9 are located on the opposite side of the cleft where the target DNA is bound and nicked (Fig. 2b), we reasoned that a direct fusion of the exonuclease might not

https://doi.org/10.1038/s41592-023-02162-w

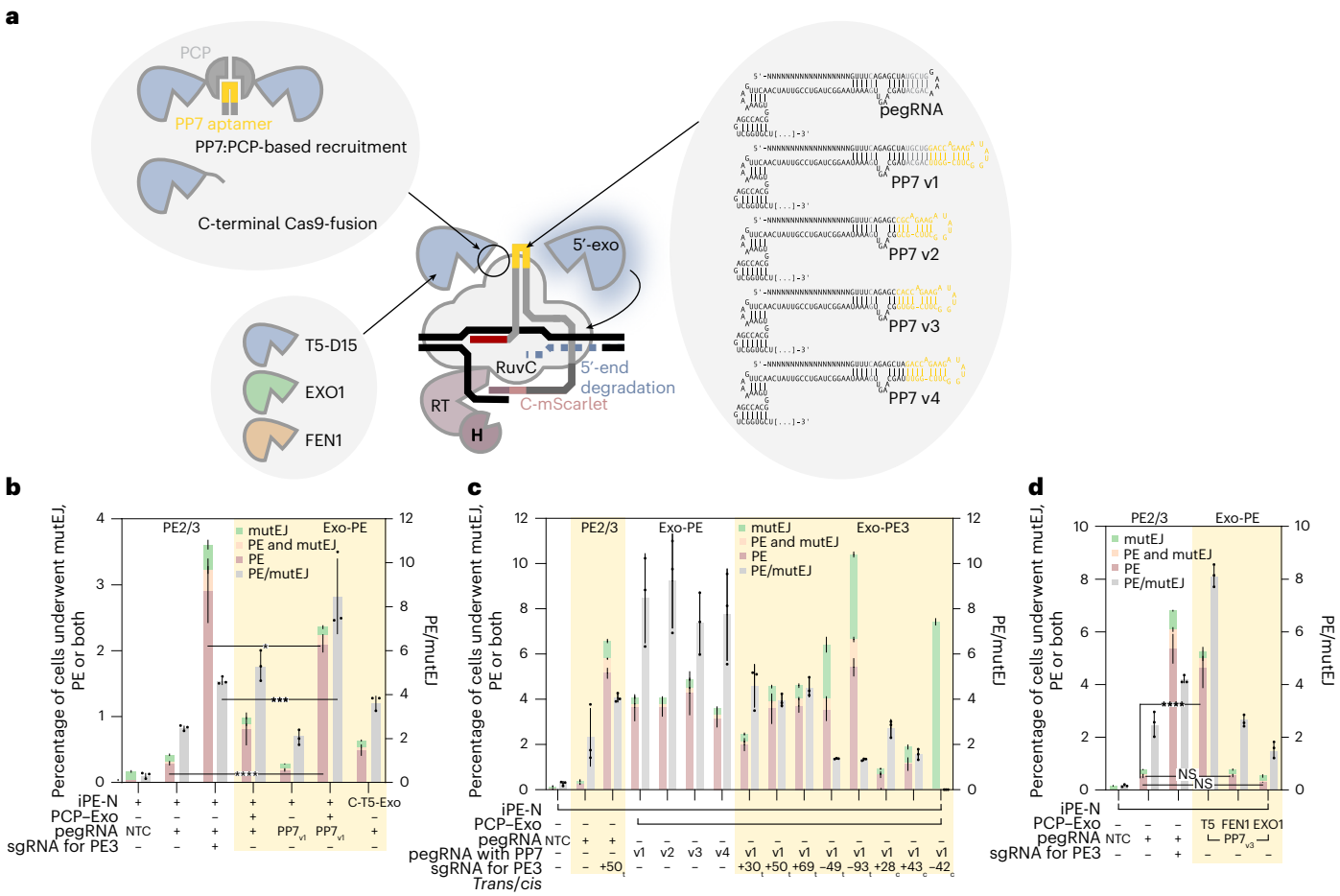

Fig. 3 | Development of an Exo-PE strategy using eTLR. a, Schematic of different Exo-PE designs varying in recruitment mechanism, choice of specific exonuclease, and version of the PP7 aptamer grafted into the pegRNA scaffold. **b**, Comparison between PE2, PE3 (white graph area) and 5c-DNA-exonuclease-enhanced PE2 (Exo-PE, yellow graph area). Selected results of Bonferroni MCT after one-way ANOVA were shown for the fractional PE events and editing precision, and are indicated by asterisks; $^{*}P < 0.05$, $^{***}P < 0.001$, $^{****}P < 0.0001$. Bars, mean ± s.d. ($n = 3$ biological replicates). **c**, Effects of different PP7/pegRNA scaffold designs (shown in **a** and the impact of an additional up- or downstream *cis*- or *trans*-acting nicking sgRNA on the efficacy and precision of Exo-PE. Bars, mean ± s.d. ($n = 3$ biological replicates). **d**, Alternative PCP fusions with human-derived 5′-DNA-exonucleases/flap endonucleases domains from FEN1 and EXO1 without their native C-terminal interaction peptides were tested as an alternative to the bacteriophage 5′-DNA-exonuclease/flap endonuclease. Selected results of Bonferroni MCT after one-way ANOVA were shown for the fractional PE events, and are indicated by asterisks; NS $P > 0.05$, $^{****}P < 0.0001$. Bars, mean ± s.d. ($n = 3$ biological replicates).

be an optimal configuration and therefore opted for aptamer-based recruitment[10]. We thus introduced the *Pseudomonas* phage PP7 aptamer[11] into the tetraloop junction between the crRNA and the tracrRNA. We also fused the 5′–3′-exonuclease to the PP7 aptamer binding coat protein (PCP) together with an NLS (PP7:PCP-based recruitment; Fig. 3a). When coexpressing the PP7-tagged pegRNA and the PCP–NLS–5′-Exo, a substantial sevenfold increase in efficacy compared with PE2 could be observed ($P < 0.0001$; one-way ANOVA all versus all excluding nontargeting controls; Bonferroni MCT; Fig. 3b), whereas, without exonuclease recruitment (using a pegRNA lacking the PP7 aptamer), efficacy dropped to only twofold above PE2 level. By contrast, a direct fusion of the 5′–3′-DNA-exonuclease to the C-terminus of nCas9 (C-T5-Exo, last bars) barely improved the editing efficacy. Compared with the PE3 strategy, the editing efficacy of Exo-PE was slightly lower ($P = 0.0149$) but with a higher editing precision ($P = 0.0008$; one-way ANOVA all versus all excluding non-targeting controls; Bonferroni MCT).

Subsequently, we refined the PP7 aptamer-tagged pegRNA for Exo-PE, and continued with PP7 v3 (Fig. 3a, right schematic), which showed a trend towards increased efficacy while maintaining improved precision (Fig. 3c). Additional modifications of iPE were shown to be beneficial in a previous study (a mutation in nCas9 (K918N) and a histone-like dsDNA binding protein (Sso7d) (iPE$_{K918N,Sso7d}$, see sketch in Extended Data Fig. 3a))[12,13], but were not consistently shown to be beneficial, and were therefore omitted them from subsequent experiments. Other conditions such as the combination of Exo-PE with PE3 (Exo-PE3) (Fig. 3c), catalytically inactive sgRNAs[14] (dsgRNA; Extended Data Fig. 2d), ssDNA-binding domains (Pot1pC[15]) (Extended Data Fig. 3b), or replacement of phage-derived exonucleases with human exonucleases FEN1 and EXO1 (Fig. 3d) did not yield any additional benefit. More interestingly, the T5-like exonuclease from *Klebsiella pneumoniae* siphophage Sugarland was nearly as effective for Exo-PE as T5 (80% homology of T5; Extended Data Fig. 3b) when tevopreQ1 (Q1) was used to increase the steady-state concentration of full-length pegRNAs[16] ($P = 0.0221$, ANOVA all versus iPE-N$_{K918N}$ (ref. 12) + T5 with Bonferroni MCT). By contrast, T7 exonuclease showed a decreased efficacy ($P < 0.0001$). Thus, we conclude that the best 5′-exonuclease for iPE used with the Exo-PE strategy remained the T5 phage exonuclease C-terminally fused to PCP.

We also re-examined whether further optimization of the pegRNAs could improve Exo-PE performance even more. For our initial experiments, we already used an optimized sgRNA scaffold in which

we removed the polyT/U-stretch and introduced either an RNA folding nucleation site via an extended neutral hairpin[17] or the PP7 aptamer hairpin to improve RNA folding. Removing the 3′-tRNA from the pegRNA (which cleaves off the 3′-uridine stretch via endogenous RNAse P/Z) led to a strong decrease in efficacy in PE3 (iPE-$N_{K918N\text{-}Sso7d}$; all 3′-modified pegRNA versus 3′-unmodified pegRNA; $P = 0.0001$; one-way ANOVA with Bonferroni MCT; Extended Data Fig. 3a,c), probably due to RNA destabilization[18]. Similarly, removing the 3′-uridines by HDV ribozymes was almost as effective ($P = 0.0412$) as tRNAs. However, prolonging the pegRNA half-life by adding the 3′-pseudoknot tevopreQ1 (ref. 16), which we had also already used in previous experiments, was more effective than removing the destabilizing terminal U-stretch ($P < 0.0001$). The minimal pseudoknot (mpknot) from the same study[16] as tevopreQ1 was not effective ($P > 0.9999$; Extended Data Fig. 3c), while other pseudoknots (BWYV, PEMV) or hairpin structures were similarly effective as tevopreQ1 in Exo-PE (all versus tevopreQ1; $P = 0.1736$ and $P > 0.9999$ for BWVV and PEMV, respectively; one-way ANOVA with Bonferroni MCT; Extended Data Fig. 3d).

The best editing efficacy for iPE on eTLR was thus obtained with a pegRNA containing a $PP7_{v3}$ aptamer and tevopreQ1 (7_{v3}/Q1), resulting in a ~50-fold better efficacy than the original editor[1] for PE3 and ~30-fold better efficacy for Exo-PE (all versus all; $P < 0.0001$; one-way ANOVA with Bonferroni MCT; Extended Data Fig. 3e). Compared with the optimized PE enzyme, termed PEmax[2], $iPE_{K918N\text{-}Sso7d}$ had a 50% higher efficacy while maintaining the same editing precision in PE3 ($P < 0.0001$; Extended Data Fig. 3e). iPE_{K918N} in Exo-PE was as effective as PEmax in PE3 ($P = 0.1620$), but with higher editing precision ($P = 0.0019$).

Benchmarking of Exo-PE against PE2

After extensive optimization of the prime editor complex using the eTLR reporter, we derived an optimal configuration (Fig. 4a) and validated its performance with the Exo-PE strategy against standard PE strategies at established reference sites in the HEK293T genome[16] (Figs. 4–6).

We hypothesized that Exo-PE would be particularly advantageous for challenging larger insertions and therefore selected a 30-base pair (bp) stretch encoding a Flag-tag and a 54-bp flippase recognition target (FRT) site as the insertions. Editing efficacy and precision were determined from amplicon sequencing data, with efficacy given as the total percentage of correct edits and precision calculated as the percentage of correct edits versus all edits.

Please note that the *HEK3* locus in HEK293T contains a monoallelic SNP 9 bp downstream of the *HEK3* editing site in the flap incorporation area. For the *VEGFA* locus, we had constructed a similar case in which complete PE introduced an additional substitution 5 bp downstream of the insertion site (Fig. 4b). Both outcomes (insertion with and without the additional substitution) were registered separately as correct edits (Figs. 4c,d and 5, blue and light blue bars) and subsequently aggregated.

We first compared Exo-PE with PE2 (Fig. 4c), which is the most direct benchmark as it also requires only a single pegRNA and no additional nicking sgRNA (required for PE3) or second pegRNA (used in paired PE). For editing efficacy, a three-way ANOVA reported significant effects for PE strategy ($F = 1{,}538.637$, $P < 0.0001$), locus ($F = 265.677$, $P < 0.0001$), and iPE-N/C ($F = 14.545$, $P = 0.0005$), as well as an interaction for locus and PE strategy ($F = 193.464$, $P < 0.0001$). Since the factor iPE-N/C and its interactions explained less than 2% of the variance, we averaged over this factor to conduct Bonferroni MCT for Exo-PE versus PE2 at each locus, showing that Exo-PE significantly increased editing efficacy for the 30-bp Flag insertion over PE2 in all tested loci except *RNF2* (Fig. 4c and see full statistical results in Supplementary Table 1), corresponding to a mean increase of 14.4 percentage points averaged across loci and iPE-N/C.

For editing precision, an analogous analysis revealed that Exo-PE over PE2 achieved an at least equal precision for all loci except *RUNX1* (Bonferroni MCT from a three-way ANOVA with effects for PE strategy ($F = 32.712$, $P < 0.0001$), locus ($F = 5.182$, $P = 0.0087$) and iPE-N/C ($F = 6.665$, $P = 0.0164$; Fig. 4c).

We also tested Exo-PE against PE2 for the insertion of a 54-bp sequence containing an FRT site (Fig. 4d) and found an average increase (over loci and iPE-N/C) in editing efficacy of 9.96 percentage points (three-way ANOVA with effects for PE strategy ($F = 511.47$, $P < 0.0001$), locus ($F = 288.548$, $P < 0.0001$), iPE-N/C ($F = 12.5$, $P = 0.0017$) and a PE strategy/locus interaction ($F = 156.780$, $P < 0.0001$)). The editing efficacies for FRT and Flag insertion were correlated for Exo-PE and lower for FRT (Fig. 4e).

We then repeated the experiment with identical conditions in HeLa cells and again found an improved, or on par, editing efficacy of Exo-PE compared with PE2 for Flag and FRT insertions for all loci (three-way ANOVA with Bonferroni MCT; Extended Data Fig. 4a,b). The editing efficacy from HeLa cells was correlated to that in HEK293T cells, but was generally lower, causing higher variance for FRT insertion data (Extended Data Fig. 4c).

We also examined off-target activity of Exo-PE compared with PE2 for four known Cas9 off-targets of the *HEK3* locus[19]. Although no off-target activity was detected for most loci, the most commonly affected *HEK3* off-target site ('OT1'), with a perfectly matching PBS of the pegRNA, displayed an increased number of editing events when Exo-PE was used (Supplementary Table 2).

Comparison of Exo-PE with PE4

We also assessed the effect of MMR inhibition via the coexpression of dominant-negative MLH1 (MLH1dn), which was recently shown to improve PE2 efficacy and precision for small edits without secondary nicking sgRNAs.

Similarly, Exo-PE displayed improved editing efficacy compared with PE4 (mean difference across loci and iPE-N/C was 12.55 percentage points, from a three-way ANOVA identifying main effects for PE strategy ($F = 438.402$, $P < 0.0001$), locus ($F = 499.14$, $P < 0.0001$), iPE-N/C ($F = 17.035$, $P < 0.0001$) and an interaction of PE strategy/locus ($F = 49.917$, $P < 0.0001$); Fig. 5).

Exo-PE4 (a combination of Exo-PE and PE4) did not seem to provide an additional increase in efficacy over Exo-PE. The effect of iPE-C/N, while significant for efficacy, was small and accounted for only 0.42% of the total variation.

Fig. 4 | Editing efficacy and precision of Exo-PE benchmarked against PE2 for two different insertions in multiple loci. a, Schematic of the final prime editor system for the Exo-PE strategy, composed of an iPE combined with an engineered pegRNA bearing a PP7 aptamer to recruit a T5 phage 5′–3′-DNA-exonuclease C-terminally fused to PCP to facilitate the integration of the de novo synthesized 3′ flap carrying the desired edit. **b**, HEK293T contains a heterozygous SNP 9 bp downstream of the insertion site in the *HEK3* locus. For *VEGFA*, an additional substitution of 5 bp downstream of the insertion site was also included in the pegRNA design. Both SNP and substitution increase the effective insertion size while narrowing the extent of the homology region of the pegRNA. **c**,**d**, Editing efficacy (correct edits) and precision were determined for two insertion types, Flag (**c**) and FRT (**d**), for iPE-N (N) and iPE-C (C) with either the PE2 or the Exo-PE editing strategy in HEK293T cells by amplicon sequencing. Precision was calculated as the proportion of correctly edited reads within all altered (nonwild-type) reads. Correct editing outcomes merely lacking the additional substitution as shown in **b** were registered separately as correct edits (light blue). Selected results of Bonferroni MCT averaged over iPE-N/C after three-way ANOVA (locus, PE strategy, iPE-N/C) for editing efficacy (results reported in the text) are indicated by asterisks; NS $P > 0.05$, $^{*}P < 0.05$, $^{****}P < 0.0001$. Bars, mean ± s.d. ($n = 3$ biological replicates). **e**, Replotting of the editing efficacies shown in **c** and **d** for FRT against Flag insertions for the loci *DNMT1*, *RNF2* and *VEGFA*. A linear regression is shown for Exo-PE (Pearson $r = 0.9244$, $P = 0.0084$) with 0.95 confidence bands shown in dashed lines. See Supplementary Table 1 for complete statistical results.

https://doi.org/10.1038/s41592-023-02162-w

Again, Exo-PE exhibited a similar editing precision to that of PE2/PE4, with overall levels at ~90% for all loci except *RUNX1* (Fig. 5). Detailed analysis of *RUNX1* editing outcomes revealed a propensity for a specific thymidine insertion in all conditions, as well as a (partial) duplication of the pegRNA homology region at the insertion site only in Exo-PE conditions (Extended Data Fig. 5). The duplication effect also occurred occasionally at other loci, but for both Exo-PE and PE2 and at very low frequencies (<0.2%). In this context, we also evaluated cell viability and proliferation and found a slight reduction of the bioluminescent signal in a commercial assay for Exo-PE and PE4 at times, indicating that both editing strategies can lead to a slight reduction of the proliferation rate during transient expression (Extended Data Fig. 6).

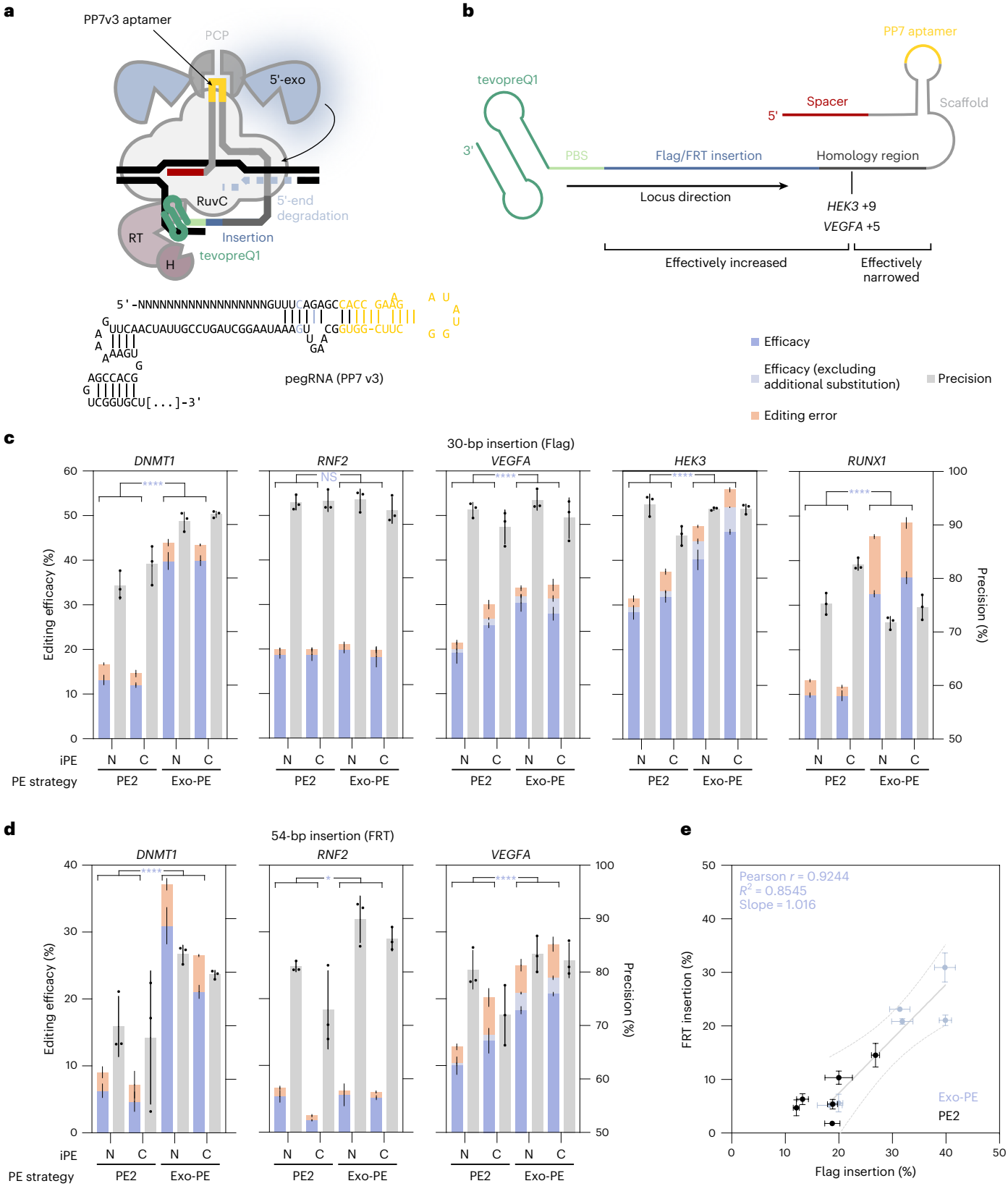

https://doi.org/10.1038/s41592-023-02162-w

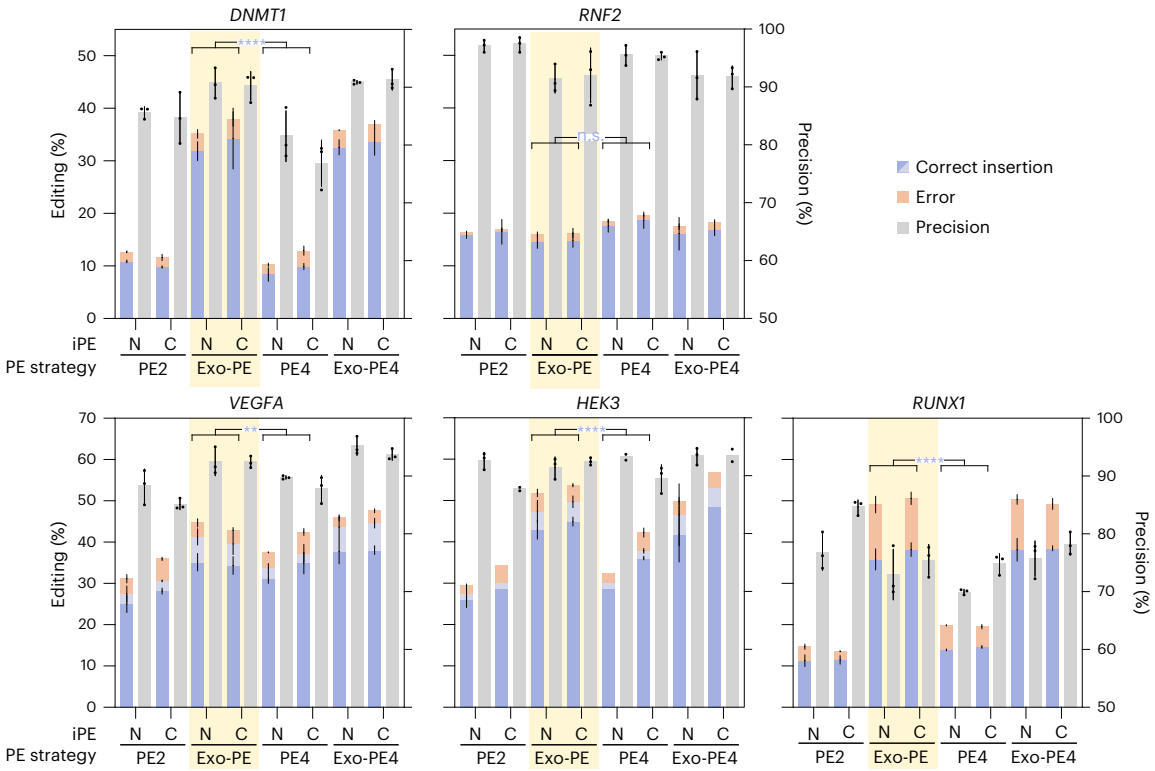

Fig. 5 | Benchmarking of the Exo-PE strategy for 30-bp insertions against PE4. Editing efficacy (correct edits) and precision (correct edits divided by all altered (nonwild-type) reads) were determined from amplicon sequencing. PE4 refers to PE2 + MLH1dn to inhibit MMR, Exo-PE4 refers to Exo-PE + MLH1dn. Each strategy was evaluated using both iPE-N and iPE-C. HEK293T contains a heterozygous SNP 9 bp downstream of the insertion site in the *HEK3* locus; for *VEGFA*, an additional substitution 5 bp downstream of the insertion site was included in the pegRNA design (Fig. 4b). Selected results of Bonferroni MCT averaged over iPE-N/C (after three-way ANOVA with results reported in the text) are indicated by asterisks; NS $P > 0.05$, $^{**}P < 0.01$, $^{***}P < 0.001$, $^{****}P < 0.0001$. Bars, mean ± s.d. ($n = 3$ biological replicates, except for *HEK3* C-PE2, N-PE4 and C-Exo-PE4 where $n = 2$).

In addition, we examined the performance of Exo-PE at genomic sites associated with diseases such as prion disease[20] and *CDKL5* deficiency disorder[21] for both the 30-bp insertion (Extended Data Fig. 7a) and therapeutically relevant substitutions (Extended Data Fig. 7b). Compared to PE2, Exo-PE again increased efficacy for insertions (three-way ANOVA with Bonferroni MCT) but not for substitutions, consistent with previous observations for the respective edit types at other loci.

Exo-PE for protein tagging via fluorescence complementation

We next sought to use Exo-PE for a practical application in biomedical research, inspired by a large-scale in-situ protein tagging study[22]. We designed pegRNAs to extend the endogenous locus with sequences coding for the 11 amino acids of a split fluorescent protein, namely monomeric mNeonGreen2 (mNG2)[23]. A HEK293T cell line containing the stably integrated split-mNG2(1–10) was subjected to PE for inserting the missing mNG2(11) peptide at the N or C terminus of functionally expressed genes. Fluorescence complementation consequently indicates the successful insertion of the peptide without compromising the expression of the tagged gene (Extended Data Fig. 8a). We observed a main effect of Exo-PE across the first panel of loci (two-way ANOVA, Exo-PE/PE2, locus; $F(1, 28) = 40.35$, $P < 0.0001$; Extended Data Fig. 8b). We also targeted two additional loci (*GAPDH* and *ENO1*-N, Extended Data Fig. 8c) and again found that Exo-PE had a greater editing efficacy than PE2 ($P = 0.0349$ for both loci, Bonferroni MCT), while PE3 also showed substantial efficacy.

Comparison of Exo-PE with PE3 and PE5

We then extended the comparison with PE3 and PE5, both of which require a secondary nick, for the 30-bp Flag insertion in an additional set of loci. We again selected the reference loci tested in ref. 2, so that we could use the identical nicking sites (Fig. 6).

As before, Exo-PE demonstrated superior editing efficacy for the insertions across loci, with precision also being similar or better in all cases (Bonferroni MCT based on a three-way ANOVA with significant main effects for PE strategy ($F = 1135.566$, $P < 0.0001$), locus ($F = 262.932$, $P < 0.0001$) and the interaction of both factors ($F = 39.102$, $P < 0.0001$); Fig. 6). However, both PE3 and PE5 showed a substantial reduction in mean editing precision across loci and iPE-N/iPE-C by 66.4 and 63.2 percentage points, respectively, compared with Exo-PE. Closer investigation revealed that both strategies suffered from a large proportion of indels occurring between the two nicking sites, even when the insertion was incorporated successfully (Extended Data Fig. 9).

When we subsequently evaluated Exo-PE performance on single-base substitutions at the same endogenous sites, no improvements in efficacy were found over PE2, while PE4 resulted in a mean increase across loci and iPE-N/C of 5.485 percentage points (based on a three-way ANOVA identifying main effects for PE strategy ($F = 34.091$, $P < 0.0001$), locus ($F = 499.217$, $P < 0.0001$), iPE-N/C ($F = 11.273$, $P = 0.001$), and an interaction of PE strategy/locus ($F = 31.973$, $P < 0.0001$); Extended Data Figs. 7b and 10a,b). The average precision of PE3 and PE5 across loci and iPE-N/C was much higher (53.4% and 60.5%) on substitution-type edits (Extended Data Fig. 10a) than for mid-size insertions (5.3% and 8.7%), respectively (Fig. 6).

In summary, we found that Exo-PE to exhibited a significantly higher, or at least equal editing efficacy against PE2, PE4 (PE2 with MMR inhibition), and dual-nick strategy without (PE3) and with MMR inhibition (PE5) in each of the independent benchmarking experiments (Figs. 4–6 and see full statistical results in Supplementary Table 1).

https://doi.org/10.1038/s41592-023-02162-w

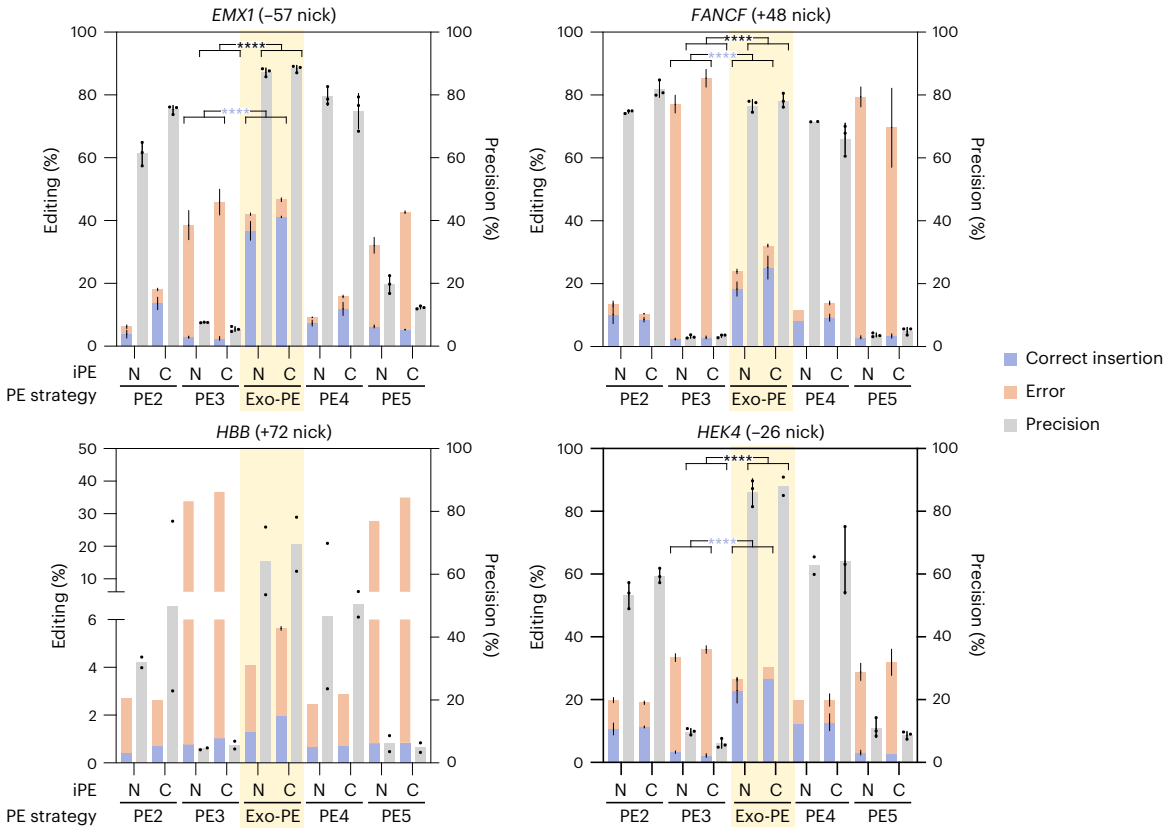

Fig. 6 | Comparison of the Exo-PE strategy for 30-bp insertions with dual-nick strategies. Exo-PE was benchmarked against the dual-nick strategies PE3 and PE5 (PE3 + MLH1dn) for 30-bp insertions on an additional set of endogenous loci. Nick positions of ngRNAs for PE3/PE5 strategies are indicated in parentheses. Selected results of Bonferroni MCT averaged over iPE-N/C (from three-way ANOVA with results reported in the text) are indicated by asterisks; ****$P < 0.0001$. Bars, mean ± s.d. ($n = 3$, biological replicates, except for *FANCF* (N-PE4), *HEK4* (C-Exo-PE), *HEK4* (N-PE4) and *HBB* (all conditions) where $n = 2$).

Over all 11 loci in which Exo-PE was compared directly against PE2 for Flag insertions in HEK293T cells, Exo-PE showed a significant increase in efficacy in 9 out of 11 loci with an average difference across loci and iPE-N/C of 14.2 percentage points (Supplementary Fig. 1) based on a three-way ANOVA with factors PE strategy ($F = 1{,}079.564$, $P < 0.0001$), locus ($F = 167.58$, $P < 0.0001$) and iPE-N/C ($F = 20.203$, $P < 0.0001$), with the latter factor accounting for only 0.59% of the total variation. We also observed an interaction of Locus/Strategy ($F = 46.9$, $P < 0.0001$, 13.69% of total variation) driven by the *RNF2* locus, for which Exo-PE did not show an increased efficacy (full statistical results in Supplementary Table 1). Except for the *RUNX1* locus (Extended Data Fig. 5), Exo-PE displayed similar or slightly increased precision at all nine loci where it significantly increased efficacy.

Discussion

We demonstrated that we could iteratively achieve substantial improvements in the PE machinery using an improved reporter system (eTLR) which, in contrast to previous versions[4], indicates all mutagenic indel events. eTLR allowed us to rapidly identify an improved PE with optimized codons and linkers, including a potent superNLS (iPE-C/N), which, combined with engineered pegRNAs protected by (t)evopreQ1 (ref. 16), offered the best alternative to PEmax.

We then tackled the flap competition as a central bottleneck for PE efficacy, especially for larger insertions, by recruiting a 5′–3′ exonuclease to iPE via aptamer-mediated recruitment to create space for the invasion of the reverse-transcribed 3′ flap. Exo-PE was then validated on several endogenous loci and showed a substantial improvement in editing efficacy for 30–57-bp insertions (Flag, FRT sites, split C-mNeonGreen) in several cell lines when benchmarked against the standard techniques PE2, PE3, PE4 and PE5. Exo-PE improved editing efficacy without compromising editing precision compared with PE2 and PE4. Although iPE-C displayed a slightly better performance than iPE-N for many loci, it may be beneficial to test both variants for a specific target locus.

The preserved editing precision of Exo-PE is particularly valuable when contrasted with the dual-nicking strategy PE3, which displayed substantially increased indel rates for the insertion-type edits. An increased indel frequency was reported previously for larger insertions[24], while smaller substitutions and insertions generated with PE3 resulted in only a minor increase in indel frequency in most cases[1]. In general, single-nick techniques such as PE2/PE4 and base editing hold a key advantage over DSB-induced HDR-dependent CRISPR editing techniques in that staggered DSBs can be avoided. While Exo-PE inherits this safety feature from PE2 and thus maintains high editing precision, it is conceivable that two nicking sites used in PE3 (and paired PE strategies) could generate a staggered DSB break leading to increased editing errors. Furthermore, nicking at the secondary site in PE3 is likely to occur even after successful editing as long as the PE machinery is expressed, which may (or needs to) be the case for a prolonged period of time, for example, after virus-mediated gene delivery. Nonetheless, if increased editing efficacy is the primary objective in a given experimental setting where indels can be tolerated, PE3 could be highly effective also for longer insertions.

It is conceivable that the flap competition contributes to an apparent specificity for on-target versus off-target effects. Since this competition is mitigated by Exo-PE, it might explain the increased editing versus PE2 on the main OT1 for the *HEK3* locus, for which the PBS of the reference pegRNA[24] provides a perfect match. It may thus be important when using Exo-PE to ensure that the PBS does not perfectly match

other sites to maintain the specificity benefit of each hybridization event before flap binding[24].

MMR inhibition via PE4/PE5 did not provide any benefit when inserting large sequences such as a Flag-tag, most likely as a consequence of ≥14-bp insertions not being recognized by the MMR pathway, a PE-inhibiting process[22,25]. We also observed that either exonuclease or MLHdn expression could transiently lead to a mild reduction in proliferation. While this did not affect the quality of our experiments, one could reduce the amount of exonuclease in situations where viability is a major concern, or even invest in a split-exonuclease recruitment approach.

In contrast to the improvements in editing efficacy for insertions, we did not observe a similar benefit of Exo-PE for short substitutions, although it occasionally outperformed PE4 at certain loci. In our experiments, we also did not find PE4 to be substantially more effective than PE2, as reported in the initial publication[2]. This may be due to differences in the pegRNA/nicking sgRNA scaffold compared to the literature[26,27] and the lower amount of MLH1dn plasmid (~33% less) we used to keep the concentration of other genetic components constant.

With PE-mediated insertions gaining increasing interest[25], Exo-PE thus provides a complementary strategy to PE4, with Exo-PE showing superior performance for larger edits and PE4 for smaller edits. Exo-PE may therefore be particularly useful for applications in basic research or biological engineering, where the addition of epitopes, affinity handles or degradation motifs may be of interest. During the revision of this manuscript, a study in plants showed an improvement in the efficacy of PE2 by adding a T5 exonuclease to the PE editor, but only when fused to the N terminus of nCas9 and not when they attempted to recruit it via a tandem insertion of MS2/F6 aptamers[28].

For larger insertions, we showed that the editing efficacy of Exo-PE can approach or even exceed that of PE3, while maintaining the superior precision of PE2. The Exo-PE approach may thus be attractive in cases where PE3 or paired PE are not feasible, for instance, if a high editing precision is desired, in the absence of a second suitable proximal PAM or in other organisms in which PE3 did not lead to enhanced editing efficacy[29]. The lack of a second nick also considerably reduces the combinatorial complexities for pegRNA optimization.

In the future, it will be interesting to directly benchmark Exo-PE against the many different variants of paired PE strategies, which have been shown to enable substantially longer insertions than Exo-PE, although these methods necessitate a careful optimization of the paired pegRNAs for specific loci[3]. Exo-PE may also catalyze those paired pegRNA approaches by degrading the endogenous 5′-intermediates, but active flap degradation could also abolish the target site for the paired pegRNA. As shown by the increased efficacy for inserting the FRT site, Exo-PE may also be beneficial for combining PE with recombinase-dependent insertions of longer DNA stretches[30].

Given the complex orchestration of multiple processes required for PE, Exo-PE adds an effective functionality to the PE machinery, which can further advanc the versatility of this powerful gene-editing technology.

Online content

Any methods, additional references, Nature Portfolio reporting summaries, source data, extended data, supplementary information, acknowledgements, peer review information; details of author contributions and competing interests; and statements of data and code availability are available at https://doi.org/10.1038/s41592-023-02162-w.

References

1. Anzalone, A. V. et al. Search-and-replace genome editing without double-strand breaks or donor DNA. *Nature* **576**, 149–157 (2019).
2. Chen, P. J. et al. Enhanced prime editing systems by manipulating cellular determinants of editing outcomes. *Cell* **184**, 5635–5652. e29 (2021).
3. Choi, J. et al. Precise genomic deletions using paired prime editing. *Nat. Biotechnol.* **40**, 218–226 (2022).
4. Certo, M. T. et al. Tracking genome engineering outcome at individual DNA breakpoints. *Nat. Methods* **8**, 671–676 (2011).
5. Yeh, J. T.-H., Nam, K., Yeh, J. T.-H. & Perrimon, N. eUnaG: a new ligand-inducible fluorescent reporter to detect drug transporter activity in live cells. *Sci. Rep.* **7**, 41619 (2017).
6. Hebsgaard, S. M. et al. Splice site prediction in *Arabidopsis thaliana* pre-mRNA by combining local and global sequence information. *Nucleic Acids Res.* **24**, 3439–3452 (1996).
7. Spencer, J. M. & Zhang, X. Deep mutational scanning of *S. pyogenes* Cas9 reveals important functional domains. *Sci. Rep.* **7**, 16836 (2017).
8. Garforth, S. J. & Sayers, J. R. Structure-specific DNA binding by bacteriophage T5 5′–>3′ exonuclease. *Nucleic Acids Res.* **25**, 3801–3807 (1997).
9. Garforth, S. J., Ceska, T. A., Suck, D. & Sayers, J. R. Mutagenesis of conserved lysine residues in bacteriophage T5 5′–3′ exonuclease suggests separate mechanisms of endo-and exonucleolytic cleavage. *Proc. Natl Acad. Sci. USA* **96**, 38–43 (1999).
10. Konermann, S. et al. Genome-scale transcriptional activation by an engineered CRISPR–Cas9 complex. *Nature* **517**, 583–588 (2014).
11. Lim, F. & Peabody, D. S. RNA recognition site of PP7 coat protein. *Nucleic Acids Res.* **30**, 4138–4144 (2002).
12. Hand, T. H. et al. Catalytically enhanced Cas9 through directed protein evolution. *CRISPR J.* **4**, 223–232 (2021).
13. Choli, T., Henning, P., Wittmann-Liebold, B. & Reinhardt, R. Isolation, characterization and microsequence analysis of a small basic methylated DNA-binding protein from the Archaebacterium, *Sulfolobus solfataricus*. *Biochim. Biophys. Acta* **950**, 193–203 (1988).
14. Park, S.-J. et al. Targeted mutagenesis in mouse cells and embryos using an enhanced prime editor. *Genome Biol.* **22**, 170 (2021).
15. Dickey, T. H., McKercher, M. A. & Wuttke, D. S. Nonspecific recognition is achieved in Pot1pC through the use of multiple binding modes. *Structure* **21**, 121–132 (2013).
16. Nelson, J. W. et al. Engineered pegRNAs improve prime editing efficiency.*Nat. Biotechnol.* **40**, 402–410 (2022).
17. Gao, Z., Herrera-Carrillo, E. & Berkhout, B. Delineation of the exact transcription termination signal for type 3 polymerase III. *Mol. Ther. Nucleic Acids* **10**, 36–44 (2018).
18. Menezes, M. R., Balzeau, J. & Hagan, J. P. 3′ RNA uridylation in epitranscriptomics, gene regulation, and disease. *Front Mol. Biosci.* **5**, 61 (2018).
19. Tsai, S. Q. et al. GUIDE-seq enables genome-wide profiling of off-target cleavage by CRISPR-Cas nucleases. *Nat. Biotechnol.* **33**, 187–197 (2015).
20. Asante, E. A. et al. A naturally occurring variant of the human prion protein completely prevents prion disease. *Nature* **522**, 478–481 (2015).
21. Olson, H. E. et al. Cyclin-dependent kinase-like 5 deficiency disorder: clinical review. *Pediatr. Neurol.* **97**, 18–25 (2019).
22. Cho, N. H. et al. OpenCell: endogenous tagging for the cartography of human cellular organization. *Science* **375**, eabi6983 (2022).
23. Feng, S. et al. Improved split fluorescent proteins for endogenous protein labeling. *Nat. Commun.* **8**, 370 (2017).
24. Anzalone, A. V. et al. Programmable deletion, replacement, integration and inversion of large DNA sequences with twin prime editing.*Nat. Biotechnol.* **40**, 731–740 (2022).
25. Koeppel, J. et al. Prediction of prime editing insertion efficiencies using sequence features and DNA repair determinants.*Nat. Biotechnol.* **41**, 1446–1456 (2023).

26. Chen, B. et al. Dynamic imaging of genomic loci in living human cells by an optimized CRISPR/Cas system. *Cell* **155**, 1479–1491 (2013).
27. Dang, Y. et al. Optimizing sgRNA structure to improve CRISPR–Cas9 knockout efficiency. *Genome Biol*. **16**, 280 (2015).
28. Liang, Z., Wu, Y., Guo, Y. & Wei, S. Addition of the T5 exonuclease increases the prime editing efficiency in plants.*J. Genet. Genomics* **50**, 582–588 (2023).
29. Scholefield, J. & Harrison, P. T. Prime editing—an update on the field. *Gene Ther.* **28**, 396–401 (2021).
30. Yarnall, M. T. N. et al. Drag-and-drop genome insertion of large sequences without double-strand DNA cleavage using CRISPR-directed integrases.*Nat. Biotechnol.* **41**, 500–512 (2023).

Methods

Molecular cloning

Genetic constructs. All pegRNAs used in this study (unless indicated) contained a modified pegRNA scaffold containing modifications from ref. 26 and ref. 27, to improve expression yield and a 3′-tRNA (M1–7 tRNA[31]) or an evopreQ1 (ref. 2) motif upstream of the 6× T-DNA-dependent RNA polymerase III termination signal. All pegRNA sequences used in this study are provided in Supplementary Table 3. All amino acid sequences of coding components of iPE can also be found in Supplementary Table 3, as well as corresponding codon-optimized nucleotide sequences including the RT domain in which we removed a potential splice site. The expression constructs for iPE-N (214734), iPE-C (214735), PCP-Exo (214736), and the AAVS1-eTLR donor construct (214737) have been provided to Addgene.

Polymerase chain reaction. Single-stranded primer deoxyribonucleotides (Integrated DNA Technologies) were resolubilized (100 µM) in nuclease-free water. A PCR reaction with plasmid and genomic DNA templates was performed with Platinum SuperFi II PCR Master Mix (Thermo Fisher Scientific) according to the manufacturer's protocol. PCR reactions were purified by DNA agarose gel electrophoresis and subsequent DNA extraction using Monarch DNA Gel Extraction Kit (New England Biolabs (NEB)).

DNA digestion with restriction enzymes. DNA products were digested with restriction enzymes according to the manufacturer's protocol (NEB) in 40 µl with 2–3 µg of plasmid DNA. Afterward, fragments were gel-purified by DNA agarose gel electrophoresis, and DNA was extracted using Monarch DNA Gel Extraction Kit (NEB).

Molecular cloning. Concentration of purified DNA was measured using a spectrophotometer (NanoDrop 1000, Thermo Fisher Scientific). For ligations with T4 DNA ligase (Quick Ligation Kit, NEB), 50–100 ng backbone DNA (DNA fragment containing the DNA replication origin) was used in 20-µl volume, with molar 1:1–3 backbone:insert ratios, at room temperature for 5–10 min. Gibson assemblies were performed with ~75 ng backbone DNA and a molar 1:1–5 backbone:insert ratios in a 15-µl reaction volume, using NEBuilder HiFi DNA Assembly Master Mix (2×) (NEB) for 15–60 min at 50 °C.

DNA agarose gel electrophoresis. Agarose (Agarose Standard, Carl Roth) gels (1% (m/m)) were prepared in 1× Tris-acetate-EDTA buffer and 1:10,000 SYBR Safe stain (Thermo Fisher Scientific). Gel electrophoresis was carried out for 20–40 min at 120 V. For size determination, the 1-kb Plus DNA Ladder (NEB) was used. DNA samples were mixed before loading with Gel Loading Dye (Purple, 6×) (NEB).

Bacterial strains for molecular cloning. Chemically competent stable *Escherichia coli* cells (NEB) were used to propagate circular plasmid DNA. Carbenicillin (Carl Roth) was used for selection during plasmid amplification at a final concentration of 100 µg ml^{-1}. All bacterial cultures were prepared in Lysogeny Broth (LB) medium and on LB agar plates with carbenicillin (Carl Roth).

Bacterial transformations. Chemical transformation of *E. coli* was performed by mixing 1–5 µl of ligation or Gibson reaction with 50 µl thawed, chemically competent stable *E. coli* (NEB) and incubating on ice for 5–30 min. Cells were subsequently heat-shocked at 42 °C for 30 s, followed by a 5 min incubation on ice, and, finally, 950 µl SOC-medium (NEB) was added to the cell suspension. After outgrowth for 10–30 min at 37 °C, cells were plated on agar plates containing appropriate antibiotics, followed by overnight incubation at 37 °C or 48 h incubation at room temperature.

Plasmid purification and Sanger sequencing. *E. coli* colonies with correct potential constructs were inoculated from agar plates in 2 ml LB medium at 37 °C with the respective antibiotics and incubated for at least 6 h or overnight. Plasmid DNA was extracted with QIAprep Plasmid MiniSpin (Qiagen) according to the manufacturer's protocol and sent for Sanger sequencing (GENEWIZ, Azenta Life Sciences). Sanger-sequencing-validated clones were inoculated into 100 ml LB medium containing the respective antibiotic selection agent and incubated overnight at 37 °C. Plasmid DNA was extracted using the Plasmid Maxi Kit (Qiagen).

Genomic DNA isolation. At 72 h after transfection in 96-well format, genomic DNA was isolated with the Quick-DNA 96 Kit (Zymo Research) according to the manufacturer's protocol, with an elution volume of 30 µl.

Amplicon PCR and purification. PCR was performed as described above using ~50 ng of gDNA and appropriate primers for each target. Amplicon lengths were designed to approach 250 bp for sequencing. PCR purification was performed using the DNA Clean and Concentrator-5 Kit (Zymo Research) according to the manufacturer's protocol, with an elution volume of 30 µl. All primer sequences are provided in Supplementary Table 3.

Amplicon sequencing and analysis. Following an initial PCR on genomic DNA, a second outer PCR using barcoded primers was performed. PCR products of each experiment were purified as described above, normalized and combined into a single tube. The mixture was gel-purified, normalized to 20 ng µl^{-1}, and submitted for Amp-EZ sequencing (Azenta). The resulting fastq files containing paired reads were analyzed with Geneious via barcode separation and CRISPR editing analysis within the entire range covered by reads or at least the full sequence area between the genomic primer-binding sites.

Mammalian cell culture

Cell lines and maintenance. HEK293T (Sigma-Aldrich, catalog no. ECACC 12022001), HEK293 eTLR (originating from HEK293, catalog no. ECACC 85120602) and HeLa cells (catalog no. ECACC 93021013) were cultivated at 37 °C and 5% CO_2 in an H_2O-saturated atmosphere in Gibco Advanced DMEM (Thermo Fisher Scientific) with 10% FBS (Gibco, Thermo Fisher Scientific), GlutaMAX (Gibco, Thermo Fisher Scientific) and 100 µg ml^{-1} penicillin-streptomycin (Gibco, Thermo Fisher Scientific). Cells were passaged twice a week at 90% confluency by aspirating the medium, washing with DPBS (Gibco, Thermo Fisher Scientific), and detaching the cells with 2–3 ml of an Accutase solution (Gibco, Thermo Fisher Scientific) for 5–10 min at room temperature until a visible detachment of the cells was observed. Accutase was subsequently inactivated in 7.5 ml FBS-containing medium. Cells were then transferred into a new flask at an appropriate density for maintenance or were counted and plated in multiwell plates for subsequent plasmid transfection.

Generation of eTLR reporter line. The HEK293 eTLR cell line, which reports all three frames after an NHEJ/MMEJ-mediated indel event, was created by cloning the reporter coding sequencer between a CAG promoter and a bovine growth hormone (bGH) polyadenylation (pA) signal. This CAG_eTLR_bGH-pA construct was again cloned into a vector containing homology arms for the first intron of the PPP1R12C gene (alias AAVS1) with 0.8 kbp for each homology arm. In addition, for selection, a puromycin N-acetyltransferase (PuroR) gene trap was created by inserting a splice acceptor, the coding sequence for puromycin N-acetyltransferase and a bGH-pA between the CAG promoter and the 5′-homology arm. This donor construct was provided to Addgene. To create a HEK293 cell line containing the eTLR reporter, HEK293 cells were cotransfected with this donor, a Cas9-NLS expression plasmid

and a gRNA plasmid (spacer sequence GGGGCCACTAGGGACAGGAT) 24 h postseeding in a six-well plate (600,000 cells per 3 ml per well in a six-well plate) following the manufacturer's protocol (X-tremeGENE HP, Roche). At 48 h after transfection, cells were selected for 2 weeks with 0.5 µg ml^{-1} puromycin dihydrochloride (Gibco, Thermo Fisher Scientific) in the presence of 0.5 µM AZD7648 (MedChemExpress, catalog no. HY-111783) (a DNA-PKcs inhibitor[32]) and a CAG-promoter-driven i53 (a 53BP1 inhibitor) to inhibit NHEJ and shift the DNA repair towards HDR[33,34]. The surviving polyclonal population carrying the eTLR system stably in the AAVS1 locus was monoclonalized using limiting dilution in 96-well plates. Clones were tested for the number of eTLR copies by transfecting the clones in a 48-well with a CRISPR–Cas9 plasmid against the eTLR system and a donor to repair the C-terminally truncated mScarlet-I. Clones that showed mutually exclusive fluorescence (either red or green, but not green and red) contained one copy of the eTLR reporter. Clones that also showed green and red fluorescence in parallel had two copies of the eTLR system. We chose a clone containing two copies of the eTLR system to mimic the diploid nature of most autosomal genes.

Plasmid transfection into mammalian cells. Cells were transfected with X-tremeGENE HP (Roche) or jetOPTIMUS (Polyplus Transfection) according to the manufacturer's protocol. Total DNA amounts were kept constant in all transient experiments to yield reproducible complex formation and comparable results. In 96-well plate experiments, a total of 100 ng, 300 ng and 2.4 µg in total per well was used for 96-well, 48-well and 6-well plate transfections, respectively. The ratios of plasmid DNA were 1:1 for pegRNAs to prime editors and 2:1 for pegRNAs to auxiliary components like exonucleases, nicking gRNAs and MLHdn. Cells were plated 1 day before transfection (25,000 cells per well in 100 µl for 96-well plates; 75,000 cells per well in 500 µl for 48-well plates; 600,000 cells per well in 3 ml for 6-well plates). At 24 h after transfection, 100 µl fresh medium was added per well in a 96-well transfection and at 48 h after transfection 100 µl medium per well was removed and replaced with fresh medium in 96-well transfections.

Small molecule manipulation of NHEJ. For modulation of NHEJ in the HEK293 eTLR line with NU7441 (MedChemExpress) or KU0060648 (alias KU-57788, MedChemExpress), the compounds were added to the cells 24 h after transfection. Control cells received the same volume of DMSO. HEK293 eTLR cells were transfected in a 48-well plate with a plasmid harboring the indicated gene-editing constructs to analyze repair events. At 72 h after transfection, cells were detached with Accutase, pelleted (200 relative centrifugal force, 5 min), and resuspended in ice-cold 0.4% formalin for 10 min. Fixed cells were pelleted again (200 relative centrifugal force, 5 min) and resuspended in ice-cold 200 µl DPBS for FACS analysis.

Viability assay. The viability of transfected cells was assessed 72 h after transfection before gDNA isolation using the RealTime-Glo MT Cell Viability Assay (Promega) according to the manufacturer's instructions (endpoint method, sample volume 20 µl, incubation time 60 min). Luminescence was measured on the Centro LB 960 plate reader (Berthold Technologies) with 0.5-s acquisition time.

FACS analysis. FACS analysis was performed on the BD FACSaria II system (controlled with the BD FACSDiva Software (v.6.1.3, BD Biosciences)). In brief, the main population of cells was gated first according to their FSC-A and SSC-A. Second, single cells were gated using FSC-A and FSC-W. The final gate (red and green fluorescence) was used to determine the number of undergoing mutEJ or PE. The events in the red/green/red-green gate were normalized to the number of cells in the single-cell gate. See Supplementary Information for a depiction of the FACS gating strategy.

Statistics and reproducibility

Statistics were calculated as specified in each figure using R (ref. 35) (v.4.3.1 with the emmeans package[36] to calculate multiple comparisons and marginal effects) and Prism (v.9, GraphPad). Mean and s.d. were calculated across biological replicates.

For experiments on eTLR, the precision was calculated as the ratio of PE/HDR events over mutEJ events. For next-generation sequencing experiments, precision was calculated as the proportion of correct editing events among all editing events (correct/(correct + error) × 100).

We did not use statistical analysis to determine sample size or to randomize the experiments, nor did we blind the investigators to the allocation of the experiments or their outcomes. Despite those limitations, we made an effort to reduce any biases introduced during the sample preparation by using the use of master mixes and multichannel pipettes.

No data were excluded from the analyses except for some next-generation sequencing experiments (Fig. 5 and 6 and Extended Data Figs. 4, 7 and 10) for which certain replicates had to be excluded from calculating the mean value due to obvious technical errors (no reads). For the HBB locus in Fig. 6, one replicate was lost during sample processing.

The comparison Exo-PE versus PE2 from Fig. 4c was reproduced independently several months later on the identical loci, as shown in Fig. 5. with highly correlated efficacies for both editing strategies (Pearson $r(8) = 0.8646$ and 0.915, $P = 0.0012$ and 0.0002, respectively; Supplementary Fig. 2). Tables of all statistical tests are provided in Supplementary Table 1. While Bonferroni-corrected MCT of the three-way ANOVA was conducted with averaging over the weak factor iPE-N/C, test results from nonaveraged data are also provided in Supplementary Table 1.

Reporting summary

Further information on research design is available in the Nature Portfolio Reporting Summary linked to this article.

Data availability

PDB-ID of shown *Sp*Cas9 structure (Fig. 2b) is https://doi.org/10.2210/pdb6VPC/pdb. The plasmids for iPE-N, iPE-C, PCP-Exo and the AAVS1-eTLR donor construct are available via Addgene. Source data are provided with this paper.

References

31. Bogerd, H. P. et al. A mammalian herpesvirus uses noncanonical expression and processing mechanisms to generate viral microRNAs. *Mol. Cell* **37**, 135–142 (2010).
32. Robert, F., Barbeau, M., Éthier, S., Dostie, J. & Pelletier, J. Pharmacological inhibition of DNA-PK stimulates Cas9-mediated genome editing. *Genome Med.* **7**, 93 (2015).
33. Truong, D.-J. J. et al. Intron-encoded cistronic transcripts for minimally invasive monitoring of coding and non-coding RNAs. *Nat. Cell Biol.* **24**, 1666–1676 (2022).
34. Truong, D.-J. J., Armbrust, N., Geilenkeuser, J. & Westmeyer, G. G. Generation of cell lines for the usage of intron-encoded scarless programmable extranuclear cistronic transcripts (INSPECT). *Protocol Exchange* https://doi.org/10.21203/rs.3.pex-2000/v1 (2023).
35. R Core Team. *R: A Language and Environment for Statistical Computing* (R Foundation for Statistical Computing, 2023).
36. Lenth, R. emmeans: Estimated Marginal Means, aka Least-Squares Means. R package version 1.8.8 (2023).

Acknowledgements

We thank R. Le Gleut and R. Meixner from the Core Facility Statistical Consulting at Helmholtz Munich as well as S. Haug from TUM for statistical consulting. We acknowledge support from the Federal Ministry of Education and Research (BMBF) and the Free State of Bavaria under the Excellence Strategy of the Federal Government

and the Länder through the ONE MUNICH project Munich Multiscale Biofabrication (to J.G. and G.G.W.). G.G.W. acknowledges support from the European Research Council (ERC-CoG 865710), G.G.W. and D.-J.J.T. acknowledge support from the European Innovation Council (EIC Pathfinder 101115574).

Author contributions

D.-J.J.T. conceived the study, designed all constructs, cogenerated all constructs, coconducted all cell and biochemical experiments, coanalyzed all data and generated all figures. J.G., S.V.W., J.C.H.W., N.A., E.M.H.B., T.H.S., A.S. and C.G. cogenerated all constructs, coconducted all cell and biochemical experiments and coanalyzed all data regarding PE. T.P. and M.Ž. coconducted cell and biochemical experiments to initially characterize the eTLR system. J.G. and S.V.W. conducted the editing experiments on endogenous loci and cogenerated the corresponding figures. D.-J.J.T., J.G., S.V.W., N.A. and G.G.W. designed the experiments. J.G, D.-J.J.T., S.V.W. and G.G.W. wrote the manuscript. D.-J.J.T. coordinated the experimental activities. G.G.W. supervised the research.

Funding

Open access funding provided by Helmholtz Zentrum München - Deutsches Forschungszentrum für Gesundheit und Umwelt (GmbH).

Competing interests

The authors declare no competing interests.

Additional information

Extended data is available for this paper at https://doi.org/10.1038/s41592-023-02162-w.

Supplementary information The online version contains supplementary material available at https://doi.org/10.1038/s41592-023-02162-w.

Correspondence and requests for materials should be addressed to Gil Gregor Westmeyer.

Peer review information *Nature Methods* thanks Hui Yang and the other, anonymous, reviewer(s) for their contribution to the peer review of this work. Peer reviewer reports are available. Primary Handling Editor: Madhura Mukhopadhyay, in collaboration with the *Nature Methods* team.

https://doi.org/10.1038/s41592-023-02162-w

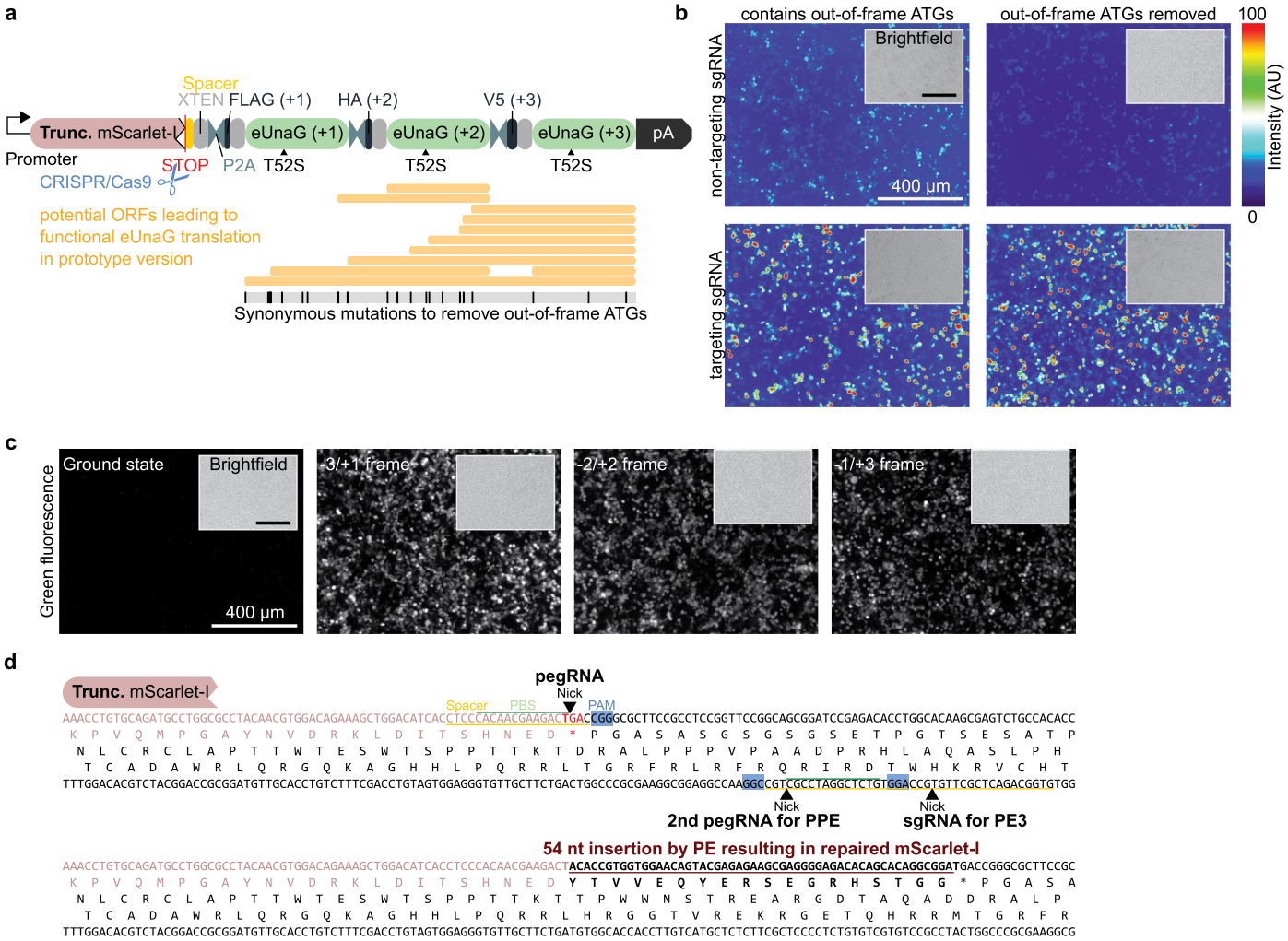

Extended Data Fig. 1 | Optimization and validation of the enhanced Traffic Light Reporter (eTLR). a, Depiction of possible ORFs inducing the functional translation of eUnaG in the prototype version of eTLR and incorporated mutations to remove these out-of-frame ATGs, resulting in the final version of eTLR. A prototype version of the eTLR system, which contains out-of-frame ATGs, was compared with the final version of the eTLR that does not have out-of-frame ATGs, which may otherwise result in the cryptic translation from internal 'noisy' transcription within the reporter's coding sequences. **b**, Representative false-colored epifluorescence images from HEK293T cells two days after transfection with the indicated reporter constructs with non-targeting controls (ntc) or targeting sgRNA against the cotransfected reporter. Results shown were reproduced for a total of two times independently. **c**, Representative epifluorescence images from HEK293T cells, transfected with the eTLR reporter shown in a, but carrying a −1, −2, and −3 nt deletion at the potential nick/DSB site to mimic the three possible eUnaG-T52S reading frames after an error-prone repair. Results shown were reproduced for a total of two times independently. **d**, Depiction of the eTLR reporter editing site for PE analysis with annotated nicking/cuttings sites of the used pegRNAs/sgRNAs in this study.

https://doi.org/10.1038/s41592-023-02162-w

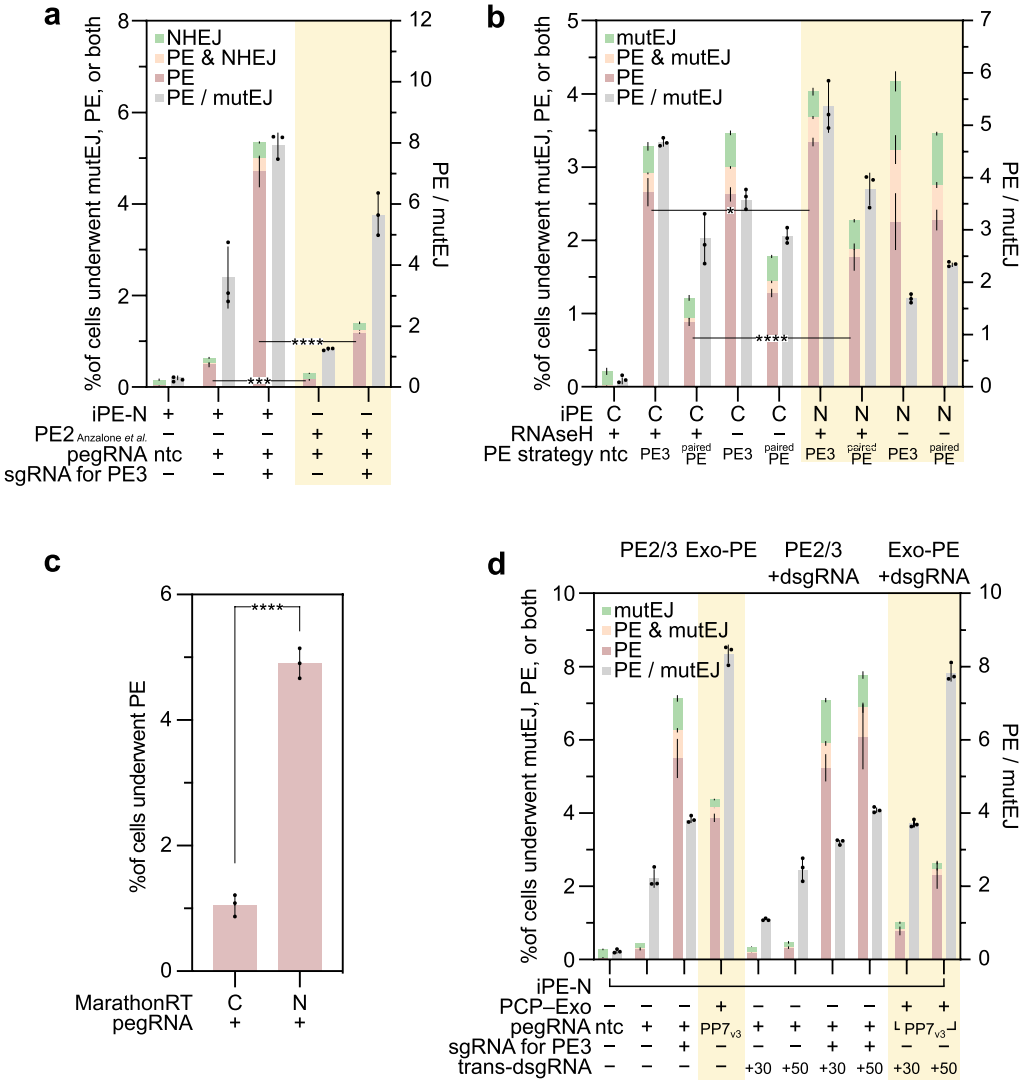

Extended Data Fig. 2 | Screening for additional optimizations of the improved Prime Editor protein (iPE) architecture. a, Comparison of the performance in 'PE2' or 'PE3' of the best RT variant identified in b (N-terminal RT with RNAse H) with the original PE2 construct (see a, top construct) from the original study[2]. Two-tailed unpaired *t*-tests were shown on the fractional PE events; ***$P < 0.001$, ****$P < 0.0001$. Data are shown as the mean ± SD ($n = 3$, biological replicates). **b**, Effects of iPE-C (C) or iPE-N (N) fusions of nucleotide-optimized versions of the hexamutant (x6) Moloney murine leukemia virus (MLV) reverse transcriptase with or without its RNAse H domain, analyzed by eTLR in HEK293. ntc: non-targeting control pegRNA; PE3: 'PE3' strategy. PE, mutEJ, and PE & mutEJ events (colored bars, left y-axis) and PE/mutEJ-ratio (gray bars, right y-axis). Selected results of Bonferroni MCT after one-way ANOVA were shown on the PE events and are indicated by asterisks; *$P < 0.05$, ***$P < 0.001$, ****$P < 0.0001$. Bars represent the mean ± SD ($n = 3$, biological replicates). **c**, Comparison of an N-terminal or C-terminal fusion variant of the MarathonRT reverse transcriptase (group II intron maturase) to Cas9 nickase (nCas9) on prime editing efficacy. In this case, a prototype variant of the reporter shown in Fig. 1 without UnaG was co-transfected instead of genomically integratedused, in which PE recovers repairs the missing C-terminus (54 nt, 18 aa) of a reporter expressing a C-terminally truncated mScarlet-I, resulting in red fluorescence. Result of a two-tailed unpaired *t*-tests is shown for the PE events; ****$P < 0.0001$. Data represent the mean ± SD ($n = 3$, biological replicates). **d**, Effects of an additional proximal binding of a catalytically dead sgRNA (dsgRNAs) on 'PE2', 'PE3', and 'Exo-PE'. Bars represent the mean ± SD ($n = 3$, biological replicates).

https://doi.org/10.1038/s41592-023-02162-w

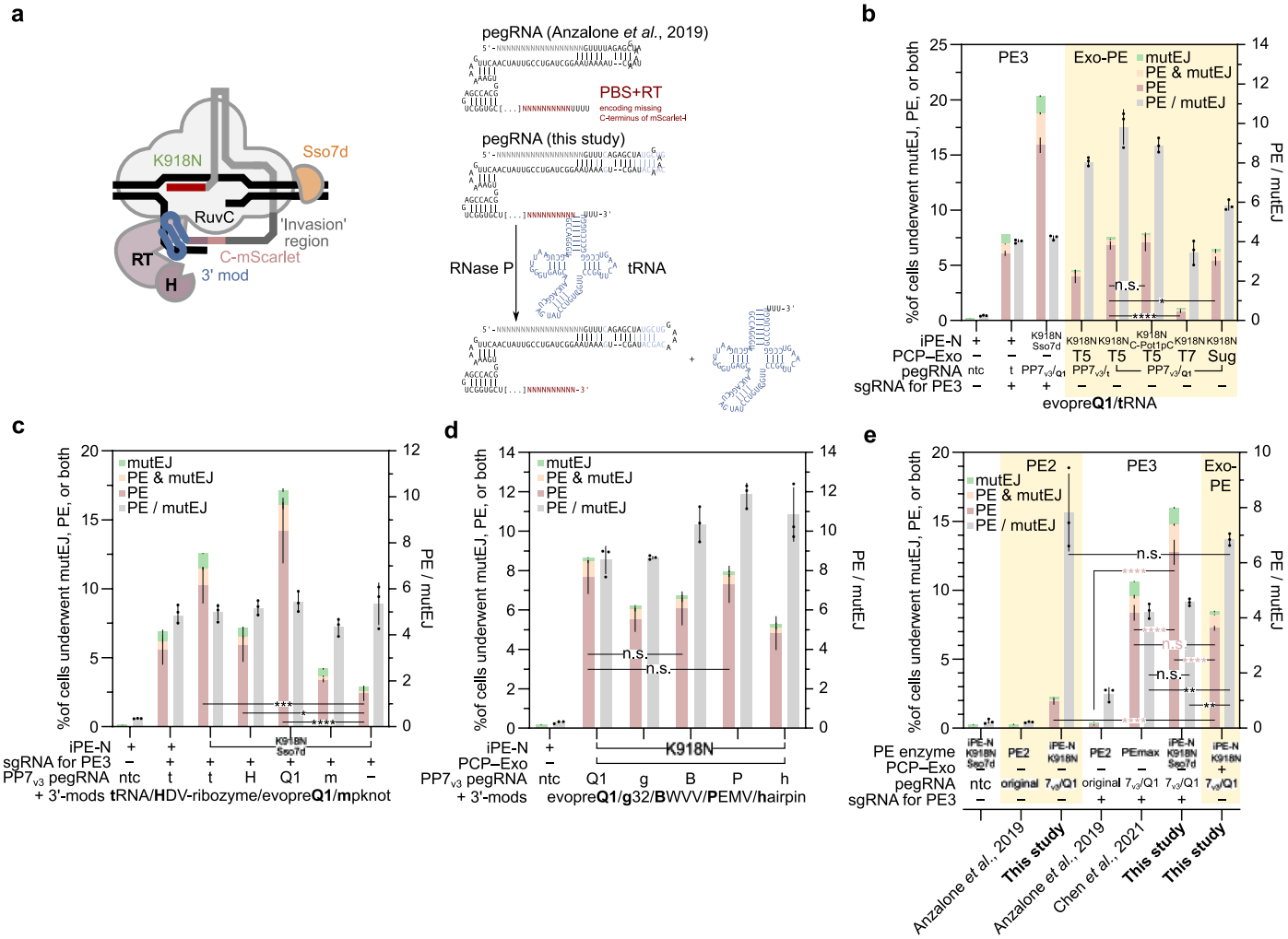

Extended Data Fig. 3 | Screening for additional optimizations of the pegRNA architecture. a, Schematic depiction of various modifications made to the PE architecture such as different 3′ modifications of the pegRNA, mutations to the Cas9 enzyme (K918N), and addition of a dsDNA binding domain (Sso7d). We also compare a detailed depiction of the pegRNA from the original publication to the optimized pegRNA used in this study. **b**, An ssDNA binding domain (Pot1pC) was tested for its ability to enhance 'Exo-PE'. Furthermore, T5-like 5′-3′-DNA-exonuclease from *Klebsiella pneumoniae* Siphophage Sugarland as well as from *Escherichia* phage T7 was tested as an alternative 5′-3′-DNA-exonuclease/flap endonuclease. For all subfigures, additional modifications (K918N and Sso7d) were utilized as described in the respective labels. Selected results of Bonferroni MCT after one-way ANOVA were shown for the fractional PE events, and are indicated by asterisks; n.s. $P > 0.05$, $^{*}P < 0.05$, $^{****}P < 0.0001$. Data are given as the mean ± SD ($n = 3$, biological replicates). **c**, Comparison of different 3′-modifications instead of the 3′-tRNA (t) with $iPE_{K918N\text{-}Sso7d}$ in 'PE3'. Selected results of Bonferroni MCT after one-way ANOVA were shown for the fractional PE events, and are indicated by asterisks; $^{*}P < 0.05$, $^{***}P < 0.001$, $^{****}P < 0.0001$. Bars represent the mean ± SD ($n = 3$, biological replicates). **d**, Comparison of additional 3′- secondary or tertiary motifs for 3′-stabilization to increase Exo-PE efficacy. Different secondary or tertiary RNA structures were tested for their ability to enhance Exo-PE:, M1-7 tRNA, evopreQ1 pseudoknot, g32 pseudoknot, BWYV-FL1 pseudoknot, PEMV pseudoknot, and a simple RNA stem-loop (hairpin). Selected results of Bonferroni MCT after one-way ANOVA were shown for the fractional PE events; n.s. $P > 0.05$. Bars represent the mean ± SD ($n = 3$, biological replicates). **e**, Comparison of the top-performing iPE versions (iPE alterations are depicted in the sketch) to the original editor complex (PE2)[1] and the improved editor PEmax[2] for the editing strategies 'PE2', 'PE3', and 'Exo-PE'. iPE-N has a pegRNA harboring a PP7 aptamer (7_{v3}) and 3′-tevopreQ1[16] motif (Q1). Selected results of Bonferroni MCT after one-way ANOVA are shown for the fractional PE events and editing precision and are indicated by asterisks; n.s. $P > 0.05$, $^{**}P < 0.01$, $^{****}P < 0.0001$. Bars represent the mean ± SD (n = 3, biological replicates).

https://doi.org/10.1038/s41592-023-02162-w

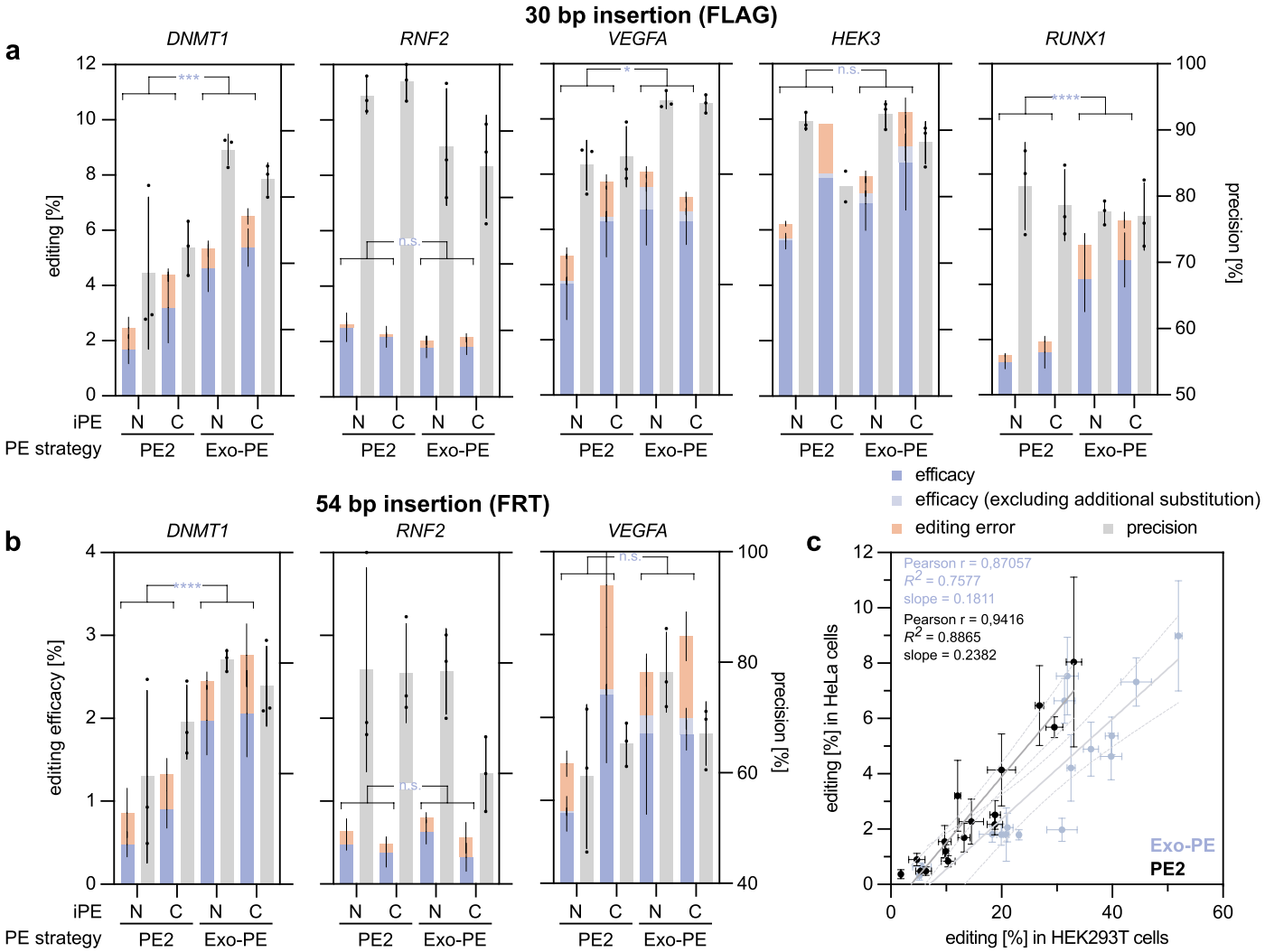

Extended Data Fig. 4 | Editing efficacy and precision of 'Exo-PE' and 'PE2' for two different insertions in HeLa cells. a, b, Experimental conditions and analyses are analogous to HEK293T data in Fig. 4c,d. Efficacy in HeLa was lower than in HEK293T cells, resulting in a larger SD for editing precision. Selected results of Bonferroni MCT for efficacy averaged over iPE-N/C after three-way ANOVA (showing main effects for panel a: PE strategy ($F = 32.762$, $P < 0.0001$), locus ($F = 46.97$, $P < 0.0001$), ($F = 9.085$, $P = 0.0045$), and the PE strategy/locus interaction ($F = 5.738$, $P = 0.001$) and panel b: PE strategy ($F = 13.665$, $P = 0.0011$), locus ($F = 25.373$, $P < 0.0001$) and PE strategy/locus interaction ($F = 7.46$, $P = 0.003$)) are indicated by asterisks; n.s. $P > 0.05$, *$P < 0.05$, ***$P < 0.001$, ****$P < 0.0001$. Bars represent mean ± SD ($n = 3$, biological replicates, except for *HEK3* C-PE2 where $n = 2$). **c**, Replotting of all efficacy data points for FLAG insertion from this figure and Fig. 4c,d shows the correlations of editing performance between HEK293T and HeLa ($P < 0.0001$ for both editing strategies). Gray lines indicate the 0.95 confidence bands of the linear regression. Please see Supplementary Table 1 for complete statistical results.

https://doi.org/10.1038/s41592-023-02162-w

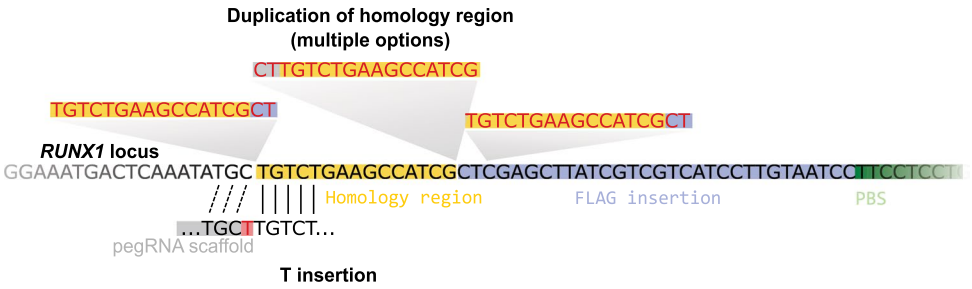

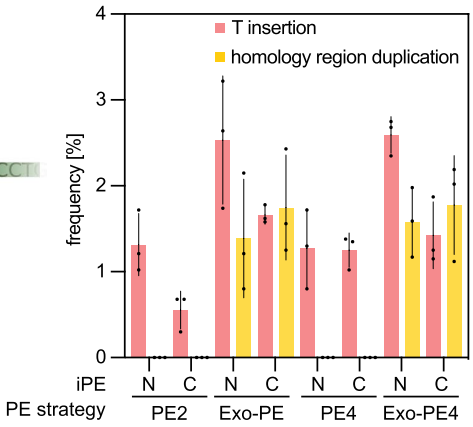

Extended Data Fig. 5 | Editing errors in the *RUNX1* locus. All conditions featuring 'Exo-PE' ('Exo-PE', 'Exo-PE4') led to a (partial) duplication of the pegRNA homology region at the insertion site (yellow), as well as an increased insertion of a single T at the end of the homology region (red). The T insertion could be linked to additional homology (dotted lines) in the pegRNA scaffold. Bars represent the mean ± s.d ($n = 3$, biological replicates).

https://doi.org/10.1038/s41592-023-02162-w

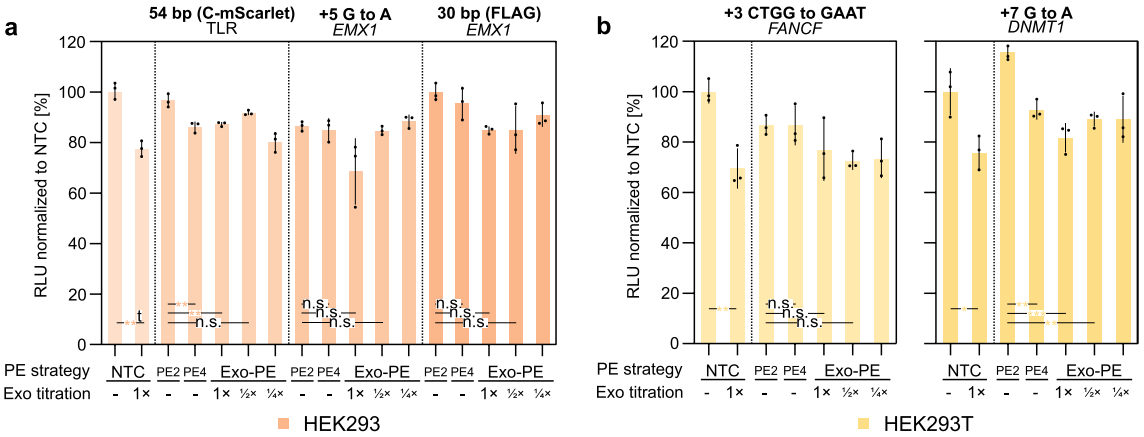

Extended Data Fig. 6 | Evaluation of viable cell abundance upon 'Exo-PE' editing. The abundance of viable cells was determined with a bioluminescent assay based on the cellular conversion of a luciferase substrate (see methods). iPE-C was tested in either 'PE2', 'PE4', or 'Exo-PE' for different insertion and substitution edits of varying length in **a**, HEK293, or **b**, HEK293T. For 'Exo-PE', the amount of T5-Exonuclease added to the experimental setup was titrated ('Exo-PE' with ½ Exo, ¼ Exo). Relative light unit [RLU] values were normalized against the non-targeting control (NTC). Cell viability significantly decreased upon the addition of untargeted T5-exonuclease (NTC+Exo). In comparison, 'Exo-PE' and 'PE4' showed a trend towards decreased RLU values compared to 'PE2', which was, however, not consistently observed across the different loci and different amounts of 'Exo-PE'. Selected results of Bonferroni MCT after a one-way ANOVA for each edit type are indicated by asterisks; n.s. $P > 0.05$, $^{*}P < 0.05$, $^{**}P < 0.01$, $^{***}P < 0.001$. For the comparison of NTC vs. NTC+ 1x Exo, unpaired two-tailed t-tests were performed. Bars represent the mean ± s.d ($n = 3$, biological replicates).

https://doi.org/10.1038/s41592-023-02162-w

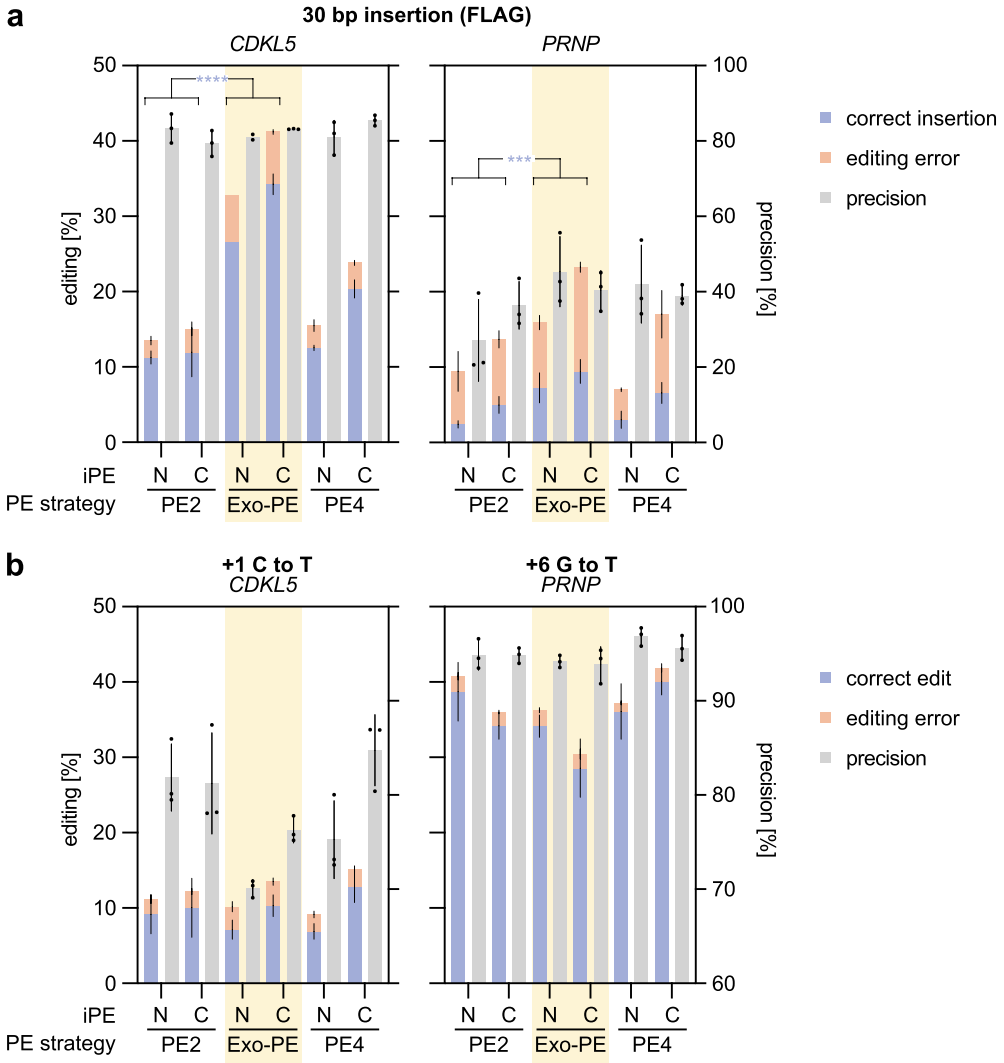

Extended Data Fig. 7 | Performance of 'Exo-PE' at additional genomic sites with biomedical relevance. a, Evaluation of 'Exo-PE' against the single-nick strategies 'PE2' and 'PE4' at disease-associated sites within the *CDKL5* and *PRNP* gene for 30 bp FLAG insertions. Selected results of Bonferroni MCT for efficacy averaged over iPE-N/C after three-way ANOVA (showing main effects for PE strategy ($F = 185{,}354$, $P < 0.0001$), locus ($F = 699.236$, $P < 0.0001$), iPE-N/C ($F = 68.975$, $P < 0.0001$), and the PE strategy/locus interaction ($F = 70.895$, $P < 0.0001$) are indicated by asterisks; ***P < 0.001, ****P < 0.0001. Bars represent the mean ± SD (n = 3, biological replicates, except for *CDKL5* N-Exo-PE (FLAG insertion) where n = 2). **b**, Evaluation of 'Exo-PE' against the single-nick strategies 'PE2' and 'PE4' for single-base therapeutic substitutions at the same genomic sites. Bars represent the mean ± SD (n = 3, biological replicates).

https://doi.org/10.1038/s41592-023-02162-w

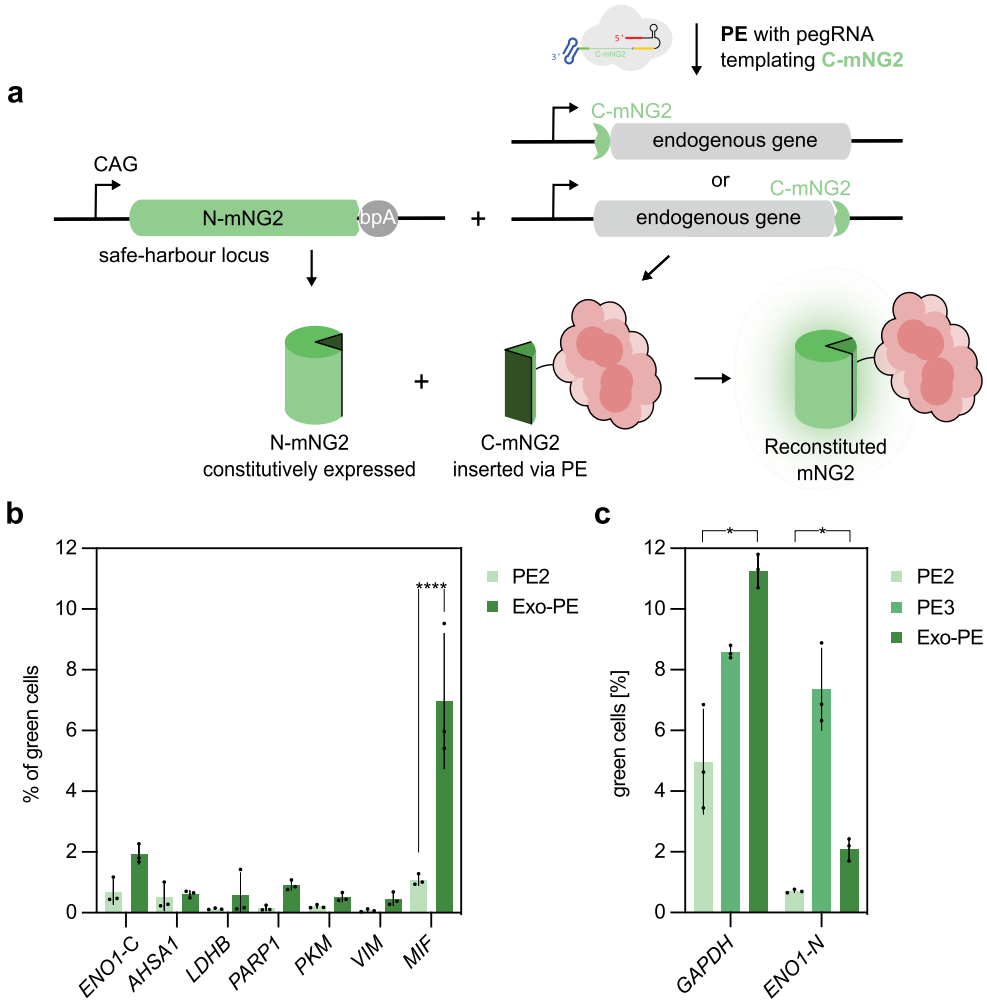

Extended Data Fig. 8 | Insertion of a protein tag for bimolecular fluorescence complementation. a, Schematic showing the Insertion of 48-57 bp (depending on 3xGly linker) coding for 11 amino acids of the split mNeonGreen (C-mNG2) to the C- or N-terminus of a target of interest. Corresponding proteins can be fluorescently labeled by on-target complementation of the split mNG2(1-10) (N-mNG2) co-expressed in a respective reporter cell line (HEK293T N-mNG2). **b,c**, Nine loci were targeted (*ENO1* was tagged either C- or N-terminally), and % of green cells was determined via FACS. **b**, 'Exo-PE' showed an overall higher editing efficacy (Two-way ANOVA, $F(1, 28) = 40.35$, $P < 0.0001$), selected results of Bonferroni MCT are shown as $^{****}P < 0.0001$. Bars represent the mean ± SD ($n = 3$, biological replicates). **c**, A direct comparison of iPE for the three editing strategies 'PE2', 'PE3', and 'Exo-PE' (PCP-Exo) was conducted. Selected results of Bonferroni MCT from a two-way ANOVA (locus, editing strategy) are shown as $^{*}P < 0.05$. Bars represent the mean ± SD (n = 3, biological replicates).

https://doi.org/10.1038/s41592-023-02162-w

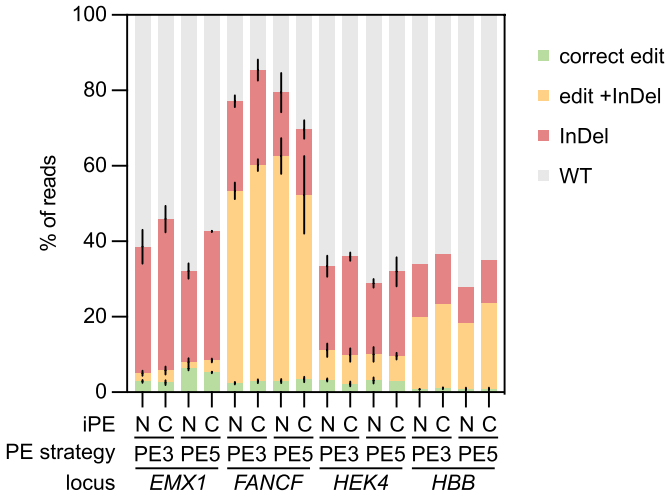

Extended Data Fig. 9 | Frequency of editing errors (InDel events) in editing strategies with a secondary nick ('PE3'/'PE5') for the 30 bp FLAG-tag insertion. Secondary nicks led to a substantial reduction in precision for insertion-type edits due to InDel events, which, depending on the target locus, often co-occurred with the incorporation of the intended edit (orange). The analysis is based on data shown in Fig. 6. Stacked bars represent the mean ± SD (n = 3, biological replicates, except *HBB* where n = 2).

https://doi.org/10.1038/s41592-023-02162-w

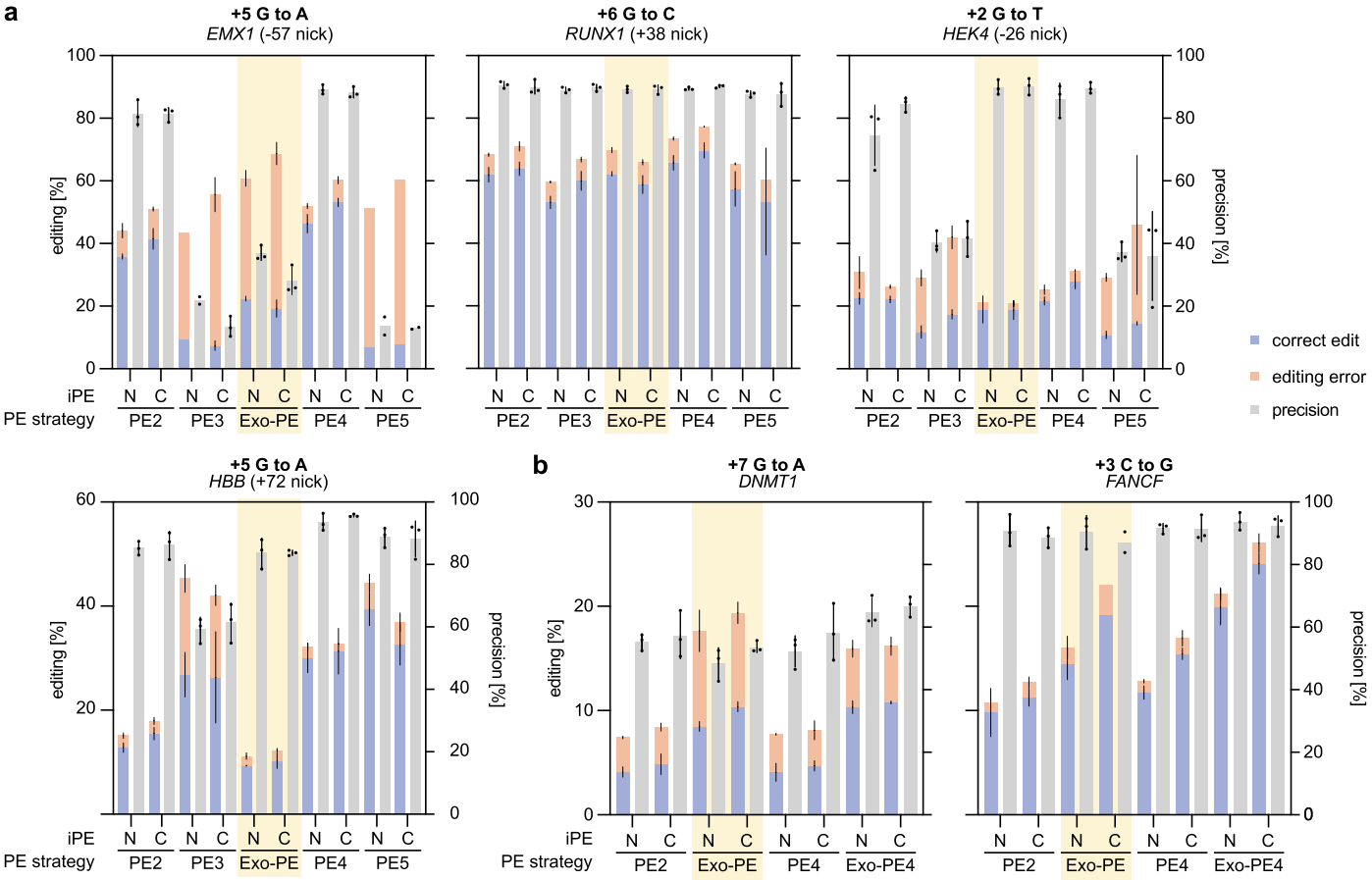

Extended Data Fig. 10 | Benchmarking of the 'Exo-PE' strategy for substitution edits. a, Substitutions on loci according to Fig. 4c. Nick positions of ngRNAs for 'PE3'/'PE5' strategies are indicated in brackets. **b**, Substitutions on two additional loci. Bars represent the mean ± SD ($n = 3$, biological replicates, except for *EMX1* N-PE3, *EMX1* N-PE5, *EMX1* C-PE5 and *FANCF* C-Exo-PE where $n = 2$).

Publication: Engineered nucleocytosolic vehicles for loading of programmable editors

In this publication, we describe the development of ENVLPE, a virus-like particle technology with optimized properties to deliver gene editor ribonucleoproteins (RNPs) to target cells, with a particular focus on prime editing (PE). We realized that pegRNA stability and its effective concentration in the form of RNPs at the plasma membrane as the site of cargo recruitment is a critical bottleneck for packaging functional editor RNPs. By combining aptamer-based RNP recruitment with additional pegRNA stabilization and active shuttling of the pre-assembled RNP from the nucleus into the cytoplasm, a substantial increase in editing efficacy over competitor systems was achieved. At the same time, the modularity of the aptamer recruitment mechanism provides the opportunity to seamlessly switch between Cas effectors without any modifications to the editor protein, and also deliver mRNA transcripts with high efficacy. We show that ENVLPE matches or outperforms state-of-the-art competitor technologies in multiple editing modes, across various endogenous sites and cell types, and even in primary T cells and *in vivo* mouse models. We further assessed toxicity and off-target activity in comparison to the VLP competitor and found no significant increase for either.

Enabled by the non-covalent recruitment mechanism, we further systematically removed structural and functional components of the gag polyprotein to generate a minimal vehicle (miniENVLPE) that retains functionality. The generated insights led to the development of an ENVLPE design principle, which could serve as a platform for the engineering of custom particles with non-viral origin.

My contribution to this study entails the co-execution of all experiments, data visualization and manuscript writing together with my co-first author. More specifically, I co-developed the foundational VLP framework, led efforts for the initial RNP delivery experiments, the pegRNA stabilization module and the study on minimized vehicles. I further coordinated and supervised the benchmarking experiments on endogenous sites as well as the design and production of any material required for the *in vivo* and *ex vivo* studies carried out by our collaborators.

Parts of this publication have also been described in the dissertation “Engineering of non-invasive tools towards OMICs analysis of coding and non-coding gene expression” by co-first author Niklas Armbrust, submitted to Technical University Munich on March 31st, 2025.

Cell

Article

Engineered nucleocytosolic vehicles for loading of programmable editors

Graphical abstract

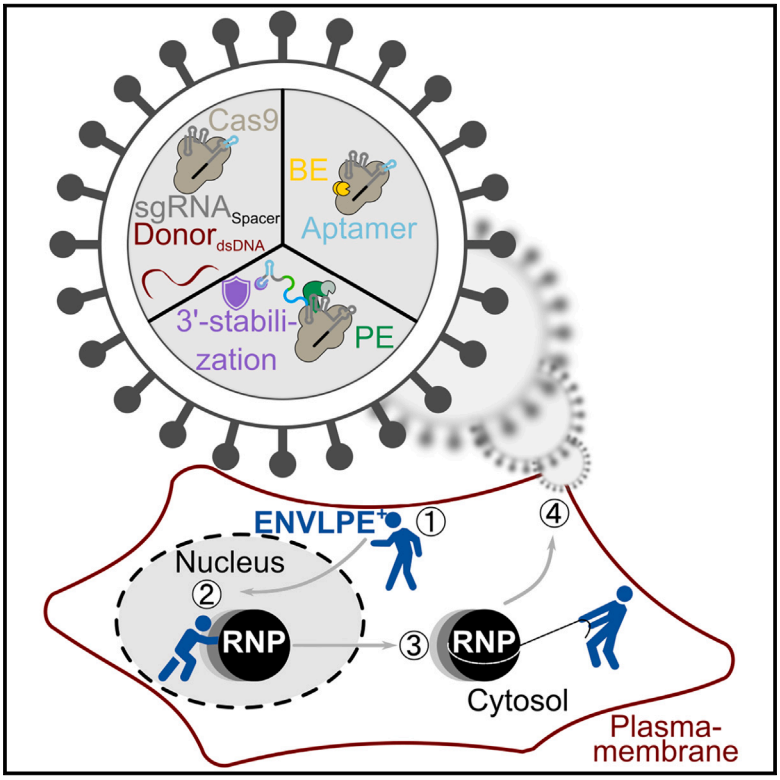

Highlights

- Nucleocytosolic shuttling allows modular loading of gene editors into VLPs via aptamers
- ENVLPE$^+$ VLPs achieve superior per-particle editing efficiency compared with previous VLPs
- 3′-pegRNA protection with Csy4 improves prime editing efficiency in VLP-based delivery
- ENVLPE$^+$ efficiently restores gene function in mouse models of inherited eye disease

Authors

Julian Geilenkeuser, Niklas Armbrust, Emily Steinmaßl, ..., Krzysztof Palczewski, Gil Gregor Westmeyer, Dong-Jiunn Jeffery Truong

Correspondence

gil.westmeyer@tum.de (G.G.W.), jeffery.truong@helmholtz-munich.de (D.-J.J.T.)

In brief

Engineered nucleocytosolic vehicles for loading of programmable editors (ENVLPE) with enhanced CRISPR ribonucleoprotein (RNP) loading and stabilization enable the efficient delivery of gene-editing effectors, such as nuclease, base, and prime editors. ENVLPE$^+$ outperforms existing VLP systems for *ex vivo* and *in vivo* gene editing, including the restoration of gene function in retinal disease models.

Geilenkeuser et al., 2025, Cell *188*, 1–19
May 15, 2025
https://doi.org/10.1016/j.cell.2025.03.015

CellPress

Cell

CellPress
OPEN ACCESS

Article

Engineered nucleocytosolic vehicles for loading of programmable editors

Julian Geilenkeuser,[1,2,10] Niklas Armbrust,[1,2,10] Emily Steinmaßl,[1,2] Samuel W. Du,[3,4] Sebastian Schmidt,[1,2,5] Eva Maria Hildegard Binder,[1,2] Yuchun Li,[1,2] Niklas Wilhelm Warsing,[1,2] Stephanie Victoria Wendel,[1,2] Florian von der Linde,[1,2] Elisa Marie Schiele,[1,2] Xiya Niu,[1] Luisa Stroppel,[1,2] Oleksandr Berezin,[1,2] Tobias Heinrich Santl,[1,2] Tanja Orschmann,[1,5] Keith Nelson,[1,2] Christoph Gruber,[5] Grazyna Palczewska,[3] Carolline Rodrigues Menezes,[3,4] Eleonora Risaliti,[3,4] Zachary J. Engfer,[3,4] Naile Koleci,[6] Andrea Schmidts,[6] Arie Geerlof,[7] Krzysztof Palczewski,[3,4,8,9] Gil Gregor Westmeyer,[1,2,*] and Dong-Jiunn Jeffery Truong[1,2,11,*]

[1]Institute for Synthetic Biomedicine, Helmholtz Munich, Neuherberg, Germany
[2]Department of Bioscience, TUM School of Natural Sciences, Technical University of Munich, Munich, Germany
[3]Gavin Herbert Eye Institute – Center for Translational Vision Research, Department of Ophthalmology, University of California, Irvine, Irvine, CA, USA
[4]Department of Physiology & Biophysics, University of California, Irvine, Irvine, CA, USA
[5]Institute of Developmental Genetics, Helmholtz Munich, Neuherberg, Germany
[6]Department of Medicine III: Hematology/Oncology, Klinikum rechts der Isar of the Technical University of Munich, TUM School of Medicine and Health, Munich, Germany
[7]Institute of Structural Biology, Helmholtz Munich, Neuherberg, Germany
[8]Department of Chemistry, University of California, Irvine, Irvine, CA, USA
[9]Department of Molecular Biology and Biochemistry, University of California, Irvine, Irvine, CA, USA
[10]These authors contributed equally
[11]Lead contact
*Correspondence: gil.westmeyer@tum.de (G.G.W.), jeffery.truong@helmholtz-munich.de (D.-J.J.T.)
https://doi.org/10.1016/j.cell.2025.03.015

SUMMARY

Advanced gene editing methods have accelerated biomedical discovery and hold great therapeutic promise, but safe and efficient delivery of gene editors remains challenging. In this study, we present a virus-like particle (VLP) system featuring nucleocytosolic shuttling vehicles that retrieve pre-assembled Cas-effectors via aptamer-tagged guide RNAs. This approach ensures preferential loading of fully assembled editor ribonucleoproteins (RNPs) and enhances the efficacy of prime editing, base editing, *trans*-activators, and nuclease activity coupled to homology-directed repair in multiple immortalized, primary, stem cell, and stem-cell-derived cell types. We also achieve additional protection of inherently unstable prime editing guide RNAs (pegRNAs) by shielding the 3′-exposed end with Csy4/Cas6f, further enhancing editing performance. Furthermore, we identify a minimal set of packaging and budding modules that can serve as a platform for bottom-up engineering of enveloped delivery vehicles. Notably, our system demonstrates superior per-VLP editing efficiency in primary T lymphocytes and two mouse models of inherited retinal disease, highlighting its therapeutic potential.

INTRODUCTION

The rapid development of various gene editing technologies over the past decade has revolutionized the field of molecular biology, allowing the precise manipulation of virtually any gene with single nucleotide precision. In particular, the recent development of base editors[1–8] and prime editors,[9] which mediate single-nucleotide conversions, deletions/insertions, or even whole gene insertions,[10,11] all without the need for mutagenic double-stranded DNA breaks (DSBs), represents a substantial advance toward genome editing. However, the efficient and safe delivery of these editing complexes remains challenging.

Viral vectors, particularly adeno-associated viruses (AAVs), are widely used for *in vivo* genome editing. Despite their safety and efficacy, AAVs have limitations, such as constrained cargo capacity, potential immunogenicity, and the risk of insertional mutagenesis and unintended mutations at on- and off-target sites due to their long persistence. Other viral vectors, including lentiviruses commonly employed in chimeric antigen receptor (CAR)-T cell therapies, integrate into the host genome, which may raise safety concerns due to insertional mutagenesis causing potential malignancy.[12]

Regardless of the delivery method, prolonged expression of genome editors can increase the risk of off-target effects

Please cite this article in press as: Geilenkeuser et al., Engineered nucleocytosolic vehicles for loading of programmable editors, Cell (2025), https://doi.org/10.1016/j.cell.2025.03.015

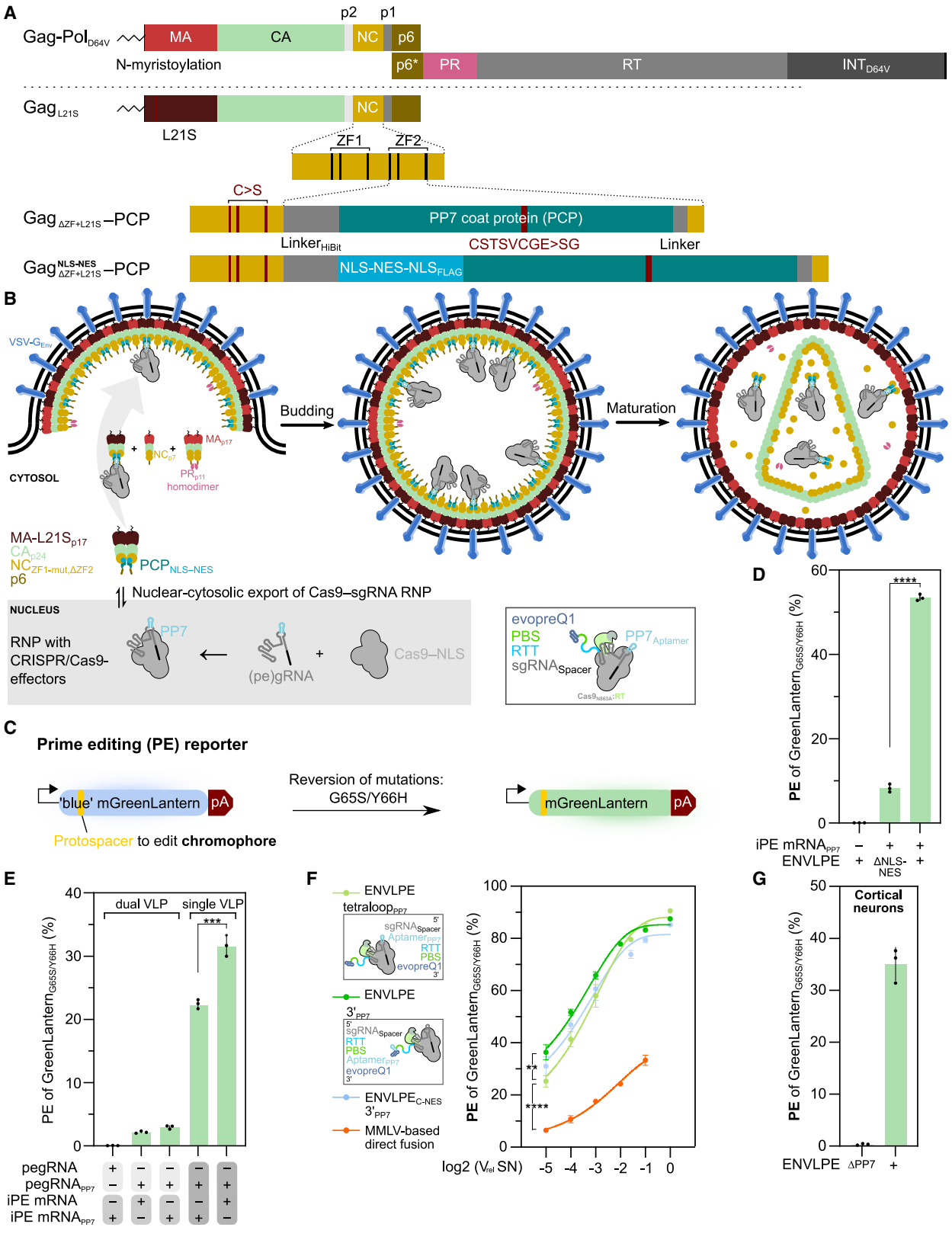

(legend on next page)

Please cite this article in press as: Geilenkeuser et al., Engineered nucleocytosolic vehicles for loading of programmable editors, Cell (2025), https://doi.org/10.1016/j.cell.2025.03.015

and immune responses. Therefore, there is a need for delivery systems that allow the cargo to persist only for a limited duration, enough to execute the desired edit but short enough to circumvent the harmful impacts of long-term expression.

In this context, lipid nanoparticles (LNPs) have gained attention as non-viral delivery vehicles for nucleic acids.[12] However, they often have limited cell-type specificity and require complex formulation and optimization for efficient delivery.

In contrast, virus-like particle (VLP) systems offer several advantages, including their capacity for pseudotyping,[13–16] enabling modulation of cell or tissue tropism by exploiting the diversity of known viruses with different tropisms. This facilitates the re-engineering of glycoproteins to target specific cell types or tissues, further enhancing the versatility and applicability of VLP systems. Importantly, VLP systems can package and deliver genome editing complexes as ribonucleoproteins (RNPs) without the risk of insertional mutagenesis or activation of the host immune response due to viral components or persistent transgene expression. Recent strategies rely on packaging the RNP editor via the Cas component, primarily by direct fusion to Gag,[17–21] which requires complex design considerations and optimization of the linker and the protease site depending on the editor protein of choice to enable efficient obligatory proteolytic cargo release.[22]

However, not only is a Cas9 apoenzyme less stable than a corresponding RNP complex,[23] the half-life of single guide RNAs (sgRNAs) is also orders of magnitude shorter than sgRNAs embedded into RNP complexes.[24–26] This characteristic leads to the conclusion that prime editing guide RNAs (pegRNAs), which carry a 3′-extended region encoding the desired edit as a reverse transcription template (RTT) followed by a primer binding site (PBS), are particularly prone to exonucleolytic degradation.[27,28]

We, therefore, opted for a recruitment mechanism based on RNA aptamers grafted onto (pe)gRNAs[29,30] to increase the likelihood of packaging functional RNPs. We further reasoned that such a VLP system could substantially benefit from the active transport of (pe)gRNAs from the nucleus to the cytosol, as (pe)gRNAs do not naturally reside in the cytosol where VLP cargo packaging occurs.

Thus, we have developed an optimized VLP system based on nucleocytosolic-shuttling vehicles that can load a Cas9 editor of choice via the (pe)gRNA, further stabilized by a dedicated 3′ protection mechanism. This design increases the fraction of functional RNP editors, which can be released in the target cell without proteolytic processing. We characterize the function of the individual features of this genetically engineered VLP-packaging system, which we call engineered nucleocytosolic vehicles for loading of programmable editors (ENVLPE). We benchmark ENVLPE's performance and demonstrate its utility in *ex vivo* and *in vivo* applications.

RESULTS

Gag-PCP shuttling enables efficient loading of (pe)gRNAs

To achieve packaging of the RNP editors via aptamer-tagged (pe)gRNAs, we inactivated the first zinc finger (ZF1) motif and installed the PP7 coat protein (PCP)[31] in lieu of the second zinc finger (ZF2) motif within the nucleocapsid (NC) domain of the HIV-1 Gag polyprotein (Figure 1A). We then introduced L21S into the matrix (MA) domain, which has been shown to enhance membrane trafficking,[32] as modifications within the NC domains

Figure 1. Development of nucleocytosolic shuttling vehicles to package editor-RNPs

(A) The top schematic diagram shows HIV-1-derived Gag-Pol$_{D64V}$, a lentiviral packaging vector encoding Gag (matrix [MA], capsid [CA], nucleocapsid [NC], and p6 domain), and the alternative reading frame encoding the enzymatic components, such as protease (PR), reverse transcriptase (RT), and an inactivated integrase (INT$_{D64V}$) as reference. The initial ENLVPE design is based on a codon-optimized Gag with L21S, which improves membrane-targeting, combined with the grafting of a PP7 coat protein (PCP) into the second zinc-finger motif within the NC domain to enable binding to PP7-aptamer-tagged guide RNAs. The first zinc-finger motif was inactivated by C>S mutations. The bottom illustration shows the additional insertions of a concatenation of nuclear localization (NLS) and export sequences (NES) to facilitate Gag shuttling between the nucleus and cytosol.

(B) Schematic of the RNP-packaging and budding mechanism. In the nucleus (gray shading), co-expression of PP7-aptamer-tagged (pe)gRNAs and Cas9 with an NLS (Cas9-NLS) leads to the formation of the RNP editor, which stabilizes the (pe)gRNA. The box on the right illustrates PP7-tagged (pe)gRNA used for prime editing (PE), with further 3′-protection by the evopreQ1 motif. Gag-PCP with nucleocytosolic shuttling functionality (NLS-NES) then relocates the RNP editor to the cytosol via the PP7 handle on the (pe)gRNA. At the plasma membrane, the RNP-editor is packaged into VLPs. Proteolytic cleavage of Gag can then lead to the structural maturation of the VLPs.

(C) The PE reporter system expresses a stably integrated mGreenLantern harboring two mutations in the chromophore (G65S, Y66H), resulting in a hypsochromic emission shift from green to blue fluorescence. Successful PE reverts the mutations to their original state, resulting in green fluorescence.

(D) The effect of the NLS-NES shuttling motif for the PE efficacies of ENVLPE delivering improved PE (iPE), quantified by fluorescence-activated cell sorting (FACS) of the blue mGL reporter HEK293T cell line. Bars represent mean ± SD (n = 3 biological replicates).

(E) Co-transduction of HEK293T with two separate ENVLPE preparations that deliver PP7-tagged pegRNA or mRNA coding for iPE (dual VLP), respectively, in comparison with delivery of all components in a single ENVLPE (single VLP). For each group, the pegRNA or the mRNA encoding iPE was either PP7-tagged or not. Bars represent mean ± SD (n = 3 biological replicates).

(F) Comparison of the initial pegRNA design with the PP7 aptamer inserted in the tetraloop (tetraloop$_{PP7}$) and a version with the PP7 aptamer moved toward the 3′-end to prevent packaging of 3′ truncated pegRNAs (3′$_{PP7}$). A variant with the NES shifted to the C terminus of Gag was also tested (C-NES). As a control (orange line), we compared a system with direct protein fusion of a prime editor to MMLV-gag (by switching the BE for a PE in v4 BE-eVLP [orange]). Experiments were performed on the blue mGL HEK293T line. Dots represent mean ± SD (n = 3 biological replicates). Log$_2$(V_{rel}SN): relative transduction volumes in 2× dilution steps. Editing rates of the lowest VLP titer were analyzed via Bonferroni multiple comparisons test (MCT) after one-way ANOVA ($p < 0.0001$; $^{**}p < 0.01$).

(G) PE performance of ENVLPE on human induced pluripotent stem cell (hiPSC)-derived cortical neurons carrying the blue mGL reporter. Bars represent mean ± SD (n = 3 biological replicates).

The results of two-tailed unpaired t tests are shown for (D) and (E) ($^{****}p < 0.0001$; $^{***}p < 0.001$; $^{**}p < 0.01$).

See also Figures S2, S3, and S17.

Please cite this article in press as: Geilenkeuser et al., Engineered nucleocytosolic vehicles for loading of programmable editors, Cell (2025), https://doi.org/10.1016/j.cell.2025.03.015

may negatively correlate with membrane recruitment and budding.[33] To enable packaging via PCP, a PP7 aptamer was grafted into the tetraloop of the SpCas9 gRNA/pegRNA scaffold (Figure 1B). In contrast to VLP-packaging mechanisms that use Gag-Cas fusions, this mode of gRNA recruitment binds the RNP complex at its least stable component to favor the packaging of fully assembled RNPs.

As a first characterization of the vesicular stomatitis virus G protein (VSV-G) pseudotyped VLP system, we confirmed proteolytic maturation of Gag-PCP, enhanced budding efficiency of the L21S mutation, and packaging of PP7-tagged mRNA (see design considerations in STAR methods; Figure S1). To assess the gene editing performance of the delivered prime editors, we generated a "blue" mGreenLantern fluorescent reporter HEK293T line (blue mGL) in which mutations in the chromophore of mGreenLantern (G65S and Y66H) can be reverted to shift the fluorescence profile from blue back to green (Figure 1C).

Since (pe)gRNAs are localized in the nucleus, we hypothesized that shuttling a Gag-PCP component between the nucleus and cytosol would allow active nuclear export of PP7-tagged (pe)gRNAs, which would otherwise rely on passive diffusion through the nuclear pore or nuclear envelope breakdown during mitosis. Therefore, we introduced an HIV-1 nuclear export sequence (NES) flanked by two nuclear localization sequences (NLSs) (MYC and a synthetic NLS) into the NC domain upstream of PCP to allow nucleocytosolic shuttling of the packaging component (Figure 1A).

For VLP production, we co-expressed the engineered Gag variants and wild-type (WT) Gag/Gag-Pol$_{D64V}$ to form mosaic VLPs and mitigate possible steric hindrance by PCP insertion. As prime editor, we used the "improved PE" (iPE) with C-terminal fusion of the Moloney murine leukemia virus (MMLV) pentamutant RT.[34] Indeed, the shuttling motif (NLS-NES-NLS) led to a substantial increase in PE activity when delivered to the blue mGL reporter cell line, suggesting that (pe)gRNA packaging was otherwise limited by low cytosolic concentration (Figure 1D). Immunofluorescence imaging revealed that the steady-state localization of the engineered shuttling Gag was in the cytosol as long as an NES motif was present (Figures S2A–S2C). Nuclear accumulation of Gag-PCP was evident as early as 1 h after the addition of leptomycin B, a nuclear export inhibitor. This observation suggests that Gag-PCP is continuously shuttled between the nucleus and cytosol (Figure S2C).

VLP delivery of prime editors as RNPs

Next, we sought to evaluate the potential contribution of mRNA recruitment to our delivery system. To this end, we tagged the 3′ UTR of the iPE mRNA with a single PP7. We then compared the prime editing (PE) efficacy in blue mGL HEK293T cells transduced with VLPs carrying the editor as RNP or as protein and pegRNA in separate particles (Figure 1E). Alternatively, only the mRNA or the pegRNA was delivered separately, while the other component was complemented by plasmid transfection (Figure S3A). Critically, we observed substantial editing only in those conditions where both the prime editor and the pegRNA were loaded into the same particle, independent of whether the mRNA encoding iPE was PP7-tagged (Figure 1E). In addition, we observed an increased editing efficacy for a non-tagged mRNA encoding iPE, compared with a PP7-tagged version, suggesting that more iPE proteins than mRNAs can be packaged into VLPs (Figure S3A). Jointly, these data indicate that the VLPs delivered the editors primarily as RNPs.

We transfected the blue mGL receiver cells with microRNAs (miRs)[35] targeting the 3′ UTR of the PP7-tagged prime editor mRNA prior to VLP delivery and observed no decrease in editing efficacy, documenting that there is no significant contribution of potentially co-packaged mRNA coding for iPE (Figure S3B). The functionality of the miR was validated by delivering a mGreenLantern mRNA with the same 3′ UTR. Transfection of the receiver cells with the miR prior to VLP transduction strongly suppressed mGreenLantern translation (Figure S1E).

ENVLPE design and pegRNA refinements

After completing additional validation experiments and optimizing the stoichiometry (Figures S3C–S3F), we also attempted to simplify the system to a single-component-packaging plasmid based on Gag-Pol$_{D64V}$, but the mosaic composition of Gag/Gag-Pol$_{D64V}$ and shuttling Gag-PCP was still superior (Figure S3G).

Despite using 3′ pseudoknot motifs such as evopreQ1 (Q1), packaged pegRNAs may be partially degraded. By moving the PP7 aptamer out of the gRNA scaffold to the 3′ end of the pegRNA between PBS and Q1, we limited packaging to only pegRNAs with intact 3′ ends (RTT and PBS), resulting in slightly increased editing efficacy, especially under low VLP doses. Both versions outperformed a Gag-PE fusion design, an architecture previously used for RNP delivery of Cas9, base-,[19,20] and prime-editors[17,18] (Figure 1F).

Moving the NES component of the shuttling domain to the Gag C terminus to improve cargo release was not beneficial (Figures 1F and S3H), indicating that cargo release was not limited by aptamer dissociation (see design considerations in STAR methods). Using this ENVLPE architecture, we achieved prime editing efficacies of up to 35% in human induced pluripotent stem cell (hiPSC)-derived cortical neurons carrying the blue mGL reporter system (Figure 1G).

Delivery of Cas9 effectors for KO and edits mediated by HDR

To utilize the high modularity of the guide-mediated packaging mechanism, we continued to test the capability of ENVLPE to deliver other Cas9-based effectors. Compared with pegRNAs, sgRNAs are bound with high affinity to *apo*-Cas9 (K_d ~5–20 nM[27] vs. ~10–300 pM[36,37]) and are more stable without a 3′ extension. Therefore, it appears that the loading capability of unaltered sgRNAs may be sufficient to enable efficient packaging in Gag-Cas9 fusion systems as well.

We thus conducted a comparison in HEK293T and hiPSCs, which revealed that Cas9 ENVLPE performed comparably to v4 Cas9 eVLPs[17] in a titration assay for targeted insertions and deletions (indels) at the *B2M* locus (Figure 2A). We then validated that Cas9 nuclease ENVLPEs were also effective in post-mitotic hiPSC-derived cortical neurons equipped with an "enhanced traffic-light reporter" (eTLR),[34] which reports all occurring mutagenic end-joining (mutEJ) indel events (Figure S4A).

Please cite this article in press as: Geilenkeuser et al., Engineered nucleocytosolic vehicles for loading of programmable editors, Cell (2025), https://doi.org/10.1016/j.cell.2025.03.015

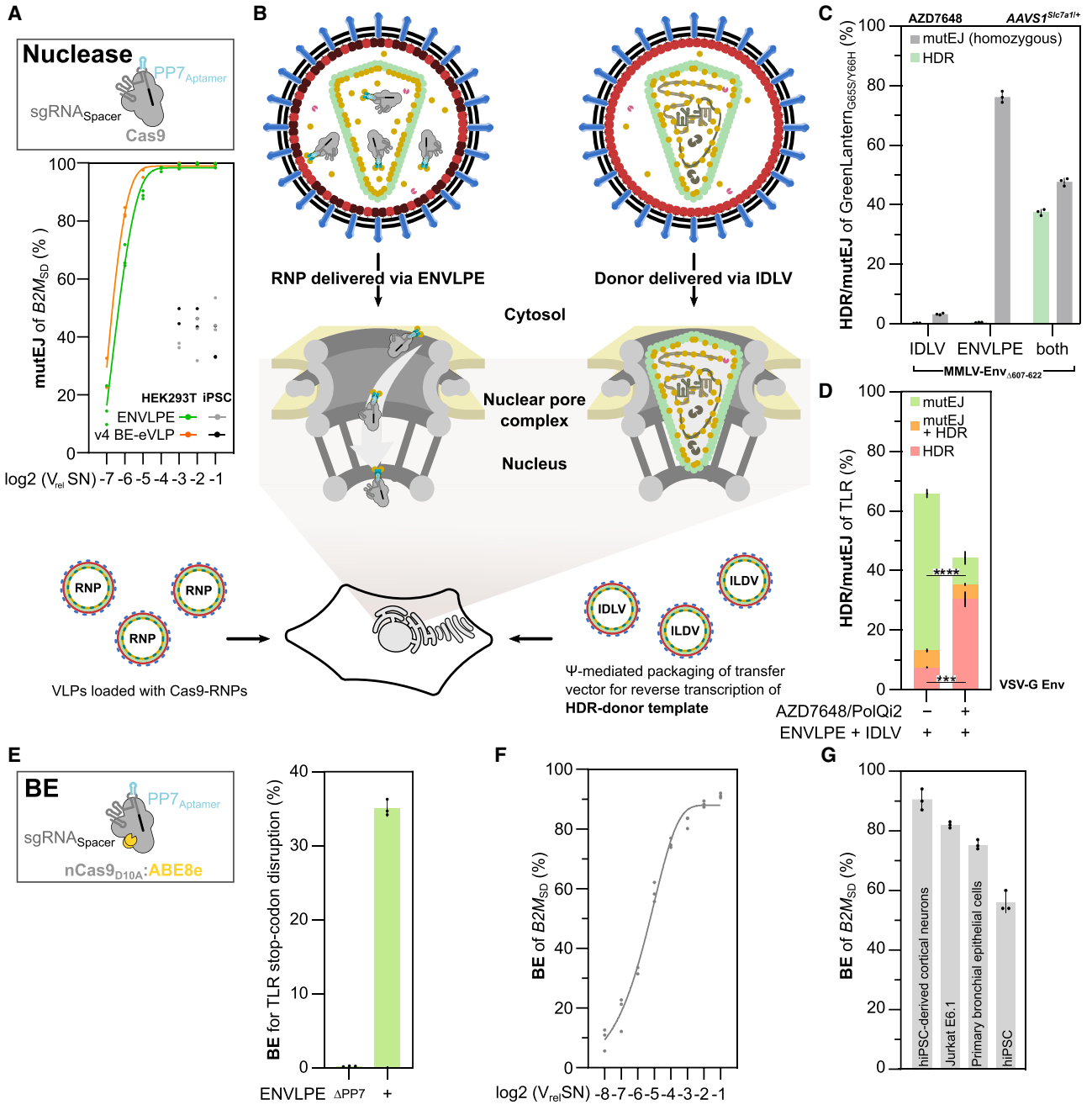

Figure 2. Delivery of various Cas9 effectors for mutEJ, HDR, and BE

(A) Cas9 ENVLPE was compared against v4 Cas9 eVLPs in targeting *B2M* in HEK293T cells and iPSCs. Indels were quantified via NGS, with points representing $n = 3$ biological replicates (except for HEK293T eVLP "−1" and "−2," iPSC ENVLPE "−3," and iPSC eVLP "−3," where $n = 2$). $Log_2(V_{rel}SN)$: relative transduction volumes in 2× dilution steps.

(B) To enable homology-directed repair (HDR), Cas9 ENVLPE was co-delivered with an HIV-1-based integrase-deficient lentivirus (IDLV) to revert the blue mGL reporter locus to its original green-fluorescent state. The IDLV delivers the reverse-transcribed donor template directly to the recipient cell's nucleus. The transfer plasmid contains the promoterless mGL HDR template, which includes homology arms to provide a DNA template for HDR.

(C) FACS-quantified percentages of HDR (green) and mutEJ (gray) events after transduction of the HEK293T blue mGL reporter cell line with Cas9 ENVLPE and HDR-donor IDLV in the presence of 0.5 μM AZD7648, a non-homologous end-joining (NHEJ) inhibitor. ENVLPE and IDLV were pseudotyped with ecotropic envelope proteins of the Moloney murine leukemia virus with deletion of the R-peptide (MMLV $Env_{\Delta 607-622}$); "blue mGL" reporter cells stably express the murine SLC7A1 receptor making them permissive for MMLV Env pseudotyped VLPs/IDLVs. Bars represent mean ± SD; $n = 3$ biological replicates.

(D) FACS-quantified percentages of HDR (red), mutEJ (green), or both (1st allele HDR, 2nd allele mutEJ, orange) of HEK293T eTLRv2 reporter cells after transduction with Cas9 ENVLPE and HDR-donor IDLV in the presence of 0.5 μM AZD7648 (NHEJ inhibitor) and 3 μM PolQi2 (MMEJ inhibitor) to promote HDR by

(legend continued on next page)

Please cite this article in press as: Geilenkeuser et al., Engineered nucleocytosolic vehicles for loading of programmable editors, Cell (2025), https://doi.org/10.1016/j.cell.2025.03.015

Nuclease-mediated editing is especially useful in stimulating homology-directed repair (HDR) to incorporate larger edits at a target site. In the context of HDR, VLPs have been used only in combination with other delivery modalities, such as co-precipitation of VLPs with dsDNA donors using polybrene or additionally electroporating the dsDNA donor into the recipient cells.[20] Many cell types, such as T lymphocytes, have sensitive innate immune responses toward cytosolic double-stranded DNA (dsDNA), resulting in massive cell death,[38,39] precluding direct delivery of dsDNA. Thus, *in vitro* generated single-stranded DNA (ssDNA)-based donors or AAVs (ssDNA genome) are common alternatives as HDR repair templates.

On the other hand, lentiviruses, such as HIV-1, can deliver their reverse-transcribed and capsid-shielded pseudo-genome directly to the nucleus without requiring the breakdown of the nuclear envelope,[40–42] thereby remaining undetected by cytosolic nucleic acid sensors.[38,39,43] Hence, we wondered whether Cas9 ENVLPEs could be combined with integrase-defective lentiviruses (IDLVs) that provide nuclear DNA templates after reverse transcription of the Ψ-tagged cargo RNA[44,45] (Figure 2B).

As a proof of concept, we provided IDLVs containing a promoterless mGreenLantern HDR template to repair the blue mGreenLantern back to its green-fluorescent state and co-delivered them with Cas9-ENVLPE into the recipient reporter cells. To show the flexibility of using fusogens other than VSV-G, we used the ecotropic MMLV envelope protein (MMLV-Env$_{\Delta 607\text{-}622}$)[46] to pseudotype both particles. Such pseudotyped particles cannot enter human cells unless the murine SLC7A1 receptor (mCAT1)[47] is heterologously expressed,[48] as in our modified blue mGreenLantern reporter HEK293T cell line. Upon co-delivery of Cas9 ENVLPEs together with the donor IDLVs in the presence of a non-homologous end-joining (NHEJ) inhibitor (0.5 μM AZD7648[49,50]), we observed chromophore repair in ∼40% of the population (Figure 2C), indicating highly efficient HDR. To raise the level of editing complexity, we increased the edit size from a 2 nt substitution in blue mGL to a 244 bp insertion to repair a truncated red fluorescent mScarlet-I protein in the eTLR reporter cell line, which reports mutEJ events as green fluorescence and successful HDR events as red fluorescence.[34] We observed 7% HDR, which could be increased to 30% in the presence of NHEJ/microhomology-mediated end-joining (MMEJ) inhibitors[51] (Figure 2D).

Delivery of Cas9 *trans*-activators and base editors

Next, we wondered whether functional CRISPR *trans*-activators, such as dCas9-miniVPR[52] RNPs, could be delivered using ENVLPE to induce *MAPT* expression in a HEK293T reporter cell line, which reports *MAPT* expression as a firefly luciferase (FLuc) activity.[53] We observed a significant 2-fold increase in reporter signal 48 h after CRISPRa-ENVLPE transduction, indicating successful gene activation (Figure S4B).

Lastly, we sought to extend ENVLPE to base editing (BE),[5–8] a double-strand-break-free and therapeutically promising gene editing technology. We first evaluated ENVLPE-mediated BE in our HEK293-TLR reporter cell line, which can also report the stop codon removal via a>g editing as green fluorescence, and observed that 35% of the cells were successfully edited (Figure 2E). We next tested BE ENVLPE on the *B2M* locus (Figures 2F and 2G) on multiple common cell types, where BE ENVLPE was able to facilitate BE with high efficacy at the *B2M* locus in all of the cell lines tested, reaching 90% in hiPSC-derived cortical neurons, and >55% in hiPSCs (Figure 2G). The latter cells are typically challenging to access with conventional techniques, such as lipofection or electroporation, which require tedious optimization.

3′ protection of pegRNA with Csy4 increases editing efficacy

Compared with gRNAs, pegRNAs particularly have a short half-life because of their degradation-prone 3′ extension.

Although our current design prioritizes packaging of PE RNPs with intact 3′ ends protected by the evopreQ1 pseudoknot,[27] we hypothesized that pegRNA stability may still limit the full potential of PE-ENVLPE. Accordingly, we used the CRISPR protein Csy4 (alias Cas6f) from *Pseudomonas aeruginosa*, which binds to a highly conserved 16 nt RNA motif (Csy4 motif, C4), wherein the nucleotides 2–16 form a hairpin with a 5 bp stem and a 5 nt loop. Csy4's processing activity has been used extensively in various CRISPR-Cas9 systems, e.g., to process arrays of gRNAs/crRNAs into individual gRNA/crRNAs for multiplexed gene editing,[54,55] or to enhance PE efficiency by preventing the pegRNA from folding back on itself due to the complementarity between the spacer and the PBS region.[56]

Importantly, the C4 RNA aptamer is bound by Csy4 with an exceptionally high affinity (K_d ∼50 pM[57]) that is ∼20-fold higher than the PCP-PP7 interaction (K_d ∼1 nM[58]). The C4 aptamer is precisely cleaved 3′ proximal to the hairpin without leaving any unpaired nucleotides as 3′-overhang. Csy4 remains bound with an unchanged affinity and thus may shield the 3′ end from a potential 3′ exonucleolytic attack.[57]

Although C4-modified pegRNAs showed no additional benefits in transient transfection experiments, in which pegRNA levels are naturally elevated (Figure S5A), we hypothesized that Csy4-mediated 3′ protection of the pegRNA could prove advantageous in conditions where RNA stability is limiting, such as during RNP delivery (Figure 3A). When Csy4 is co-expressed in the VLP-production cells, recruitment of the RNP complex is still

blocking NHEJ/MMEJ. Stacked bars represent mean ± SD; n = 3 biological replicates. Results from a two-tailed unpaired t test are shown (****$p < 0.0001$; ***$p < 0.001$); conditions were compared in the context of total indel rates (green + orange), as well as total editing rates (red + orange).

(E) ABE ENVLPE for disruption of the stop codon of an integrated eTLRv1 reporter in HEK293 cells, leading to green fluorescence by read-through. Editing was quantified via FACS; bars represent mean ± SD; n = 3 biological replicates.

(F and G) ABE ENVLPE for the disruption of a splice donor (SD) site of the first intron in the *B2M* gene was transduced into the indicated cell lines. Editing was quantified in HEK293T via NGS (F) or Sanger sequencing (G) 72 h after transduction. Points in (F) and bars in (G) represent n = 3 biological replicates. $Log_2(V_{rel}SN)$: relative transduction volumes in 2× dilution steps.

See also Figures S4 and S18.

Please cite this article in press as: Geilenkeuser et al., Engineered nucleocytosolic vehicles for loading of programmable editors, Cell (2025), https://doi.org/10.1016/j.cell.2025.03.015

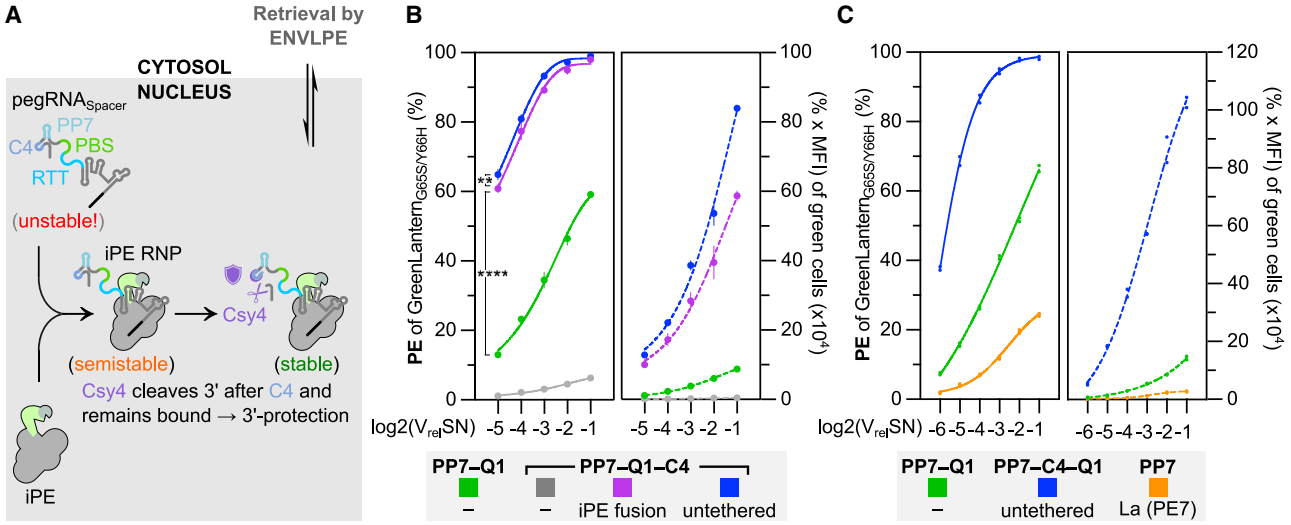

Figure 3. Implementation of Csy4 for improved PE pegRNA stability

(A) Schematic of Csy4-protected PE-RNP complex formation for packaging via ENVLPE. Csy4 cleaves off the 3′ overhanging nucleotides at the pegRNA's C4 aptamer and remains bound, thereby providing additional 3′-stabilization against exonucleolytic attack. The PE-RNP complex is then exported by the shuttling ENVLPE and combined with the budding module.

(B) Comparison of ENVLPE VLPs packaged with different 3′-stabilized PE-RNP complexes comprising the indicated 3′-modifications and covalent or non-covalent Csy4 tethers across a range of VLP doses. PE-mediated reversion of the blue mGL reporter in HEK293T cells is quantified via FACS and displayed as a percentage of green cells (left plot) or the percentage multiplied by the median fluorescence intensity (MFI) of green cells (right plot). PP7, PP7 aptamer bound by PP7 coat protein (PCP); Q1, evopreQ1 pseudoknot; C4, Csy4 aptamer hairpin bound and processed by Csy4; elements are described from 5′ to 3′ as they appear at the 3′-end of the respective pegRNA. Points represent mean ± SD (n = 3 biological replicates). $Log_2(V_{rel}SN)$: relative transduction volumes in 2× dilution steps. Editing rates of the lowest VLP titer were analyzed via Bonferroni multiple comparisons test (MCT) after one-way ANOVA (****$p < 0.0001$; **$p < 0.01$).

(C) Comparison of different VLP systems packaged with PE RNPs with different 3′-protection strategies applied to blue mGL HEK293T cells across a range of VLP doses. La indicates the fusion of the N-terminal fragment (amino acid [aa] 1–194) of La (SSB) used in PE7. The two plots represent the metrics as defined in (B). Points represent n = 3 individual replicates (orange) and n = 2 (green and blue). $Log_2(V_{rel}SN)$: relative transduction volumes in 2× dilution steps.

See also Figures S5–S10.

mediated by the PCP-PP7 system, and the 3′ end of the pegRNA in our initial setup contains an additional C4 motif downstream of the essential elements (RTT, PBS, and PP7). The editing efficacy in the recipient cells was strongly improved when Csy4 was co-expressed in the producer cells, either as a direct fusion to iPE or as an untethered module via a 2A peptide (iPE_{Csy4}) (Figure 3B), indicating that the increased efficacy is solely due to the 3′ protective effect of Csy4. Notably, the median fluorescence intensity (MFI) was strongly elevated for cells edited in the presence of Csy4, indicating either multi-allelic editing, faster editing kinetics, or a combination of both. We further observed that expressing Csy4 in an untethered fashion resulted in slightly higher % × MFI values than the fusion of Csy4 to iPE (Figure 3B). Interestingly, we observed an almost complete loss of editing activity in the control condition without Csy4, suggesting that unprocessed 3′-terminal nucleotides downstream of the C4 aptamer are highly susceptible to degradation (Figure 3B).

Evaluation of pegRNA 3′ end motifs

The effectiveness of PCP grafting into Gag was evaluated at different grafting positions to confirm that the observed improvement in protective Csy4 efficacy was not due to compensation for potentially suboptimal PCP grafting (Figure S5B). Alternative aptamer recruitment systems, such as Com (Figure S5C) or Csy4 alone, as a dual-purpose protection and recruitment module (Figure S6), did not provide additional benefits (see design considerations in STAR methods).

Therefore, we chose the 3′ configuration "PP7-C4-Q1" as the preferred mode for iPECsy4 because it can be used without Csy4 and thus provides the highest flexibility (Figure S7A).

We next compared iPE_{Csy4} with PE7, which utilizes the N-terminal fragment of the La protein fused to the prime editor to protect the 3′ ends of pegRNAs by binding to the 3′ poly(U) nucleotides, a scar left by RNA polymerase III termination.[28] With ENVLPE-mediated delivery, iPE_{Csy4} clearly outperformed PE7 in editing the blue mGL reporter line (Figure 3C). PE7-ENVLPE performance was increased by adding a tevopreQ1 motif to the pegRNA 3′ end but still displayed lower editing rates compared with iPE_{Csy4} ENVLPE (Figure S7B).

Evaluation of cell viability post-PE_{Csy4} delivery and potential application of Csy4 for canonical gRNAs

To evaluate the potential toxicity of Csy4 due to its RNA processing activity,[54] we investigated the effect of PE_{Csy4} transductions via ENVLPE on cellular fitness in recipient HEK293T and hiPSCs. However, we could not find relevant differences in cell viability compared with the non-VLP control condition and no difference in cytotoxicity compared with other VLP-transduced conditions lacking Csy4 (Figures S8A and S8B). We conclude that previous reports of Csy4's cytotoxic effect arise from circumstances

Please cite this article in press as: Geilenkeuser et al., Engineered nucleocytosolic vehicles for loading of programmable editors, Cell (2025), https://doi.org/10.1016/j.cell.2025.03.015

where Csy4 is excessively overexpressed in transient transfection settings.[54] Alternative strategies in which the protection and processing of the pegRNA 3′ end are separated into distinct processes did not prove to be beneficial (Figure S9; see design considerations in STAR methods).

We further tested whether Csy4-mediated 3′-stabilization of pegRNAs would also translate to conventional gRNA-based effectors that do not carry 3′-extensions. Likely due to the absence of 3′-vulnerable ends, gRNA-based nuclease and base-editing systems do not benefit from additional 3′-protection (Figure S10). In summary, Csy4 expressed via a 2A peptide with iPE (PE_{Csy4}), combined with PP7-C4-Q1 pegRNAs, substantially improves prime editing efficacy in ENVLPE-mediated RNP delivery.

Engineering of minimal, homomeric shuttling vehicles

Current VLP-delivery tools based on cargo fusion utilize co-assembly with virally derived Gag/Gag-Pol domains, as they are obligatorily dependent on the protease domain contained in the Pol frame for proteolytic cargo release.[14,17] We hypothesized that due to its aptamer recruitment and release mechanism, ENVLPE is not fundamentally dependent on protease-mediated release, even though it still utilizes mosaic assemblies with Gag/Gag-Pol domains composed of $Gag_{L21S,NLS\text{-}NES}$-PCP, Gag, and Gag-Pol.

Omitting Gag/Gag-Pol_{D64V} in the ENVLPE setup only resulted in a modest decrease in efficacy (Figure S11A), indicating that Gag/Gag-Pol_{D64V} was not essential. In contrast, omitting Csy4 led to a strong decrease in RNP transfer efficacy, indicating that RNP stability is a major bottleneck in aptamer-based RNP delivery systems (Figure S11A).

We identified the relatively mild impact of Gag/Gag-Pol_{D64V} omission as an opportunity to create a minimal VLP-like delivery system inspired by a previous publication.[59] We thus attempted to replace as many HIV-1 elements as possible with functional equivalents of non-viral elements (Figures 4A and 4B).

While preserving the nucleocytosolic shuttling motif and the aptamer-binding domain PCP, most of the MA/CA/NC regions were removed (ΔMA12–114, ΔCA133–277, ΔNC), except for the parts necessary to act as a spacer to induce membrane curvature during budding, as well as the budding domain p6 (Figure 4A). To compensate for Gag's eliminated oligomerization function, we incorporated GCN4 coiled coils, which form homomeric parallel dimers and trimers. Examining the functionality of this minimal design (miniENVLPE), we again found that the nucleocytosolic shuttling component is a key element in forming an efficient RNP packaging and delivery system (Figure 4C). Replacing the N-myristylation signal (MY) with a pleckstrin homology domain from phospholipase C-δ1 (PH)[60] that binds to phosphatidylinositol lipids, a component of the plasma membrane, further increased efficacy (Figure 4C). Remarkably, these miniature systems contained less than 13% of WT HIV-1 Gag sequences but were almost as active as full-length, homomeric $Gag_{L21S,NLS\text{-}NES}$-PCP setups (ENVLPE ΔGag/Gag-Pol_{D64V}; Figure 4D).

Since the minimal system is considerably decreased in size, which may shift its nucleocytosolic equilibrium, we re-tested several NES-NLS combinations on the miniENVLPE system. Still, we found no substantial improvement over the original nucleocytosolic shuttling sequence (Figure 4D).

Cryo-electron microscopy in our experiment revealed that HIV-1 Gag VLPs had a median radius of ∼55 nm, while ENVLPE and miniENVLPE had a smaller median radius of ∼31.5 nm (Figure S11B).

Mechanistic insights yield optimized ENVLPE$^+$

Further experiments on homomeric and minimal assemblies with different aptamers for recruitment provided additional evidence for our mechanistic insights on the ENVLPE system for PE (see design considerations in STAR methods). First, the PE efficacy improvement of PE_{Csy4} is also compatible with homomeric and minimal ENVLPE variants (Figures 4E and S11A). Second, cargo release is sufficient without proteolytic activity but is restricted to aptamer systems with intermediate affinities (nM range) since ultra-high-affinity aptamer systems (pM range) limit cargo release in the recipient cells (Figures 4F, S5C, and S11C). Last, Gag/Gag-Pol is not essential for particle assembly but is still generally beneficial (Figures 4F, S11A, S11C, and S11D).

Since GCN4 coiled coils were successfully applied in miniENVLPE, we also introduced them into ENVLPE (Figure 5A). Remarkably, this led to another significant increase in efficacy (Figure 5A), probably by enhancing productive PCP-PCP homodimerization. We termed this GCN4-enhanced final configuration ENVLPE$^+$.

Characterization of cargo loading efficiency

We next combined ENVLPE$^+$ with PE_{Csy4} as the optimal configuration for PE and conducted comparisons with v3 and v3b PE-eVLPs. As they are based on distinct packaging mechanisms compared with ENVLPE$^+$ (Figure S12), we chose to compare the amount of pegRNA and Cas9 effector protein per VLP. We found that one ENVLPE$^+$ particle was loaded with an average of 78 Cas9 molecules and 77 pegRNAs (ratio 0.99). In contrast, similar Cas9 levels were observed for v3 and v3b PE-eVLPs but distributed in a higher number of VLPs per volume and with a Cas9:pegRNA ratio of 0.58 and 0.61 for v3 and v3b PE-eVLPs, respectively (Figures S13A and S13B). This result aligns with our hypothesis that ENVLPE favors packaging of pegRNA:Cas9 complexes, while packaging of pegRNAs or Cas9 apoenzymes alone is improbable due to instability or absence of a recruitment handle. This observation is additionally supported by the findings of An et al., which suggested that improved RNP packaging could be a result of the additional introduction of Gag-aptamer-binding-proteins in v3 and v3b PE-eVLP.[18]

Benchmarking ENVLPE$^+$ against eVLP on endogenous targets

We proceeded to benchmark the editing efficacy and precision of ENVLPE$^+$ in base- and prime-editing modes on established endogenous loci against the MMLV-based v4 BE-eVLP and v3b PE-eVLP systems (see Figure S12 for the mechanistic differences). Because eVLP production is driven by CMV promoters, which are considered to be one of the strongest promoters in HEK293T cells,[61] we also switched ENVLPE$^+$ to CMV promoter-driven expression and optimized the plasmid stoichiometries again (Figure S13C). We wondered whether v3 or v3b

Please cite this article in press as: Geilenkeuser et al., Engineered nucleocytosolic vehicles for loading of programmable editors, Cell (2025), https://doi.org/10.1016/j.cell.2025.03.015

CellPress
OPEN ACCESS

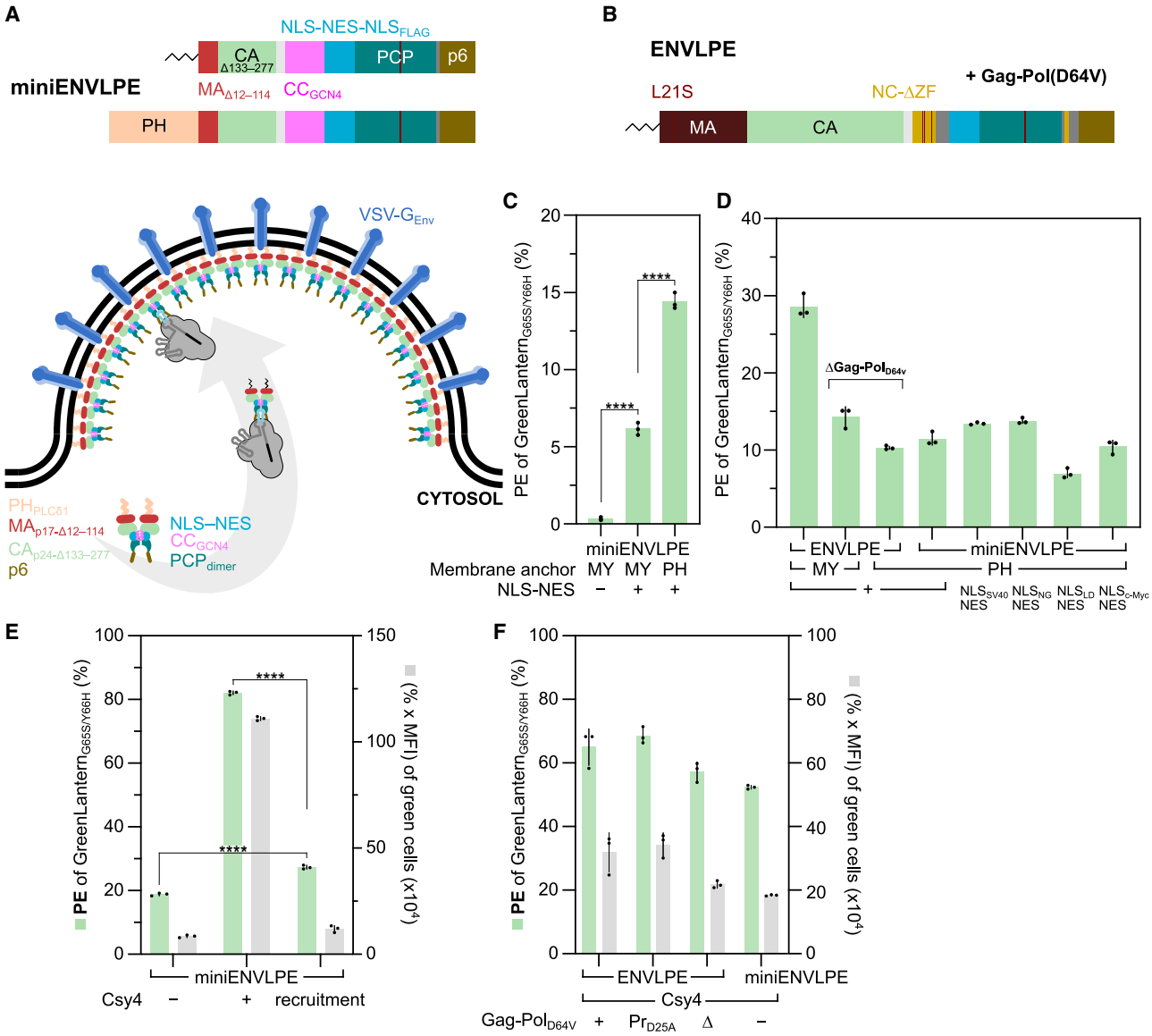

Figure 4. Engineering of a minimal Gag variant for delivery of functional RNPs

(A) Schematic representation of engineered minimal Gag versions with a majority of MA and CA deleted as indicated. The shuttling motif and PCP replace the complete NC domain, which also ablates the function of Gag to homo-oligomerize. Homo-oligomerization is restored by the introduction of GCN4 coiled coils (CC_{GCN4}). A PH was fused to the N terminus to replace the native N-myristoylation site. The resulting particles are formed from homomeric assemblies.

(B) Schematic representation of full-length Gag-PCP as used in ENVLPE for reference.

(C) Quantification of PE events in the blue mGL HEK293T reporter cell line via flow cytometry 72 h after transduction. Respective ENVLPE variants, shuttling domain variants, and membrane anchors (MY, HIV-1 N-myristoylation; PH, phospholipase C-δ1 pleckstrin homology domain) are indicated. Bars represent mean ± SD (n = 3 biological replicates).

(D) Comparison of the original ENVLPE (left) with variants without Gag/Gag-Pol_{D64V} and the addition of PH to full-length Gag-PCP as in (A, top) to miniENVLPE versions with different engineered nucleocytosolic shuttling motifs. PE was quantified in the blue mGL reporter HEK293T cell line via flow cytometry 72 h after transduction with VLPs. Bars represent mean ± SD (n = 3 biological replicates).

(E) Validation of the Csy4-C4 3′-protection module in the untethered or direct recruitment mode (see Figure S6) in the context of miniENVLPE. Experiments were conducted in the blue mGL HEK293T cell line. Bars represent mean ± SD (n = 3 biological replicates).

(F) The influence of proteolytic activity on PE efficacy in the blue mGL HEK293T reporter cell line in the context of the ENVLPE/Gag-Pol_{D64V} mosaic setup and the homomeric miniENVLPE. Bars represent mean ± SD (n = 3 biological replicates).

Selected results of Bonferroni MCT after one-way ANOVA analysis are shown for (C) and (E) (****$p < 0.0001$).

See also Figure S11.

Please cite this article in press as: Geilenkeuser et al., Engineered nucleocytosolic vehicles for loading of programmable editors, Cell (2025), https://doi.org/10.1016/j.cell.2025.03.015

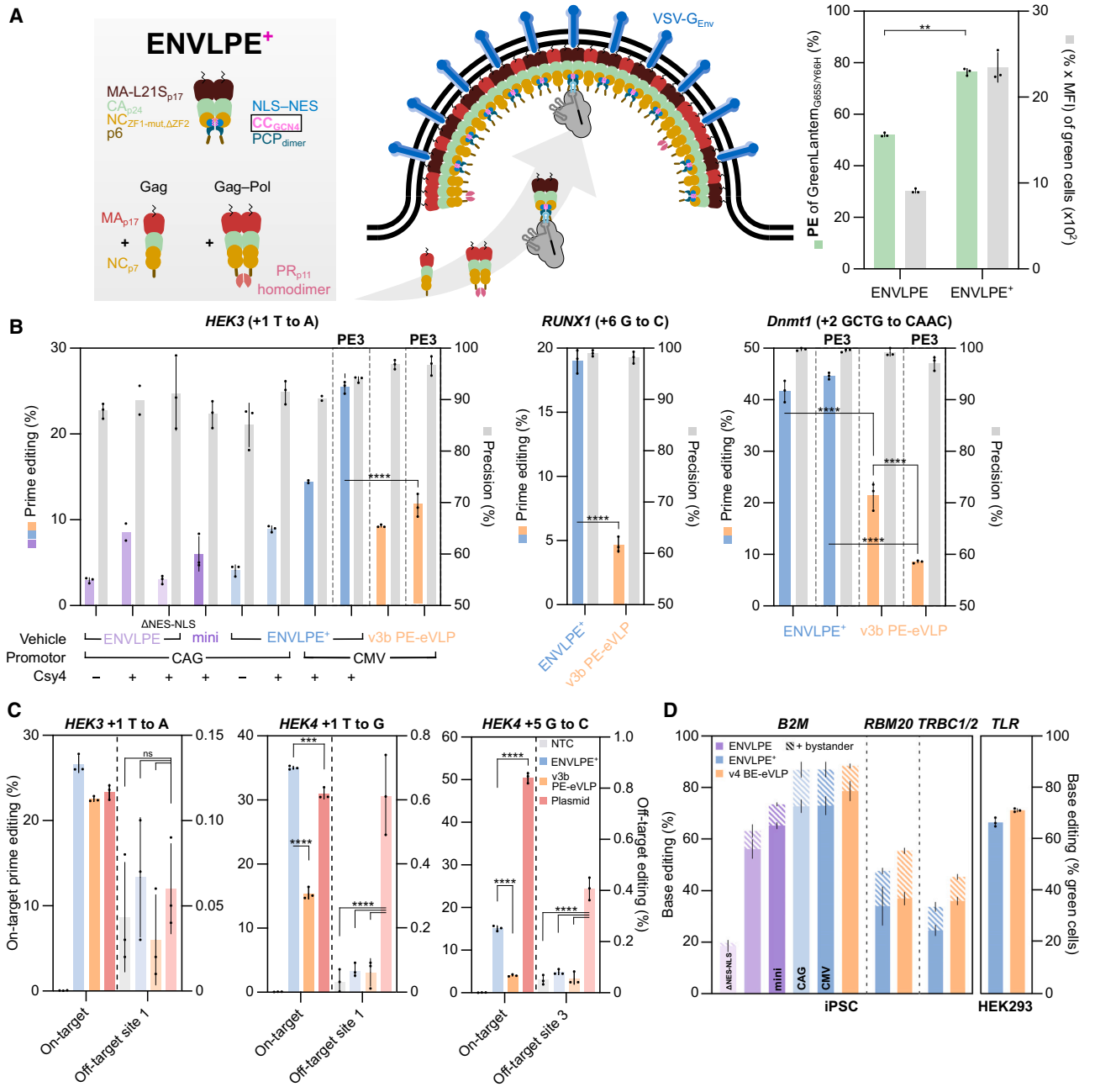

Figure 5. Optimized ENVLPE+ benchmarked for PE and BE at several endogenous sites

(A) Depiction of the improved module with an additional GCN4 domain (ENVLPE+) to assist Gag oligomerization (left). Editing performance of ENVLPE+ compared with ENVLPE (right). Experiments were performed on the blue mGL HEK293T line. Bars represent mean ± SD (n = 3 biological replicates). Results from a paired t test are indicated (**p < 0.01).

(B) Evaluation of ENVLPE, miniENVLPE, ENVLPE+, and v3b PE-eVLP delivery on several endogenous loci in HEK293T cells (*HEK3* and *RUNX1*) and in Neuro-2a cells (*Dnmt1*) using either the PE2 (default) or PE3 (indicated on top) strategy. Editing efficacy was analyzed via targeted amplicon sequencing, and precision was calculated by the ratio of intended edits divided by the total number of all non-WT reads × 100%. Bars represent mean ± SD (n = 3 biological replicates, except in *HEK3* PE$_{Csy4}$ ENVLPE [CAG] and PE$_{Csy4}$ ENVLPE+ [CMV] where n = 2). *HEK3* and *Dnmt1* data were analyzed using two-way ANOVA with Bonferroni MCT (****p < 0.0001). The conditions of *RUNX1* editing were analyzed by an unpaired two-tailed t test (****p < 0.0001).

(C) Additional assessment of on- and off-target editing in HEK293T of the respective VLP systems in HEK293T cells compared with plasmid-transfection of PE components targeting the respective targets. The same non-targeting control (NTC) of *HEK4* on-target editing is shown for both edit types. The off-target % is

(legend continued on next page)

Please cite this article in press as: Geilenkeuser et al., Engineered nucleocytosolic vehicles for loading of programmable editors, Cell (2025), https://doi.org/10.1016/j.cell.2025.03.015

PE-eVLP systems would benefit from Csy4 protection as well, and while both v3 and v3b PE-eVLP showed improvements with the additional 3′-protection to varying extents, ENVLPE$^+$ still achieved the highest prime-editing efficacy of all tested conditions (Figure S13D).

We then performed a detailed comparison of the endogenous *HEK3* locus (+1 t>a editing), including additional controls and comparisons with individual features of the ENVLPE system in HEK293T cells (NLS-NES, PE$_{Csy4}$, miniENVLPE, GCN4 coiled coils, CMV promoter). Evaluation of the editing performance at endogenous loci again demonstrated the functional relevance of the features built into ENVLPE$^+$ and reaffirmed CMV-driven PE$_{Csy4}$ ENVLPE$^+$ as the optimal configuration. This configuration also outperformed the state-of-the-art v3b PE-eVLP system[18] in both prime editing modes, "PE2" and "PE3" (Figure 5B).

We continued to benchmark our system across three additional loci and further editing types (t>a, g>c, t>g, +2 gctg>cacc), which showed that iPE$_{Csy4}$ ENVLPE$^+$ displayed consistently higher editing than v3b PE-eVLP across multiple endogenous sites in HEK293T and in Neuro-2a cells (Figures 5B and 5C). No significant increase in off-targets[62] compared with v3b PE-eVLP was found despite higher on-target efficacy (Figure 5C). On the other hand, plasmid-transfection of prime-editing components led to elevated off-target rates (Figure 5C). As expected for PE, editing precision (proportion of correct edits within all edited reads) was consistently high across all systems, mostly above 90%.

We extended ENVLPE$^+$ benchmarking against eVLPs to include BE and found similar rates for editing of multiple endogenous sites as observed with v4 BE-eVLPs in HEK293T and hiPSCs, with miniENVLPE also mediating comparable editing efficacies (Figure 5D).

BE with ENVLPE$^+$ for *ex vivo* T cell engineering

We next sought to assess the use of ENVLPE for generating hypo-immunogenic T cells suitable for cell-based therapeutic interventions. To achieve sufficient titers, we scaled up ENVLPE$^+$ particle production and transitioned to ultracentrifuge precipitation for enrichment.

We then administered ENVLPE$^+$ to primary T lymphocytes, facilitating a base edit in splice donor sites of the *B2M* and *TRBC1/2* loci to knock out major histocompatibility complex (MHC) class I and T cell receptor (TCR), two common knockout (KO) targets to generate hypoimmunogenic CAR-T cells[63] (Figure 6A). ENVLPE$^+$ facilitated both base edits at high efficacy and in a dose-dependent fashion (Figures 6B and 6C).

For *B2M* modification, we observed a direct correlation between editing efficacy and surface protein expression that is consistent with the requirement for biallelic modification to achieve complete KO (Figure 6B). This relation was less clear for *TRBC1/2*, where the KO of CD3 more closely follows editing (Figure 6C). It is likely that this pattern is caused by only one TRBC locus being transcriptionally active at a time,[64] resulting in a bias in both editing and expression toward the same allele.

We then proceeded to compare the efficacy of a simultaneous gene KO with a single transduction of either ENVLPE$^+$ or v4 BE-eVLPs. Our findings revealed comparable performance for both systems, albeit at a remarkably 40-fold higher titer of v4 BE-eVLPs (5.43×10^{11} v4 BE-eVLP particles and 1.34×10^{10} ENVLPE$^+$ particles per 50,000 cells; Figure 6D).

Distribution of ENVLPE *in vivo* after subretinal injection

We next set out to evaluate ENVLPE's editing performance in an *in vivo* setting and chose an ophthalmology context, since the eye has been used as a potent testbed for precision genome editing.[65] Multiple BE and PE strategies have been demonstrated in a diverse set of inherited retinal degeneration models, though virally delivered BE and PE limit the clinical applicability of the studies.[66–68]

To first test ENVLPE's transduction efficacy and local distribution of ENVLPE upon subretinal injection, we applied VSV-G-pseudotyped ENVLPE loaded with Cre$_{NLS}$ mRNA$_{PP7}$ to mT/mG mice (Figure 7A), which report Cre-recombinase activity as a conversion from red to green fluorescence. We injected 1.0, 1.5, and 2.0 μL of an ENVLPE solution (2.53×10^8 particles μL^{-1} in PBS) and observed broad and homogeneous green fluorescence-reporter activation across the retinal pigment epithelium (RPE) in 17/18 injected eyes 1 week after injection (Figures 7B and S14A). More importantly, no gross change of the compact RPE layer's pentagonal and hexagonal cell morphology was evident, suggesting ENVLPE was well tolerated. Consistent with these results, ENVLPE also performed well as an mRNA-delivery tool in a titration experiment in a Cre-dependent green-to-red-reporter HEK293 line (Figure S14B).

Prime editing of inherited retinal degeneration mouse models with PE$_{csy4}$ ENVLPE$^+$

Encouraged by the results from mRNA delivery, we sought to benchmark the performance of VLP-mediated PE in our optimized configuration iPE$_{Csy4}$ ENVLPE$^+$. To this end, we chose mouse models of retinitis pigmentosa (*rd6*) and of Leber congenital amaurosis (*rd12*), which have recently been used to measure the editing performance of v3 PE-eVLPs after subretinal injection.[18]

The loss-of-function phenotype in the *rd6* mouse model is caused by a 4 bp deletion in the splice donor region of *Mfrp* intron 4, abolishing protein expression (Figure 7C). To enable a direct head-to-head comparison with the recently published v3 PE-eVLP systems *in vivo*,[18] we employed the identical PE3b strategy for ENVLPE$^+$ (including identical spacers and 3′ extensions of the pegRNA but adapted to our scaffold and with 3′-modifications required for the Csy4/C4 protection; Figure 7C). We then produced both VLP systems in parallel from 15 cm dishes with 12.5×10^6 HEK293T cells/dish using original

calculated by subtracting the number of WT reads from the total reads of the indicated off-target loci. Bars represent mean ± SD (n = 3 biological replicates). Selected results of Bonferroni MCT after one-way ANOVA are indicated (****$p < 0.0001$; ***$p < 0.001$; ns $p > 0.05$).

(D) Evaluation of VLP-mediated BE in the HEK293 traffic-light reporter (TLR) cell line and other endogenous sites and cell lines. Editing efficacy was analyzed via targeted amplicon sequencing; bars represent mean ± SD (n = 3 biological replicates).

See also Figures S12 and S13.

Please cite this article in press as: Geilenkeuser et al., Engineered nucleocytosolic vehicles for loading of programmable editors, Cell (2025), https://doi.org/10.1016/j.cell.2025.03.015

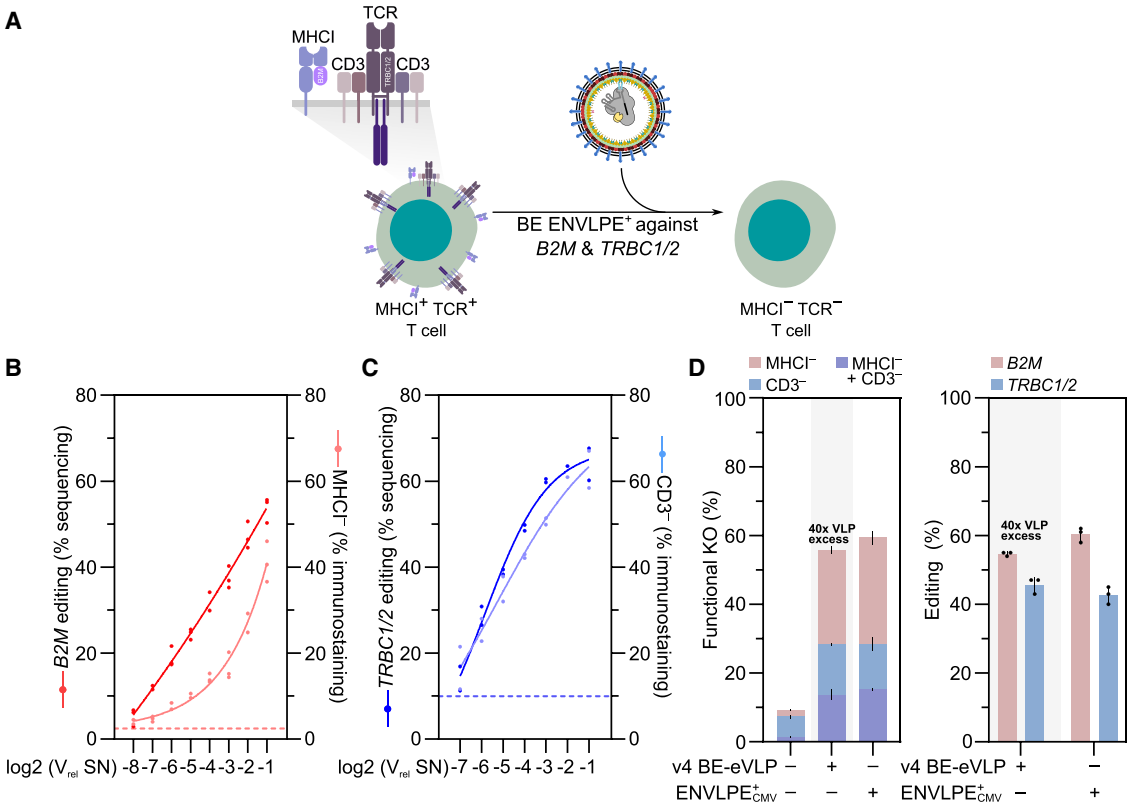

Figure 6. Using ENVLPE⁺ to generate hypoimmunogenic T cells *ex vivo*

(A) Schematic illustration of T cell receptor (TCR)/CD3 and MHC class I knockout (KO) by targeting *B2M* and *TRBC1/2* in primary T lymphocytes.

(B) *Ex vivo* delivery of adenine BE RNPs via $_{CAG}$ENVLPE⁺ to primary T lymphocytes. Quantification of *B2M* KO and the effect on MHC class I surface expression were analyzed 72 h after VLP delivery via NGS or flow cytometry (FC) after MHC class I immunostaining, respectively. $Log_2(V_{rel}SN)$, relative transduction volumes in 2× dilution steps.

(C) *Ex vivo* delivery of adenine BE RNPs via $_{CAG}$ENVLPE⁺ to primary T lymphocytes. Quantification of *TRBC1/2* KO and the effect on TCR surface expression were analyzed 72 h after VLP delivery via NGS or FC after CD3 immunostaining, respectively.

(D) Analysis of functional MHC class I⁻/CD3⁻ double KO in primary T lymphocytes by BE ENVLPE⁺ vs. v4 BE-eVLPs. KO efficiency was quantified via FC (functional) and NGS 72 h after delivery of the indicated VLP systems. Bars represent mean ± SD ($n = 3$). Titers of the respective VLP systems were measured via ELISA (5.43×10^{11} v4 BE-eVLP particles per 50,000 cells; 1.34×10^{10} ENVLPE⁺ particles per 50,000 cells; Figure S15). For dual targeting, 46 μL of VLPs containing either *B2M*-targeting sgRNAs or *TRBC1/2*-targeting sgRNAs were used for the eVLP or ENVLPE system, respectively.

See also Figures S12, S13, and S15.

plasmids for v3 PE-eVLPs[18] (from Addgene; see STAR Methods for details), concentrated the VLPs by ultracentrifuge precipitation using a sucrose cushion, and quantified the titers by ELISA against the capsid proteins in ENVLPE⁺ (HIV-1 p24) or v3 PE-eVLP (MMLV p30), respectively (Figure S15). 5- to 7-week-old *rd6* mice were injected with equal doses of $PE3b_{Csy4}$ ENVLPE⁺ or v3 PE3b-eVLP (1.6×10^9 particles μL^{-1} in 1 μL PBS). 3 weeks post-injection, we analyzed the protein expression of *Mfrp* in the eye cup via immunoblot and assessed the editing outcomes via targeted amplicon sequencing. Only ENVLPE⁺-treated eyes showed visibly restored MFRP protein expression (Figure 7D), mediated by the restoration of the splice donor site (median 8.6%; Figure 7E) with no detectable indels (Figure 7F), while samples from v3 PE3b-eVLP-treated mice exhibited MFRP levels beyond detection limit.

We repeated our head-to-head comparison on a second mouse model, *rd12*, which displays a more severe loss-of-function phenotype caused by a nonsense mutation in exon 3 of *Rpe65*, which abolishes the canonical visual cycle leading to visual impairment (Figure 7G). 3 weeks after subretinal injection of equal doses (1×10^9 particles μL^{-1} in 1 μL PBS) of both preparations into the RPE of 5- to 7-week-old *rd12* mice, immunoblot analysis of RPE homogenates revealed that the restored RPE65 protein could only be detected in eyes treated with $PE3b_{Csy4}$ ENVLPE⁺, whereas protein levels in eyes treated with v3 PE3b-eVLP remained below the detection limit (Figure 7H).

Comparable results were found by analyzing *Rpe65* exon 3 via targeted amplicon sequencing, which revealed substantial successful prime editing events with a median of 6.3% for $PE3b_{Csy4}$ ENVLPE⁺ (Figure 7I) without detectable indels (Figure 7J). In comparison, editing levels in the v3 PE3b-eVLP condition were below the detection threshold. The electroretinography (ERG) response correlated with the observed editing results across all samples from ENVLPE⁺ (Figure S16).

rd12 mice display a virtually absent light-dependent retinal activity that can be quantified via ERG (Figures 7K and 7L).

Please cite this article in press as: Geilenkeuser et al., Engineered nucleocytosolic vehicles for loading of programmable editors, Cell (2025), https://doi.org/10.1016/j.cell.2025.03.015

CellPress
OPEN ACCESS

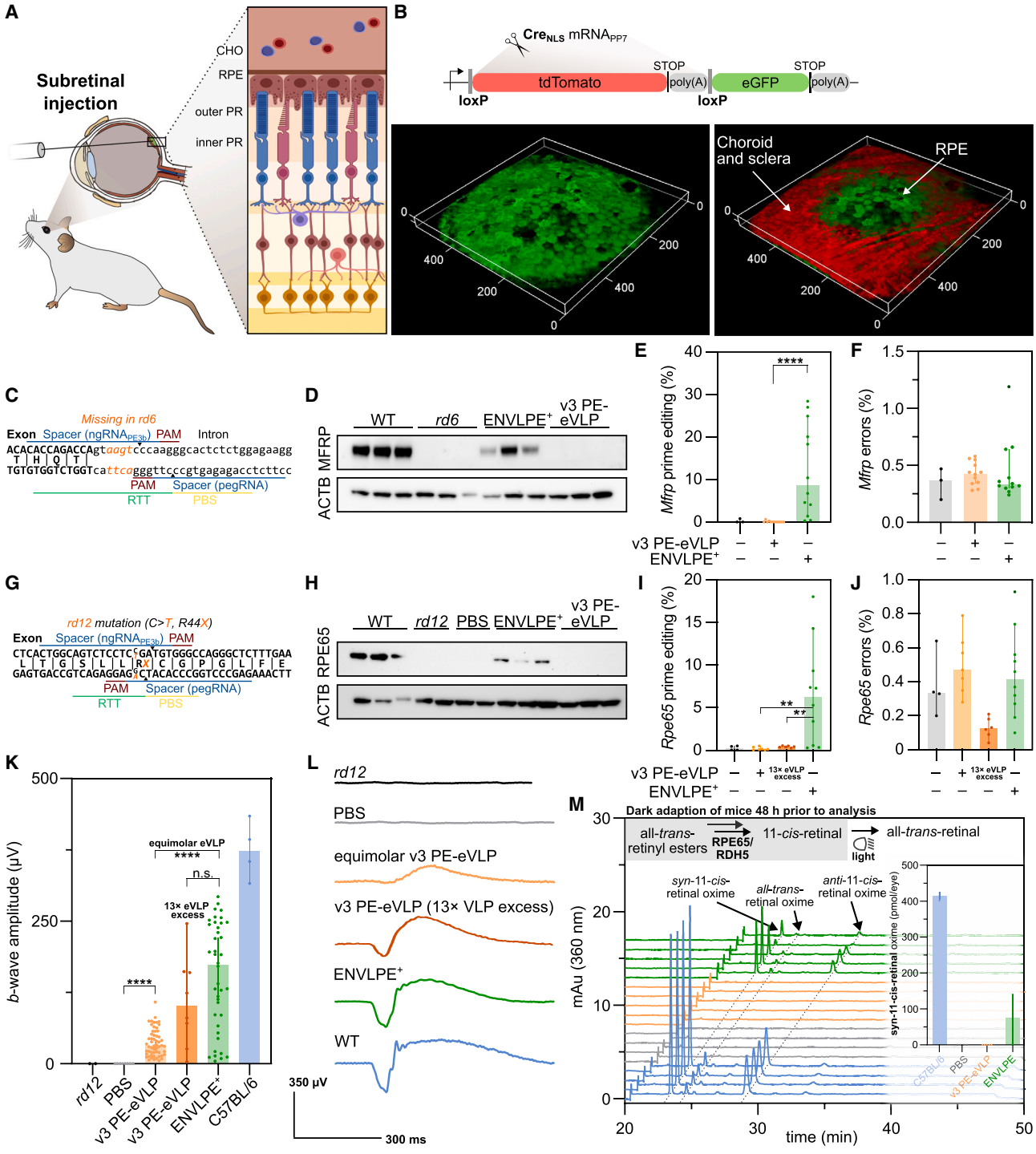

Figure 7. Subretinal injection of ENVLPE particles for mRNA delivery into Cre-reporter mice and for PE-RNP delivery to mouse models for inherited retinal degeneration

(A) Depiction of subretinal injection of VLPs into mouse retina. CHO, choroid; RPE, retinal pigment epithelium; PR, photoreceptor.

(B) Genetic construct of the reporter mouse indicating delivery of mRNA-encoded Cre activity with a red-green switch of fluorescent proteins expressed in RPE. Example 3D rendering of an imaging volume of the posterior portion of the intact eye acquired by two-photon imaging after subretinal injection of 1.5 μL sample (containing 3.63×10^8 ENVLPE particles). Left: green channel only; Right: green-red overlay. The units on the axes are in micrometers. Green fluorescence was observed in 17 out of 18 eyes; additional images are shown in Figure S14.

(C) Schematic diagram of 4 bp deletion in the SD region of exon 4 of *Mfrp* in *rd6* mice.

(legend continued on next page)

Please cite this article in press as: Geilenkeuser et al., Engineered nucleocytosolic vehicles for loading of programmable editors, Cell (2025), https://doi.org/10.1016/j.cell.2025.03.015

Treatment with ENVLPE$^+$ evoked ~5.5-fold higher *b*-wave signal (median 173.5 μV) compared with an equal dose of v3 PE-eVLPs (median 31.52 μV). A response of the comparable magnitude (median 102.2 μV) was evoked only after injecting a dose of v3 PE-eVLP that was approximately one order of magnitude higher (13.7×10^9 particles μL^{-1}; Figures 7K and 7L).

In *rd12* mice, the absence of RPE65 disrupts the visual cycle, leading to a deficiency of 11-*cis*-retinal. High-performance liquid chromatography (HPLC) analysis of retinoids in PE3b$_{Csy4}$ ENVLPE$^+$-treated *rd12* mouse eyes revealed significant restoration of 11-*cis*-retinal after dark adaptation, reaching ~20% of WT levels, suggesting a partially restored visual cycle (Figure 7M). Instead, 11-*cis*-retinal levels in v3-PE3b-eVLP-treated samples were below the detection limit, though some restoration must have occurred due to the recordable *b*-wave signals (Figures 7K and 7L).

DISCUSSION

We have introduced a highly effective and versatile tool for delivering all major classes of RNA-guided gene editors into a variety of cell types. Ultimately, we demonstrated its applicability for *in vivo* studies by restoring visual function in *rd12* mice and correcting the *rd6* mutation.

By systematically analyzing VLP methods for the delivery of gene editing RNP complexes, we identified three interrelated bottlenecks that limit their performance. First, the formation of guide RNA/Cas complexes in the nucleus is spatially separated from the budding process at the plasma membrane. Second, unbound guide RNAs, especially pegRNAs, are the least stable RNP components in the packaging cells. Third, the transport and packaging of RNP editors via protein fusions of an adapter to Gag protein instead of RNA aptamers limits the efficiency and modularity of the resulting VLPs.

Therefore, we have incorporated both NLS and NES and adjusted their relative strengths to enable an active nucleocytosolic export of editor-RNP complexes via an aptamer tag attached to the guide RNAs. This is in distinction to v3 and v3b PE-eVLP systems where multiple NES were added to the NLS motifs already contained in Gag-PE (v3) or P4-PE (v3b) but not inserted into the respective fusions of Gag and aptamer-binding proteins (Gag-MCP-Pol, v3; Gag-COM-Pol, v3b).[18] Thus, the purpose of the NES was to override the NLS on the Cas-containing fusion proteins to facilitate cytoplasmic packaging at the plasma membrane. Moreover, VLP-packaging mechanisms that recruit the RNP editor via the Cas protein component, either as direct fusions to Gag[17,19–21] or via coiled-coil adapters,[18] can result in empty *apo*-Cas packaging directly after cytosolic translation. Instead, ENVLPE ensures that the PP7-tagged stabilized RNP complex is directly picked up by the shuttling Gag-PCP component and then actively exported out of the nucleus for packaging at the plasma membrane. The Cas-effector concentration can be adjusted independently to maximize the transport of fully functional RNP editors, such that the dominant transport form is a fully assembled RNP.

Moreover, the aptamer-based recruitment mechanism of ENVLPE provides a high level of modularity, as the aptamer-tagged guide RNA serves as a universal interface to essentially any Cas effector of choice, which can be replaced without the need to re-optimize the editing performance. This also opens up the possibility of recruiting other RNA-guided effector proteins, given that their incorporation of an aptamer-tagged RNA is sufficiently stable. In the context of Cas9 effectors, this design enables seamless transitions between PE, nuclease + HDR, and BE functionalities without altering core components or stoichiometries of ENVLPE.

For PE-ENVLPE, we found that the pegRNA benefits from additional protection via Csy4/Cas6f beyond the evopreQ1 pseudoknot. While Csy4/Cas6f has been used in the past to enable multiplexed (pe)gRNA expression,[54,55] we found that Csy4/Cas6f resulted in at least an order of magnitude increase in PE efficacy.

Although this increased PE performance was also observed when Csy4 was used as a full replacement for PCP as an adapter (ENVLPE$_{Csy4}$), we suggest using Csy4 protection together with PCP-PP7-mediated recruitment strategy for maximum flexibility. In this mode, pegRNAs comprising a unified handle (3′-PP7-C4-Q1) can be used with or without Csy4. Csy4 can then be co-expressed as an untethered

(D) Immunoblot analysis of MFRP protein levels in *rd6* mouse eyes, 3 weeks after prime editing.
(E and F) Analysis of gDNA-editing efficacy and indel rate. Bars represent median with 95% CI ($n = 12$ biological replicates, except for "untreated" where $n = 3$). Selected statistical comparisons using the Kolmogorov-Smirnov test are shown (****$p < 0.0001$).
(G) Schematic diagram of the nonsense-mutation in exon 3 of *Rpe65* in *rd12* mice.
(H) Immunoblot analysis of RPE65 protein levels in *rd12* mice after prime editing.
(I and J) Analysis of the corresponding editing efficacy and error rate, including indels. Bars represent median with 95% CI ($n = 4$ [untreated]; $n = 7$ [eVLP]; $n = 6$ [eVLP 13× excess]; $n = 10$ [ENVLPE$^+$] biological replicates). Selected statistical comparisons using the Kolmogorov-Smirnov test are shown (**$p < 0.01$).
(K) Scotopic electroretinogram (ERG) *b*-wave amplitudes upon the light stimulus of −0.3 log[cd s m^{-2}] flash 3 weeks after injection of the different VLP systems or controls. Bars represent median with 95% CI ($n = 2$ [*rd12*]; $n = 9$ [PBS]; $n = 56$ [v3 PE-eVLP light orange]; $n = 8$ [v3 PE-eVLP dark orange], $n = 40$ [ENVLPE$^+$]; $n = 10$ [C57BL/6] biological replicates). Mice were dark-adapted overnight prior to analysis. Selected statistical comparisons using the Kolmogorov-Smirnov test are shown (****$p < 0.0001$; ns $p > 0.05$).
(L) Representative ERG traces from (K). Traces are represented as plots of potential (μV) versus time (ms).
(M) Schematic diagram of a portion of the visual cycle. Extracted whole-eye retinoids were analyzed by HPLC to quantify *syn*-11-*cis*-retinal. The mobile phase for retinal oxime elution was 90% hexanes and 10% ethyl acetate; the mobile phase for the earlier all-*trans*-retinyl ester elution (not shown in figure) was 99.4% hexanes and 0.6% ethyl acetate. Retinoid levels were determined using a standard curve. Results on the right show median and 95% CI for $n = 4$ control samples and $n = 5$ ENVLPE$^+$ and eVLP samples.
In (D)–(M), injection volumes were adjusted to equalize the injected VLP titers from v3 PE-eVLP and ENVLPE$^+$ particles per eye. VLP titers were quantified via ELISA (Figure S15).
See also Figures S12–S16.

Please cite this article in press as: Geilenkeuser et al., Engineered nucleocytosolic vehicles for loading of programmable editors, Cell (2025), https://doi.org/10.1016/j.cell.2025.03.015

protective module during VLP production. In this configuration, Csy4 protection is decoupled from the recruitment mechanism and can, therefore, be applied to other delivery systems that might benefit from pegRNA stabilization, as we have demonstrated exemplary for PE-eVLP.

We further found that the combination of HDR-donor IDLVs, Cas9 ENVLPEs, and DNA repair pathway modulators efficiently promotes knockins, useful for targeted integration of larger cassettes into safe-harbor loci or tagging of endogenous loci by homologous recombination. One important advantage of using our HIV-1-based ENVLPE + IDLV as dsDNA carriers is that the IDLV capsid acts as a molecular "Trojan horse" to deliver reverse-transcribed dsDNA donor directly into the nucleus, therefore likely circumventing the host's innate immune system (cGAS-STING).[43] Of note, MMLV or FMLV-based integrase-defective retroviruses (IDRV) rely on the dissolution of the nuclear envelope during mitosis, which is followed by the G1 phase. Homologous recombination, however, is restricted to the late G2/S phase, making MMLV/FMLV-based IDRVs a suboptimal choice as donor carriers for HDR. It remains to be seen whether an "all-in-one" VLP, encompassing both the RNP and the HDR template, is a viable option.

In ENVLPE, the RNP can dissociate from the aptamer interface without proteolytic Gag maturation, unlike direct fusions of Gag to CRISPR effectors. A non-maturing homomeric ENVLPE formulation still achieved 50% editing efficacy compared with the mosaic ENVLPE system. Understanding the mechanisms of efficient budding led us to the further improved ENVLPE^{+} by facilitating Gag-PCP oligomerization via coiled coils. It also allowed us to create a minimal variant (miniENVLPE) with ~13% of the original HIV-1 Gag/Gag-Pol sequence, achieving comparable editing efficacies. Given its independence from proteolytic maturation and co-expression of unmodified Gag/Gag-Pol, miniENVLPE can serve as a blueprint for future Gag-independent budding modules, e.g., by incorporating *de novo* cages or bacterial encapsulins.

For the *ex vivo* generation of T cells, we observed editing efficiencies comparable to v4 BE-eVLPs but at much lower titers, which is particularly relevant when injection volumes are limited.

The *in vivo* comparisons in several ophthalmologic mouse models showed potent mRNA delivery and superior "per VLP" editing efficacies with increased RNP loading compared with PE-eVLPs. Although we observed a higher per VLP editing efficacy of ENVLPE^{+} compared with PE-eVLPs, the titer (1×10^{9} particles per μL) we obtained for our equimolar comparison was 26-and 40-fold lower than in the referenced study for PE-eVLPs in the *rd6* or *rd12* models, respectively.[18] Moreover, we observed a higher variability of the protein levels, most likely because we did not control the selection of the tissue via a co-expressed fluorescent protein, as was done previously via AAV1-eGFP co-transductions.[18]

In summary, our characterization and application of the ENVLPE mechanism revealed that an optimized (pe)gRNA-mediated VLP packaging of gene editors as RNPs substantially improves editing efficacy per particle. This makes ENVLPE a potent delivery tool for base- and prime-editing, as well as HDR-based insertions or transactivation.

Limitations of the study

While extensive PE and BE data highlight the modularity of ENVLPE, experiments for CRISPRa and HDR were not carried out beyond proof of principle. Such future applications of ENVLPE could also include other Cas effectors, such as CRISPRi or CRISPRoff, and other RNA-targeting Cas enzymes, which were not explicitly considered here.

The transient nature of VLP-based delivery vehicles, as reported before,[17,19–21,29] decreases the risk of off-target edits due to prolonged expression of the editor complex. VLP systems may further attenuate potential immune responses, observed for traditional AAV-based gene therapy vectors that can continuously express their cargo for months to years in non-dividing cells. However, to deliver the desired genetic edits during the limited time window of transient expression, the VLP system must be highly optimized. In any case, the immunogenicity of different VLP systems should be closely examined in follow-up studies to compare their immunogenic potential. Additionally, immunogenic epitopes should be eliminated to minimize immune responses triggered by multiple VLP administrations. In this regard, our efforts to construct minimal packaging modules can serve as a blueprint for developing such low-immunogenic variants.

A key benefit of VLP strategies over LNP formulations is that tropism can be modified more easily via pseudotyping. We have demonstrated that ENVLPE can be pseudotyped with ecotropic glycoproteins, and it will be interesting to explore recent advancements in glycoprotein engineering to further refine and restrict VLP tropism to specific cell types.[13,14]

Our study also found a clear benefit of Csy4 for the efficacy of VLP-delivered prime editors across all experiments. Nevertheless, additional investigations into its generalizability across a broader range of targets and with other delivery systems would be advantageous.

Please note that despite our best efforts to prepare v4 BE-eVLPs and v3/v3b PE-eVLPs using original plasmids deposited at Addgene and the methods for VLP preparation described in the original documentation,[17,18] we cannot rule out the possibility that minor discrepancies in the protocol may have resulted in a slight reduction in the efficacy of the eVLPs compared with those used in previous studies. Moreover, in the rapidly evolving field of VLP development, the fifth version of the BE-eVLPs has recently been published. It is thus likely that an updated PE-eVLP will prove more effective than the current v3/v3b version. Nevertheless, we consider the per-particle editing efficacy to be an important metric for further optimization of VLP technology for *in vivo* applications.

RESOURCE AVAILABILITY

Lead contact

Requests for further information and resources should be directed to the lead contact, Dong-Jiunn Jeffery Truong (jeffery.truong@helmholtz-munich.de).

Materials availability

Plasmids generated in this study have been deposited to Addgene (details are provided in the key resources table).

Data and code availability

Source data are provided in this paper. All other data reported will be shared by the lead contact upon request.

ACKNOWLEDGMENTS

We thank Janna Nawroth and Tankut G. Güney for kindly providing primary bronchial epithelial cells (hBECs). We acknowledge the technical support of Flow Cytometry Core Facility at Helmholtz Munich. We would like to thank Dr. Carsten Peters and the TUM Electron Microscopy Facility for conducting sample preparation and image acquisition in automated cryo-EM. We also appreciate the assistance of Dr. Zhiqian Dong and Dr. Aleksander Tworak with mouse colony maintenance. We thank the members of the Center for Translational Vision Research and the Gavin Herbert Eye Institute for their comments and insights into this manuscript.

We acknowledge the support of the German Federal Ministry of Education and Research (BMBF) and the Free State of Bavaria within the framework of the Excellence Strategy of the Federal Government and the Länder through the ONE MUNICH project Munich Multiscale Biofabrication (J.G. and G.G.W.). G.G.W. acknowledges support from the European Research Council (ERC-CoG 865710 and ERC-PoC 101138939). J.G., N.A., G.G.W., and D.-J.J.T. acknowledge support from the European Innovation Council (EIC Pathfinder 101115574). This work was also supported in part by grants from the National Institutes of Health (NIH), including R01EY009339 (K.P.), R01EY034501 (K.P.), R01EY036994 (K.P.), T32GM008620 (S.W.D.), F30EY033642 (S.W.D.), and F31EY034027 (Z.J.E.). We acknowledge support frrom the Department of Ophthalmology, Gavin Herbert Eye Institute at the University of California, Irvine, from an unrestricted Research to Prevent Blindness award, from NIH core grant P30EY034070, and from a University of California, Irvine School of Medicine Dean's Office grant.

AUTHOR CONTRIBUTIONS

N.A. and J.G. contributed equally to this study. The exact order of the co-first authors was decided by a coin flip. J.G. and N.A. performed all experiments with the help of E.S., E.M.H.B., Y.L., N.W.W., S.V.W., F.v.d.L., E.M.S., X.N., L.S., T.H.S., K.N., C.G., and D.-J.J.T. D.-J.J.T. conceptualized and coordinated the study and oversaw the construct designs. S.S. and T.O. generated and differentiated the hiPSC reporter lines. C.G. provided the EPN-24-PCP construct for benchmarking. N.K. and A.S. performed the experiments with T lymphocytes. S.W.D. and K.P. designed the *rd6* and *rd12* study. S.W.D., G.P., C.R.M., E.R., and Z.J.E. performed *in vivo* injection experiments and their downstream analysis. S.W.D., G.P., C.R.M., E.R., and Z.J.E. analyzed data associated with *rd6* and *rd12*. K.P. analyzed data associated with *rd6* and *rd12* and supervised the *rd6* and *rd12* mouse experiments. A.G. produced the recombinant LgBiT, which was used for the quality control assays of the VLPs. O.B. performed the cryo-EM measurements to determine the size of the VLPs. D.-J.J.T. generated the sketches with modifications from J.G. and N.A. J.G., N.A., E.S., and D.-J.J.T. analyzed and visualized the data. J.G., N.A., D.-J.J.T., and G.G.W. wrote the manuscript. D.-J.J.T. and G.G.W. supervised the research.

DECLARATION OF INTERESTS

D.-J.J.T., J.G., N.A., and G.G.W. are inventors of the described technology and have filed patent applications through Helmholtz Munich and the Technical University of Munich (TUM). K.P. is a consultant for Polgenix Inc. and serves on the Scientific Advisory Board at Hyperion Eye Ltd. This work does not pertain to the above activities.

STAR★METHODS

Detailed methods are provided in the online version of this paper and include the following:

SUPPLEMENTAL INFORMATION

Supplemental information can be found online at https://doi.org/10.1016/j.cell.2025.03.015.

Received: February 16, 2024
Revised: January 3, 2025
Accepted: March 7, 2025
Published: April 9, 2025

REFERENCES

1. Richter, M.F., Zhao, K.T., Eton, E., Lapinaite, A., Newby, G.A., Thuronyi, B.W., Wilson, C., Koblan, L.W., Zeng, J., Bauer, D.E., et al. (2020). Phage-assisted evolution of an adenine base editor with improved Cas domain compatibility and activity. Nat. Biotechnol. *38*, 883–891. https://doi.org/10.1038/s41587-020-0453-z.
2. Neugebauer, M.E., Hsu, A., Arbab, M., Krasnow, N.A., McElroy, A.N., Pandey, S., Doman, J.L., Huang, T.P., Raguram, A., Banskota, S., et al. (2023). Evolution of an adenine base editor into a small, efficient cytosine base editor with low off-target activity. Nat. Biotechnol. *41*, 673–685. https://doi.org/10.1038/s41587-022-01533-6.
3. Lam, D.K., Feliciano, P.R., Arif, A., Bohnuud, T., Fernandez, T.P., Gehrke, J.M., Grayson, P., Lee, K.D., Ortega, M.A., Sawyer, C., et al. (2023). Improved cytosine base editors generated from TadA variants. Nat. Biotechnol. *41*, 686–697. https://doi.org/10.1038/s41587-022-01611-9.
4. Chen, L., Zhu, B., Ru, G., Meng, H., Yan, Y., Hong, M., Zhang, D., Luan, C., Zhang, S., Wu, H., et al. (2023). Re-engineering the adenine deaminase TadA-8e for efficient and specific CRISPR-based cytosine base editing. Nat. Biotechnol. *41*, 663–672. https://doi.org/10.1038/s41587-022-01532-7.
5. Kurt, I.C., Zhou, R., Iyer, S., Garcia, S.P., Miller, B.R., Langner, L.M., Grünewald, J., and Joung, J.K. (2020). CRISPR C-to-G base editors for inducing targeted DNA transversions in human cells. Nat. Biotechnol. *39*, 41–46.
6. Komor, A.C., Kim, Y.B., Packer, M.S., Zuris, J.A., and Liu, D.R. (2016). Programmable editing of a target base in genomic DNA without double-stranded DNA cleavage. Nature *533*, 420–424. https://doi.org/10.1038/nature17946.

7. Gaudelli, N.M., Komor, A.C., Rees, H.A., Packer, M.S., Badran, A.H., Bryson, D.I., and Liu, D.R. (2017). Programmable base editing of A•T to G•C in genomic DNA without DNA cleavage. Nature *551*, 464–471. https://doi.org/10.1038/nature24644.

8. Tong, H., Wang, X., Liu, Y., Liu, N., Li, Y., Luo, J., Ma, Q., Wu, D., Li, J., Xu, C., et al. (2023). Programmable A-to-Y base editing by fusing an adenine base editor with an N-methylpurine DNA glycosylase. Nat. Biotechnol. *41*, 1080–1084. https://doi.org/10.1038/s41587-022-01595-6.

9. Anzalone, A.V., Randolph, P.B., Davis, J.R., Sousa, A.A., Koblan, L.W., Levy, J.M., Chen, P.J., Wilson, C., Newby, G.A., Raguram, A., et al. (2019). Search-and-replace genome editing without double-strand breaks or donor DNA. Nature *576*, 149–157. https://doi.org/10.1038/s41586-019-1711-4.

10. Anzalone, A.V., Gao, X.D., Podracky, C.J., Nelson, A.T., Koblan, L.W., Raguram, A., Levy, J.M., Mercer, J.A.M., and Liu, D.R. (2022). Programmable deletion, replacement, integration and inversion of large DNA sequences with twin prime editing. Nat. Biotechnol. *40*, 731–740. https://doi.org/10.1038/s41587-021-01133-w.

11. Yarnall, M.T.N., Ioannidi, E.I., Schmitt-Ulms, C., Krajeski, R.N., Lim, J., Villiger, L., Zhou, W., Jiang, K., Garushyants, S.K., Roberts, N., et al. (2023). Drag-and-drop genome insertion of large sequences without double-strand DNA cleavage using CRISPR-directed integrases. Nat. Biotechnol. *41*, 500–512. https://doi.org/10.1038/s41587-022-01527-4.

12. Raguram, A., Banskota, S., and Liu, D.R. (2022). Therapeutic in vivo delivery of gene editing agents. Cell *185*, 2806–2827. https://doi.org/10.1016/j.cell.2022.03.045.

13. Strebinger, D., Frangieh, C.J., Friedrich, M.J., Faure, G., Macrae, R.K., and Zhang, F. (2023). Cell type-specific delivery by modular envelope design. Nat. Commun. *14*, 5141. https://doi.org/10.1038/s41467-023-40788-8.

14. Hamilton, J.R., Chen, E., Perez, B.S., Sandoval Espinoza, C.R., Kang, M.H., Trinidad, M., Ngo, W., and Doudna, J.A. (2024). In vivo human T cell engineering with enveloped delivery vehicles. Nat. Biotechnol. *42*, 1684–1692. https://doi.org/10.1038/s41587-023-02085-z.

15. Höfig, I., Barth, S., Salomon, M., Jagusch, V., Atkinson, M.J., Anastasov, N., and Thirion, C. (2014). Systematic improvement of lentivirus transduction protocols by antibody fragments fused to VSV-G as envelope glycoprotein. Biomaterials *35*, 4204–4212. https://doi.org/10.1016/j.biomaterials.2014.01.051.

16. Dobson, C.S., Reich, A.N., Gaglione, S., Smith, B.E., Kim, E.J., Dong, J., Ronsard, L., Okonkwo, V., Lingwood, D., Dougan, M., et al. (2022). Antigen identification and high-throughput interaction mapping by reprogramming viral entry. Nat. Methods *19*, 449–460. https://doi.org/10.1038/s41592-022-01436-z.

17. Banskota, S., Raguram, A., Suh, S., Du, S.W., Davis, J.R., Choi, E.H., Wang, X., Nielsen, S.C., Newby, G.A., Randolph, P.B., et al. (2022). Engineered virus-like particles for efficient in vivo delivery of therapeutic proteins. Cell *185*, 250–265.e16. https://doi.org/10.1016/j.cell.2021.12.021.

18. An, M., Raguram, A., Du, S.W., Banskota, S., Davis, J.R., Newby, G.A., Chen, P.Z., Palczewski, K., and Liu, D.R. (2024). Engineered virus-like particles for transient delivery of prime editor ribonucleoprotein complexes in vivo. Nat. Biotechnol. *42*, 1526–1537. https://doi.org/10.1038/s41587-023-02078-y.

19. Hamilton, J.R., Tsuchida, C.A., Nguyen, D.N., Shy, B.R., McGarrigle, E.R., Sandoval Espinoza, C.R., Carr, D., Blaeschke, F., Marson, A., and Doudna, J.A. (2021). Targeted delivery of CRISPR-Cas9 and transgenes enables complex immune cell engineering. Cell Rep. *35*, 109207. https://doi.org/10.1016/j.celrep.2021.109207.

20. Mangeot, P.E., Risson, V., Fusil, F., Marnef, A., Laurent, E., Blin, J., Mournetas, V., Massouridès, E., Sohier, T.J.M., Corbin, A., et al. (2019). Genome editing in primary cells and in vivo using viral-derived Nanoblades loaded with Cas9-sgRNA ribonucleoproteins. Nat. Commun. *10*, 45. https://doi.org/10.1038/s41467-018-07845-z.

21. Haldrup, J., Andersen, S., Labial, A.R.L., Wolff, J.H., Frandsen, F.P., Skov, T.W., Rovsing, A.B., Nielsen, I., Jakobsen, T.S., Askou, A.L., et al. (2023). Engineered lentivirus-derived nanoparticles (LVNPs) for delivery of CRISPR/Cas ribonucleoprotein complexes supporting base editing, prime editing and *in vivo* gene modification. Nucleic Acids Res. *51*, 10059–10074. https://doi.org/10.1093/nar/gkad676.

22. Kaczmarczyk, S.J., Sitaraman, K., Young, H.A., Hughes, S.H., and Chatterjee, D.K. (2011). Protein delivery using engineered virus-like particles. Proc. Natl. Acad. Sci. USA *108*, 16998–17003. https://doi.org/10.1073/pnas.1101874108.

23. Jiang, F., Taylor, D.W., Chen, J.S., Kornfeld, J.E., Zhou, K., Thompson, A.J., Nogales, E., and Doudna, J.A. (2016). Structures of a CRISPR-Cas9 R-loop complex primed for DNA cleavage. Science *351*, 867–871. https://doi.org/10.1126/science.aad8282.

24. Wang, H., Nakamura, M., Abbott, T.R., Zhao, D., Luo, K., Yu, C., Nguyen, C.M., Lo, A., Daley, T.P., La Russa, M., et al. (2019). CRISPR-mediated live imaging of genome editing and transcription. Science *365*, 1301–1305. https://doi.org/10.1126/science.aax7852.

25. Hendel, A., Bak, R.O., Clark, J.T., Kennedy, A.B., Ryan, D.E., Roy, S., Steinfeld, I., Lunstad, B.D., Kaiser, R.J., Wilkens, A.B., et al. (2015). Chemically modified guide RNAs enhance CRISPR-Cas genome editing in human primary cells. Nat. Biotechnol. *33*, 985–989. https://doi.org/10.1038/nbt.3290.

26. Ma, H., Tu, L.-C., Naseri, A., Huisman, M., Zhang, S., Grunwald, D., and Pederson, T. (2016). CRISPR-Cas9 nuclear dynamics and target recognition in living cells. J. Cell Biol. *214*, 529–537. https://doi.org/10.1083/jcb.201604115.

27. Nelson, J.W., Randolph, P.B., Shen, S.P., Everette, K.A., Chen, P.J., Anzalone, A.V., An, M., Newby, G.A., Chen, J.C., Hsu, A., et al. (2022). Engineered pegRNAs improve prime editing efficiency. Nat. Biotechnol. *40*, 402–410. https://doi.org/10.1038/s41587-021-01039-7.

28. Yan, J., Oyler-Castrillo, P., Ravisankar, P., Ward, C.C., Levesque, S., Jing, Y., Simpson, D., Zhao, A., Li, H., Yan, W., et al. (2024). Improving prime editing with an endogenous small RNA-binding protein. Nature *628*, 639–647. https://doi.org/10.1038/s41586-024-07259-6.

29. Lyu, P., Javidi-Parsijani, P., Atala, A., and Lu, B. (2019). Delivering Cas9/sgRNA ribonucleoprotein (RNP) by lentiviral capsid-based bionanoparticles for efficient "hit-and-run" genome editing. Nucleic Acids Res. *47*, e99. https://doi.org/10.1093/nar/gkz605.

30. Lyu, P., Lu, Z., Cho, S.-I., Yadav, M., Yoo, K.W., Atala, A., Kim, J.-S., and Lu, B. (2021). Adenine base editor ribonucleoproteins delivered by Lentivirus-like particles show high on-target base editing and undetectable RNA off-target activities. CRISPR J. *4*, 69–81. https://doi.org/10.1089/crispr.2020.0095.

31. Prel, A., Caval, V., Gayon, R., Ravassard, P., Duthoit, C., Payen, E., Maouche-Chretien, L., Creneguy, A., Nguyen, T.H., and Martin, N. (2015). Highly efficient in vitro and in vivo delivery of functional RNAs using new versatile MS2-chi- meric retrovirus-like particles. Mol. Ther. Methods Clin. Dev. *2*, 15039.

32. Paillart, J.C., and Göttlinger, H.G. (1999). Opposing effects of human immunodeficiency virus type 1 matrix mutations support a myristyl switch model of gag membrane targeting. J. Virol. *73*, 2604–2612. https://doi.org/10.1128/JVI.73.4.2604-2612.1999.

33. Grigorov, B., Décimo, D., Smagulova, F., Péchoux, C., Mougel, M., Muriaux, D., and Darlix, J.L. (2007). Intracellular HIV-1 Gag localization is impaired by mutations in the nucle- ocapsid zinc fingers. Retrovirology *4*, 54.

34. Truong, D.-J.J., Geilenkeuser, J., Wendel, S.V., Wilming, J.C.H., Armbrust, N., Binder, E.M.H., Santl, T.H., Siebenhaar, A., Gruber, C., Phlairaharn, T., et al. (2024). Exonuclease-enhanced prime editors. Nat. Methods *21*, 455–464. https://doi.org/10.1038/s41592-023-02162-w.

35. Fellmann, C., Hoffmann, T., Sridhar, V., Hopfgartner, B., Muhar, M., Roth, M., Lai, D.Y., Barbosa, I.A.M., Kwon, J.S., Guan, Y., et al. (2013). An optimized microRNA backbone for effective single-copy RNAi. Cell Rep. *5*, 1704–1713. https://doi.org/10.1016/j.celrep.2013.11.020.

36. Wright, A.V., Sternberg, S.H., Taylor, D.W., Staahl, B.T., Bardales, J.A., Kornfeld, J.E., and Doudna, J.A. (2015). Rational design of a split-Cas9 enzyme complex. Proc. Natl. Acad. Sci. USA *112*, 2984–2989. https://doi.org/10.1073/pnas.1501698112.

37. Yourik, P., Fuchs, R.T., Mabuchi, M., Curcuru, J.L., and Robb, G.B. (2019). *Staphylococcus aureus* Cas9 is a multiple-turnover enzyme. RNA *25*, 35–44. https://doi.org/10.1261/rna.067355.118.

38. Motwani, M., Pesiridis, S., and Fitzgerald, K.A. (2019). DNA sensing by the cGAS–STING pathway in health and disease. Nat. Rev. Genet. *20*, 657–674. https://doi.org/10.1038/s41576-019-0151-1.

39. An, J., Zhang, C.-P., Qiu, H.-Y., Zhang, H.-X., Chen, Q.-B., Zhang, Y.-M., Lei, X.-L., Zhang, C.-X., Yin, H., and Zhang, Y. (2024). Enhancement of the viability of T cells electroporated with DNA via osmotic dampening of the DNA-sensing cGAS–STING pathway. Nat. Biomed. Eng. *8*, 149–164. https://doi.org/10.1038/s41551-023-01073-7.

40. Zila, V., Margiotta, E., Turoňová, B., Müller, T.G., Zimmerli, C.E., Mattei, S., Allegretti, M., Börner, K., Rada, J., Müller, B., et al. (2021). Cone-shaped HIV-1 capsids are transported through intact nuclear pores. Cell *184*, 1032–1046.e18. https://doi.org/10.1016/j.cell.2021.01.025.

41. Dickson, C.F., Hertel, S., Tuckwell, A.J., Li, N., Ruan, J., Al-Izzi, S.C., Ariotti, N., Sierecki, E., Gambin, Y., Morris, R.G., et al. (2024). The HIV capsid mimics karyopherin engagement of FG-nucleoporins. Nature *626*, 836–842. https://doi.org/10.1038/s41586-023-06969-7.

42. Fu, L., Weiskopf, E.N., Akkermans, O., Swanson, N.A., Cheng, S., Schwartz, T.U., and Görlich, D. (2024). HIV-1 capsids enter the FG phase of nuclear pores like a transport receptor. Nature *626*, 843–851. https://doi.org/10.1038/s41586-023-06966-w.

43. Papa, G., Albecka, A., Mallery, D., Vaysburd, M., Renner, N., and James, L.C. (2023). IP6-stabilised HIV capsids evade cGAS/STING-mediated host immune sensing. EMBO Rep. *24*, e56275. https://doi.org/10.15252/embr.202256275.

44. Cornu, T.I., and Cathomen, T. (2007). Targeted genome modifications using integrase-deficient lentiviral vectors. Mol. Ther. *15*, 2107–2113. https://doi.org/10.1038/sj.mt.6300345.

45. Lombardo, A., Genovese, P., Beausejour, C.M., Colleoni, S., Lee, Y.-L., Kim, K.A., Ando, D., Urnov, F.D., Galli, C., Gregory, P.D., et al. (2007). Gene editing in human stem cells using zinc finger nucleases and integrase-defective lentiviral vector delivery. Nat. Biotechnol. *25*, 1298–1306. https://doi.org/10.1038/nbt1353.

46. Tschorn, N., Söhngen, C., Berg, K., and Stitz, J. (2022). Ecotropic HIV-1 vectors pseudotyped with R-peptide-deleted envelope protein variants reveal improved gene transfer efficiencies. Virology *577*, 124–130. https://doi.org/10.1016/j.virol.2022.09.008.

47. Albritton, L.M., Tseng, L., Scadden, D., and Cunningham, J.M. (1989). A putative murine ecotropic retrovirus receptor gene encodes a multiple membrane-spanning protein and confers susceptibility to virus infection. Cell *57*, 659–666. https://doi.org/10.1016/0092-8674(89)90134-7.

48. Mangeot, P.-E., Dollet, S., Girard, M., Ciancia, C., Joly, S., Peschanski, M., and Lotteau, V. (2011). Protein transfer into human cells by VSV-G-induced nanovesicles. Mol. Ther. *19*, 1656–1666. https://doi.org/10.1038/mt.2011.138.

49. Fok, J.H.L., Ramos-Montoya, A., Vazquez-Chantada, M., Wijnhoven, P.W.G., Follia, V., James, N., Farrington, P.M., Karmokar, A., Willis, S.E., Cairns, J., et al. (2019). AZD7648 is a potent and selective DNA-PK inhibitor that enhances radiation, chemotherapy and olaparib activity. Nat. Commun. *10*, 5065. https://doi.org/10.1038/s41467-019-12836-9.

50. Truong, D.-J.J., Armbrust, N., Geilenkeuser, J., Lederer, E.-M., Santl, T.H., Beyer, M., Ittermann, S., Steinmaßl, E., Dyka, M., Raffl, G., et al. (2022). Intron-encoded cistronic transcripts for minimally invasive monitoring of coding and non-coding RNAs. Nat. Cell Biol. *24*, 1666–1676. https://doi.org/10.1038/s41556-022-00998-6.

51. Wimberger, S., Akrap, N., Firth, M., Brengdahl, J., Engberg, S., Schwinn, M.K., Slater, M.R., Lundin, A., Hsieh, P.-P., Li, S., et al. (2023). Simultaneous inhibition of DNA-PK and Polθ improves integration efficiency and precision of genome editing. Nat. Commun. *14*, 4761. https://doi.org/10.1038/s41467-023-40344-4.

52. Vora, S., Cheng, J., Xiao, R., VanDusen, N.J., Quintino, L., Pu, W.T., Vandenberghe, L.H., Chavez, A., and Church, G. (2018). Rational design of a compact CRISPR-Cas9 activator for AAV-mediated delivery. Preprint at bioRxiv. https://doi.org/10.1101/298620.

53. Truong, D.-J.J., Phlairaharn, T., Eßwein, B., Gruber, C., Tümen, D., Baligács, E., Armbrust, N., Vaccaro, F.L., Lederer, E.-M., Beck, E.M., et al. (2021). Non-invasive and high-throughput interrogation of exon-specific isoform expression. Nat. Cell Biol. *23*, 652–663. https://doi.org/10.1038/s41556-021-00678-x.

54. Nissim, L., Perli, S.D., Fridkin, A., Perez-Pinera, P., and Lu, T.K. (2014). Multiplexed and programmable regulation of gene networks with an integrated RNA and CRISPR/Cas toolkit in human cells. Mol. Cell *54*, 698–710. https://doi.org/10.1016/j.molcel.2014.04.022.

55. Kurata, M., Wolf, N.K., Lahr, W.S., Weg, M.T., Kluesner, M.G., Lee, S., Hui, K., Shiraiwa, M., Webber, B.R., and Moriarity, B.S. (2018). Highly multiplexed genome engineering using CRISPR/Cas9 gRNA arrays. PLoS One *13*, e0198714. https://doi.org/10.1371/journal.pone.0198714.

56. Liu, Y., Yang, G., Huang, S., Li, X., Wang, X., Li, G., Chi, T., Chen, Y., Huang, X., and Wang, X. (2021). Enhancing prime editing by Csy4-mediated processing of pegRNA. Cell Res. *31*, 1134–1136. https://doi.org/10.1038/s41422-021-00520-x.

57. Sternberg, S.H., Haurwitz, R.E., and Doudna, J.A. (2012). Mechanism of substrate selection by a highly specific CRISPR endoribonuclease. RNA *18*, 661–672. https://doi.org/10.1261/rna.030882.111.

58. Lim, F., Downey, T.P., and Peabody, D.S. (2001). Translational Repression and Specific RNA Binding by the Coat Protein of the Pseudomonas Phage PP7. J. Biol. Chem. *276*, 22507–22513. https://doi.org/10.1074/jbc.M102411200.

59. Accola, M.A., Strack, B., and Göttlinger, H.G. (2000). Efficient Particle Production by Minimal Gag Constructs Which Retain the Carboxy-Terminal Domain of Human Immunodeficiency Virus Type 1 Capsid-p2 and a Late Assembly Domain. J. Virol. *74*, 5395–5402. https://doi.org/10.1128/jvi.74.12.5395-5402.2000.

60. Urano, E., Aoki, T., Futahashi, Y., Murakami, T., Morikawa, Y., Yamamoto, N., and Komano, J. (2008). Substitution of the myristoylation signal of human immunodeficiency virus type 1 Pr55Gag with the phospholipase C-δ1 pleckstrin homology domain results in infectious pseudovirion production. J. Gen. Virol. *89*, 3144–3149. https://doi.org/10.1099/vir.0.2008/004820-0.

61. Qin, J.Y., Zhang, L., Clift, K.L., Hulur, I., Xiang, A.P., Ren, B.-Z., and Lahn, B.T. (2010). Systematic comparison of constitutive promoters and the doxycycline-inducible promoter. PLoS One *5*, e10611. https://doi.org/10.1371/journal.pone.0010611.

62. Malinin, N.L., Lee, G., Lazzarotto, C.R., Li, Y., Zheng, Z., Nguyen, N.T., Liebers, M., Topkar, V.V., Iafrate, A.J., Le, L.P., et al. (2021). Defining genome-wide CRISPR-Cas genome-editing nuclease activity with GUIDE-seq. Nat. Protoc. *16*, 5592–5615. https://doi.org/10.1038/s41596-021-00626-x.

63. Madison, B.B., Patil, D., Richter, M., Li, X., Tong, M., Cranert, S., Wang, X., Martin, R., Xi, H., Tan, Y., et al. (2022). Cas-CLOVER is a novel high-fidelity nuclease for safe and robust generation of TSCM-enriched allogeneic CAR-T cells. Mol. Ther. Nucleic Acids *29*, 979–995. https://doi.org/10.1016/j.omtn.2022.06.003.

64. Horna, P., Weybright, M.J., Ferrari, M., Jungherz, D., Peng, Y., Akbar, Z., Tudor Ilca, F., Otteson, G.E., Seheult, J.N., Ortmann, J., et al. (2024). Dual T-cell constant β chain (TRBC)1 and TRBC2 staining for the identification of T-cell neoplasms by flow cytometry. Blood Cancer J. *14*, 34. https://doi.org/10.1038/s41408-024-01002-0.

65. Suh, S., Choi, E.H., Raguram, A., Liu, D.R., and Palczewski, K. (2022). Precision genome editing in the eye. Proc. Natl. Acad. Sci. USA *119*, e2210104119. https://doi.org/10.1073/pnas.2210104119.

66. Du, S.W., Newby, G.A., Salom, D., Gao, F., Menezes, C.R., Suh, S., Choi, E.H., Chen, P.Z., Liu, D.R., and Palczewski, K. (2024). In vivo photoreceptor base editing ameliorates rhodopsin-E150K autosomal-recessive retinitis pigmentosa in mice. Proc. Natl. Acad. Sci. USA *121*, e2416827121. https://doi.org/10.1073/pnas.2416827121.

67. Suh, S., Choi, E.H., Leinonen, H., Foik, A.T., Newby, G.A., Yeh, W.-H., Dong, Z., Kiser, P.D., Lyon, D.C., Liu, D.R., et al. (2021). Restoration of visual function in adult mice with an inherited retinal disease via adenine base editing. Nat. Biomed. Eng. *5*, 169–178. https://doi.org/10.1038/s41551-020-00632-6.

68. Choi, E.H., Suh, S., Foik, A.T., Leinonen, H., Newby, G.A., Gao, X.D., Banskota, S., Hoang, T., Du, S.W., Dong, Z., et al. (2022). In vivo base editing rescues cone photoreceptors in a mouse model of early-onset inherited retinal degeneration. Nat. Commun. *13*, 1830. https://doi.org/10.1038/s41467-022-29490-3.

69. Shi, Y., Kirwan, P., and Livesey, F.J. (2012). Directed differentiation of human pluripotent stem cells to cerebral cortex neurons and neural networks. Nat. Protoc. *7*, 1836–1846. https://doi.org/10.1038/nprot.2012.116.

70. Votteler, J., Ogohara, C., Yi, S., Hsia, Y., Nattermann, U., Belnap, D.M., King, N.P., and Sundquist, W.I. (2016). Designed proteins induce the formation of nanocage-containing extracellular vesicles. Nature *540*, 292–295. https://doi.org/10.1038/nature20607.

71. Horns, F., Martinez, J.A., Fan, C., Haque, M., Linton, J.M., Tobin, V., Santat, L., Maggiolo, A.O., Bjorkman, P.J., Lois, C., et al. (2023). Engineering RNA export for measurement and manipulation of living cells. Cell *186*, 3642–3658.e32. https://doi.org/10.1016/j.cell.2023.06.013.

Please cite this article in press as: Geilenkeuser et al., Engineered nucleocytosolic vehicles for loading of programmable editors, Cell (2025), https://doi.org/10.1016/j.cell.2025.03.015

STAR★METHODS

KEY RESOURCES TABLE

REAGENT or RESOURCE	SOURCE	IDENTIFIER
Antibodies		
anti-RPE65 clone KPSA1	UC Irvine	N/A
anti-beta-actin clone 13E5	Cell Signaling Tech-nologies	4970; RRID:AB_2223172
anti-MFRP	R&D Systems	AF3445; RRID:AB_2142759
donkey anti-goat IgG HRP	Thermo Thermo Fisher Scientific	A16005; RRID:AB_2534679
anti-mouse IgG HRP	Cell Signaling Technologies	7076; RRID:AB_330924
anti-rabbit IgG HRP	Cell Signaling Technologies	7074S; RRID:AB_2099233
PE anti-human HLA-A,B,C Antibody	Biolegend	311406; RRID:AB_314875
APC anti-human CD3 Antibody	Biolegend	317318; RRID:AB_1937212
Bacterial and virus strains		
NEB Stable Competent *E. coli*	New England BioLabs	C3040H
Chemicals, peptides, and recombinant proteins		
Poly-L-lysine solution	Sigma-Aldrich, Merck	P4832
Advanced DMEM	Gibco, Thermo Thermo Fisher Scientific	12491015
RPMI 1640 Medium	Gibco, Thermo Thermo Fisher Scientific	11875093
Essential 8 Flex Medium Kit	Gibco, Thermo Thermo Fisher Scientific	A2858501
Geltrex LDEV-Free Reduced Growth Factor Basement Membrane Matrix	Gibco, Thermo Thermo Fisher Scientific	A1413201
Fetal Bovine Serum	Gibco, Thermo Thermo Fisher Scientific	A5256701
Penicillin-Streptomycin	Sigma-Aldrich, Merck	P4333
Accutase - Enzyme Cell Detachment Medium	Invitrogen, Thermo Fisher Scientific	00-4555-56
DPBS, calcium, magnesium	Gibco, Thermo Thermo Fisher Scientific	14190144
D(+)-Saccharose	ROTH	9097
anti-CD3/CD28 Dynabeads	Gibco, Thermo Thermo Fisher Scientific	40203D
recombinant human IL-2	Peprotech	200-02
jetOPTIMUS® transfection reagent	Polyplus	101000006
Critical commercial assays		
Plasmid Maxi Kit	QIAGEN	12165
Nano-Glo® HiBiT Lytic Detection System	Promega	N3030
Lenti-X p24 Rapid Titer Kit	Takara Bio	631476
QuickTiter MuLV p30 Core Antigen ELISA Kit	Cell Biolabs	VPK-156
Quick-DNA 96 Kit	Zymo Research	D3011
Experimental models: Cell lines		
HEK293T as producer cell line	ECACC	12022001; RRID:CVCL_0063
HEK293	ECACC	85120602; RRID:CVCL_0045
Jurkat E6.1	ECACC	88042803; RRID:CVCL_0367
Neuro-2a	ECACC	89121404; RRID:CVCL_0470
hiPSCs	Helmholtz Zentrum München (HMGU)	ISFi001-A; RRID:CVCL_YT30
primary human T cells	Technical University Munich	N/A
Small airway epithelial cells	Cell Systems	FC-0106
Experimental models: Organisms/strains		
C57BL/6J mice	Jackson Laboratory	RRID:IMSR_JAX:000664
rd6 mice	Jackson Laboratory	RRID:IMSR_JAX:003684

(*Continued on next page*)

Please cite this article in press as: Geilenkeuser et al., Engineered nucleocytosolic vehicles for loading of programmable editors, Cell (2025), https://doi.org/10.1016/j.cell.2025.03.015

Continued

REAGENT or RESOURCE	SOURCE	IDENTIFIER
rd12 mice	Jackson Laboratory	RRID:IMSR_JAX:005379
Oligonucleotides		
NGS_B2M_fw	CGGTCTCACAAGCATGGATGC TTGTTGGGAAGGTGGAAGCTC	N/A
NGS_B2M_rv	CACAATCGAGCTCCATCTGTGG ACCAGTCCTTGCTGAAAGACAAG	N/A
NGS_TRBC1/2_fw	CGGTCTCACAAGCATGGATGCT CAATGACTCCAGATACTGCCTG	N/A
NGS_TRBC1/2_rv	CACAATCGAGCTCCATCTGTGGC TACCTGGATCTTTCCATTTTCC	N/A
rd6_genomic_HTS_F	ACACTCTTTCCCTACACGACGCTCTTCCG ATCTNNNNAAGAACCCACTGCTCACCCGA	N/A
rd6_genomic_HTS_R	TGGAGTTCAGACGTGTGCTCTTCCGATC TAGAGGTCTTCCCCAACCTGCAA	N/A
rd12_genomic_HTS_F	ACACTCTTTCCCTACACGACGCTCTTCCG ATCTNNNNTGATATCTCACTTTGCTGCAGG	N/A
rd12_genomic_HTS_R	TGGAGTTCAGACGTGTGCTCTTCCGATCTA TGGCTAGACCATGAAGAAAGAAG	N/A
Recombinant DNA		
pCMV-VSV-G	Addgene	8454
pRSV-REV	Addgene	12253
psPAX2-D64V	Addgene	63586
pCMV_ENVLPE^{+}	This study	232427
pCMV_iPE-C_P2A_Csy4	This study	232428
pCMV_ABE8e	This study	232429
pCMV_Cas9	This study	232430
pCMV_miniENVLPE	This study	232431
pU6_empty-sgRNA(PP7)	This study	232432
pU6_rd6_pegRNA_(PP7-C4-Q1)	This study	232433
pU6_rd6_nsgRNA(PP7)	This study	232434
pU6_rd12_pegRNA_(PP7-C4-Q1)	This study	232435
pU6_rd12_nsgRNA(PP7)	This study	232436
pU6_HEK3+1T>A_(PP7-C4-Q1)	This study	232437
pU6_HEK3_nsgRNA(PP7)	This study	232444
pU6_B2M_sgRNA(PP7)	This study	232438
pCMV_CreNLS_PP7	This study	232439
pCMV_mGL_PP7	This study	232440
Software and algorithms		
Geneious Prime 2022/2023/2024	Biomatters (https://www.geneious.com/)	N/A
Prism 9/10	GraphPad (https://www.graphpad.com)	N/A
FlowJo v10	BD Biosciences (https://www.flowjo.com/solutions/flowjo)	N/A
Other		
38.5 mL, Open-Top Thinwall Ultra-Clear Tube, 25 x 89 mm	Beckman Coulter	344058
Millex®-HV Filter Unit (Sterile)	Merck Millipore	SLHV033RS
BD Plastipak™ Plastic Concentric Luer-Lock Syringe	BD	300865
Injekt® Solo Luer, disposable syringes 5 mL	Braun	4606051V
Sterican needle 0.80 x 120 mm	Braun	4665643
Swinging-bucket centrifuge rotor	Beckman Coulter	SW 28

(*Continued on next page*)

Please cite this article in press as: Geilenkeuser et al., Engineered nucleocytosolic vehicles for loading of programmable editors, Cell (2025), https://doi.org/10.1016/j.cell.2025.03.015

Continued

REAGENT or RESOURCE	SOURCE	IDENTIFIER
Cotton Swabs 2,2/145 mm	Greiner Bio-One	421084
Ultrafree-CL Centrifugal Filter	Merck Millipore	UFC40GV0S
Amicon® Ultra-4 Centrifugal Filter Unit	Merck Millipore	UFC810024

EXPERIMENTAL MODEL AND STUDY PARTICIPANT DETAILS

Animals

Mouse experiments and procedures were approved by the Institutional Animal Care and Use Committee at the University of California, Irvine and conform to the Association for Research in Vision and Ophthalmology Statement for the Use of Animals in Ophthalmic and Vision Research. Breeding colonies of wild-type C57BL/6J (000664), *rd6* (003684), and *rd12* (005379) mice were established by purchase from the Jackson Laboratory (Bar Harbor, ME). Mice were housed in the specific pathogen-free vivarium of the University of California, Irvine on a 12 h/12 h light/dark cycle and fed *ad libitum*. 5–7 weeks old homozygous mouse littermates were randomly assigned to experimental groups. Both male and female mice were used equally. No mice were involved in previous procedures.

Cell lines and cultivation

Cells were cultured at 37 °C, 5% CO_2, and an H_2O-saturated atmosphere.

HEK293T (ECACC: 12022001, Sigma-Aldrich) and HEK293 (ECACC 85120602) cells were maintained in advanced DMEM (Gibco, Thermo Fisher Scientific) supplemented with 10% FBS (Gibco, Thermo Fisher Scientific), GlutaMAX (Gibco, Thermo Fisher Scientific), 100 μg/ml Penicillin-Streptomycin (Gibco, Thermo Fisher Scientific), 10 μg/ml Piperacillin (Sigma-Aldrich), and 10 μg/ml Ciprofloxacin (Sigma-Aldrich). Cells were passaged at 90% confluence by removing the medium, washing with DPBS (Gibco, Thermo Fisher Scientific) and detaching the cells with Accutase solution (Gibco, Thermo Fisher Scientific). Cells were then incubated for 5–10 min at room temperature until a visible detachment of the cells was observed. Accutase was subsequently inactivated by addition of pre-warmed DMEM including 10% FBS and all supplements. Cells were then transferred into a new flask at an appropriate density, or counted and distributed on 96-well or 6-well plates for plasmid transfection or VLP transduction.

Jurkat E6.1 cells (ECACC 88042803) were maintained in RPMI media 1640 (Gibco, Thermo Fisher Scientific) with GlutaMAX (Gibco, Thermo Fisher Scientific) and 100 μg/ml Penicillin-Streptomycin (Gibco, Thermo Fisher Scientific). For transduction, they were seeded into 96-well plates at 25,000 cells/well. The proper density was achieved by centrifugation at 200 relative centrifugal force (rcf) for 2 min and subsequent dilution with RPMI 1640 to the desired density.

Human induced pluripotent stem cells (hiPSCs (ISFi001-A) were incubated in Essential 8 (E8) Flex medium (Thermo Fisher Scientific, A2858501) at 37 °C under 5% CO2 saturation on (v/v) Vitronectin-coated (A31804, Thermo Fisher Scientific) plates. At 70% confluency, the cells were subcultivated using StemMACS Passaging Solution XF (Miltenyi Biotec) by incubating the cells for 6 min at room temperature. Subsequently, StemMACS Passaging Solution XF was removed by aspiration, and hiPSC colonies were harvested in E8 flex medium and chopped using a 1000 μl pipette tip. Collected cells were seeded on 96-, 48-, 24-, or 6-well plates at the appropriate cell densities.

Small airway epithelial cells (donor 08938, purchased from Cell systems) were thawed in a 37 °C water bath and seeded onto a 10 cm^2 petri dish containing 15 ml warm medium (airway epithelial growth medium (Promocell) supplemented with bovine pituitary extract, hydrocortisone, human epidermal growth factor (hEGF), epinephrine, transferrin, insulin, retinoic acid, and triiodothyronine (Promocell) according to the company's instructions, further supplemented with Primocin (Invivogen) at 100 μg ml^{-1}). The medium was changed every 2 days until the culture was 80% confluent, before being detached using Accutase (Sigma) and seeded into 96-well plates at 25k cells/well in 200 μl of airway-epithelial growth medium, 24 hours before transduction.

METHOD DETAILS

Molecular cloning and DNA analysis

Genetic constructs

The ENVLPE packaging plasmid is based on psPAX2$_{D64V}$ encoding CAG-driven Gag/Gag–Pol with a D64V mutation in the HIV-1-integrase domain. During optimization, Gag/Gag–Pol (psPAX2$_{D64V}$) and shuttling Gag-PCP variants were co-expressed on separate plasmids. Later, we grafted the optimized CAG-driven shuttling Gag-PCP/Gag–Csy4 expression cassettes to yield equimolar expression of Gag/Gag–Pol and Gag-PCP/Gag–Csy4 into psPAX2$_{D64V}$. For CMV-driven ENVLPE$^+$, the CAG promoters were exchanged for CMV promoters taken from pCMV-VSV-G. All core plasmids will be deposited on Addgene. (pe)gRNA sequences are listed in Table S1.

Please cite this article in press as: Geilenkeuser et al., Engineered nucleocytosolic vehicles for loading of programmable editors, Cell (2025), https://doi.org/10.1016/j.cell.2025.03.015

PCR

Single-stranded primer deoxyribonucleotides (Integrated DNA Technologies (IDT)) were resolubilized (100 μM) in nuclease-free water. PCR reactions with plasmid and genomic DNA templates were performed with Platinum SuperFi II PCR Master Mix (Thermo Fisher Scientific) according to the manufacturer's protocol. PCR reactions were purified by DNA agarose gel electrophoresis and subsequent DNA extraction using a Monarch DNA Gel Extraction Kit (New England Biolabs (NEB)).

DNA digestion with restriction endonucleases

Samples were digested with NEB restriction enzymes according to the manufacturer's protocol in a total volume of 40 μl with 1–3 μg of plasmid DNA. Afterwards, DNA fragments were purified by agarose gel-electrophoresis and subsequent purification using Monarch DNA Gel Extraction Kit (NEB).

Ligation and Gibson assembly

Concentrations of agarose-gel purified DNA fragments were determined by a spectrophotometer (NanoDrop 1000, Thermo Fisher Scientific). Ligations were carried out at room temperature for 5–10 min, with 50–100 ng backbone-DNA (DNA fragment containing the ori) in a 20 μl volume, with molar backbone:insert ratios of 1:1–3, using T4 DNA ligase (Quick Ligation Kit, NEB). Gibson assemblies were performed with 75 ng of backbone DNA in a 15 μl reaction volume and molar backbone:insert ratios of 1:1–5, using NEBuilder HiFi DNA Assembly Master Mix (2×) (NEB) for 20–60 min at 50 °C.

DNA agarose gel-electrophoresis

1% (m/m) agarose (Agarose Standard, Carl Roth) gels were prepared in 1× TAE buffer and 1:10,000 SYBR Safe stain (Thermo Fisher Scientific). Gel electrophoreses were carried out for 20–40 min at 100 V. For size determination, 1 kb Plus DNA Ladder (NEB) was used. DNA samples were mixed prior to loading with Gel Loading Dye (Purple, 6×) (NEB).

Bacterial strains (E. coli) for molecular cloning

Chemically competent *E. coli* K12 cells (NEB Stable) were used for transformation of circular plasmid DNA. For plasmid amplification, carbenicillin (Carl Roth) was used as a selection agent at a final concentration of 100 μg/ml. All bacterial cells were incubated in Lysogeny Broth (LB) medium or on LB agar plates, including the respective antibiotics.

Bacterial transformation with plasmid DNA

Transformation was performed by mixing 1-5 μl of ligation- or Gibson-reaction mixture with 50 μl of thawed, chemically competent cells, which were incubated on ice for 30 min before heat shocking at 42 °C for 30 s. Afterward, cells were incubated on ice for 5 min and mixed with 450 μl of SOC-medium (NEB). Transformed cells were then plated on agar plates containing an appropriate type and concentration of antibiotics according to the supplier's information. Plates were incubated overnight at 37 °C.

Plasmid DNA purification and Sanger sequencing

E. coli colonies with correct potential constructs were inoculated from agar plates in 2 ml LB medium at 37 °C with the respective antibiotics, and incubated for at least 6 h or overnight. Plasmid DNA was extracted with a Monarch Plasmid Miniprep Kit (NEB) according to the manufacturer's protocol, and sent out for Sanger sequencing (GENEWIZ, Azenta Life Sciences). Sanger-sequencing-validated clones were inoculated in 100 ml LB medium overnight at 37 °C containing the respective antibiotic selection agent. Plasmid DNA was extracted using a Plasmid Maxi Kit (QIAGEN).

Genomic DNA isolation

72 hours after transfection or transduction in 96-well format, genomic DNA was isolated with a Quick-DNA 96 Kit (Zymo Research) according to the manufacturer's protocol, with an elution volume of 30 μl.

For animal experiments, after the mice were euthanized, the anterior segment (iris, lens, cornea, ciliary body) was removed by dissection, and the neural retina was peeled from the posterior eyecup (RPE, choroid, and sclera). The eyecup was then immediately immersed in buffer RLT Plus with 1% beta-mercaptoethanol (Qiagen # 1053393), and the RPE was disassociated from the eyecup by pipetting before homogenization by QiaShredder (Qiagen # 79654). DNA was then isolated with the AllPrep DNA/RNA Micro kit according to manufacturer instructions (Qiagen # 80284).

Amplicon PCR and purification

Primer sequences are provided in Table S1. PCR was performed as described above using ~50 ng of gDNA and appropriate primers for each target. Amplicon lengths were designed to approach 250 bp for sequencing. PCR purification was performed using the DNA Clean & Concentrator-5 Kit (Zymo Research) according to the manufacturer's protocol with an elution volume of 30 μl.

For analysis of animal experiments, PCR was performed with Phusion Plus green mastermix (Thermo # F632S) and PCR products were checked by electrophoresis on a 1% agarose TAE gel. PCR products were then purified with a QiaQuick MinElute PCR kit (Qiagen # 28004) and quantified spectrophotometrically with a NanoDrop 1000 spectrophotometer.

Amplicon sequencing and analysis

Genomic DNA was used as a template for PCR on the locus of interest (40 cycles). For pooled analysis of multiple samples, a second outer PCR using barcoded primers was performed and the samples were subsequently pooled. PCR products were gel-purified as described above, normalized to 20 ng/μl and submitted for Amp-EZ sequencing (GENEWIZ, Azenta Life Sciences). For samples from animal experiments, next-generation sequencing was performed commercially by Quintara Biosciences (Hayward, CA) by Illumina MiSeq utilizing 2 × 250 bp chemistry.

The resulting fastq files containing paired reads were analyzed with Geneious (including barcode separation for pooled samples), trimming all merged reads shorter than 200 bp and using an analysis window spanning at least 50 bp around the nicking site.

Please cite this article in press as: Geilenkeuser et al., Engineered nucleocytosolic vehicles for loading of programmable editors, Cell (2025), https://doi.org/10.1016/j.cell.2025.03.015

Alternatively, PCR amplicons were analyzed *via* Sanger sequencing followed by chromatogram quantification with interference of CRISPR edits (ICE, Synthego).

Mammalian cell culture

HEK293T 'blue' mGreenLantern reporter generation

Cell lines were created by cloning the reporter coding for the blue-shifted mGreenlantern mutant (G65S, Y66H) with a CAG-promoter, a bovine growth hormone (bGH) polyadenylation signal (pA) flanked by homology arms for a safe-harbor locus of choice. To create a HEK293T reporter cell line, cells were transfected with the CRISPR donor plasmid and a second plasmid encoding Cas9 and the corresponding gRNA. Cells were transfected according to the manufacturer's protocol (jetOPTIMUS, Polyplus) 24 hours post-seeding on a 6-well plate (600k cells in 3 ml per well) in the presence of 0.5 μM AZD7648 (HY-111783; MedChemExpress), a DNA-PKcs inhibitor, and a CAG-promoter-driven i53, a 53BP1 inhibitor, to inhibit NHEJ and thereby shifting the DNA repair towards HDR. The surviving polyclonal population was monoclonalized using limiting dilution in 96-well plates, and selected clones were genotyped to determine homozygosity.

hiPSC reporter lines generation

The hiPSC reporter cell lines were generated by integrating the blue-shifted mGreenlantern mutant (G65S, Y66H) (Figure S17A) or the enhanced traffic light reporter v2 (eTLRv2) (Figure S18A) version 2 into the human safe-harbor locus *AAVS1*.

hiPSCs (ISFi001-A (RRID:CVCL_YT30)) were passaged using Accutase (Sigma, A6964-500ML) for 10 min at 37 °C, counted using a Neubauer improved cell-counting chamber (Carl Roth, PK361), and electroporated as single cells in a 100 μl cuvette using the CB-156 program with the P3 Primary Cell 4D-Nucleofector X Kit (Lonza Group Ltd) and the 4D Nucleofector (Lonza Group Ltd) according to the manufacturer's instructions (2×10^6 hiPSCs, 1 μg Cas9-gRNA plasmid, 2 μg integration plasmid). After nucleofection, hiPSCs were seeded on one well of a Vitronectin-coated 6-well plate, and incubated in E8 flex medium supplemented with 10 μM Y27632 (Enzo Life Sciences, ALX-270333-M005) and 0.5 μM AZD7648 (HY-111783; MedChemExpress) for 24 h. Cells were allowed to recover to ~70 % confluency in E8 flex medium. Gene-edited hiPSCs were selected with puromycin (A1113803, Thermo Fisher Scientific) at a concentration of 0.5μg/ml in E8 flex medium for 3 days; then at 1 μg ml^{-1} puromycin for 4 additional days. Subsequently, hiPSC colonies were clonalized and expanded. For characterization, genomic DNA was isolated using the QIAamp DNA Mini Kit (Qiagen) according to the manufacturer's instructions for cultured cells. A correct integration was verified by genotyping PCRs and Sanger sequencing of amplicons reaching over the 5' homology arm into the CAG promoter (P1: CCACTCTGTGCTGACCACTC; P2: AGGCGGGCCATTTACCGTAAG), over the 3' homology arm into the puromycin resistance gene (P3: GAGTTTGCCAAGC AGTCACC; P4: CCTGAGGGCCCTAGAACCT), and within the knock-in from the CAG promoter to the pA

(P5: TTCGGCTTCTGGCGTGTG; P6: CGAGGCTGATCAGCGAGCTC). Heterozygosity was confirmed by a genotyping PCR amplifying the region of the homology arms (P1; P3). The expression and functionality of the integrated reporter were verified by FACS analysis. In total, 2 clones per reporter cell line ('blue' mGreenLantern reporter or eTLR) were selected and further quality controlled.

Quality control of edited hiPSCs

Karyotyping

Single-nucleotide polymorphism (SNP) array-based karyotyping was performed as described previously. The genomic DNA of the hiPSCs was extracted using the QIAamp DNA Mini Kit (Qiagen) according to the manufacturer's instructions. The DNA concentration was measured using Quant-iT PicoGreen (Invitrogen, Thermo Fisher Scientific) according to the Infinium HTS Assay Protocol Guide (Illumina). SNPs were identified using an Infinium Global Screening Array-24 v3.0 Kit (Illumina) and an iScan system (Illumina) according to the Infinium HTS Assay Protocol Guide.

The assay was performed by the Genomics Core Facility of Helmholtz Munich. Clustering, quality control, and SNP calling were done using GenomeStudio 2.0.5 (Illumina) as described. Copy number variations (CNVs) on autosomes were determined using the cnvPartition v3.2.1 (Illumina) plugin with default settings, including a confidence threshold of 50. No CNVs exceeding 1 kbp could be identified for the 'blue' mGreenLantern reporter (Figure S17B), nor the eTLRv2 (Figure S18B) hiPSC lines.

Pluripotency staining

hiPSC were cultured on Vitronectin-coated glass coverslips for 5 days. Cells were fixed with 10% Formalin (Sigma, F5554) for 20 min at 37 °C, washed twice with PBS (Thermo Fisher Scientific), and permeabilized/blocked using a blocking solution (PBS containing 1 % BSA (Sigma-Aldrich, A7906-500G) and 0.3% Triton X-100 (Sigma-Aldrich, T9284)) for 15 min at room temperature. Primary antibodies were diluted in a blocking solution, and antibody incubation was performed at 4 °C overnight. Cells were washed twice with PBS and incubated in a blocking solution containing secondary antibodies for 2 h at room temperature. Nuclei were stained with PBS containing 0.1 μg/ml DAPI (Thermo Fisher Scientific, 62248) for 10 min at room temperature. Cells were washed twice with PBS and coverslips were mounted using Aqua-Poly/Mount (Polysciences Inc., 18606-20). Primary antibodies were diluted as follows: NANOG (AF1997, R&D Systems; 1:200), POU5F1 (2840 S, Cell Signaling; 1:500), SOX2 (sc-365823, Santa Cruz; 1:500). Secondary antibodies were diluted as follows: donkey-anti-mouse IgG Alexa 488 (A21202, Thermo Fisher Scientific; 1:500), donkey-anti-goat IgG Alexa 594 (A11058, Thermo Fisher Scientific; 1:500), donkey-anti-rabbit IgG Alexa 594 (A21207, Thermo Fisher Scientific; 1:500). Fluorescence images were acquired using an EVOS FL Auto Imaging System (Thermo Fisher Scientific) (Figures S17C and S18C).

Please cite this article in press as: Geilenkeuser et al., Engineered nucleocytosolic vehicles for loading of programmable editors, Cell (2025), https://doi.org/10.1016/j.cell.2025.03.015

Trilineage differentiation

The differentiation potential of edited cells was verified by trilineage differentiation into the ectoderm, mesoderm, and endoderm lineage. hiPSCs were maintained on Vitronectin-coated 6-well plates. At 70% confluency, hiPSCs were passaged using Accutase for 10 min at 37 °C, sheared to single cells by pipetting using a 1,000 μl tip, and diluted in E8 flex medium containing 10 μM ROCK inhibitor Y27632. hiPSCs were harvested at 200 rcf for 5 min and resuspended in E8 flex medium containing 10 μM ROCK inhibitor Y27632. Cell number was determined using a Neubauer improved cell counting chamber, and 50,000 cells per well with 9 replicates per cell line were seeded in E8 flex medium containing 10 μM ROCK inhibitor Y27632 on Vitronectin-coated 96-well plates. Trilineage differentiation was performed in triplicates using the STEMdiff Trilineage Differentiation Kit (StemCell Technologies) according to the manufacturer's instructions. Subsequently, cells were fixed with 10% Formalin (Sigma, F5554) for 20 min at 37 °C. Differentiation efficiency was quantified by immunostainings as described above for the pluripotency staining. Primary antibodies were diluted as follows: SOX2 (sc-365823, Santa Cruz; 1:500), NES (Ma1110, Thermo Fisher Scientific; 1:250), AFP (MAB1368, R&D; 1:500), SOX17 (AF1924, R&D Systems; 1:500), NCAM1 (Sc-106, Santa Cruz; 1:500), TBXT (ab209665, Abcam; 1:500). Secondary antibodies were diluted as follows: donkey-anti-mouse IgG Alexa 488 (A21202, Thermo Fisher Scientific; 1:500), donkey-anti-goat IgG Alexa 594 (A11058, Thermo Fisher Scientific; 1:500), donkey-anti-rabbit IgG Alexa 594 (A21207, Thermo Fisher Scientific; 1:500). Fluorescence images were acquired using an EVOS FL Auto Imaging System (Thermo Fisher Scientific) (Figures S17D and S18D).

Generation of hiPSC-derived cortical neurons

hiPSCs were differentiated into neuronal precursor cells and further into cortical neurons by using a dual SMAD-signaling inhibition strategy as described.[69] At 70% confluency, hiPSCs were passaged using Accutase for 10 min at 37 °C, sheared to single cells by pipetting using a 1000 μl tip and diluted in E8 flex medium containing 10 μM ROCK inhibitor Y27632. hiPSCs were harvested at 200f rcf for 5 min and resuspended in E8 flex medium containing 10 μM ROCK inhibitor Y27632. Cell number was determined using a Neubauer improved cell-counting chamber, and hiPSC were seeded on Vitronectin-coated 6-well plates at a density of 30,000 cells/cm^2. The next day (day 0), differentiation was started by replacing the E8 flex medium with neural-induction medium (50% DMEM/F12-GlutaMAX (Thermo Fisher Scientific, 31331093), 50% Neurobasal medium (Thermo Fisher Scientific, 21103049) supplemented with 1% B27 (Thermo Fisher Scientific, 17504044), 0.5% N2 (Thermo Fisher Scientific, 17502048), 0.5% GlutaMAX (Thermo Fisher Scientific, 35050061), 0.5% non-essential amino acids (Thermo Fisher Scientific, 11140035), 1% Penicillin-Streptomycin (Thermo Fisher Scientific, 15070063), 2.5 g/ml Insulin (Sigma, I3536-100MG), 10 μM SB431542 (Miltenyi Biotec, 130-106-275), 100 nM LDN193189 (Tocris Bioscience, 6053), and 0.02 % beta-mercaptoethanol (Thermo Fisher Scientific, 31350010)). The medium was replaced daily until day 21. On day 14, cells were reseeded on a 15 μg/ml poly-L-ornithine and 10 μg/ml laminin-coated 6-well plate at a ratio of 1:2. The neuroepithelial sheet was collected using a StemPro EZPassage tool (Thermo Fisher Scientific, 23181010) and transferred using a 1,000 μl tip. On day 21, neuronal precursor cells were reseeded and expanded. The medium was removed by aspiration, cells were washed once with PBS, and detached using Accutase for 10 min at 37 °C. Dissociated cells were diluted in neural-induction medium, centrifuged at 200 rcf for 5 min, and resuspended in neural-induction medium containing 10 μM ROCK inhibitor Y27632. Cell number was determined using a Neubauer improved cell-counting chamber, and neuronal precursor cells were seeded on poly-L-ornithine-laminin-coated 6-well plates at a density of 200,000 cells cm^2. On day 22, the medium was changed to neural-maintenance medium (50% DMEM/F12-GlutaMAX, 50% Neurobasal supplemented with 1% B27, 0.5% N2, 0.5% GlutaMAX, 0.5% non-essential amino acids, 1% penicillin-streptomycin, 2.5 g ml^{-1} insulin, 0.02 % beta-mercaptoethanol, 200 μM ascorbic acid 2-phosphate (Sigma, A8960-5G), and 20 ng/ml human BDNF (Miltenyi Biotec, 130-093-811)). The medium was replaced daily until day 50. On day 50, cortical neurons were reseeded on poly-L-ornithine-laminin-coated glass coverslips, and 96-, 48-, 24-, or 6-well plates for direct use. The medium was removed by aspiration, the cells were washed once with PBS, and detached using Accutase for 10 min at 37 °C. Dissociated cortical neurons were diluted in neural-maintenance medium, centrifuged at 200 rcf for 5 min, and resuspended in neural-maintenance medium containing 10 μM ROCK inhibitor Y27632. Cell number was determined using a Neubauer improved cell-counting chamber and cortical neurons were seeded on the desired vessels at a density of 200,000 cells/cm^2. Before use, cortical neurons were maintained at 37 °C under 5% CO2 saturation for 14 additional days, with medium changes every second day. Differentiation efficiency was verified by immunostainings as described above for the pluripotency staining. Cortical neurons grown on glass coverslips were fixed with 10% Formalin (Sigma, F5554) for 20 min at 37 °C. Primary antibodies were diluted as follows: BCL11B (Abcam, ab18465; 1:500), CUX1 (Sigma Aldrich, SAB1405681; 1:500), TUBB3 (T5076, Sigma-Aldrich; 1:1000), MAP2 (Sigma Aldrich, AB5622-I; 1:500). Secondary antibodies were diluted as follows: donkey-anti-mouse IgG Alexa 488 (A21202, Thermo Fisher Scientific; 1:500), donkey-anti-mouse IgG Alexa 594 (A21203, Thermo Fisher Scientific; 1:500), donkey-anti-rat IgG Alexa 488 (A21208, Thermo Fisher Scientific; 1:500), donkey-anti-rabbit IgG Alexa 594 (A21207, Thermo Fisher Scientific; 1:500). Fluorescence images were acquired using an EVOS FL Auto Imaging System (Thermo Fisher Scientific) (Figures S17E and S18E).

VLP production

A general schematic depiction of the VLP production process can be found in Figure S19.

Plasmid transfection for VLP production

For production on 6-well plates (poly-D-lysine-coated), 750,000 cells were seeded at 3 ml per well in full DMEM with 10% FBS 24 h prior to transfection. The cells were transfected (jetOPTIMUS, Polyplus) with a total of 1.2 μg plasmid DNA using JetOPTIMUS

transfection reagent. The reagent volume to DNA mass ratio (V/m) was 1:1 in a total volume of 120 μl (fill-up with JetOPTIMUS Buffer, 10 min incubation at room temperature for complex formation). The detailed plasmid stoichiometries of the different systems are shown in Table S1.

For production on 15 cm dishes (poly-D-lysine-coated), 12.5×10^6 cells were seeded in 50 ml per well in full DMEM with 10% FBS 24 h prior to transfection. The cells were transfected (jetOPTIMUS, Polyplus) with a total of 19.2 μg plasmid DNA using JetOPTIMUS transfection reagent. The reagent volume to DNA mass ratio (V/m) was 1:1 in a total volume of 1.92 ml (fill-up with JetOPTIMUS Buffer, 10 min incubation at room temperature for complex formation). The detailed plasmid stoichiometries of the different systems are shown in Table S1.

Concentration and transduction of VLPs

The supernatant (SN) containing the VLPs was sterile-filtered to remove cell debris and remaining lipofection reagents. Subsequently, the filtered SN was concentrated to approximately 1/30 of the original volume using a 100 kDa molecular weight cutoff filter (Amicon Ultra-4, UFC810024 (Merck)). For transduction (TD), the respective reporter cell line was seeded on a 96-well plate (25,000 cells in 200 μl advanced DMEM). 6 h post-seeding, the supernatant of one 6-well production (or a corresponding dilution in 2-fold steps) was applied to a triplicate of receiver cells on the 96-well plate without exceeding 20% of the total volume of the receiver cell's original growth medium. For optimizing the VLP system, cells were analyzed at 72 h post-TD when delivering an RNP complex, and 24 h post-TD when delivering mRNA.

Storage capabilities of the ENVLPE VLPs vary depending on pseudotyping. VSV-G pseudotyped VLPs can be stored at 4 °C for at least three days without significant loss of infectivity. For other pseudotyped VLPs it is recommended to quick-freeze the VLPs using liquid nitrogen and avoid repeated freeze-thaw cycles.

Ultracentrifugation of VLPs

For experiments with primary T lymphocytes and all animal studies, VLPs were purified by ultracentrifugation. After 72 hours of expression in a 15 cm dish (12,500,000 cells in 50 ml advanced DMEM), the supernatant was harvested and sterile-filtered (0.45 μm). 35 ml of the filtrate was transferred into a Beckman Coulter Ultra-Clear Tube, and 3 ml of a 20% sucrose PBS solution was layered below the supernatant. The supernatants were spun for two hours at 26,000 rpm in a Beckman LE-70 ultracentrifuge. The SW28 swinging-bucket rotor was cooled to 4 °C. After removing the supernatant, the rim of the centrifugation tubes were dried with cotton swabs and pellets were resuspended in 1/1000 of the original volume using PBS supplemented with 10% sucrose and 1× PenStrep.

IDLV production and transduction

For the production of ecotropic integrase-defective lentiviruses (IDLV) to facilitate editing of the 'blue' mGL reporter locus, HEK293T cells were seeded 1 day prior transfection on a 6-well plate in 3 ml advanced DMEM with a concentration of 200,000–250,000 cells/ml. The cells were transfected according to the manufacturer's protocol (jetOPTIMUS, Polyplus) with the following components: 400 ng psPAX2$_{D64V}$ (a gift from David Rawlings & Andrew Scharenberg (Addgene # 63586)), 600 ng lentiviral transfer vector encoding the HDR-donor, and 200 ng of the CMV promoter-driven ecotropic MMLV envelope protein (MMLV-Env$_{\Delta607\text{-}622}$). The IDLVs were purified as described for VLPs and then co-transduced with Cas9-ENVLPE. 4 days after transduction, green fluorescence was measured *via* FACS to quantify HDR events. Additionally, the decrease of blue fluorescence indicated the indel rate.

To facilitate the larger edit of the TLR locus, we produced VSV-G-pseudotyped IDLVs. For lipofection, 12,500,000 HEK293T cells were seeded on a 15 cm dish (poly-L-lysine coated) in 50 ml DMEM. 5376 ng psPAX2$_{D64V}$ (Addgene # 63586), 8064 ng lentiviral transfer vector encoding the HDR-donor, 2688 ng pRSV-REV (Addgene #12253) and 3072 ng of pCMV-VSV-G (Addgene #8454) were co-transfected according to the manufacturer's protocol (jetOPTIMUS, Polyplus). The Cas9-ENVLPE was also produced in a 15 cm dish. Both ENVLPE and IDLV were purified *via* ultracentrifugation and resuspended in PBS at 1/1000 of the original volume.

Cas9-ENVLPE and IDLVs were co-transduced in a 1:1 ratio.

Anti-FLAG staining

HEK293T cells were seeded (80,000 cells in 300 μl advanced DMEM) one day before transfection in 8-well μ-Slides (Ibidi). 48 hours post-TF, half of the medium was removed, and cells were pre-fixed with 10% neutral-buffered formalin (Sigma-Aldrich) for 5 minutes at room temperature, followed by fixation with 10% neutral buffered formalin for 10 min at room temperature. Afterward, cells were washed three times with DPBS before incubation for 2 h at room temperature with 1:1000 Monoclonal ANTI-FLAG M2 antibody from mouse (Sigma-Aldrich, 1 mg/ml) in DPBS containing 1% BSA (Sigma-Aldrich) and 1% Triton X-100 (Sigma-Aldrich) for permeabilization. Following three additional washing steps with DPBS, cells were treated with Cy3-conjugated goat anti-mouse IgG (2 mg/ml stock), diluted 1:100 in DPBS with 1% BSA, and incubated for 45 min at room temperature. The next washing step included Hoechst 33342 stain (10 mg/ml stock diluted 1:10,000 in DPBS), followed by two additional washing steps with DPBS. Confocal microscopy was performed using a Leica SP5 system (Leica Microsystems) under identical conditions for all samples across all experimental conditions.

Delivery of VLPs in primary T lymphocytes

Cryopreserved primary human T cells, isolated in-house (# 19661; Stem Cell Technologies) from anonymous healthy donors under an institutional review board-approved protocol, were thawed on day 0 and activated with anti-CD3/CD28 Dynabeads (#40203D; Gibco)

Please cite this article in press as: Geilenkeuser et al., Engineered nucleocytosolic vehicles for loading of programmable editors, Cell (2025), https://doi.org/10.1016/j.cell.2025.03.015

in RPMI medium (10% FBS and 1% P/S), supplemented with 20 IU/ml recombinant human IL-2 (#200-02; Peprotech). 50,000 T cells/well were plated in a 96-well U-bottom plate. One day afterward, the activated T cells were treated with VLPs, prepared *via* ultracentrifugation, targeting B2M and/or TRBC1/2 in duplicates or triplicates per condition. On the third day after T cell activation, cells were split in half, and fresh RPMI medium with recombinant IL-2 was added. On the fifth day following T cell activation, anti-CD3/CD28 beads were removed magnetically, and MHCI (#311406; Biolegend) and CD3 (#317318; Biolegend) surface presentation was analyzed by flow cytometry, while the respective *TRBC1/2* and *B2M* loci were analyzed *via* NGS following gDNA isolation and PCR.

For flow cytometry, cells were washed with FC buffer (PBS + 2% FBS), stained with the indicated antibodies (1:100 dilution) for 30 min at 4 °C in the dark, washed twice to remove unbound antibodies, and resuspended in FC buffer with DAPI (Thermo Fisher, #62247). Samples were acquired on a BD LSRFortessa and analyzed using FlowJo software (v10).

Viability and toxicity assays

To assess viability and cytotoxicity in receiver cells, HEK293T cells were seeded in a 96-well format (25,000 cells in 200 μl advanced DMEM) and transduced six hours post-seeding with the equivalent of half the supernatant of one 6-well production distributed across a triplicate. Additionally, hiPSCs cells were seeded as single cells (25,000 cells) on a Geltrex-coated 96-well plate in 100 μl E8 flex media supplemented with 10 μM Y27632 (Enzo Life Sciences, ALX-270333-M005). One day post-seeding, cells were washed with DPBS, 100 μl new E8 flex media was added and transduced with the equivalent of half the supernatant of one 6-well production distributed across a triplicate. One day post-TD, receiver cells were washed with DPBS, new pre-warmed media was added, and puromycin (2 μg/ml) was administrated in triplicate as a control. The CellTiter-Glo 2.0 Cell Viability Assay (Promega, G9241), as well as LDH-Glo Cytotoxicity Assay (Promega, J2380) were performed according to the manufacturer's protocol, 48 hours post-TD for HEK293T, and 24 hours post-TD for hiPSCs. Measurements were taken on a Varioskan LUX microplate reader (Thermo Fisher Scientific).

Flow cytometry

72 h post-transduction, cells were gently detached in a suitable volume of Accutase, pelleted (200 rcf, 5 min), and resuspended in ice-cold 0.4% formalin for 10 min. Fixed cells were pelleted again (200 rcf, 5 min) and resuspended in 200 μl ice-cold DPBS. Analysis was performed on the BD FACSaria II or the BD FACSymphony A3 Cell Analyzer (BD Biosciences). Data were analyzed with FlowJo (10.10.0, BD BioSciences). Briefly, the main population of the cells was gated according to their FSC-A and SSC-A. Secondly, single cells were gated using FSC-A and FSC-W (FACSAria II) or FSC-H (FACSymphony A3). The final gate (green fluorescence plotted against red fluorescence to compensate for autofluorescence artefacts) was used to determine the proportion of successfully edited or transduced cells, as well as their median fluorescence intensity.

Bioluminescence quantification

For dual-luciferase readout using the Nano-Glo Dual-Luciferase Reporter Assay System (Promega), NLuc and FLuc signals were read on-plate 48 hours post-transfection. Measurements were taken on a Centro LB 960 plate reader (Berthold Technologies) with 0.5 s acquisition time 10 min after the addition of Reagent 1 (ONE-Glo EX Luciferase) for FLuc, and 10 min after the addition of Reagent 2 (NanoDLR Stop & Glo) for NLuc. Reagent 2 contains a FLuc inhibitor.

Cryo-electron microscopy

After production of VLPs in HEK293T, the supernatant was sterile filtered and the VLPs purified *via* ultracentrifugation. VLPs were resuspended in 1/1000th of the original volume. 4 μL of the ultracentrifuged material for each of the samples was applied onto carbon-coated 200 mesh copper grids R2/1 (Quantifoil Micro Tools), blotted, and immediately plunged frozen in liquid ethane, using Vitrabot Mark 4 (Thermo Scientific). The grids were loaded into the autoloader of a 200 kV Glacios cryo-TEM, equipped with a Falcon4i direct electron detector camera (Thermo Scientific). EPU software (Thermo Scientific) was used for automatic image acquisition in different grid squares to streamline data generation. Acquired data was manually checked for the ice quality and the particles' presence. Selected sets of foil hole images with a pixel size of 0.246 nm were passed for downstream image analysis. Images were grouped by the sample origin. The contrast of the images was enhanced in Fiji image software through the application of the Contrast Limited Adaptive Histogram Equalization (CLAHE) plugin (block size 127, histogram bins 256, maximum slope 1.5). The visibility of the particles was further enhanced by 2× application of Despeckle (median filter) operation in Fiji image software. Vesicle lipid envelopes were manually segmented, avoiding damaged or distorted particles. The segmented areas were used to create the binary masks and the binary masks were quantified in Fiji to acquire area per particle with subsequent conversion of circular area to a radius individually for each of the particles.

p24 (HIV-1) and p30 (MMLV) quantification

VLP titers after ultracentrifugation were determined using commercial ELISA kits. For HIV-1-derived ENVLPE, the Lenti-X p24 Rapid Titer Kit (Takara Bio, 631476) was used according to the manufacturer's protocol.

The MMLV-derived eVLPs were quantified using the QuickTiter MuLV p30 Core Antigen ELISA Kit (Cell Biolabs, VPK-156) according to the manufacturer's protocol.

Please cite this article in press as: Geilenkeuser et al., Engineered nucleocytosolic vehicles for loading of programmable editors, Cell (2025), https://doi.org/10.1016/j.cell.2025.03.015

In both ELISAs, titers were calculated by using the recommended dilution series of recombinant antigens and at least two different dilutions of the VLP solution in PBS. For calculations, we assumed that one particle contains, on average, 2500 HIV-1-Gag monomers or 1800 MMLV-Gag monomers.

Cas9 protein quantification

Samples were concentrated *via* ultracentrifugation and the concentration of editor protein was determined using the Cas9 ELISA Kit (Cell Biolabs, PRB-5079) according to the manufacturer's protocol. For VLP lysis, 25 μl of Triton-X100 was added to 225 μl of the sample (experimental or standard) and incubated for 30 min at 37 °C before application to the anti-Cas9 antibody-coated plate. The concentration was calculated using the recommended dilution series of recombinant *S. pyogenes* Cas9 and at least two different dilutions of the VLP solution in PBS.

pegRNA quantification

For pegRNA quantification, RNA was extracted from the purified VLPs, which were also used for Cas9 quantification by the Quick-RNA Viral 96 Kit, following the manufacturer's protocol. Purified RNA was stored at −80 °C. RNA samples were subjected to DNase digestion with DNase I (NEB) with the following protocol changes: the DNase concentration was doubled, and the incubation time was extended to 15 min.

For standard curve generation, plasmids encoding pegRNAs were *in vitro* transcribed using the Quick T7 High Yield RNA Synthesis Kit (NEB #E2050), following the manufacturer's protocol, which was adjusted for sgRNA synthesis as instructed by the manufacturer. Transcribed RNA was purified using the Monarch RNA Cleanup Kit (50 μg) (NEB #T2040), and subsequently subjected to DNase digestion as described above. The RNA concentration was quantified using the Qubit RNA High Sensitivity (HS) assay kit (Thermo Fisher) according to the manufacturer's protocol.

Standard and experimental samples were serially diluted in nuclease-free water. Reverse transcription was performed using SuperScript IV Reverse Transcriptase (Invitrogen, 18090010) following the manufacturer's protocol. Sequence-specific primers (Table S1) were annealed at 65 °C for 5 min ramping down, followed by reverse transcription at 65 °C for 20 min and heat inactivation at 80 °C for 10 min.

For qPCR, Power SYBR Green Master Mix (Applied Biosystems, 4368577) was used according to the manufacturer's protocol, with a primer mix containing 900 nM of each forward and reverse primer (Table S1). Reactions were run in 384-well plates (11 μl per well) in technical duplicates for 45 cycles. Control amplification reactions without reverse transcriptase were carried out as a reference for each RT-qPCR run. The reactions were performed and monitored in an Applied Biosystems QuantStudio 12K Flex Real-Time PCR system.

Subretinal injection

Prior to injection, VLPs were clarified by centrifugation at 17,000 rcf for 1 min at room temperature. Mice were prepared for injection by sequential dilation with 1% tropicamide solution (Somerset Therapeutics #119758) and 2.5% phenylephrine solution (Akorn #118050). Mice were anesthetized with a ketamine-/xylazine cocktail and GenTeal Severe 0.3% hypromellose gel (Alcon #0065806401) was applied to the corneas. Under a surgical microscope (Zeiss), a corneal incision was made with a disposable 27G beveled needle before a 34G blunt injection needle connected to Silflex tubing (World Precision Instruments # RPE-KIT) was advanced through the incision and into the subretinal space. 1 μl of VLPs were injected at 70 nl s-1, controlled by a UMP3 pump (World Precision Instruments #UMP3-3). Anesthesia was reversed with atipamezole (Zoetis #10000449) and the mice recovered on a heating pad prior to return to their cage.

Electroretinography (ERG)

Mice were dark adapted for 24 hours preceding the ERG recordings. Under a safety light, mice were dilated with topical administration of 1% tropicamide ophthalmic solution (Akorn #17478-102-12) followed by 10% phenylephrine ophthalmic solution (MWI Animal Health #054243) and underwent anesthesia by isoflurane inhalation. The mice were placed on a Diagnosys Celeris rodent-ERG device (Diagnosys LCC, Lowell, MA, USA) equipped with a heating pad and hypromellose administration (Akorn #9050-1) for hydration. Ocular stimulator electrodes were placed on the corneas, a ground electrode was placed subdermally in the rear leg and the reference electrode was placed subdermally between the ears. Green-light stimulation (peak emission 544 nm, bandwidth ~160 nm) of -0.3 log (cd s m-2) was recorded from each eye. The responses for 10 stimuli with an inter-stimulus interval of 10 s were averaged, and the a- and *b*-wave amplitudes were acquired from the averaged ERG waveform. Data were analyzed with Espion V6 software (Diagnosys LLC).

Retinoid analysis

Mice were dark adapted for 48 hours prior to sacrifice. Single, whole eyes were enucleated under dim red light and frozen on dry ice before wrapping in aluminum foil and storing for a short-term at −80 °C. The whole eyes were unwrapped and allowed to thaw on ice prior to Dounce homogenization in 1 ml of a chilled, sodium-phosphate-based buffer containing hydroxylamine and methanol (10 mM sodium phosphate, 100 mM hydroxylamine hydrochloride, and 50% methanol by volume). Following incubation of the homogenates at room temperature for 25 min, 2 ml of 3M NaCl and 3 ml of ethyl acetate were added to each homogenate. The tubes were

Please cite this article in press as: Geilenkeuser et al., Engineered nucleocytosolic vehicles for loading of programmable editors, Cell (2025), https://doi.org/10.1016/j.cell.2025.03.015

vigorously shaken for 2 min to partition the retinoids into the ethyl acetate layer, then centrifuged at 3,220 rcf in a tabletop centrifuge for 15 min at 20 °C. The top ethyl acetate layer was collected in separate tubes, and an additional 3 ml of ethyl acetate was added to each tube. The shaking and centrifugation steps were then repeated, and the ethyl acetate fractions were consolidated for each sample. Following consolidation, each fraction was dried under vacuum at approximately 32 °C. The dried retinoids were resuspended in 400 μl of hexanes and centrifuged in a tabletop centrifuge at 16,100 rcf for 15 min at 4 °C to pellet undissolved material. All steps prior to loading onto the HPLC were done in darkroom conditions with dim red illumination. The top 350 μl of each sample were placed into amber HPLC vials and loaded into a normal-phase Agilent 1260 Infinity II high-performance liquid chromatograph (Agilent, Santa Clara, CA) equipped with an Agilent Rx-SIL HPLC column (Neta Scientific, Hainesport NJ, cat #: 880975-901). The elution protocol consisted of two steps; one less-polar elution step (99.4% hexanes: 0.6% ethyl acetate) for 20 min followed by a more polar elution step (90% hexanes: 10% ethyl acetate) for 25 min, followed by a brief shift to the less-polar elution step for 5 min. Eluted retinoids were detected spectrophotometrically by monitoring changes in absorbance at 325 nm and 360 nm. Retinoids were identified by their elution times and spectra. To quantify individual retinoids in terms of pmol/eye, areas under each retinoid peak were multiplied by conversion factors derived from standard curves that were generated for all-*trans*-retinyl esters, *syn*-11-*cis*-retinal oxime (derivative of *syn*-11-*cis*-retinal), or all-*trans*-retinal oxime (derivative of all-*trans*-retinal). These retinoid standards were dissolved in hexanes.

Western blotting

After eyecups were isolated as described above for nucleic acid extraction, eyecups were immersed into 1×c RIPA buffer with protease inhibitors (Roche # 04693132001). The eyecups were homogenized mechanically with a pestle before incubation for 20 min on ice. The homogenates were then spun at 4 °C at 21,300 rcf for 20 min and supernatants were collected. Homogenates were then cleared of mouse immunoglobulins *via* incubation for 15 min at 4 °C with Protein G Dynabeads (Invitrogen # 10003D). Protein lysates were separated on a 4-12% Bis-Tris gel (Invitrogen # NP0323BOX) in 1× MOPS running buffer before fast wet transfer (GenScript eBlot L1 # L00686) to PVDF membranes (Millipore # IPFL00010). The membranes were blocked with 5% non-fat milk in phosphate buffered saline, pH 7.4 with 0.1% Tween-20 (PBS-T) for 1 h at room temperature with constant agitation before incubation with primary antibodies in PBS-T with 1% non-fat milk overnight at 4 °C with constant agitation. Primary antibodies in this study include anti-RPE65 (1:1,000, clone KPSA1, produced in-house), anti-beta-actin (1:2,000, clone 13E5, Cell Signaling Technologies # 4970S), anti-Cas9 (1:5,000, clone 7A9, Biolegend # 844301), and anti-MFRP (1:1,000, R&D Systems # AF3445). The following day, the membranes were washed 3 times for 10 min each with PBS-T before incubation with secondary antibodies in PBS-T with 1% non-fat milk for 1 h at room temperature with constant agitation. Secondary antibodies in this study include donkey anti-goat IgG HRP (1:5,000, Thermo #A16005), anti-mouse IgG HRP (1:5,000, Cell Signaling Technologies # 7076S), and anti-rabbit IgG HRP (1:5,000, Cell Signaling Technologies # 7074S). The membranes were washed 3 times again for 10 min each with PBS-T before HRP detection with Clarity Max substrate (Bio-Rad # 1705062)and then imaged on a Bio-Rad ChemiDoc.

Two-photon imaging

Two-photon excitation imaging was accomplished using our custom TP-imaging system based on a Leica TCSSP8 and equipped with a 1.0 NA 20× water immersion objective and a Vision S (Coherent) Ti:sapphire laser delivering 950 nm 80 MHz pulsing light. To image and spectrally separate GFP and tdTomato, two internal spectral detectors were used with their detection bandwidths set to 490–545 nm for GFP, and 590–680 nm for tdTomato. Intact mouse eyes were imaged *ex vivo* after euthanasia and enucleation. Leica ASX 4.7.0.28176 and image J were used for the reconstruction of 3D stacks and quantification of transduced cells.

Design considerations

ENVLPE engineering

ENVLPE is based on the human immunodeficiency virus type 1 (HIV-1) gag protein. The first zinc finger motif within the NC domain was modified by mutation of all cysteine residues to serines to prevent unspecific RNA binding, and the second zinc finger motif was replaced with the aptamer-binding domain PP7 coat protein (PCP) to enable the binding and recruitment of mRNA molecules tagged with the PP7 aptamer (Figures 1A and S1A). VLPs containing mRNA information can be delivered to other cells when equipped with a suitable surface glycoprotein such as VSV-G. VSV-G and mGreenLantern (mGL) with a PP7 aptamer in its 3' UTR were co-expressed to determine essential elements required for efficient cargo delivery. Since proteolytic processing of VLPs is thought to be both critical and tightly regulated for VLP transduction efficacy, the most efficient VLP delivery systems are found to rely on mosaic constructs wherein protease activity is provided by lentiviral Gag/Gag-Pol plasmids, such as psPAX2 with an inactivated integrase domain ($psPAX_{D64V}$). It was observed that HIV-1 protease was essential for the delivery of PP7-tagged mRNAs encoding mGL (mGL_{PP7}), as efficient delivery was abolished when the HIV-1 protease inhibitor darunavir was added during production (Figure S1B).

L21S was introduced in the MA domain of Gag, which had previously been demonstrated to increase budding efficacy (Figure S1C). Budding efficiency was enhanced by the L21S mutation, particularly when it was present in only half of the particle-forming Gag proteins (Figure S1C). When PCP was grafted directly into the NC domain of Gag/Gag–PolD64V in an attempt to simplify the system, the capability for efficient mRNA delivery was abolished (Figure S1D). The fraction of green fluorescence that could be attributed to mRNA or protein delivery in transduced cells was subsequently investigated. When the CS1 aptamer was used to control for unspecific packaging of mGL mRNA, green fluorescence was still exhibited by almost all recipient cells, although the mean fluorescence

Please cite this article in press as: Geilenkeuser et al., Engineered nucleocytosolic vehicles for loading of programmable editors, Cell (2025), https://doi.org/10.1016/j.cell.2025.03.015

intensity (MFI) was drastically reduced. Co-transfection of microRNA (miR) targeting mGL mRNA reduced the MFI to the level of unspecific controls. This suggests that although most of the green fluorescence was a result of successful mRNA delivery, a substantial amount of mGL protein was non-specifically co-packaged into VLPs and co-transferred into recipient cells (Figure S1E).

To provide a calibration for the performance of the mosaic Gag/Gag–PolD64V + Gag-PCP system compared to recently published experiments with *de novo* protein cages,[70] EPN-24-PCP nanocages with a C-terminal fusion of PCP or single-chain tandem-PCP were compared and found its MFI to be on the same level as the Gag-PCP without Gag/Gag–Pol, but 8-fold lower than Gag-PCP co-expressed with Gag/Gag–PolD64V and the integrase-deficient Gag–Pol (Figure S1F).

Notably, observations from mRNA delivery did not translate seamlessly to RNP delivery. For example, while the unsuccessful attempts to omit Gag/Gag–PolD64V indicated that certain factors of Gag–Pol are crucial for efficient mRNA delivery, the cost of omitting Gag–PolD64V was much smaller when delivering RNPs (Figures S1F and S3C). Remarkably, while RNP delivery is apparently less dependent on Gag/Gag–PolD64V, no signal from non-specific packaging could be detected (Figure 1E), even though a substantial amount with mRNA delivery was observed (Figures S1C and S1E). This effect could be attributed to the fact that the (digital) editing reporter is less sensitive to non-specifically packaged amounts of protein, especially since this is one way that 'empty' Cas9 moieties can be packaged with VLPs.

Incorporation of the PP7 aptamer into the 3' UTR could additionally allow iPE mRNA to be packaged into the functional RNP, but instead led to a decrease in editing efficacy (Figure 1E), suggesting a potential interference of mRNA cargo recruitment/loading with transcription. Competition between mRNA and (pe)gRNA for PCP binding sites could be eliminated as the cause for this effect by including PP7-tagged decoy mRNAs with unrelated functions, which are not expected to affect editing activity. When the individual components unique to Gag/Gag–PolD64V were examined more closely, small effects were found for each, which may have the potential to add up. Interestingly, the negative effect of protease inhibition by darunavir or knockout on VLP production and/or RNP delivery was rather small compared to mRNA delivery and occurred even when darunavir was added during transduction (Figures S1B and S3D). Beyond the protease, it remains unclear how the effects of the respective KO variants in Figure S3D are mechanistically related to VLP assembly or RNP packaging or why RNA delivery was more affected by the absence of Gag/Gag–PolD64V. While this could be related to cargo size (as RNPs are much more spatially compact than mRNAs), it is conceivable that HIV-1 Gag/Gag–Pol is also mechanistically involved in mRNA cargo loading, *e.g.*, by providing a properly matured nucleocapsid (NC) structure and thus mediating mRNA condensation.

Next, the stoichiometry of all ENVLPE components was optimized (Figures S3E and S3F). Optimal results were obtained when a slight excess (2:1) of cargo over VLP was used. Regarding the ratio of each budding component, Gag/Gag–PolD64V gave ideal results when supplied in slight deficit in relation to engineered Gag-PCP. As a ratio of 1:1 was already close to optimal, a combined plasmid was constructed where both components are expressed at identical strength (Gag/Gag–PolD64V & GagNLS-NES_ΔZF2+L21S-PCP, both driven by a separate hybrid CAG promoter on the same plasmid). The optimal ratio for RNP formation appeared to be a 3-fold excess of pegRNA over the prime editor, which should be transferrable to other Cas9 effector strategies as well.

The cargo release mechanism was investigated and optimized in the next step. If the RNP remained tethered to the NC domain in the recipient cell after maturation, the NES of the shuttling domain would likely prevent the nuclear import of the genome editing RNP complex. However, no additional benefit was observed when the NES was repositioned to the C-terminus downstream of the budding domain (p6) (Figures 1H and S3H), indicating that the non-covalent interaction of PCP–PP7 is sufficiently amenable to a local concentration decrease in the recipient cell to shift the equilibrium and facilitate cargo release.

Csy4 increases PE efficacy by 3' protection

To ensure that the improved efficacy of protective Csy4 did not just compensate for potential suboptimal PCP grafting into Gag, the PCP–PP7 system (PCP grafting in NC) was benchmarked to variants with alternative grafting positions (grafting downstream of the p6 domain), which has been previously reported to be a viable option.[71] Since PCP binds as a homodimer to the PP7 aptamer, variants encoding tandem copies of PCP (tdPCP) were compared. Indeed, the previous PCP–PP7-based setup was already the best performing compared to alternative graft positions and tandem variants (Figure S5B, PCP_{ZF2} > $tdPCP_{C\text{-}terminus}$ > $tdPCP_{ZF2}$ > $PCP_{C\text{-}terminus}$).

Harnessing the COM–Com aptamer system as an alternative for PCP–PP7 was also evaluated by introducing Com into either the scaffold or the 3' end of the pegRNA while fusing the Com-binding protein COM to the C-terminus of Gag (Figure S5C). While COM-based ENVLPE worked in general, its performance was reduced compared to the PCP-based ENVLPE setup, which could be explained either by the lower affinity of the COM-Com system or suboptimal RNA-folding of the *com* aptamer. This result still emphasizes the modularity of an aptamer-based recruitment mechanism that can be quickly adapted to other aptamer systems of choice.

Csy4 for 3'-protection and cargo recruitment

After discovering that the recruitment functionality in ENVLPE can be quickly adapted to other aptamer systems beyond PCP–PP7 (Figure S5C), the possibility of Csy4 fulfilling both functions simultaneously was investigated: 3' protective function and cargo loading, harnessing its exceptionally high affinity for the C4 aptamer. For that experiment, the PCP domain was replaced with a C-terminally fused Csy4 domain (Figure S6A), which would be responsible for both recruiting and stabilizing the RNP complex (Figure S6B). Remarkably, this mode of packaging ($ENVLPE_{Csy4}$) also drastically improved prime editing efficacy (Figure S6C), similar to the combination of PCP–PP7 recruitment and untethered Csy4-mediated stabilization. Initially, a fusion of Csy4 to the C-terminus of Gag was tested since Csy4, in contrast to PCP, is monomeric, so the assumption was made that interference with the budding process is less likely. Indeed, no differences were evident in whether Csy4 was C-terminally fused or, as PCP previously, grafted into the NC domain

Please cite this article in press as: Geilenkeuser et al., Engineered nucleocytosolic vehicles for loading of programmable editors, Cell (2025), https://doi.org/10.1016/j.cell.2025.03.015

of Gag (Figure S6D). In this instance, the effect of the omission of PP7 and evopreQ1 was investigated, as Csy4 now covered both functions, recruitment and protection. PP7 could be eliminated without consequence if the C4 aptamer was moved downstream of evopreQ1 to the 3' of the pegRNA, suggesting that a linker sequence separating C4 from the PBS is required for optimal ENVLPE$_{Csy4}$ performance (Figure S6D).

Alternative strategies for 3' protection

Alternative strategies were explored in which the protection and processing of the pegRNA 3' end are performed in separate steps. For this experiment, a cleavage-inactive dCsy4 (Csy4$_{H29A}$) mutant of Csy4 was tested, which supposedly fully retains its high affinity for the C4 aptamer, and combined with the self-cleaving HDV ribozyme motif added to the 3' end of the pegRNA (Figure S9A). While this strategy should, in theory, lead to the same protected 3' end as with active Csy4, it could not provide any additional benefit over evopreQ1 alone (Figure S9B). Placing an HDV ribozyme between evopreQ1 (Q1) and the polyU motif with varied spacer nucleotides between Q1 and HDV led to a significant improvement over Q1 alone (Figure S9B), indicating that precise processing by HDV ribozyme to remove 3'-unpaired nucleotides provided additional protection against 3'-exonucleolytic attack, but still was outperformed by the dedicated Csy4/C4 protection module. Attempts using alternative structured motifs were also proven unsuccessful when compared to evopreQ1 alone (Figure S9C).

Evaluation of 3' protection in BE and Cas9 mode

Next, it was investigated whether the improvements of Csy4 protection can be transferred to conventional gRNA-based effectors. Since 3' extensions are usually accompanied by a major decrease in Cas9 activity (while loop modifications are generally better tolerated), both PP7 aptamer engraftments were examined (Figure S10A) but no benefits of Csy4/C4 protection in Cas9 ENVLPE (Figure S10B) or BE ENVLPEs (Figure S10C) were found.

Engineering minimal, homomeric shuttling vehicles

In-depth investigations into the necessary functionalities in a minimal budding and RNP transfer system resulted in miniENVLPE that also benefits from the dedicated untethered Csy4/C4 protection; however, functional replacement of PCP by Csy4 for direct recruitment of the cargo in miniENVLPE (miniENVLPE$_{Csy4}$) performed very poorly in a direct comparison (Figure 4E).

When the protease (Pr$_{D25A}$) in ENVLPE$_{Csy4}$ and PCP-based ENLVPE was inactivated, it only caused a significant 20% decrease in efficacy for ENVLPE$_{Csy4}$ (Figure S11C) but not in PCP-based ENVLPE (Figure 4F), indicating that ENVLPE$_{Csy4}$ is more dependent on proteolytic release. Also, the omission of Gag/Gag–Pol$_{D64V}$ (containing the protease domain in the Pol frame) is much more detrimental for ENVLPE$_{Csy4}$ (Figure S11D) than for PCP–PP7-based ENVLPE (Figure S11A). This result supports the proposed aptamer-mediated release mechanism for the PCP–PP7 pair since the more stable Csy4–C4 interaction presumably adds a constraint to cargo release, which can then be alleviated again by additional proteolytic activity.

Importantly, ENVLPE$_{Csy4}$ with ΔGag/Gag–Pol$_{D64V}$ was almost completely inactive as a homomeric formulation (Figure S11D), beyond what was to be expected from the data on miniENVLPE$_{Csy4}$ (Figure 4E). It is, therefore, possible that the dimerization of PCP could have contributed to particle assembly, while Csy4 lacks such a property but was compensated for in miniENVLPE with GCN4.

QUANTIFICATION AND STATISTICAL ANALYSIS

Statistics were calculated as specified in each figure using Prism (v.10, GraphPad). Mean and standard deviation (SD) were calculated across biological replicates.

For next-generation sequencing experiments, precision was calculated as the proportion of correct editing events among all editing events (correct/(correct + error) × 100).

We made an effort to reduce any biases introduced during the sample preparation by using master mixes and multichannel pipettes.

No data were excluded from the analyses except for some FACS analyses where replicates were lost during sample processing, and some next-generation sequencing analyses for which certain replicates had to be excluded from calculating the mean value due to obvious technical errors (no reads).

Details on all performed statistical tests are provided in Table S2.

CellPress
OPEN ACCESS

Supplemental figures

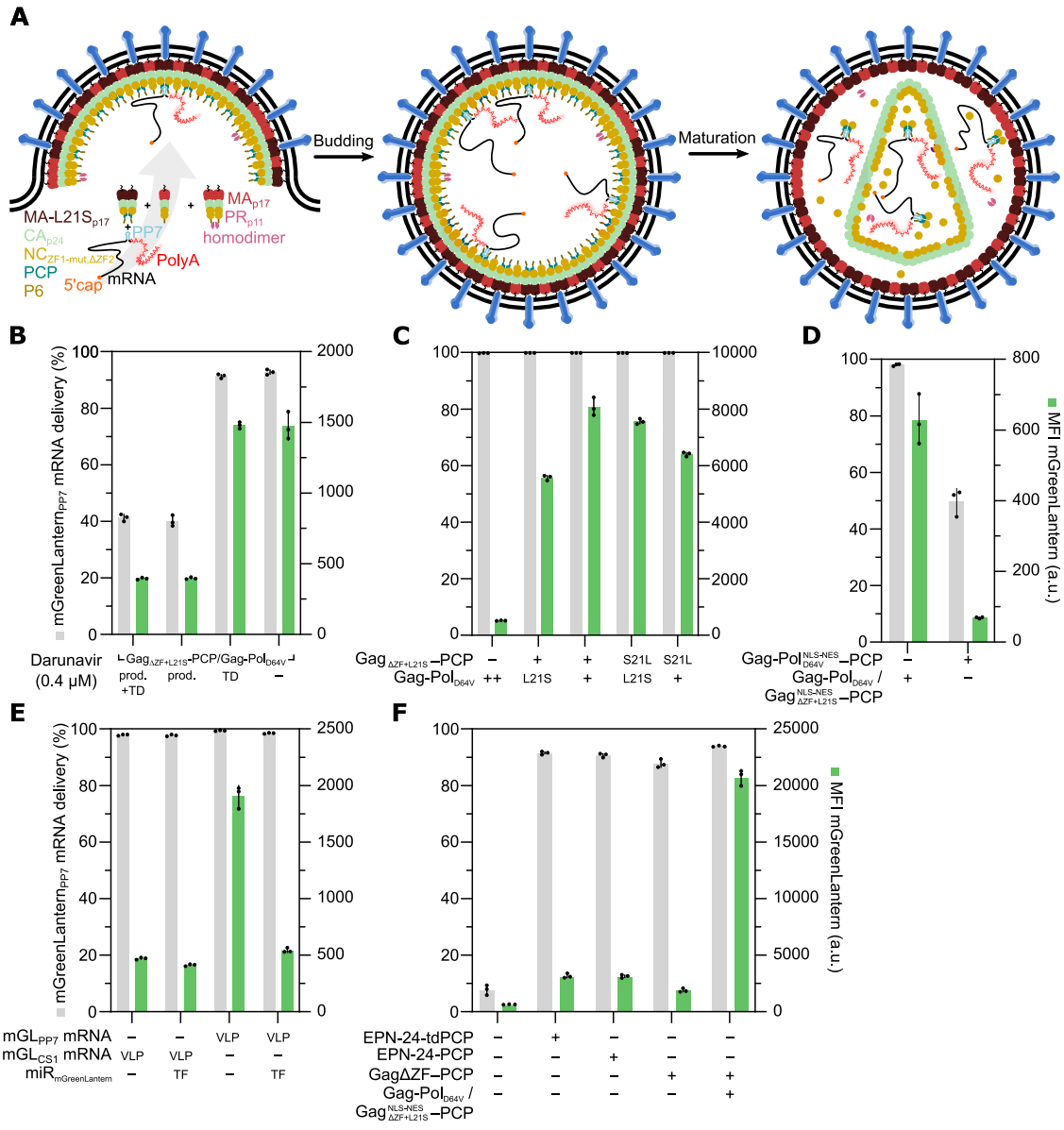

Figure S1. Investigation of relevant factors and general capability of ENVLPE to facilitate mRNA delivery in HEK293T cells, related to design considerations in STAR Methods

(A) Illustration of mRNA packaging using non-shuttling Gag-PCP. The PP7 aptamer is encoded in the 3′ UTR of the cargo mRNA. The VLPs were pseudotyped with VSV-G.

(B) Effect of the protease inhibitor darunavir on mGreenLantern mRNA delivery. Darunavir was added during production (prod.), during transduction (TD), or both (prod. + TD).

(C) Impact of including L21S mutation in the MA domain of Gag when introduced in Gag-PCP or Gag/Gag-Pol$_{D64V}$.

(D) Comparison of mGreenLantern mRNA delivery via Gag-Pol$_{D64V}$-PCP or the mosaic setup using Gag/Gag-Pol$_{D64V}$ and Gag-PCP.

(E) Specificity of Gag-PCP toward PP7-tagged aptamers and the effect of microRNA (miR) transfection (depicted by TF).

(F) Comparison of EPN-24-PCP nanocage variants with Gag-PCP ± Gag/Gag-Pol$_{D64V}$ setups.

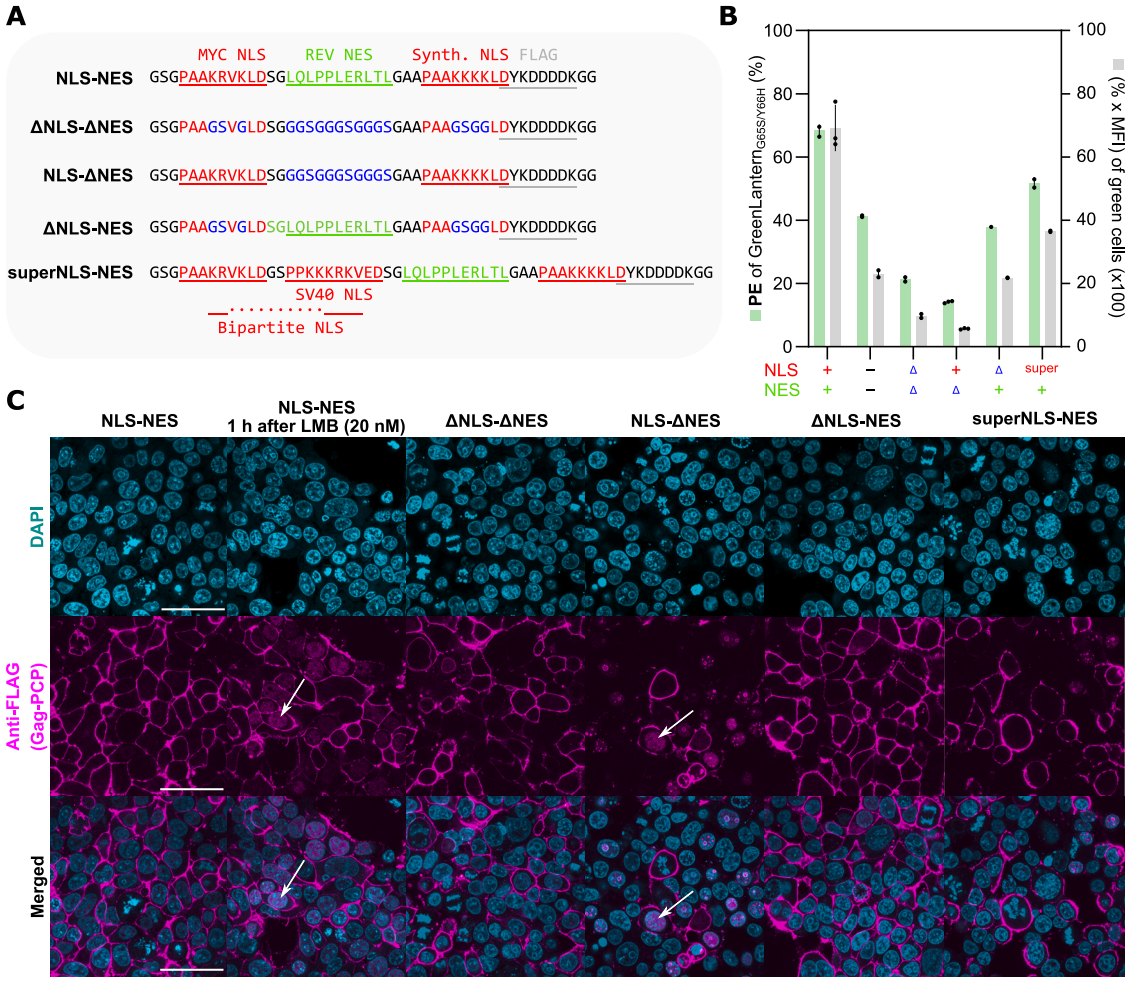

Figure S2. Impact of nucleocytosolic shuttling motifs on VLP-mediated packaging of CRISPR RNPs, related to Figure 1

(A) aa sequences of respective combinations of nuclear localization (NLS) and nuclear export sequences (NES) variants used in (B) and (C).

(B) Evaluation of different combinations of NLS or NES on the delivery of prime editors into the blue mGL HEK293T reporter line.

(C) Immunofluorescence staining of FLAG-tagged Gag variants carrying NLS or NES depicted in (A); 48 h post-transfection into HEK293T cells. Addition of 20 nM leptomycin B (LMB) blocks XPO1/CRM1-mediated nuclear export of HIV-1 REV NES, resulting in nuclear accumulation of a nucleocytosolic shuttling protein (indicated with a white arrow). The scale bar represents 50 μm.

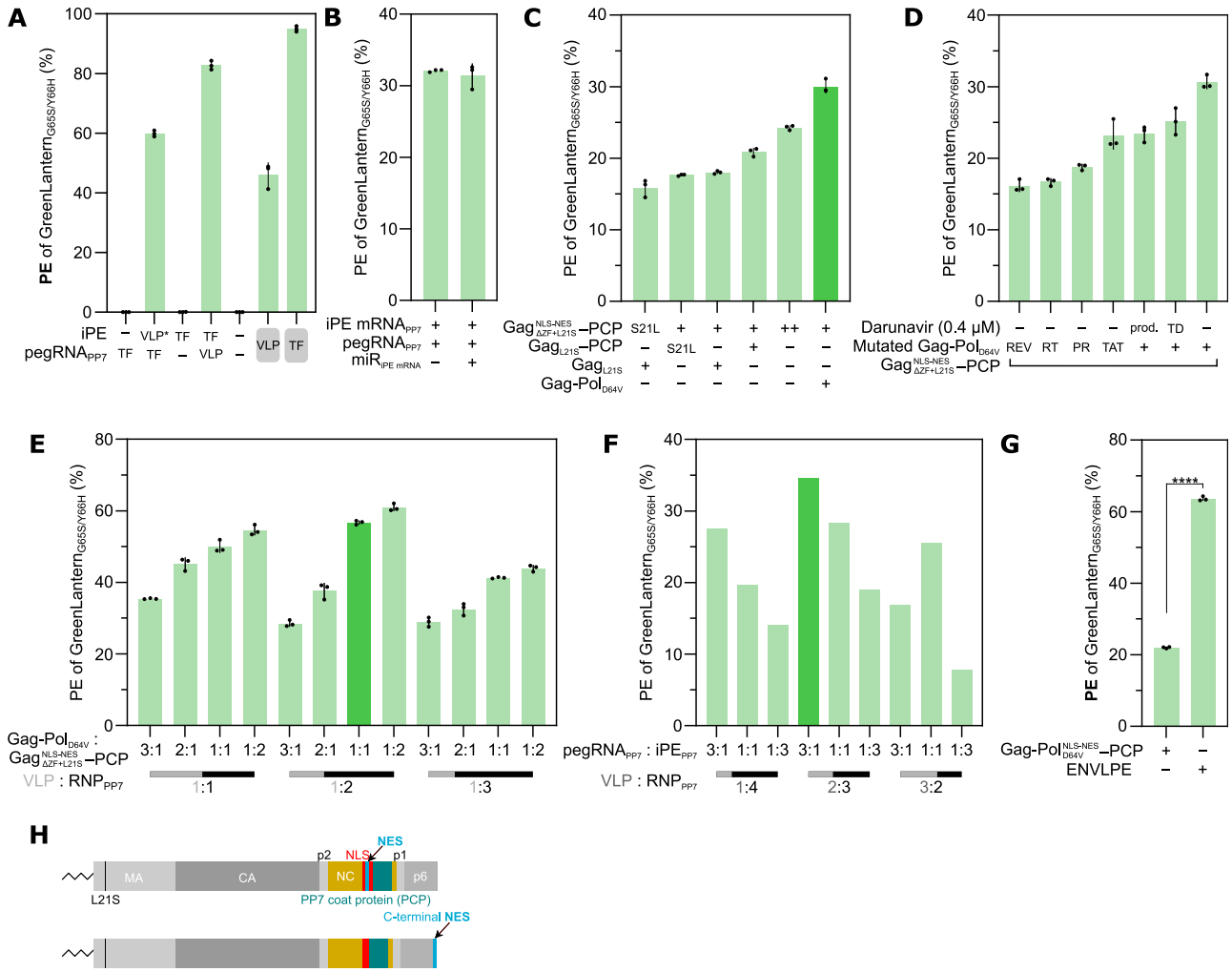

Figure S3. Optimization and characterization of the ENVLPE system for PE-RNP delivery in HEK293T blue mGL cells, related to Figure 1

(A) To determine the limiting component of the prime editor complex, either the mRNA encoding the prime editor protein or the pegRNA was transfected (TF), while the complementary component was transduced (VLP). For the condition where only iPE was delivered via VLP, the iPE mRNA was tagged with a PP7 aptamer to enable recruitment (VLP*).

(B) While being transduced with ENVLPE carrying PE RNPs targeting the blue mGreenLantern reporter, recipient cells were additionally transfected with a miR targeting the 3′ UTR of the iPE mRNA to investigate if any proportion of PE efficacy originated from mRNA delivery instead. miR functionality was independently verified in Figure S1E.

(C) Analysis of the impact on PE delivery when the L21S mutation, as well as the PCP domain, is included in one or both packaging components. To normalize the total amount of packaging plasmid, the amount of an individual plasmid was doubled when used alone (++).

(D) Inactivation of indicated domains encoded in the 2nd generation IDLV packaging vector psPAX2$_{D64V}$ and the impact of the protease inhibitor darunavir.

(E) Co-optimization of mass stoichiometry between Gag/Gag-Pol$_{D64V}$ and Gag-PCP (packaging plasmids) and the ratio between packaging and cargo plasmids. The pegRNA:iPE ratio was set to 3:1 in all conditions.

(F) Co-optimization of mass stoichiometry between pegRNA and iPE (cargo plasmids), and the ratio between packaging and cargo plasmids. Gag/Gag-Pol$_{D64V}$ and Gag-PCP (packaging plasmids) were expressed 1:1 for all conditions.

(G) Effect of inserting the nucleocytosolic shuttling motif and PCP directly into the NC domain of Gag-Pol$_{D64V}$. Bars represent mean ± SD (n = 3 biological replicates). Results of an unpaired t test are shown (****$p < 0.0001$).

(H) Illustration of NES repositioning from NC to C terminus of HIV-1 Gag, as used in Figure 1G.

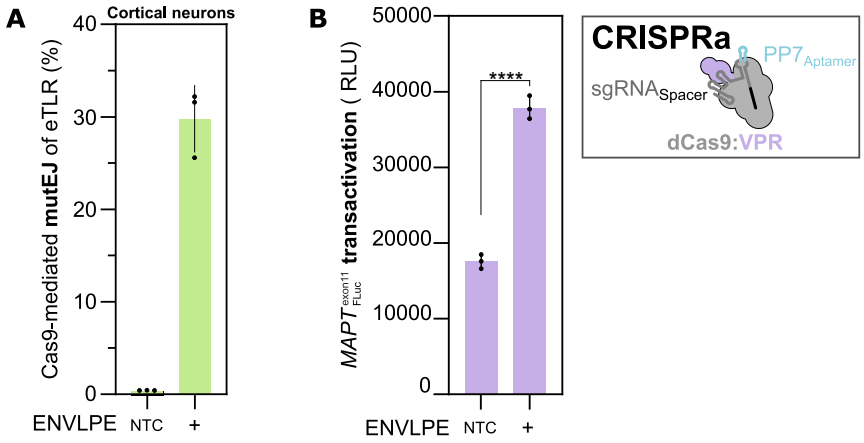

Figure S4. ENVLPE-mediated Cas9 delivery in reporter cortical neurons and transactivation of *MAPT* in HEK293T cells, related to Figure 2

(A) Delivery of Cas9 and PP7-tagged gRNA as RNPs targeting the enhanced traffic-light reporter (eTLRv2); eTLRv2 signals all possible indel events via read-through activation of mGreenLantern in any of the three downstream ORFs. Double-strand breaks (DSBs) were quantified in hiPSC-derived cortical neurons stably expressing eTLRv2 via FC. Bars represent mean ± SD (n = 3 biological replicates).

(B) Relative light units (RLUs) of a *MAPT* HEK293T reporter cell line after transduction with dCas9-miniVPR ENVLPE to induce *MAPT* via CRISPRa. Bars represent mean ± SD (n = 3 biological replicates). Results of an unpaired t test are shown (****$p < 0.0001$).

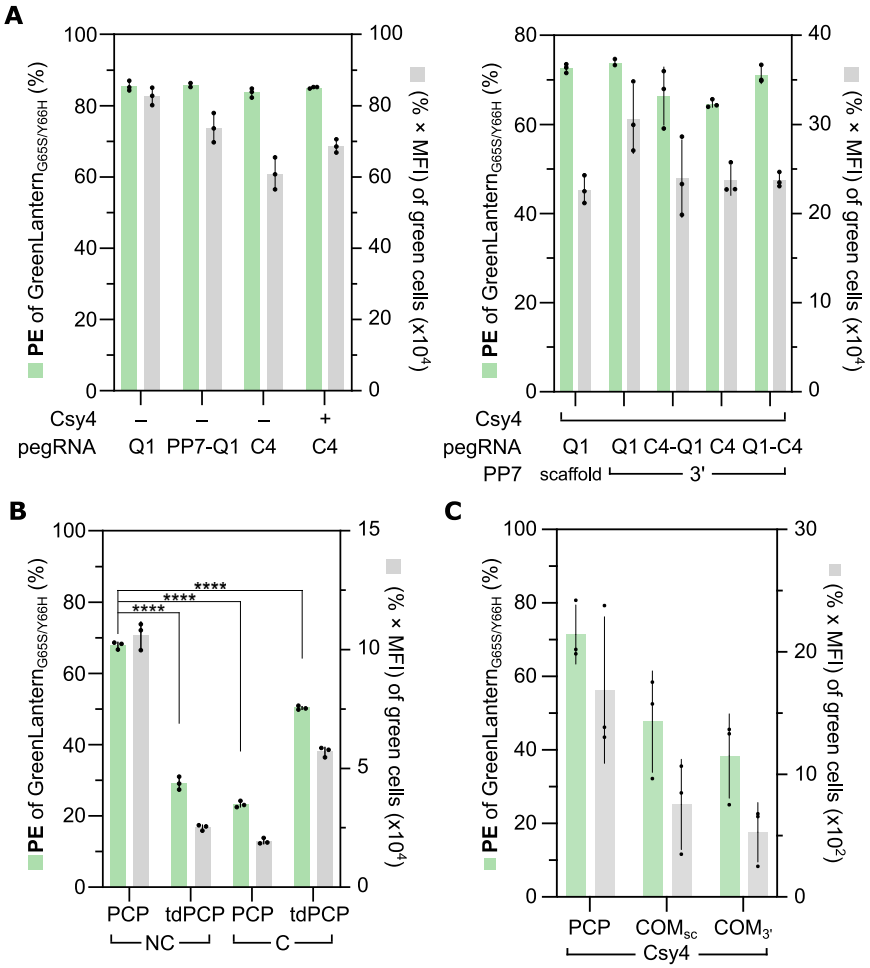

Figure S5. Impact of Csy4/C4 protection in transient transfection settings, validation of PCP-grafting position, and assessment of the versatility of the final pegRNA 3′ configuration, related to Figure 3

(A) PE efficacies in blue mGL reporter HEK293T line transfected with plasmids (i.e., not transduced with ENVLPE) coding for iPE and different pegRNAs with the indicated 3′-modified pegRNAs in the presence or absence of Csy4.

(B) PE efficacies of ENVLPE variants with different grafting positions of PCP (dimeric) and tandem dimers of PCP (monomeric), quantified by FC of the blue mGreenLantern reporter HEK293T cell line. NC indicates the replacement of the NC ZF2 domain with (td)PCP, while C denotes the C-terminal fusion of (td)PCP downstream of Gag after p6. Bars represent mean ± SD ($n = 3$ biological replicates). Selected results are shown of Bonferroni MCT after one-way ANOVA analysis (****$p < 0.0001$).

(C) Checking the *com* aptamer as an alternative to PCP/PP7 under non-saturating conditions (8× dilution). Experiments were performed on the blue mGL HEK293T line. The position of the *com* aptamer in the pegRNA is denoted as sc, scaffold, or 3′, 3′ end. Bars represent mean ± SD ($n = 3$ biological replicates).

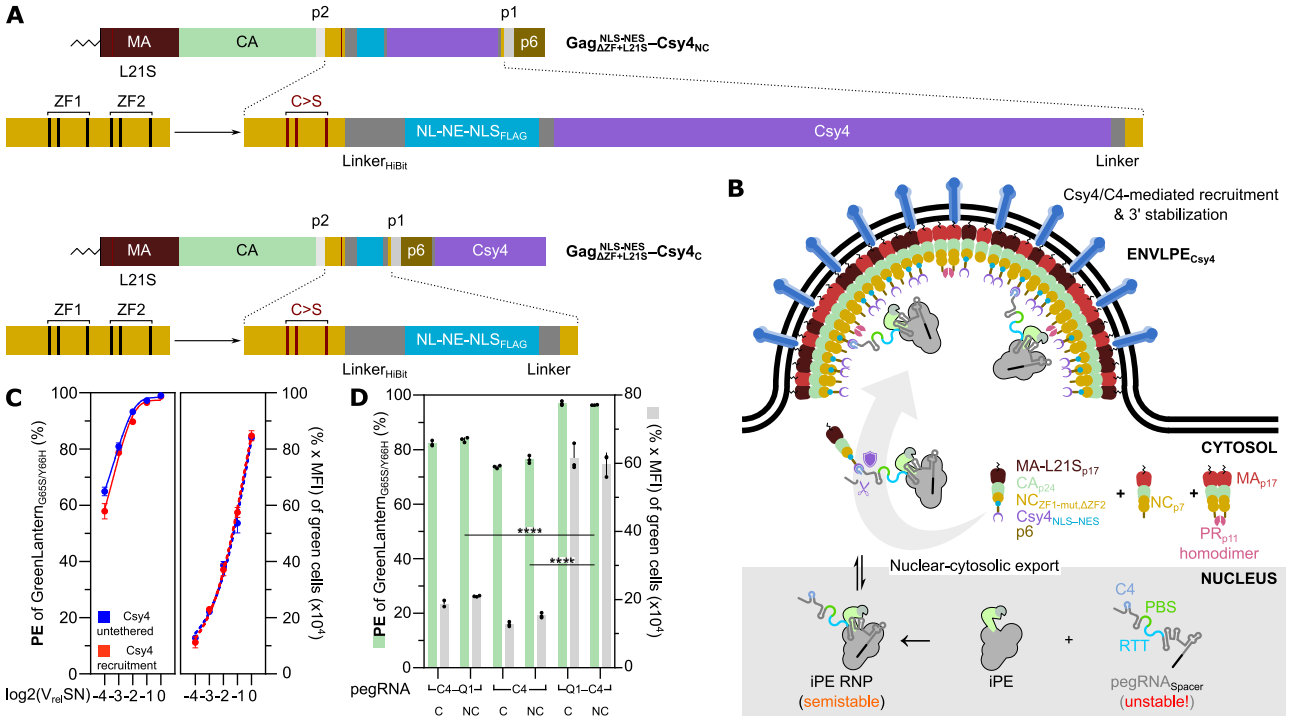

Figure S6. Using Csy4 for simultaneous high-affinity recruitment, related to Figure 3

(A and B) For the ENVLPE$_{Csy4}$ strategy, Csy4 was inserted into Gag NC analogously to ENVLPE in Figure 1A, with the only difference being that an additional C-terminal fusion of Csy4 was tested. In this instance, the Csy4-C4 system can be utilized simultaneously for RNP recruitment and pegRNA stabilization by fusing Csy4 to shuttling Gag, thereby replacing the PCP-PP7 interaction altogether.

(C) Editing efficacy in the blue mGL HEK293T line. The red curves represent ENVLPE$_{Csy4}$ (C-term. fusion), which employs the C4-Csy4 interaction for RNP packaging and pegRNA stabilization, in comparison with ENVLPE$_{PCP}$ in combination with untethered Csy4 for pegRNA protection (blue curves, duplicated from Figure 3B). Log$_2$(V$_{rel}$SN), relative transduction volumes in 2× dilution steps.

(D) Delivery of RNPs for PE via direct fusion of Csy4 to Gag (ENVLPE$_{Csy4}$) to test different orientations of the C4 and Q1 motifs on the pegRNA 3′ end. "NC" denotes Csy4 grafting into the NC domain, "C" denotes fusion to the C terminus of Gag. Experiments were performed on the blue mGL HEK293T line. Bars represent mean ± SD (n = 3 biological replicates). Data were analyzed using two-way ANOVA with Bonferroni MCT (****p < 0.0001).

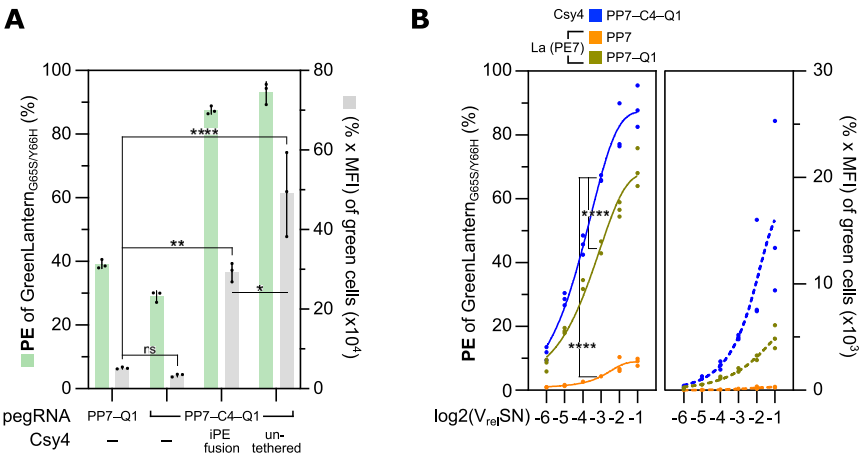

Figure S7. Evaluation of La/SSB-mediated 3′-protection in the context of ENVLPE and context specificity of Csy4/C4 PE-RNP protection system, related to Figure 3

(A) ENVLPE packaged with PE RNPs comprising the final 3′-configuration PP7-C4-Q1 was compared with and without (un)tethered Csy4 expression under non-saturated conditions (8× dilution) for prime editing efficacy on the blue mGL HEK293T line. Selected results of Bonferroni MCT after one-way ANOVA are indicated (****$p < 0.0001$; **$p < 0.01$; *$p < 0.05$; ns $p > 0.05$).

(B) Comparison of ENVLPE-mediated delivery of Csy4/C4-protected prime editors vs. La/SSB-protected prime editors (PE7) across a range of VLP doses on the blue mGL HEK293T line. The PE7 protection system is based on the fusion of an N-terminal fragment (aa 1–194) from La/SSB toward the C terminus of the prime editor to bind and shield the poly(U) stretch of the pegRNA (with or without evopreQ1) from 3′-exonucleolytic attack. $Log_2(V_{rel}SN)$, relative transduction volumes in 2× dilution steps. Points represent $n = 3$ biological replicates (except PE7 PP7-Q1, where $n = 2$).

Selected results of Bonferroni MCT after one-way ANOVA are indicated for the 8× dilution ($log_2(V_{rel}SN) = -3$, ****$p < 0.0001$).

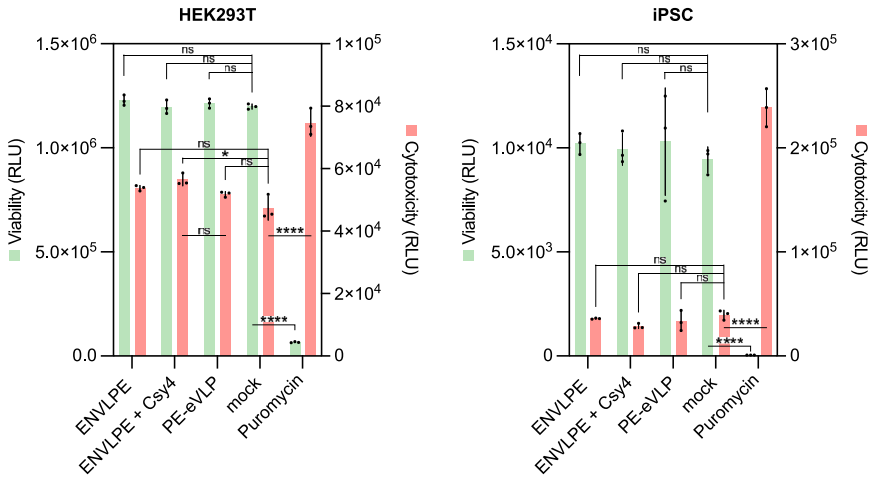

Figure S8. Impact of VLPs on cell viability and cytotoxicity, related to Figure 3

HEK293T cells and hiPSCs were transduced with the indicated VLP systems. 48 h post-TD, cell viability, and cytotoxicity assays were performed. Puromycin 2 μg mL^{-1} was used as a positive control for cytotoxicity. Selected results of Bonferroni MCT after one-way ANOVA analysis are indicated (****$p < 0.0001$; *$p < 0.05$; ns $p > 0.05$).

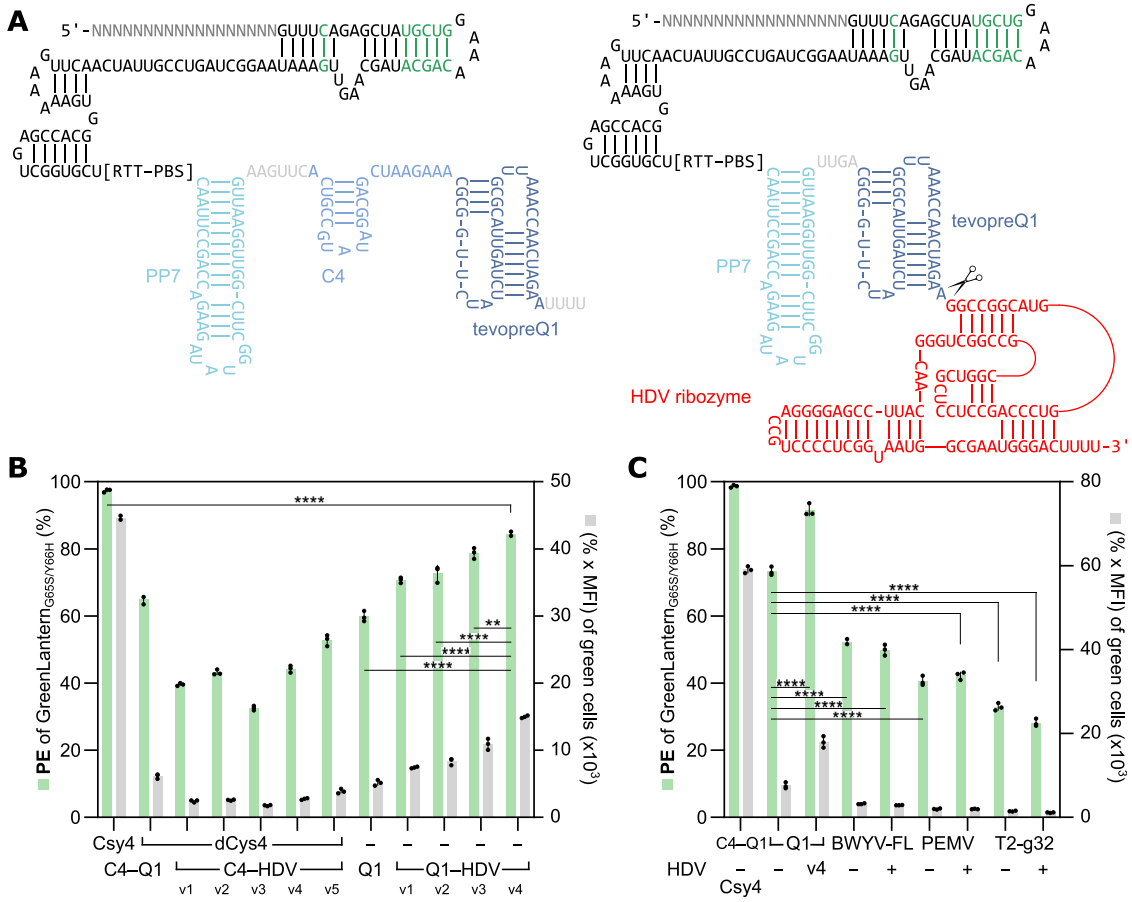

Figure S9. Evaluation of alternative Csy4-independent 3′ stabilization strategies, related to Figure 3

(A) Depiction of the secondary structure of the pegRNA variant carrying PP7-C4-Q1 (left) used throughout the manuscript; and a variant (right) in which truncated evopreQ1 (tevopreQ1) is followed by an HDV ribozyme to remove the 3′-terminal poly(U) stretch, a product of RNA polymerase III promoter termination.

(B) Comparison of the different alternative strategies for 3′-protection from 3′-exonucleolytic attack. dCsy4 indicates a processing-defective variant of Csy4 (H29A), which retains its binding capability for its C4 motif. v1-v4 indicate different minor modifications in the exact placement between C4 or Q1 to the HDV ribozyme with varying nucleotide linkers. Experiments were performed on the blue mGL HEK293T line. Data were analyzed via one-way ANOVA with Bonferroni MCT (****$p < 0.0001$; **$p < 0.01$).

(C) Comparison of a variety of pseudoknot structures with and without a downstream HDV ribozyme as alternative 3′-protection motifs. Experiments were performed on the blue mGL HEK293T line. Data were analyzed via one-way ANOVA with Bonferroni MCT (****$p < 0.0001$).

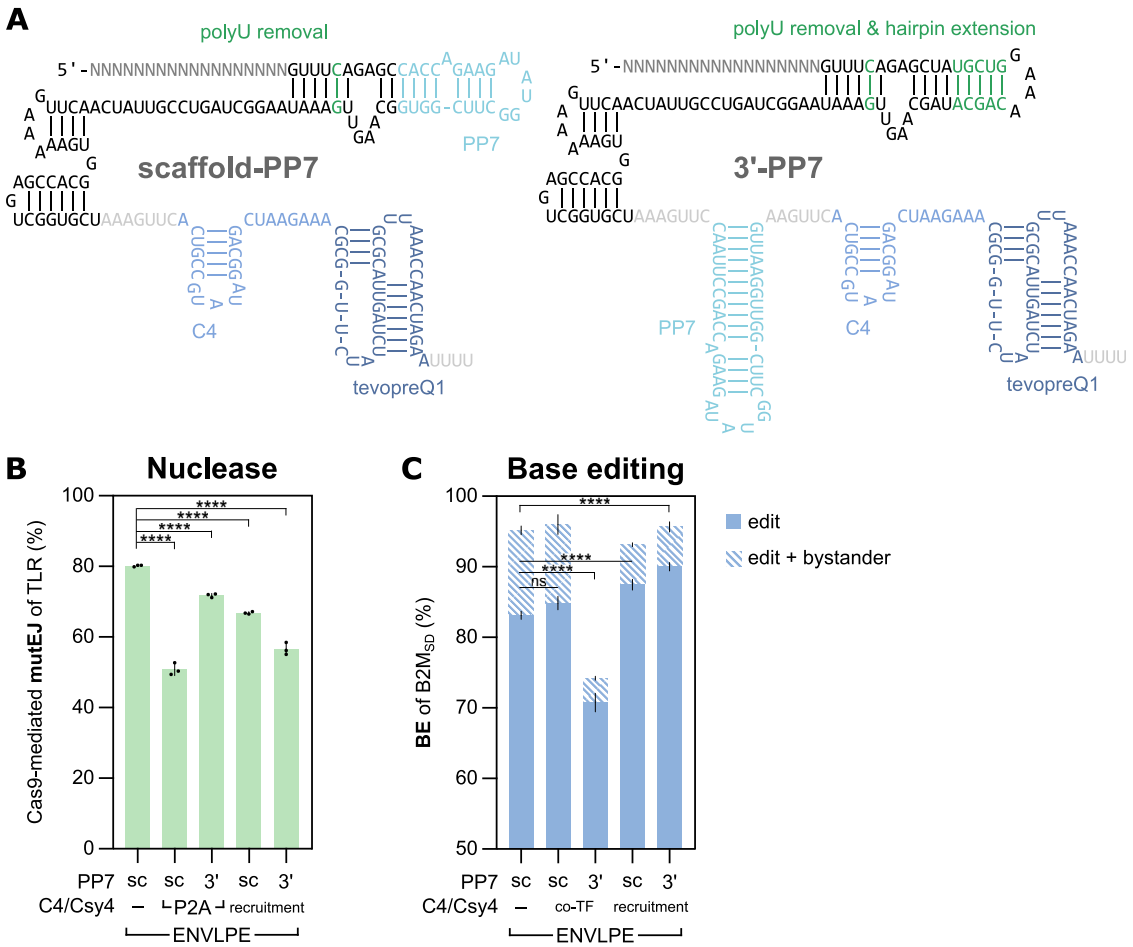

Figure S10. Effect of Csy4 protection on ENVLPE-mediated Cas9 delivery or BE, related to Figure 3

(A) Illustration of sgRNA structures, either with insertion of the PP7 aptamer into the scaffold in combination with the C4 aptamer and downstream tevopreQ1 at the 3′-end or all the components at the 3′-end.

(B and C) Investigation of the effect of the C4/Csy4 protection strategy on ENVLPE-mediated Cas9 and BE delivery using the gRNAs scaffolds depicted in (A). Csy4 was either co-expressed with the Cas9 effector via a 2A peptide ("P2A"), co-transfected as a separate plasmid ("Co-TF"), or fused to ENVLPE ("recruitment"). For (B), indels were quantified via FC analysis of the TLR reporter cell line. For (C), on-target base edits and bystander edits of the endogenous B2M locus in HEK293T cells were quantified via NGS. Results were analyzed via one-way ANOVA; selected results from Bonferroni MCT are indicated by asterisks (****$p < 0.0001$; ns $p > 0.05$). sc, scaffold-PP7; 3′, 3′-PP7.

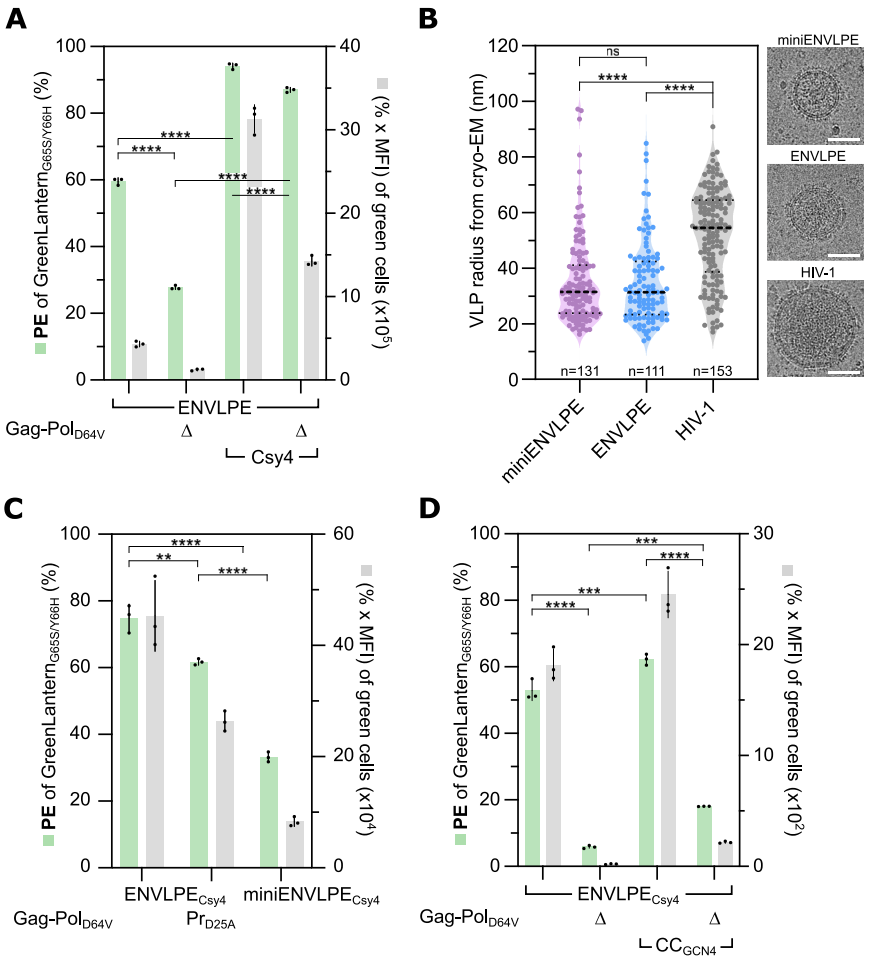

Figure S11. Investigation of the ENVLPE size distribution and release mechanism, related to Figure 4

(A) Analysis of the impact of Gag/Gag-Pol$_{D64V}$ co-expression on PE and PE$_{Csy4}$ efficacy for ENVLPE. Experiments were performed on the blue mGL HEK293T line.

(B) Distribution of VLP radii in comparison with HIV-1 Gag measured by cryoelectron microscopy. The thick dotted line represents the median, while the thin dotted lines constitute the quantiles. Results were analyzed by the Kruskal-Wallis test with Dunn's MCT (****$p < 0.0001$; ns $p > 0.05$). Representative cryo-EM micrographs of the respective species are shown on the right; HIV-1 denotes particles made of HIV-1 Gag/Gag-Pol$_{D64V}$ expressed from psPAX2$_{D64V}$. Scale bar, 50 nm.

(C) Investigating the protease dependence of ENVLPE$_{Csy4}$ by functional inactivation (Pr$_{D25A}$ or omitting Gag-Pol (Δ) under non-saturating conditions (8× dilution). Experiments were performed on the blue mGL HEK293T line.

(D) Benefit of CC$_{GCN4}$ on chimeric and homomeric ENVLPE$_{Csy4}$ assemblies assessed under non-saturating conditions (8× dilution). Experiments were performed on the blue mGL HEK293T line.

For (A), (C), and (D), selected results are shown from one-way ANOVA with Bonferroni MCT (****$p < 0.0001$; ***$p < 0.001$; **$p < 0.01$).

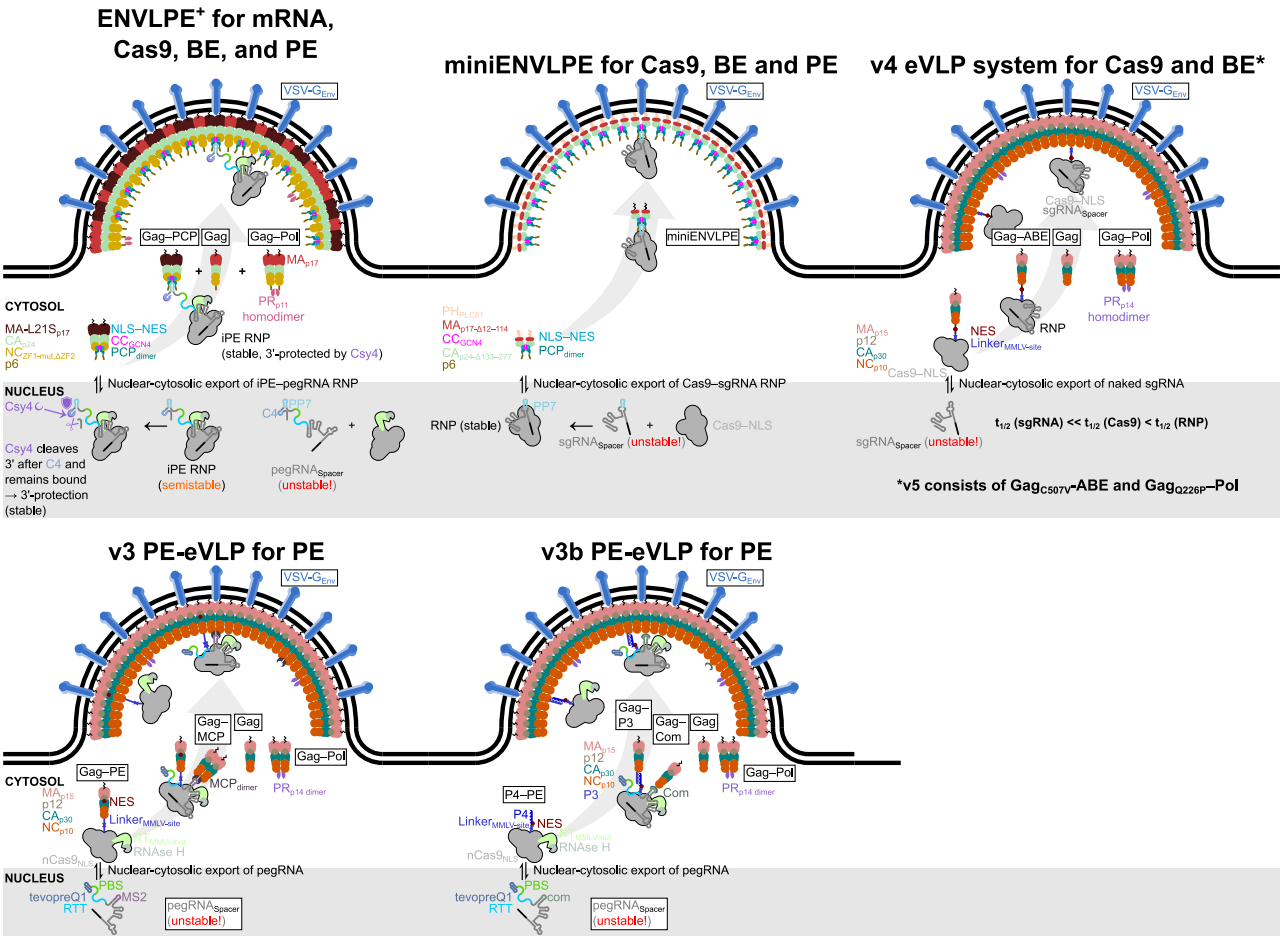

Figure S12. Assembly and RNP recruitment mechanisms in ENVLPE and eVLP variants, related to Figures 5, 6, and 7

The Cas9 effector protein binds the stabilized gRNA-Cas-effector ribonucleoprotein (RNP) complex in the nucleus; nucleocytosolic shuttling (NLS-NES) of Gag-PCP enables binding of the fully assembled RNP via PCP-PP7 interaction. The system enables modular packaging of various RNP complexes and only requires modification of the (pe)gRNA with a PP7 aptamer. Csy4 cleaves and protects the pegRNA in the RNP complex.

v·4 eVLPs consist of an MMLV-Gag fusion to a genome-editing effector protein of choice. The fusion protein shuttles between the nucleus and cytosol to package the unprotected gRNA. In contrast to ENVLPE+, packaging of the Cas *apo*-enzyme (without gRNA) is possible; the genome editor is released after budding only upon proteolytic processing of the Gag polyprotein by the protease encoded in MMLV Gag/Gag-Pol.

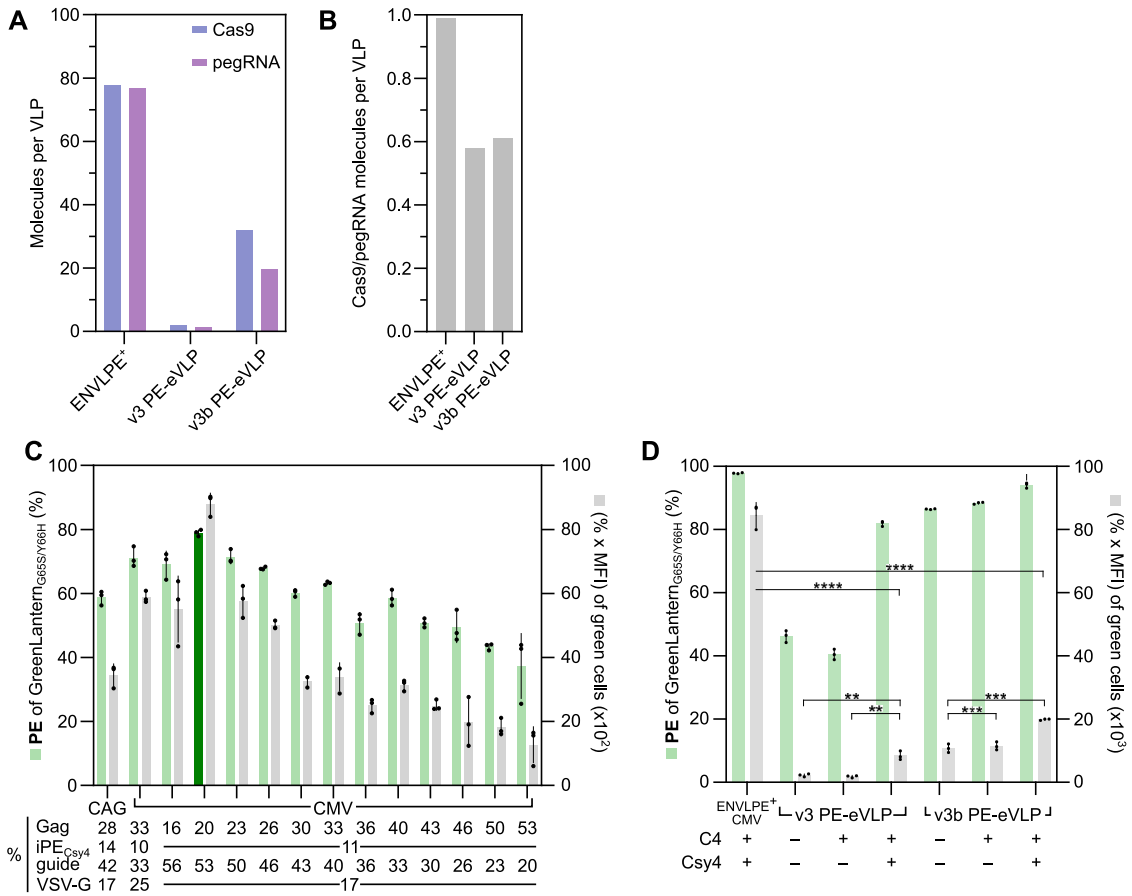

Figure S13. Characterization of RNP loading into different VLP systems, increasing ENVLPE titers by switching from CAG to CMV promoter-driven plasmids, and the benefit of PE_{Csy4} for PE-eVLP-mediated RNP delivery, related to Figures 5, 6, and 7

(A) Quantification of Cas9 molecules per VLP matched with pegRNA molecules per VLP for ENVLPE and v3(b) PE-eVLPs. VLPs produced in 15-cm dishes were purified by ultracentrifugation and resuspended in 1/1,000th of the original volume prior to analysis.

(B) Corresponding Cas9:pegRNA packaging ratios.

(C) Optimization of ENVLPE$^+$ plasmid ratios at non-saturating conditions (8× dilution) after switching ENVLPE$^+$ component expression to CMV promoter-driven plasmids. The chosen ratio for the benchmarking experiments in Figures 5B–5D is indicated in dark green.

(D) To test the compatibility of the Csy4/C4 protection system with v3/v3b PE-eVLPs, Csy4 was supplied as a co-expressing plasmid from a separate plasmid for the PE-eVLP systems. Experiments were performed on the blue mGL HEK293T line. Transduction was performed at 2× dilution. Selected results are shown of Bonferroni MCT after one-way ANOVA analysis (****$p < 0.0001$; ***$p < 0.001$; **$p < 0.01$).

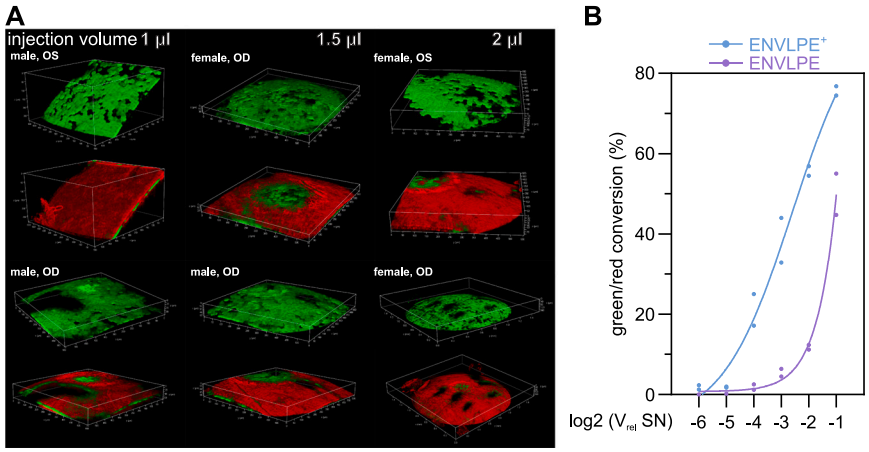

Figure S14. Delivery of Cre_{NLS} mRNA to activate a red/green-reporter locus, related to Figure 7

(A) Cre_{NLS} mRNA-loaded ENVLPEs were injected in different volumes subretinally into the eyes of mT/mG reporter mice (2.53×10^8 particles μL^{-1} in PBS). Two-photon excitation imaging-based 3D reconstruction of the posterior portion of intact mouse eyes are shown, 1 week after subretinal injection. Green-fluorescent cells indicate successful reporter activation by Cre in the red/green-reporter locus. Oculus dexter (OD) indicates the right, Oculus sinister (OS) the left eye. For each reconstruction, the total extent of x and y dimensions is 550 µm.

(B) Quantification of Cre_{NLS} mRNA delivery by ENVLPE vs. $ENVLPE^+$ to a HEK293T reporter cell line carrying a green/red-reporter locus (inverse signal logic compared with A). $Log_2(V_{rel}SN)$, relative transduction volumes in 2× dilution series.

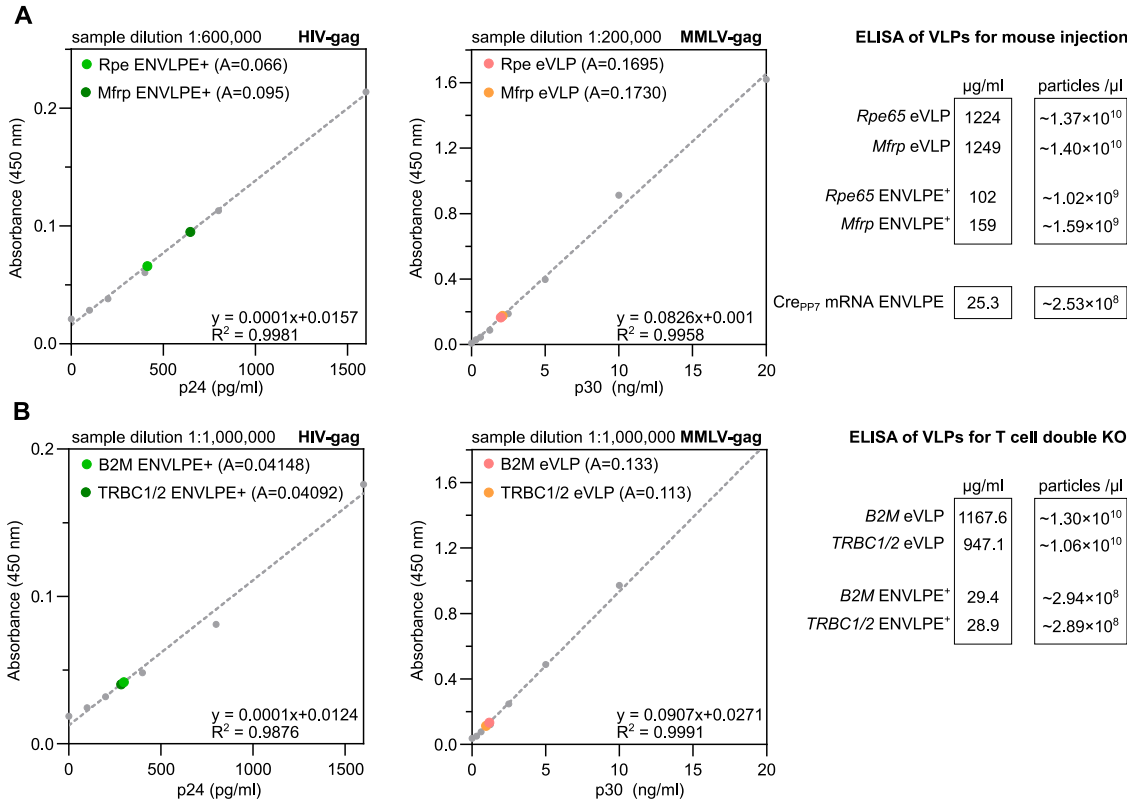

Figure S15. Quantification of VLP titers using anti-p24 (HIV-1) or anti-p30 (MMLV) ELISA, related to Figures 6 and 7

(A) Quantification of ENVLPE$^+$ and v3 PE-eVLP titers after ultracentrifugation prior to subretinal injections. The VLP amount per volume was calculated based on the assumption that 2,500 HIV-1 Gag monomers (or 1,800 MMLV Gag monomers) form the capsid.

(B) Assessment of VLP titers for *ex vivo* BE of T lymphocytes.

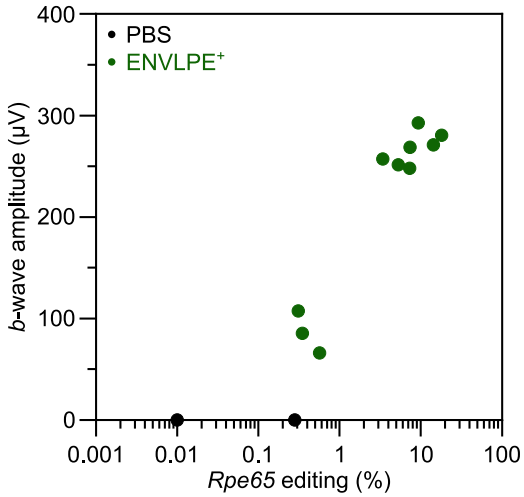

Figure S16. Correlation of *in vivo* editing of *Rpe65* in *rd12* mice with corresponding *b*-waves, related to Figure 7

Correlation plot of *Rpe65* prime editing efficacy and functional restoration quantified by *b*-wave amplitudes in response to a light stimulus after ENVLPE^{+}-mediated iPE$_{Csy4}$ delivery; points correspond to the subset of matching pairs of data points also shown in Figures 7I and 7K.

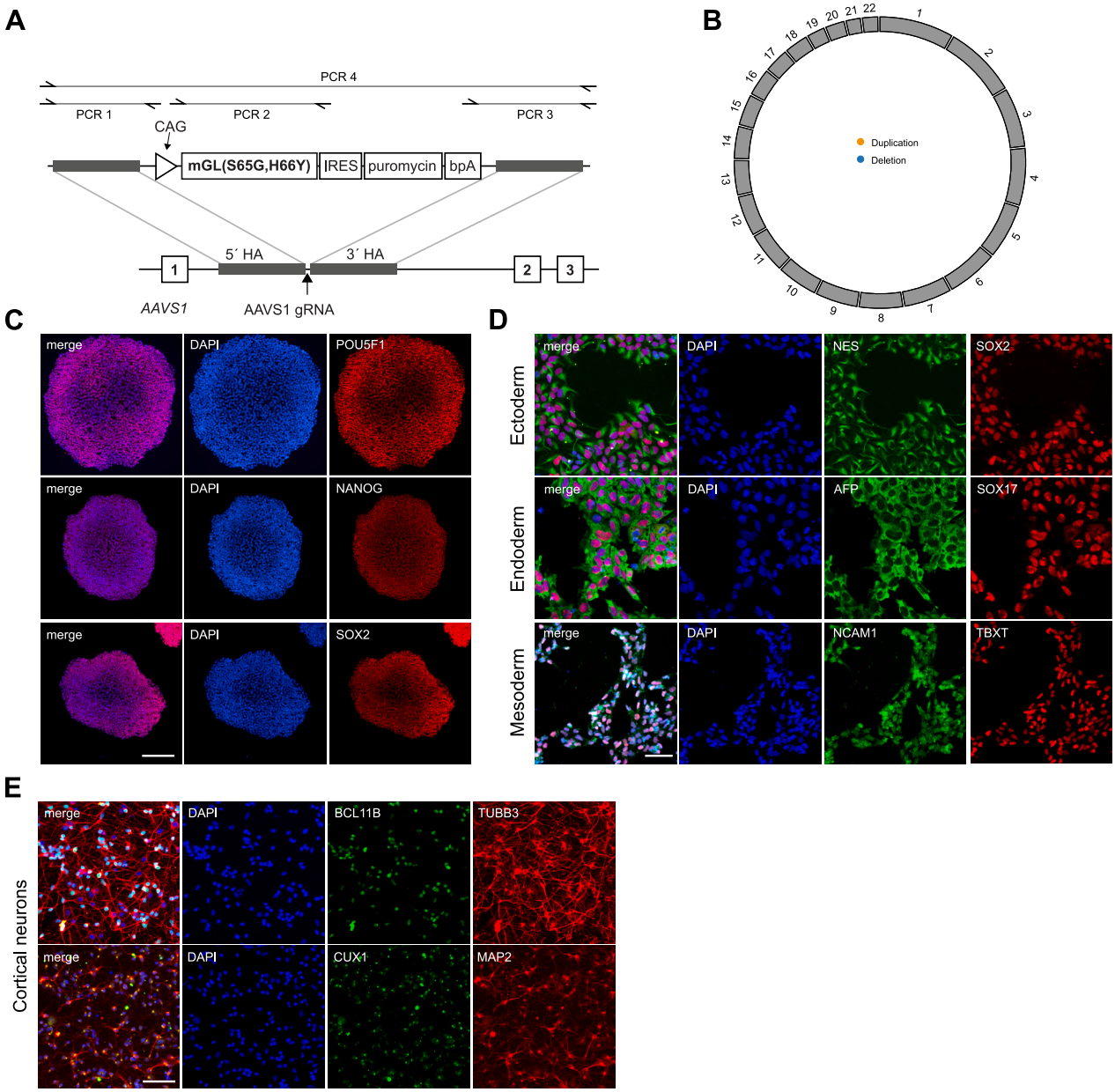

Figure S17. Characterization of pluripotency and neuronal differentiation of the blue mGL reporter iPSC line, related to Figure 1

(A) Schematic illustration of the *PPP1R12C* (*AAVS1*) locus with the inserted cassette encoding the blue mGL reporter as well as a puromycin N-acetyltransferase mediating resistance to puromycin selection.

(B) Analysis of copy-number variation (CNV) in the context of the hiPSC genotype.

(C) Example immunostainings of hiPSC cell markers (POU5F1, NANOG, and SOX2) in the blue mGL cell line after CRISPR-Cas9-mediated knockin. Scale bar, 200 μm.

(D) Immunostaining to show the ability of the generated cell line to differentiate into all three lineages. Scale bar, 50 μm.

(E) Immunostaining of the cell line after differentiation into cortical neurons. Scale bar, 50 μm.

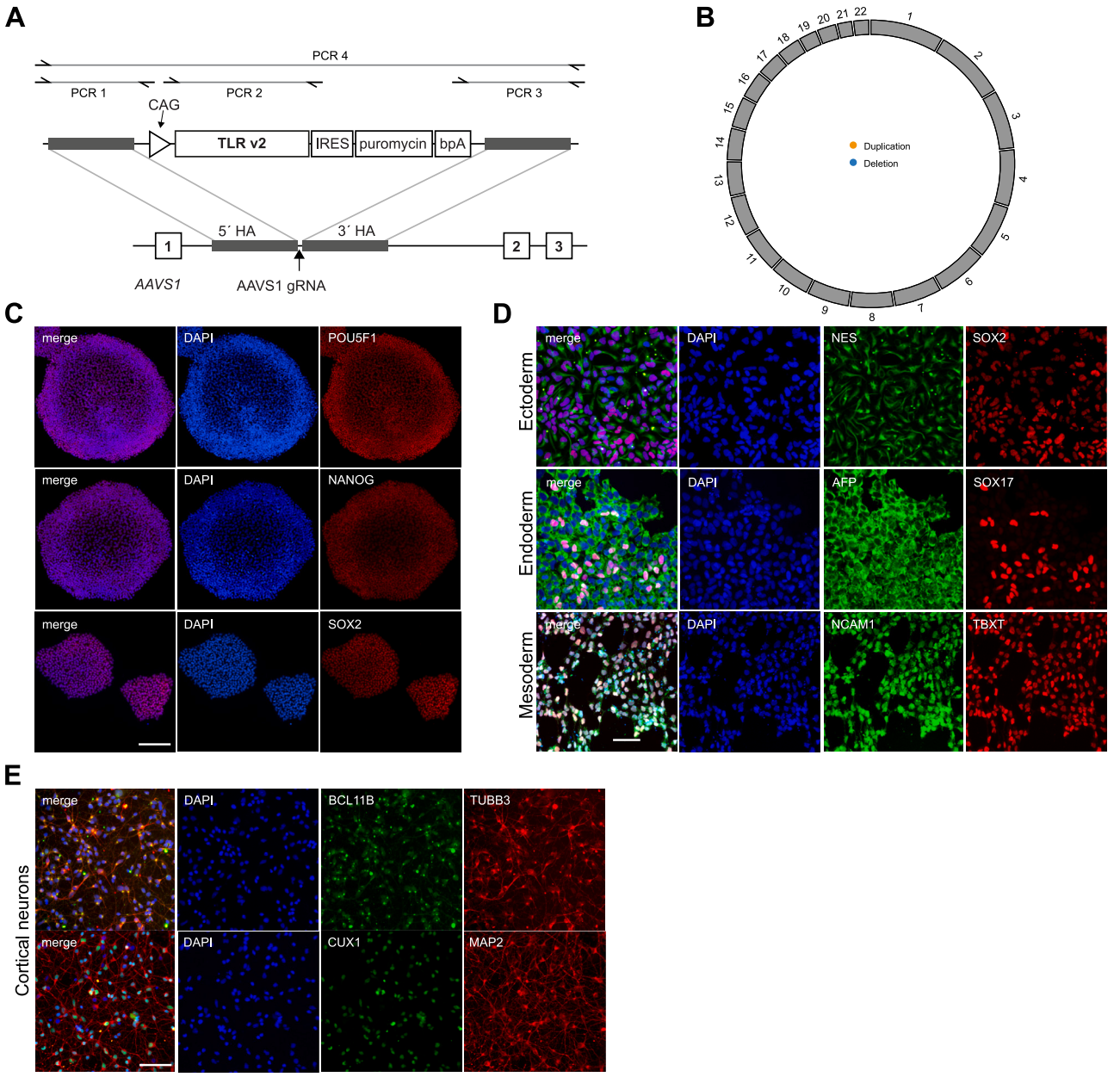

Figure S18. Characterization of pluripotency and neuronal differentiation of the eTLRv2 reporter hiPSC line, related to Figures 2 and S4

(A) Schematic illustration of the *PPP1R12C* (*AAVS1*) locus with the inserted cassette encoding the enhanced traffic-light reporter eTLRv2 as well as a puromycin N-acetyltransferase mediating resistance to puromycin selection.

(B) Analysis of copy-number variation (CNV) in the context of the hiPSC genotype.

(C) Example immunostainings of pluripotency markers (POU5F1, NANOG, and SOX2) in the eTLRv2 hiPSC, after CRISPR-Cas9-mediated knockin. Scale bar, 200 μm.

(D) Immunostaining to show the ability of the generated cell line to differentiate into all three lineages. Scale bar, 50 μm.

(E) Immunostaining of the cell line after differentiation into cortical neurons. Scale bar, 50 μm.

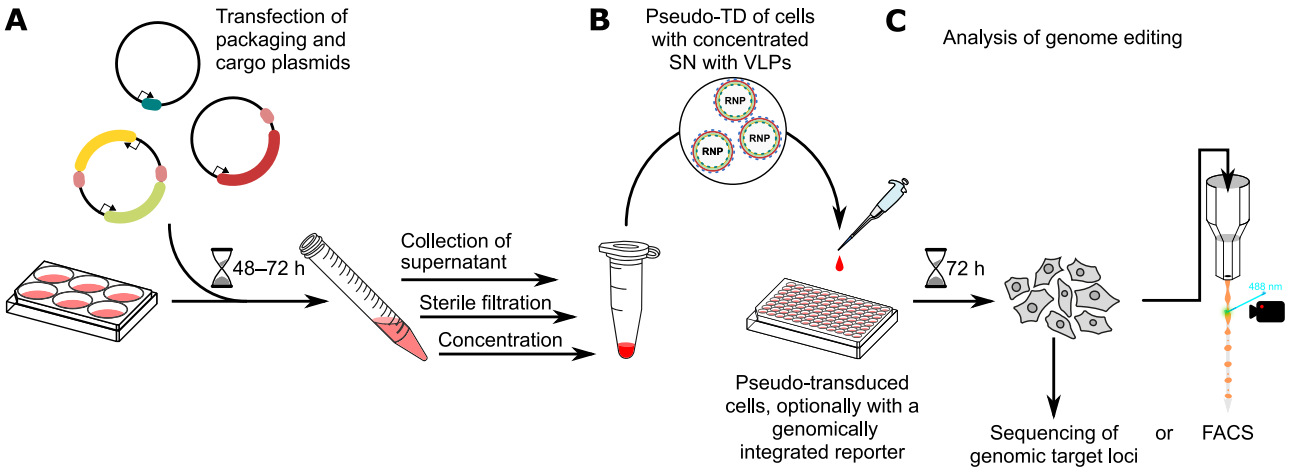

Figure S19. Workflow of ENVLPE particle production, purification, transduction, and analysis, related to VLP production in STAR Methods

(A) Co-transfection of HEK293T cells with packaging, cargo, and glycoprotein plasmids. The cargo plasmids encode a PP7 aptamer-tagged (pe)gRNA and a suitable genome-editing effector. 48–72 h post-transfection of the producer cells, the supernatant (SN) containing the VLPs was collected and sterile-filtered to remove cell debris and leftover transfection reagents. Subsequently, the filtered SN was concentrated using a molecular-weight-cutoff filter (100 kDa).

(B) For pseudo-transduction (pseudo-TD) of the target cells, the supernatant was applied to the cells without exceeding 20% of the total volume of the recipient cell's original growth medium. For simplicity, pseudo-TD is always referred to as transduction/TD.

(C) To optimize the VLP system, cells were analyzed 72 h post-TD via targeted amplicon sequencing of the respective targets or FACS analysis if fluorescence-reporter cell lines were used.

Discussion

Exonuclease-enhanced prime editors (Exo-PE)

Design rationale

Installing a prime edit requires multiple steps, which have to be completed in sequence for an edit to be successfully installed. After gRNA binding, DNA unwinding and nicking, the pegRNA PBS has to bind to the available 3' flap and the RT has to carry out reverse transcription. Subsequently, the now elongated 3' flap has to compete with the endogenous 5' flap for incorporation into the double strand, and the nick has to be repaired. Lastly, the edit has to be propagated from the incorporated flap into the complementary strand, again facilitated through endogenous DNA repair.

At each step, the process can fail: the PBS might disengage, reverse transcription could produce errors or be terminated prematurely upon RT disengagement, or the original flap might be incorporated again. Even after successful flap incorporation, cellular DNA repair might reconstitute the original sequence at the target locus. As with nucleases, the same RNP might engage a given locus again; however, this is rendered unproductive if the inherently less stable 3' extension of the pegRNA has already been degraded in the meantime by exonucleases or the RNase H domain within the RT.

It is therefore highly desirable to optimize the kinetics of prime editing to yield better results, as many studies have sought after already: Methods to prevent pegRNA self-inactivation or enhance RT activity have successfully increased PE efficacy. PE3 introduces a second nick to "confuse" endogenous DNA repair, and with both strands now having acquired a nick, the cellular repair machinery is supposedly not biased towards edit rejection anymore by the presence of an intact, unmodified strand, shifting the equilibrium towards edit propagation. PE4 also targets the last step of edit propagation, but by inhibiting MMR outright.

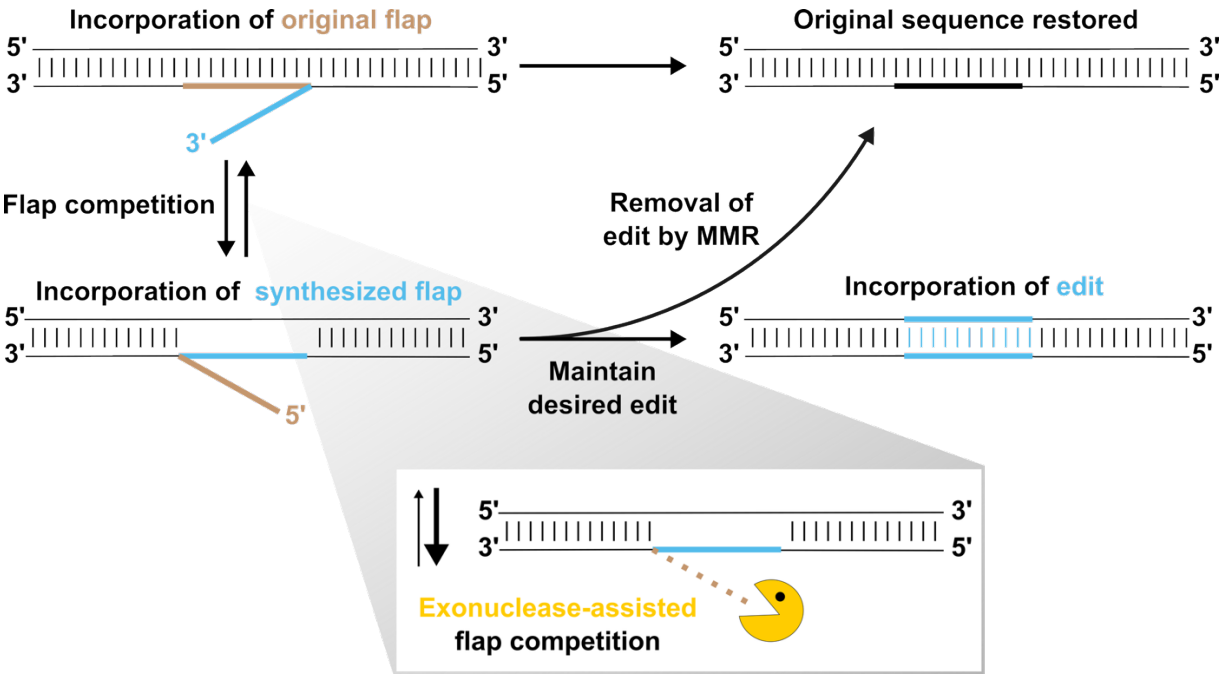

Figure 1: Continued prime editing process after a synthesized strand was reverse transcribed into the 3' flap of a target locus. After flap incorporation, the edit also needs to be propagated to the opposing strand. Flap incorporation can be supported by selectively digesting the endogenous flap via 5' exonucleases.

In contrast, the bottleneck of flap competition, while clearly identified, had intriguingly not yet been targeted further at the time. It was presumed that human endogenous exonucleases such as EXO1 and FEN1 were responsible for 5' flap degradation[6], and FEN1 knockdown did lead to a decrease in editing efficacy[8]. However, FEN1 overexpression did not yield a benefit[42,46].
We hypothesized that a beneficial effect might still materialize if a 5' exonuclease would be actively recruited to the location of the 5' flap in the correct spatial orientation, and therefore tested multiple exonucleases with different modes of recruitment. Untethered co-expression of any 5' exonuclease was unsuccessful, even though this had worked for the RT domain as another critical PE component[59].
We eventually found that only recruitment of the phage-derived T5 exonuclease, and to a lesser degree the T5-like exonuclease from *Klebsiella pneuomoniae* siphophage "Sugarland", could effectively increase PE efficacy. Unlike other tested exonucleases, T5 exonuclease and presumably also T5-like Sugarland possess 5' flap endonuclease activity[187,188], and we wondered if flap endonuclease activity might in fact be responsible for 5' flap degradation during PE. However, subsequent attempts to isolate this flap endonuclease activity by specifically inactivating the exonuclease domain[188] were unsuccessful in the PE context (not shown).
It is a possibility that there are other, more effective methods to degrade the 5' flap or assist flap incorporation in any way, either through exonucleases or other enzymatic functionalities. As of now, there is a convergence towards T5 exonuclease, even though the mechanistic and kinetic details have not yet been elucidated. An independent study on plants conducted by Liang *et al.* followed the same rationale of specific 5' flap degradation, and successfully enhanced PE via N-terminal fusion of the T5 exonuclease, which was also in their study the only effective exonuclease variant[189]. Based on their results, we had re-evaluated the N-terminal fusion of T5 exonuclease to the PE complex post-publication, but our aptamer recruitment strategy remained superior (not shown). Further contrary to our study, they also report a benefit for small and substitution-type edits. Plant cells are known to be more challenging for PE, likely due to polyploidy, limited pegRNA expression, and diverging cellular determinants[190]. These barriers could have helped to detect a benefit of 5' flap degradation for substitution-type edits that we could not observe.
Lastly, while they attempted the aptamer recruitment strategy as well, it led to a drastic decrease in editing below PE2 levels in their hands. In their design, the aptamer was presumably terminally attached to the 3' end of the pegRNA, following the design of an older study[191] where this was only shown with gRNAs. The decrease in efficacy below PE2 levels therefore might indicate suboptimal spatial orchestration of the exonuclease domain, but more fundamentally a destabilizing effect of the aptamer graft within the pegRNA itself. pegRNAs tolerate 3' modifications in principle[30], but a stable hairpin right next to the scaffold might still obstruct its secondary structure or lead to context-dependent destabilization.
A number of other studies have utilized aptamer grafts into the (pe)gRNA scaffold for various purposes such as effector recruitment[192], template recruitment[31,52,59] or packaging into cell-derived particles[137,181], finding that multiple stem loops within the gRNA scaffold are viable integration sites to some degree. While we have opted for the tetraloop in this study (historically the junction between crRNA and tracrRNA), we did not comprehensively screen other options. Therefore, the possibility remains that a different grafting position might be better for pegRNA stability or for proper orientation of the 5' exonuclease.

Compatibility with other edit types, PE strategies and PE enhancers

Exo-PE provides the biggest benefit for insertion-type edits, for which a large, thermodynamically unfavored flap has to compete against the endogenous flap. We observed that there is no benefit for single-base substitutions, suggesting that the novel flap is already thermodynamically competitive enough so that it could not be further supported through 5' flap degradation. While this was not tested in the study, Exo-PE could also be beneficial for deletions, where it would be helpful to degrade not only the 5' flap, but also more of that strand behind it. Even though exonuclease and flap endonuclease activity is generally limited to ssDNA substrates, it might still be valuable to investigate experimentally.

In many cases, additive effects can be expected from independent optimizations of the PE process. For instance, improved prime editor proteins or pegRNAs perform consistently better across a variety of combinations and strategies[8,35]. Conceiving the steps of flap competition and edit incorporation during PE as separate bottlenecks, one might correspondingly assume that a beneficial effect would arise from alleviating both bottlenecks simultaneously, such as through a combination of Exo-PE with PE3 and/or PE4. But since PE4 is only beneficial for small edits[8] and Exo-PE conversely only for larger insertions, we did not expect any additive effects from an "Exo-PE4" combination. Indeed, depending on the edit type, we observed in our study that Exo-PE4 was either on par with PE4 or with Exo-PE.
As we also observed, PE3 can efficiently facilitate larger insertions on its own, but that is associated with a substantial amount of unintended InDel events because of the staggered DSB. This was evident in particular by most deletions precisely spanning the sequence space between both nicks. In comparison, the precision profile of Exo-PE did not differ from that of PE2. Intriguingly, the combination of Exo-PE with PE3 (Exo-PE3) mainly led to an increase in InDel events compared to both Exo-PE and PE3 individually. This could suggest that the propensity of dual-nick strategies to cause deletions is actually amplified, advising caution towards combining flap degradation with dual-nicking.
Consequently, the combination of Exo-PE with dual-pegRNA strategies has not been further assessed in our study, as like PE3, they lead to a staggered DSB through dual-nicking, generally increasing the prevalence of InDel events. However, there is still some potential for an additive effect of Exo-PE: Dual-pegRNA approaches generate two perfectly complementary flaps to bypass the second bottleneck of edit incorporation entirely, as now both novel 5' flaps together replace the endogenous 3' flaps. This might change the mechanism through which InDel events occur, and Exo-PE could still aid the process towards edit incorporation by removing the endogenous flaps, perhaps even in combination with HDR enhancers to further increase precision.
In the more recent strategies prime assembly[72,73] and EXPERT[74], endogenous 5' flaps might also still compete with edit incorporation, leaving some potential for a beneficial effect with Exo-PE. Nonetheless, an additive effect is not guaranteed and hard to predict. This also holds true for the combination of Exo-PE with other PE advancements, perhaps to a lesser degree since the bottlenecks at which they engage are often quite separated. With this disclaimer in mind, it is possible that Exo-PE performance increases further, as it has before, when combined with the latest advances regarding pegRNA stabilization[51], HDR enhancement[24,193] or optimized PE proteins[53]. Improving RT activity[40,41] might be particularly helpful for longer insertions, which require correspondingly long RT templates to be successfully transcribed.

Since Exo-PE displayed scaffold readthrough and integration in some cases, chemical pegRNA modifications to prevent readthrough[36] would also be applicable.
Arguably, the biggest synergy could arise from a combination of Exo-PE with recombinase strategies, similar to PASTE[70] and PASSIGE[71] where PE was leveraged to introduce recombination site "landing pads" for the subsequent integration of multi-kilobase dsDNA donors. Exo-PE also demonstrated this utility already via FRT site insertions, but we have not yet followed that up with the corresponding Flp recombinase. Bxb1 was the recombinase of choice in the majority of studies, but there are other options[194–196].

Utility and limitations for research and therapy

We see the main utility of Exo-PE in synthetic biology and cell engineering, where it could assist researchers in their gene editing endeavors without much additional effort. An obvious application would be the introduction of affinity tags to surface proteins, or markers to other proteins of interest. We have already demonstrated the benefit of Exo-PE for tagging endogenous proteins with fluorescence complementation tags, as it was previously shown on a comprehensive level through ssODN knock-ins[197]. With prime editing however, such tags can even be installed in non-dividing cells unavailable to HDR, a capability also valuable for molecular recording techniques[198,199]. Sequential PE approaches are particularly dependent on high precision, as any editing error would likely terminate the process. Especially when longer insertions are used[199], Exo-PE could enhance efficacy without sacrificing precision. Where precision is not a concern and PAM's are widely available, dual-pegRNA approaches might remain the default option for efficacy reasons.

After the first CRISPR cell therapy had received approval in 2023, the next-generation editing techniques are now also entering the clinic: BE has recently seen remarkable success in an *in vivo* human gene therapy[200], and PE has entered its first clinical trial, although as an ex vivo therapy[201]. Based on the extended range of genetic diseases alone that could theoretically be targeted, PE as a therapeutic strategy addresses a significant unmet medical need.
To further advance PE into the clinic and make it viable also for *in vivo* therapies, a number of challenges have to be overcome, not all of which are PE-specific. While there are remaining concerns of genotoxicity[87] and even a report on unintended enzymatic activity[202], its precision and off-target editing profile seems to be generally preferable[203]. PE could also benefit from innovations to make gene editors more easily applicable[56,204–207] or more specific and effective[208–210] for any given target sequence where a genetic defect might be located. But owing to its complex process, PE still lacks efficacy compared to nucleases and also base editors, and the translation of various efficacy-enhancing strategies might prove difficult for a multitude of reasons. For instance, off-target editing and precision issues of PE3 and other dual-nick strategies might be amplified during persistent expression. Enhancer proteins and compounds would have to be assessed in regard to their immunogenicity and toxicity profile. And lastly, there might be additional issues regarding formulation, manufacturing and compatibility with suitable delivery vectors. There are a number of studies reporting PE-related innovations with a dedicated focus on clinical translation, such as AAV compatibility[58–60] and the development of minimally immunogenic nucleases[211]. A recent study even leveraged artificial intelligence to generate a synthetic CRISPR nuclease, which was released for commercial use[212].

But as mentioned in the introduction, permanent expression of gene editors is likely not a viable strategy due to elevated immunogenicity and off-target editing. Many PE(-related) strategies consist of a complex composition of different molecules (short RNA, dsDNA, protein/RNP), feature treatment with additional compounds or have specific manufacturing requirements, and their clinical (or even *in vivo*) development therefore hinges on a match with suitable delivery vectors and manufacturing processes. This would also apply to Exo-PE, and the benefit of its addition would have to outweigh its risks. It is currently unclear how efficiently any PE strategy could facilitate complex edits in a scenario where the editing machinery and any modulators are only available transiently and at low abundance. Complex edits are certainly also therapeutically relevant, from stretch replacements to cover a variety of pathogenic mutations to substituting entire genes. But while recent developments demonstrate that PE research is far from exhausted, it remains to be seen if PE is the best technology for large insertions, with other alternatives on the horizon and more contestants emerging. Naturally, those would also have to adapt to the challenges of targeted delivery if developed towards therapeutic editing.

A sizeable amount of research has focused on the ability of programmable systems and for targeted, size-unrestricted and DSB-free insertions[213], which is arguably the “holy grail” of genome editing. CRISPR-associated transposases (CASTs)[214–216] have been a major avenue towards this goal, facilitating insertions on the kilobase scale without causing DSBs. Initially displaying very low efficacy, they were continuously optimized and recently also subjected to directed evolution, which yielded evolved CAST systems[217]. In a technology called “STITCHR”, CRISPR-guided retrotransposons were recently utilized for the first time for targeted insertions[218]. But there are also non-CRISPR examples, such as recombinase fusions to DNA-binding domains to enable target site programmability[219–221]. An entirely different approach is “bridge recombination”, where recombination between two DNA molecules is guided by a programmable ncRNA[222].

Engineered nucleocytosolic vehicles for loading of programmable editors (ENVLPE)

Within the quite crowded space of VLP delivery, ENVLPE can be considered as the latest addition to the group of (pe)gRNA-focused RNP delivery tools, demonstrating for the first time recruitment of a PE complex via aptamers. In this chapter, the design rationale, particular innovations and remaining bottlenecks of ENVLPE will be discussed in detail and in context of the available literature. A major bottleneck for delivery is also targeted and tissue-specific cell entry, which VLPs facilitate like LVs via fusogenic glycoproteins. Glycoprotein engineering approaches applicable for VLP pseudotyping are therefore also discussed.

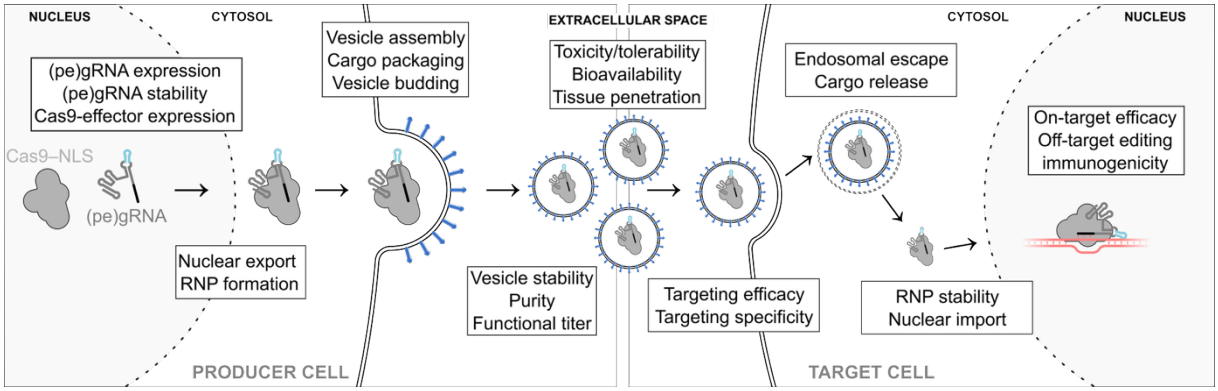

Figure 2: Parameters determining the efficacy of a cell-derived gene editor delivery technology, which can be affected/optimized explicitly or implicitly by various design choices on both the editor and the delivery vector level.

From mRNA to RNP delivery via aptamer recruitment

Our VLP design was initially conceived to package non-coding and intronic RNA transcripts[223], modeled after a design from Prel *et al.* for mRNA delivery[175]. We then adapted this to the delivery of gene editors and gRNA recruitment using the pegRNA design from our other previous study Exo-PE, even though the general concept of effector recruitment via aptamer-modified gRNAs was of course already available otherwise[191,224]. This development process bears intriguing similarity to the development of other aptamer-based VLPs[181,185], which also started out as mRNA delivery tools in the respective groups[176,178]. In fact, one of them justified their switch from mRNA delivery to RNP delivery the exact same way, also observing that separate delivery of gRNAs was highly inefficient compared to co-delivery with Cas9[185]. It is likely that all previous approaches claiming to co-deliver Cas9 mRNA with sgRNAs preferentially (or even exclusively) packaged Cas9 RNPs instead, which was notably recognized as a possibility in the first study already[179].

Another study later claimed that they had observed additional benefit by co-packaging Cas9 mRNA[184], something which we also explicitly checked but were unable to confirm. However, this disagreement could be rooted in optimization issues, as gRNA trafficking and stability in this study was arguably suboptimal compared to ENVLPE.

ENVLPE innovations, limitations and further opportunities

The aptamer recruitment mechanism enabled a number of key innovations, with overlaps and co-dependencies. Specifically, we introduced the concept of **(pe)gRNA shuttling** and put a large emphasis on **(pe)gRNA stability** and the delivery of intact RNP complexes. The high **modularity** that comes with aptamer recruitment enables **compatibility** with recent and future gene editing developments, and also positions ENVLPE as an **engineering platform for novel delivery vehicles** constructed from custom building blocks.

Active gRNA shuttling

While strategies for protein delivery are very straight-forward and similar across many studies, strategies for gRNA packaging have been more complicated and diverse. Early studies encoded it on a lentiviral transgene[150,155], but subsequent studies then compared this to mere co-expression of the gRNA in the producer cell and observed no significant difference. This led to the conclusion that the gRNA would automatically associate with Cas9, and could be easily co-packaged as RNP complex. In contrast, aptamer-based approaches actively recruit gRNA, either alongside Cas9 mRNA or deliberately as “handle” for RNP recruitment.

We showed that active trafficking of the gRNA component into the cytosol increases the editing efficacy of the resulting VLPs, reasoning that they should be preferentially localized at the site of particle assembly. However, this hypothesis is only scarcely entertained in previous literature. In the VesiCas study[126], gRNAs were produced in the cytosol via T7 polymerase-dependent transcription explicitly for this purpose, but the lack of any active recruitment, in combination with the nuclear localization of Cas9, likely had a negative impact on gRNA stability and RNP packaging efficiency. The NanoScribes study deployed Pol II-dependent transcription of gRNAs combined with intronic processing[168]. While they reference the circumvention of U6 promoter-dependent features like the +1 G transcription start and polyuridine termination as design rationale, the potential benefit of their design for pegRNA localization and stability is only acknowledged as an additional possibility in the discussion[168].

Meanwhile, ENVLPE features the most deliberate and likely most effective design to date towards optimizing the abundance of stable RNP complexes in the cytosol for packaging into VLPs. With ENVLPE, (pe)gRNAs are transcribed in the nucleus, but transported into the cytosol by a shuttling aptamer-binding protein. Nucleo-cytosolic shuttling does also exist as an endogenous process[225,226], which we mimicked through the combination and balancing of NLS and NES motifs, as shown in a study on Cas13d[227]. The same study also tested RNA export motifs attached to the gRNA, which however performed worse.
Intriguingly, a combination of NLS and NES motifs was utilized with the fusion-based eVLPs[163] and Cas9-EDVs[172], although for a different purpose: Cas9 carries NLS motifs for efficient nuclear transport in the target cell, but since nuclear localization of the gag-Cas9 fusion protein is not ideal for particle assembly in the producer cell, NES motifs are also introduced somewhere within the gag domain as compensation, separated from the NLS by a protease cleavage site. Cas9-NLS is then released after virion maturation, and can freely translocate in the target cell.
While these fusion constructs are potentially capable of shuttling, they were not specifically designed for the purpose of gRNA retrieval. This is also evident by the design of v3b PE-eVLPs: Com-tagged pegRNAs are additionally recruited by a gag-com-pol construct, which however

contains neither NLS nor NES motifs. To faciloitate pre-assembly of RNP complexes in the nucleus, shuttling of an entire gag-Cas9 fusion protein is presumably not ideal either.

(pe)gRNA design and stabilization

ENVLPE was designed under the assumption that the gRNA is the least stable component during RNP delivery, and that its design should follow the purpose of maximizing the packaging of functional RNP complexes. Therefore, gRNAs should engage into an RNP complex as early as possible, and recruiting the RNP via the gRNA ensures that no Cas9 apo-enzymes would be packaged. While packaging of a "naked" (pe)gRNA is possible in principle, it is likely highly disfavored against assembled RNPs: We and other studies have observed that packaging of naked (pe)gRNAs is highly inefficient[179,181], presumably due to their instability.
Stability is a bigger concern for pegRNAs compared to gRNAs, because their 3' end is exposed and also functionally essential. Multiple studies have therefore focused on increasing the stability of pegRNAs specifically[35,50]. Stability becomes even more important in a low-abundance environment like VLP delivery, where even chemical modification is not possible. Consequently, some VLP studies have taken additional measures[168,174]. With ENVLPE, the elevated stability requirement of pegRNAs is accounted for in two ways: By introducing the aptamer downstream of the RT template at their most vulnerable spot, it is ensured that only 3'-intact pegRNAs are packaged. More importantly though, the Cas6f/Csy4 system is deployed as an additional 3' protection mechanism.

The original function of Csy4 pertains to the processing of crRNAs[228,229], and has consequently also found use in processing gRNA arrays[230]. Csy4 binds to its target aptamer with high affinity[231], cleaves off any downstream nucleotides and remains bound tightly to the 3' end[229]. These properties make Csy4 well-suited to stabilize any RNA, and it has consequently been utilized at the 3' UTR of mRNAs[232], even to a degree where it promoted backsplicing[233]. As an aptamer, it naturally also found use for effector recruitment[191].
Csy4 has already been implemented for prime editing on multiple occasions and for various purposes: In a study by Liu *et al.*, Csy4 is used to prevent pegRNA self-inhibition, and also to process a pegRNA and an sgRNA from a single transcript[30]. Feng *et al.* used Csy4 to recruit an untethered RT domain to Cas9[31]. Lastly, Huang *et al.* deployed Csy4 to process a pegRNA from the intron of an mRNA transcript[234], which was later adopted by Halegua *et al.* in the development of the NanoScribes VLP system[168]. But intriguingly, none of these studies explicitly reference pegRNA stability as a design rationale, only Halegua *et al.* acknowledge the potential for increased stability as a possibility[168].
In each case, the aptamer was placed at the 3' end of the pegRNA in at least some designs, for which a stability increase would be expected. However, none of them except Halegua *et al.* worked on VLP delivery, but with DNA transfection instead. During the development of ENVLPE, we have also tested Csy4 in DNA transfections, but a beneficial effect on editing efficacy was only observed after implementing it into VLP delivery. Fittingly, Halegua *et al.* also reported that the strategy of intronic pegRNA processing was less beneficial in DNA transfection experiments. It is therefore likely that the effect of Csy4 on pegRNA stability remained elusive to those other studies that worked with DNA transfection exclusively, where pegRNA abundance is high and the penalty for degradation is comparatively low. These results seem to emphasize the importance of pegRNA stability in low-abundance environments, as well as the sensitivity at which changes in pegRNA stability can be observed there. It is

therefore particularly odd that we did not observe a beneficial effect of PE7[51] when combined with ENVLPE, as one would certainly expect significant benefits from DNA transfection experiments to translate to VLP delivery.
It still stands to reason that by adopting the pegRNA design from ENVLPE, the effect of Csy4-mediated pegRNA stabilization should at least translate to other VLP systems. While we could demonstrate this with PE-eVLPs in principle, one would have expected the effect to be more pronounced. This in turn seems to suggest that in the current PE-eVLP design, pegRNA stability is not the primary bottleneck.

It has been reported that unspecific cleavage by Csy4 can lead to cytotoxicity[230]. Even though Csy4 has been utilized multiple times for prime editing prior to ENVLPE, we were the first to utilize it *in vivo*, where cytotoxicity concerns carry more weight. As any concentration-dependent unspecific cleavage is likely already substantially reduced by the transient nature of VLP delivery, and while we have also not observed any cytotoxicity, it might still be useful to develop mechanisms that can further mitigate cytotoxic risks. We tried to combine a catalytically inactive variant of Csy4[231] with self-cleaving ribozymes to process the 3' end of pegRNAs, which turned out unsuccessful. However, precautious implementation of a recently developed split-Csy4 system[235] might be able eliminate the remaining cytotoxic risk while retaining on-target cleavage and protection.

Modularity and compatibility

Compared to fusion-based approaches where the protein cargo might obstruct cargo assembly, non-covalent recruitment likely alleviates cargo-specific negative effects on assembly and packaging efficiency. In fact, the coiled-coil recruitment system in PE-eVLP was introduced with the same rationale of alleviating steric hindrance of large cargo proteins during particle assembly[169]. Though in this mode of non-covalent recruitment, it is still necessary to modify the cargo protein with a coil domain, which is already a modularity improvement compared to other fusion-based approaches.
In contrast, as an aptamer-based system, ENVLPE provides full modularity to seamlessly switch between different Cas9 effectors or even package mRNA instead of RNPs as cargo. While the respective cargo (pe)gRNA or mRNA has to be equipped with an aptamer for recruitment, the Cas effector requires no modification at all, minimizing the necessary design effort. Nonetheless, editor-tailored stoichiometry optimization during production might lead to further increases in performance.

Based on its modular design, ENVLPE already demonstrated compatibility with nuclease editing, CRISPR activation, BE and PE. Hence, it stands to reason that other Cas9-fused effector strategies could be used with ENVLPE, and likely also other gRNA-associated Cas variants like Cas12 and Cas13, although this depends on the design of a suitable aptamer-grafted gRNA.
ENVLPE therefore is, in principle, compatible with PE4 and PE5, as well as any dual-pegRNA strategy. Exo-PE could also be deployed, if either Exo-PE or ENVLPE switched to the orthogonal MS2 aptamer to avoid interference with the respective recruitment process. But it remains to be seen if those strategies are still effective when transiently delivered via VLPs. Halegua *et al.* already demonstrated as much by delivering two pegRNAs in the same particle for twinPE[168], but from our own experience, the efficacy penalty associated with increased edit

complexity is amplified during VLP-mediated editing, probably as a consequence of low editor abundance. It is therefore currently unclear if sufficient editing rates can be reached i.e. for larger insertions with those delivery tools.

With ENVLPE, we also pursued transgene integration via HDR, which requires the additional delivery of a DNA donor template. This can be achieved by encoding the donor onto a lentiviral transfer vector and deliver it via an IDLV, upon which the donor RNA is reverse transcribed as part of the lentiviral replication cycle. This has been demonstrated previously both in combination with TALENs[149,236] and also Cas9[156,184]. While it is possible to deliver RNP and donor within the same particle for an "all-in-one" approach, we have opted for delivery via separate particles for simplicity reasons. To enable simultaneous recruitment of RNP and donor, the lentiviral transgene backbone can be modified with a suitable RNA aptamer, as Yadav *et al.* have demonstrated[184]. IDLVs are better suited for HDR donor delivery than MLV-derived particles, because they transfer the donor-enclosing nucleocapsid directly into the nucleus[171,237,238] while MLV-delivered DNA only has access to the nucleus during mitosis, in which no HDR takes place.
As already highlighted before, there are also other technologies for targeted transgene integration which do not rely on recombinases/integrases instead of HDR, such as PASTE[70]/PASSIGE[71], CASTs[217] or STITCHR[218]. To incorporate these technologies into VLP delivery, the required donor could be delivered in the same fashion as before via IDLVs and reverse transcription, or in the case of STITCHR even without reverse transcription. However, associated recombinases or co-factor proteins would have to be additionally recruited. Multiple studies have highlighted the potential for cargo recruitment into VLPs via non-covalent protein interactions[155,169,178], which opens up an orthogonal recruitment mechanism for ENVLPE towards the construction of all-in-one IDLV particles for HDR, or adaptation to other gene editing tools that depend on additional protein co-factors. Attaching a cargo protein to an HIV accessory protein like Vpx for co-delivery would not require changes to the ENVLPE construct and retain its modularity. Similar to complex PE-mediated edits however, it is currently unclear how efficient such approaches would be.
ENVLPE might also be compatible with a very recent addition to the gene editing toolbox called "append editing", which harnesses novel Cas9-associated effectors to ADP-ribosylate thymines and cause a base edit[239]. Beyond base editing, the authors remarkably demonstrate the capability of ADP-ribosylation to trigger DSB-free HDR if an ssODN template is also provided. This is a highly desirable mode of action, and while packaging the novel Cas9-fused effector with ENVLPE should be rather straight-forward, packaging of the ssODN component will require further innovation.

ENVLPE as particle engineering platform

In fusion-based delivery systems, the addition of a helper gag-pol construct is required to drive cargo release via proteolytic cleavage[159,163,170]. A helper was still utilized even when the protease is incorporated into the engineered gag-Cas9 fusion construct[174], presumably to support particle assembly by reducing the sterical hindrance of bulky cargo proteins. For each cargo protein, the ratio of the helper is usually readjusted.
With aptamer-mediated RNP recruitment and release, there is no explicit requirement for proteolytic maturation. Nonetheless, existing technologies have not tried to eliminate it before, mostly because they did not depend on it from the start. For instance, in LVLPs the gag-pol

polyprotein itself has been engineered with aptamer-binding proteins. In our own attempts at this design, we did not succeed to improve over helper-based assembly; we observed that it is actually quite challenging to engineer gag-pol itself without affecting the intricate composition of the construct.
For ENVLPE, additional proteolytic release only made an impact when a different aptamer (Csy4) with much higher binding affinity (and therefore presumably suboptimal release kinetics) was used for cargo recruitment. This means that in principle, it is not necessary to support ENVLPE with a helper gag-pol construct, although we did observe that "homomeric" assemblies without any helper display reduced editing efficacy. In fact, this protease-independent beneficial effect on particle assembly by the helper construct has remained elusive, despite investigations regarding the systematic elimination of individual pol domains.

Ngo *et al.* arrived at a similar conclusion with their fusion-based design (Cas9-EDV), also systematically eliminating non-essential gag components[173]. After recognizing in their previous publication already that virion maturation was not required for RNP delivery[172], they now removed protease cleavage entirely and observed that gag-Cas9 fusions were still highly active. The clear demonstration of the viability of monomeric assemblies led them to aggressively minimize the gag domain itself[173].
We had developed miniENVLPE with a very similar rationale, based on a minimized gag design from Accola *et al.* where large parts of the MA and CA domains were omitted[240]. We could show that in principle, various domains within the ENVLPE construct can be replaced by functional equivalents, occasionally even to beneficial effect. But importantly, based on the viability of homomeric particles, it was possible to modify the assembly-forming domain itself, which enables the engineering of novel particles based on non-viral, "humanized" or even fully synthetic[241] protein assemblies following the ENVLPE design principle. Engineering variants that assemble into smaller particles might also be desirable, as this was reported to correlate with higher cellular uptake and tissue penetration, although not for VLP speficically[242,243].

Targeting strategies from LVs to VLPs: Glycoprotein engineering

Tissue specificity and target cell entry is an important metric of delivery vectors, becoming even more relevant in therapeutic applications. Ideally, a given vector reaches its target cell efficiently, delivers the cargo effectively and touches nothing else in between.
The fashion in which tropism is determined can vary widely between vector types. AAVs contain a motif in the capsid shell which influence the efficacy at which a given tissue can be transduced, and library screens have identified variants that efficiently transduce specific cell types such as photoreceptors[244] or myocytes[245]. This motif in the capsid domain has also been used as integration site for ligand display to directly engage with a surface protein on the target cell[246]. LNPs are known for their inherent liver preference, and systemic application of LNPs is often associated with liver toxicity[247]. However, it is possible to actively target them to other tissues via antibodies or antibody fragments[248,249], which are conjugated to the surface via chemical coupling, or non-covalently via specific protein linkers[250]. Recent studies have even modified LNP tropism via tailored lipid compositions to facilitate gene editing in variety of non-liver tissues[117,251,252]. To increase cellular uptake and reduce toxicity after systemic administration, Brown *et al.* included fusion-associated small transmembrane (FAST) proteins in the LNP formulation[253].

Compared to other delivery vectors, tropism modulation of LVs is quite easy to execute and comes with a high variety of options. LV tropism is determined by glycoproteins that are displayed on the lipid bilayer envelope. These glycoproteins facilitate target cell entry through their fusogenic properties and targeted engagement of cell surface receptors. There is a wide variety of different glycoproteins across the domain of enveloped viruses, many of which have been utilized to pseudotype lentiviral vectors[254,255]. Arguably the most prominent one is the glycoprotein of the vesicular stomatitis virus (VSV-G), which binds to the LDL receptor (LDL-R) family[256,257]. VSV-G pseudotyping provides multiple additional advantages: Its high stability enables particle preparation through ultracentrifugation[258], and it efficiently facilitates endosomal escape through a pH-dependent conformational change[259]. VSV-G also promotes vesicle budding[125], which is highly useful for EV preparations as well[126,128].
LDL-R is expressed in many different cell types, making VSV-G pseudotyping widely applicable. However, this in turn limits its specificity, and some particularly relevant cell types such as resting lymphocytes do not express LDL-R at all and can therefore not be targeted[260]. A lot of research has consequently focused on utilizing the natural diversity of glycoproteins, sometimes while trying to preserve the non-targeting properties of VSV-G, to expand the scope of targetable cell types. This research has enormous relevance for VLPs and even EVs, since they can be pseudotyped in the same fashion as LVs. The compatibility is often implicit, and many publications that focus on EV/VLP engineering and the logistics of cargo packaging actually just rely on VSV-G throughout the entire study. ENVLPE is not an exception from this, as we have demonstrated pseudotyping capabilities only to a limited degree in an experiment with the MLV-Eco glycoprotein. However, other studies on VLP-mediated editor delivery have heavily invested into novel pseudotyping strategies[130,172,185], and their innovations will be highlighted in this chapter alongside previous work on LV targeting. These publications collectively emphasize the potential for glycoprotein-targeted RNP delivery approaches via VLPs, even accessing previously unattainable cell types. As broad compatibility of respective targeting strategies with various LV and VLP designs has already been demonstrated, it should be possible to ultimately integrate them into an RNP delivery approach with ENVLPE.

AAV pre-targeting

As noted above, VSV-G has many advantages as an envelope glycoprotein, but there are some cell types it cannot access due to a lack of LDL-R expression. This can be solved using a tissue-specific AAV to initially deliver an LDL-R encoding vector to the cell of interest, making it susceptible to VSV-G transduction. This strategy referred to as “pre-targeting” can in principle make any cell susceptible to any glycoprotein of choice, as long as it is targetable by a respective AAV. To enhance tissue specificity further, expression of the receptor can be coupled to a tissue-specific promoter.
However, the *in vivo* utility of this strategy is limited by the endogenous expression pattern of the receptor within the target organism. To maximize target cell specificity, it might be feasible to utilize fully orthogonal, engineered ligand-receptor pairs, although this raises some immunogenicity concern in return.

Glycoprotein alternatives to VSV-G

To generate particles with a differential targeting profile to VSV-G, LVs and VLPs can be pseudotyped with a variety of glycoproteins from other viruses. The cocal virus glycoprotein is highly homologous to VSV-G, targets the same receptor[261] and avoids serum inactivation in humans[262]. A very recent study even mined for VSV-G homologs to increase the delivery potency to non-activated lymphocytes[263], which is an important prerequisite for *in vivo* T-cell engineering. Other examples of targeting immune cells and hematopoietic stem cells include the Baboon retrovirus envelope glycoprotein (BaEV) which was used to pseudotype LVs[264,265] and later also VLPs[160], as well as glycoproteins from Gibbon Ape Leukemia virus (GALV)[266], Koala Retrovirus (KoRVA)[267], and RD114[268,269]. Glycoproteins from BaEV and Sendai virus were also co-expressed together with VSV-G to enhance transduction efficiency across various cell types[159,270]. Pseudotyping with rabies virus glycoprotein (RV-G) was shown to efficiently transduce neuronal cells[271].

Engineered glycoproteins

Glycoproteins can also be modified, or stitched together from different viruses to combine beneficial characteristics. For instance, Kato *et al.* replaced the cytoplasmic domain of RV-G with the corresponding one from VSV-G, yielding a chimeric glycoprotein (FuG-B) with altered properties[272]. Other studies even introduced antibody-derived targeting domains; for instance, one group modified the MLV-Eco glycoprotein with a single chain variable fragment (ScFv), having found that a variable loop within MLV-Eco which also contains the binding interface is tolerable to large insertions[273].

VSV-G is particularly difficult to modify, because it undergoes complex conformational changes upon binding and during endosomal escape[274]. Certain sites have been identified that might be tolerable to modifications[275], but successful engineering attempts have been scarce. One recent study now showed that optimization of the VSV-G backbone enables simple N-terminal fusions of nanobodies[276], which usually leads to drastically reduced viral titers[277]. This has the potential to re-vitalize direct engineering of VSV-G.

Separation of binding and fusion modalities

A major bottleneck of glycoprotein engineering is the risk of affecting the glycoprotein fusion properties while modifying its targeting domain, as these are often not spatially separated. However, there is a class of glycoproteins from the order of *paramyxoviridae*, where the fusion and binding functionality are naturally split into separate chains: The H protein is responsible for binding a target receptor, while the F protein mediates fusion. Although some co-engineering of the F protein might still be required[278], this separation enabled powerful platforms for tropism engineering via the H protein, for instance from Nipah virus[185,279,280], measles virus[281–286] and sindbis virus[287], to target a variety of cell types via single chain antibodies, ScFvs or DARPins.

The separation of binding and fusion functionalities was also achieved with VSV-G: Nikolic *et al.* showed that the interaction to its natural entry point LDL-R could be abolished via two specific mutations without affecting VSV-G fusogenicity[256], Michels *et al.* made a similar discovery with the cocal virus glycoprotein[288]. VLP tropism could now be customized using affinity ligands such as antibody fragments, co-expressed and separately displayed on the particle surface via engineered membrane anchors.

Based on this principle, two groups developed platforms for high-throughput decoding of ligand-receptor interactions, called RAPTR[289] and ENTER[290], displaying antibody fragments or peptide-MHC conjugates next to mutant VSV-G. Hamilton *et al.* expanded on their Cas9-EDV architecture with this strategy to target immune cells specifically[172]. Strebinger *et al.* additionally introduced antibody-binding proteins as a modular recruitment mechanism for targeting ligands, and applied their DIRECTED platform to various VLP designs[291].

State of gene editing VLPs for clinical translation

Current trends and competition

There is potential for the clinical adoption of VLPs both *ex vivo* and *in vivo*, although the advantages over competing technologies for *in vivo* administration are much more pronounced. While there is interest in utilizing CRISPR to transition towards targeted integration for the generation of chimeric antigen receptor T-cells (CAR-T)[292], currently approved therapies still rely on random integration via LVs. VLPs could be a viable alternative for the *ex vivo* modification of cells, but they will have to compete with highly efficient physical delivery methods that are also in development as LV alternatives, be it for autologous or allogeneic cell products. The only currently approved CRISPR-based therapy (Casgevy) relies on Cas9 RNP electroporation, and for targeted knock-ins this approach can also be supplemented with a DNA donor vector in form of an AAV[293] or IDLV[294], but also as (circular) ssDNA[295–297] as a fully transient alternative to mitigate the genotoxicity associated with LV and AAV integration.

For *in vivo* administration however, physical methods are outright not applicable, which means that VLPs mainly compete against AAVs and LNPs for gene editor delivery, with no therapy currently approved. As discussed in a previous chapter, the long-term expression of gene editors make AAVs a generally suboptimal vector choice, which leaves LNPs as the main competitor for transient delivery. While LNP therapies in the clinic mostly target the liver[79,200], VLPs arguably lag behind substantially with no active clinical trials to date. Notably, LVs have already been investigated in the clinic for systemic administration[298], and many VLP studies have demonstrated the capability of gene correction *in vivo,* although mostly via local administration[126,159,163,169,172,174,185]. Systematic administration studies are still scarce[163,172,185], but fittingly conducted by those who also emphasized glycoprotein engineering[172,185].
An intriguing recent development in the context of systemic administration is the attempt to generate CAR-T cells *in vivo*[299], primarily driven by the potential for reducing cost and manufacturing complexity of autologous cell therapies. The concept has even entered the clinic as an mRNA-LNP formulation recently[300], although notably the CAR is only transiently expressed in this case. The viability of VLPs for *in vivo* CAR-T generation would depend on the efficacy of donor delivery for HDR, which remains to be demonstrated.

Enabling systematic administration of transient gene editing vectors would be a major breakthrough for tissues unavailable to local therapy, but this requires high tissue specificity, efficacy and tolerability. Further, editing would also have to be restricted to somatic cells for ethical reasons. But based on the demonstrated efficacy and their tropism modulation capabilities, VLPs could emerge as the enabling technology for *in vivo* gene correction both systemically and locally. There is a lot of innovation in the fast-paced field of VLP engineering, seeing steady progression towards an ideal particle design and further research on custom

targeting domains and glycoproteins. Comprehensive comparison of all these novel VLP tools against LNP vehicles has not yet been carried out, likely because they require quite a diverse set of manufacturing capabilities both on the editor complex and the delivery vector level. But as VLPs are arguably still behind LNPs in terms of clinical translation, the increased traction in the field will hopefully also attract more interest towards solving the manufacturing challenges of cell-derived particles, based on already available knowledge with lentiviral production. This will help to utilize the conceptual advantage of VLPs over LNPs regarding tissue specificity, biodistribution and RNP loading. Projecting that further progress is made with the adaptation of tissue targeting strategies, and that the challenges of VLP manufacturing can be overcome at scale, VLPs could occupy a niche of extra-hepatic indications where they are preferred over LNPs and other modes of delivery. The following section briefly discusses challenges and opportunities that are associated with the clinical translation of VLPs. As the field is growing rapidly but with currently little clinical experience, regulatory guidelines regarding product quality and safety have not yet adapted and still rely on established knowledge with LV products[122].

Off-target activity

AAVs, as the currently prevalent gene editor delivery vector in the clinic, mediate persistent gene editor expression, which carries a risk of unintended DSBs over time. Because of this, AAV-mediated nuclease editing can cause genotoxicity and senescence in target cells, although this can apparently also be alleviated by transiently inhibiting corresponding DNA damage sensory pathways[293,301].

Off-target editing and particularly the prevalence of DSBs can already be addressed by next-generation editing strategies with higher fidelity. Consequently, dual-AAVs[302] have already been adapted to both BE[303–305] and PE[57,306] to circumvent size restrictions. Nonetheless, shifting to transient expression of the gene editor likely also has a major benefit for the off-target editing profile: Many of the referenced VLP studies, and also our own work, feature off-target editing investigations, utilizing one of the various tools available[307–311], or sites discovered with those tools. The observed off-target activity was generally low, and also favorable compared to other modes of delivery like plasmid transfection, electroporation or viral transduction that promote much higher or much more persistent gene editor expression. In that regard, RNP delivery is also preferred over mRNA delivery, as it minimizes the time window for off-target edits to occur.

Immunogenicity

Immunogenicity can arise from three different aspects of VLP-mediated gene editor delivery: the vehicle, the cargo molecules, and contaminants from the host cell or the production process. It is known from viral delivery that the innate immune system can recognize viral components to inhibit transduction[312], and VSV-G specifically is known to be inactivated by human serum[262]. As VLPs rely on the same targeting strategies, these issues would transfer. However, VLPs do not contain any viral genetic material such as regulatory elements or terminal repeats, and therefore avoid triggering innate DNA sensing pathways. Still, pre-existing antibodies could render a therapy ineffective, and even the adaptive immune system can promote clearance of edited cells. Though in comparison to AAVs, the human pre-exposure rate to retroviruses is comparatively low, which limits the prevalence of pre-existing anti-vehicle antibodies[122].

Adaptive immune system activation in response to gene editor cargo could also cause clearance of edited cells, and prevent re-dosing or the administration of gene editors for a different indication in the future. Immunogenicity to the gene editor itself concerns all CRISPR therapies, but the short-term presence of a hit-and-run RNP is arguably the safest option going forward. Based on the reduced time window of editor presence with transient delivery vectors, immune triggering is presumably less likely, but can still occur[185]. A safety study on RNP delivery via VLPs in mice and non-human primates to immune-privileged tissue (brain and eye) detected immune cell infiltration and macrophage enrichment shortly after treatment, but no increase in apoptosis[185]. The immunogenic response was mostly linked to VLP components, as a similar response level could be observed with empty VLP controls. But in a separate macrophage model, it was also demonstrated that the immunogenic response was lower compared to LV-delivered CRISPR[185], in which the cargo is expressed persistently.
The risk of immunogenic responses to VLP-mediated gene editor delivery certainly requires more investigation, but there are also strategies to pre-emptively mitigate them. To reduce immunogenic burden, minimally immunogenic nucleases have been developed[211]. On the vector side, human retrovirus-like proteins have been investigated as RNA transfer vehicles[313,314], although without any demonstration of CRISPR delivery so far. Within the ENVLPE framework, we have demonstrated the capability to engineer novel particles, which could facilitate the development of minimally immunogenic frameworks in the future.
Lastly, as a cell-derived product, immunogenicity can also arise from contaminants originating from the host cell or the production process. For instance, residual plasmid DNA and genomic DNA can be eliminated by limiting cell death, enzymatic digestion and proper purification[315]. But host DNA and proteins can also be stochastically co-packaged into the particle or even host surface proteins displayed on the particle membrane[316,317]. To reduce the immunogenic potential of cell-derived vesicles, it has been proposed to knock out MHC-I in producer cells[318].

Manufacturing

As transient delivery vectors, the above issues concern LNPs and VLPs often in a similar fashion. However, their stories diverge substantially on the topic of manufacturing, especially in a GMP-compliant fashion. While LNPs can be synthesized chemically in a defined process, the at-scale production and purification of VLPs is more complicated, and suitable quality and batch control parameters and instruments remain to be broadly established. There is some precedent for VLPs as vaccine carriers[319], but the majority of applicable experience originates from other cell-derived vesicles, mostly LVs[320–322] (for a comprehensive review, please refer to Lipalo *et al.*[122] or Segura *et al.*[315]).

GMP-compliant manufacturing from producer cells requires fully characterized cell lines, defined (serum-free) culture growth conditions, and a highly reproducible transfection protocol with plasmids that were also generated under GMP. Production cell lines can additionally be engineered to optimize particle yield[323], increase particle bioavailability[324], reduce retrotransduction during production[325], or tailor them to a glycoprotein of choice[326].
After harvesting and clarification of the production culture supernatant, particles have to be purified and concentrated. In pre-clinical laboratory-scale studies, this is usually accomplished by ultracentrifugation, particle precipitation, or ultrafiltration with molecular weight filters. However, these methods either scale poorly, damage the particles or massively affect particle yield, or tend to co-purify other host cell components[327,328]. There are also more gentle and

potentially scalable filtration approaches based on tangential flow[329] or membrane oscillation[330], but as the other techniques they can also not discriminate between VLPs and other cell-derived vesicles of similar size that host cells might generate[331]. A chromatography-based workflow with sequential size exclusion (SEC) and anion exchange (AEX) was proposed to increase product purity of LVs on the laboratory scale[332], and intriguingly, AEX might actually allow for selective enrichment against other types of EVs[333]. Lastly, affinity enrichment chromatography could arguably provide the highest purity[315], but its scalability severely cost-limited.

Complementary to a robust production and purification protocol, it is essential to clearly define quality attributes and their respective ranges. For VLPs, these attributes generally align with quality control for the production of LVs: Physical/morphological appearance, absence of contaminants, and functional titer. Particle size, morphology and zeta potential can be assessed with optical methods such as dynamic light scattering (DLS), nanoparticle tracking analysis (NTA)[334,335] and electron microscopy (EM)[336], but potentially also flow cytometry[336]. Impurity quantification, particularly host cell proteins (HCPs) inside the particle or on its surface, may be accomplished via mass spectrometry[337].

While it is possible to also quantify particles via optical methods, this is usually considered less accurate. For instance, NTA is very susceptible to impurities and tends to overestimate[322]. Viral titers are conventionally determined with enzyme-linked immunosorbent assay (ELISA) targeting viral capsid components[338,339] or RT-qPCR targeting the viral genome. While the latter does not apply to RNP-loaded VLPs, ELISA can still be applied, and in combination with another ELISA targeting Cas9 and RT-qPCR on the gRNA it can also provide an estimate of cargo loading efficiency. But even though capsid-targeted ELISA discriminates against non-VLP vesicles, an accurate measurement can still be obstructed by empty or damaged VLPs as well as unassembled capsid proteins[339]. To determine the proportion of empty/unproductive VLPs or other types of vesicles in the preparation, a functional titer measurement is essential. For gene editing, this requires the co-development and calibration of a corresponding reporter system, which together with optical and chromatographic parameters referenced above could provide a comprehensive quality control profile to demonstrate batch-to-batch consistency and reproducibility.

Bibliography

This bibliography contains all literature that is referenced in the introduction and discussion section of this dissertation. Please note that the attached first-author publications contain both literature references from this list as well as additional references that are not listed here.

1. Knott, G.J., and Doudna, J.A. (2018). CRISPR-Cas guides the future of genetic engineering. Science *361*, 866–869.

2. Komor, A.C., Kim, Y.B., Packer, M.S., Zuris, J.A., and Liu, D.R. (2016). Programmable editing of a target base in genomic DNA without double-stranded DNA cleavage. Nature *533*, 420–424.

3. Gaudelli, N.M., Komor, A.C., Rees, H.A., Packer, M.S., Badran, A.H., Bryson, D.I., and Liu, D.R. (2017). Programmable base editing of A•T to G•C in genomic DNA without DNA cleavage. Nature *551*, 464–471.

4. Zou, S., Sun, Y., and Tang, W. (2025). Charting the development and engineering of CRISPR base editors: lessons and inspirations. Cell Chem. Biol. *32*, 789–808.

5. Anzalone, A.V., Koblan, L.W., and Liu, D.R. (2020). Genome editing with CRISPR-Cas nucleases, base editors, transposases and prime editors. Nat. Biotechnol. https://doi.org/10.1038/s41587-020-0561-9.

6. Anzalone, A.V., Randolph, P.B., Davis, J.R., Sousa, A.A., Koblan, L.W., Levy, J.M., Chen, P.J., Wilson, C., Newby, G.A., Raguram, A., et al. (2019). Search-and-replace genome editing without double-strand breaks or donor DNA. Nature *576*, 149–157.

7. Mentani, A., Maresca, M., and Shiriaeva, A. (2025). Prime editing: Mechanistic insights and DNA repair modulation. Cells *14*, 277.

8. Chen, P.J., Hussmann, J.A., Yan, J., Knipping, F., Ravisankar, P., Chen, P.-F., Chen, C., Nelson, J.W., Newby, G.A., Sahin, M., et al. (2021). Enhanced prime editing systems by manipulating cellular determinants of editing outcomes. Cell *184*, 5635-5652.e29.

9. Gu, S., Bodai, Z., Anderson, R.A., So, H.Y.A., Cowan, Q.T., and Komor, A.C. (2025). Elucidating the genetic mechanisms governing cytosine base editing outcomes through CRISPRi screens. Nat. Commun. *16*, 4685.

10. Scully, R., Panday, A., Elango, R., and Willis, N.A. (2019). DNA double-strand break repair-pathway choice in somatic mammalian cells. Nat. Rev. Mol. Cell Biol. *20*, 698–714.

11. Chen, P.J., and Liu, D.R. (2023). Prime editing for precise and highly versatile genome manipulation. Nat. Rev. Genet. *24*, 161–177.

12. Murray, J.B., Harrison, P.T., and Scholefield, J. (2025). Prime editing: therapeutic advances and mechanistic insights. Gene Ther. *32*, 83–92.

13. Song, M., Lim, J.M., Min, S., Oh, J.-S., Kim, D.Y., Woo, J.-S., Nishimasu, H., Cho, S.-R., Yoon, S., and Kim, H.H. (2021). Generation of a more efficient prime editor 2 by addition of the Rad51 DNA-binding domain. Nat. Commun. *12*, 5617.

14. Ferreira da Silva, J., Oliveira, G.P., Arasa-Verge, E.A., Kagiou, C., Moretton, A., Timelthaler, G., Jiricny, J., and Loizou, J.I. (2022). Prime editing efficiency and fidelity are enhanced in the absence of mismatch repair. Nat. Commun. *13*, 760.

15. Park, S.-J., Jeong, T.Y., Shin, S.K., Yoon, D.E., Lim, S.-Y., Kim, S.P., Choi, J., Lee, H., Hong, J.-I., Ahn, J., et al. (2021). Targeted mutagenesis in mouse cells and embryos using an enhanced prime editor. Genome Biol. *22*, 170.

16. Chen, R., Cao, Y., Liu, Y., Zhao, D., Li, J., Cheng, Z., Bi, C., and Zhang, X. (2023). Enhancement of a prime editing system via optimal recruitment of the pioneer transcription factor P65. Nat. Commun. *14*, 257.

17. Adikusuma, F., Lushington, C., Arudkumar, J., Godahewa, G.I., Chey, Y.C.J., Gierus, L., Piltz, S., Geiger, A., Jain, Y., Reti, D., et al. (2021). Optimized nickase- and nuclease-based prime editing in human and mouse cells. Nucleic Acids Res. *49*, 10785–10795.

18. Tao, R., Wang, Y., Hu, Y., Jiao, Y., Zhou, L., Jiang, L., Li, L., He, X., Li, M., Yu, Y., et al. (2022). WT-PE: Prime editing with nuclease wild-type Cas9 enables versatile large-scale genome editing. Signal Transduct. Target. Ther. *7*, 108.

19. Peterka, M., Akrap, N., Li, S., Wimberger, S., Hsieh, P.-P., Degtev, D., Bestas, B., Barr, J., van de Plassche, S., Mendoza-Garcia, P., et al. (2022). Harnessing DSB repair to promote efficient homology-dependent and -independent prime editing. Nat. Commun. *13*, 1240.

20. Li, X., Zhang, G., Huang, S., Liu, Y., Tang, J., Zhong, M., Wang, X., Sun, W., Yao, Y., Ji, Q., et al. (2023). Development of a versatile nuclease prime editor with upgraded precision. Nat. Commun. *14*, 305.

21. Wimberger, S., Akrap, N., Firth, M., Brengdahl, J., Engberg, S., Schwinn, M.K., Slater, M.R., Lundin, A., Hsieh, P.-P., Li, S., et al. (2023). Simultaneous inhibition of DNA-PK and PolΘ improves integration efficiency and precision of genome editing. Nat. Commun. *14*, 4761.

22. Selvaraj, S., Feist, W.N., Viel, S., Vaidyanathan, S., Dudek, A.M., Gastou, M., Rockwood, S.J., Ekman, F.K., Oseghale, A.R., Xu, L., et al. (2024). High-efficiency transgene integration by homology-directed repair in human primary cells using DNA-PKcs inhibition. Nat. Biotechnol. *42*, 731–744.

23. Cullot, G., Aird, E.J., Schlapansky, M.F., Yeh, C.D., van de Venn, L., Vykhlyantseva, I., Kreutzer, S., Mailänder, D., Lewków, B., Klermund, J., et al. (2024). Genome editing with the HDR-enhancing DNA-PKcs inhibitor AZD7648 causes large-scale genomic alterations. Nat. Biotechnol., 1–5.

24. Dacquay, L.C., Antoniou, P., Mentani, A., Selfjord, N., Mårtensson, H., Hsieh, P.-P., Mustfa, S., Thom, G., Wimberger, S., Firth, M., et al. (2025). Dual inhibition of DNA-PK and PolΘ boosts precision of diverse prime editing systems. Nat. Commun. *16*, 4290.

25. Liu, N., Zhou, L., Lin, G., Hu, Y., Jiao, Y., Wang, Y., Liu, J., Yang, S., and Yao, S. (2022). HDAC inhibitors improve CRISPR-Cas9 mediated prime editing and base editing. Mol. Ther. Nucleic Acids *29*, 36–46.

26. Liu, B., Dong, X., Zheng, C., Keener, D., Chen, Z., Cheng, H., Watts, J.K., Xue, W., and Sontheimer, E.J. (2024). Targeted genome editing with a DNA-dependent DNA polymerase and exogenous DNA-containing templates. Nat. Biotechnol. *42*, 1039–1045.

27. Ferreira da Silva, J., Tou, C.J., King, E.M., Eller, M.L., Rufino-Ramos, D., Ma, L., Cromwell, C.R., Metovic, J., Benning, F.M.C., Chao, L.H., et al. (2024). Click editing enables programmable genome writing using DNA polymerases and HUH endonucleases. Nat. Biotechnol. https://doi.org/10.1038/s41587-024-02324-x.

28. Ponnienselvan, K., Liu, P., Nyalile, T., Oikemus, S., Maitland, S.A., Lawson, N.D., Luban, J., and Wolfe, S.A. (2023). Reducing the inherent auto-inhibitory interaction within the pegRNA enhances prime editing efficiency. Nucleic Acids Res. *51*, 6966–6980.

29. Zhang, W., Petri, K., Ma, J., Lee, H., Tsai, C.-L., Joung, J.K., and Yeh, J.-R.J. (2024). Enhancing CRISPR prime editing by reducing misfolded pegRNA interactions. Elife *12*. https://doi.org/10.7554/elife.90948.2.

30. Liu, Y., Yang, G., Huang, S., Li, X., Wang, X., Li, G., Chi, T., Chen, Y., Huang, X., and Wang, X. (2021). Enhancing prime editing by Csy4-mediated processing of pegRNA. Cell Res. *31*, 1134–1136.

31. Feng, Y., Liu, S., Mo, Q., Liu, P., Xiao, X., and Ma, H. (2023). Enhancing prime editing efficiency and flexibility with tethered and split pegRNAs. Protein Cell *14*, 304–308.

32. Yang, C., Fang, Q., Li, M., Zhang, J., Li, R., Zhou, T., Wang, K., Deng, J., Wang, X., Huang, C., et al. (2025). Prime editor with rational design and AI-driven optimization for reverse editing window and enhanced fidelity. Nat. Commun. *16*, 5144.

33. Liang, R., Wang, S., Cai, Y., Li, Z., Li, K.M., Wei, J., Sun, C., Zhu, H., Chen, K., and Gao, C. (2025). Circular RNA-mediated inverse prime editing in human cells. Nat. Commun. *16*, 5057.

34. Li, X., Zhou, L., Gao, B.-Q., Li, G., Wang, X., Wang, Y., Wei, J., Han, W., Wang, Z., Li, J., et al. (2022). Highly efficient prime editing by introducing same-sense mutations in pegRNA or stabilizing its structure. Nat. Commun. *13*, 1669.

35. Nelson, J.W., Randolph, P.B., Shen, S.P., Everette, K.A., Chen, P.J., Anzalone, A.V., An, M., Newby, G.A., Chen, J.C., Hsu, A., et al. (2022). Engineered pegRNAs improve prime editing efficiency. Nat. Biotechnol. *40*, 402–410.

36. Antoniou, P., Dacquay, L., Mårtensson, H., Madeyski-Bengtson, K., Loyd, A.-L., Shiriaeva, A., Gordon, E., Mustfa, S., Thom, G., Hsieh, P.-P., et al. (2025). Modified pegRNAs mitigate scaffold-derived prime editing by-products. Nat. Commun. *16*, 3374.

37. Anderson, M.V., Haldrup, J., Thomsen, E.A., Wolff, J.H., and Mikkelsen, J.G. (2021). pegIT - a web-based design tool for prime editing. Nucleic Acids Res. *49*, W505–W509.

38. Hsu, J.Y., Grünewald, J., Szalay, R., Shih, J., Anzalone, A.V., Lam, K.C., Shen, M.W., Petri, K., Liu, D.R., Joung, J.K., et al. (2021). PrimeDesign software for rapid and simplified design of prime editing guide RNAs. Nat. Commun. *12*, 1034.

39. Hwang, G.-H., Jeong, Y.K., Habib, O., Hong, S.-A., Lim, K., Kim, J.-S., and Bae, S. (2021). PE-Designer and PE-Analyzer: web-based design and analysis tools for CRISPR prime editing. Nucleic Acids Res. *49*, W499–W504.

40. Levesque, S., Cosentino, A., Verma, A., Genovese, P., and Bauer, D.E. (2025). Enhancing prime editing in hematopoietic stem and progenitor cells by modulating nucleotide metabolism. Nat. Biotechnol. *43*, 534–538.

41. Liu, P., Ponnienselvan, K., Nyalile, T., Oikemus, S., Joynt, A.T., Iyer, S., Kelly, K., Guo, D., Kyawe, P.P., Vanderleeden, E., et al. (2025). Increasing intracellular dNTP levels improves prime editing efficiency. Nat. Biotechnol. *43*, 539–544.

42. Li, X., Chen, W., Martin, B.K., Calderon, D., Lee, C., Choi, J., Chardon, F.M., McDiarmid, T.A., Daza, R.M., Kim, H., et al. (2024). Chromatin context-dependent regulation and epigenetic manipulation of prime editing. Cell *187*, 2411-2427.e25.

43. Kim, H.K., Yu, G., Park, J., Min, S., Lee, S., Yoon, S., and Kim, H.H. (2021). Predicting the efficiency of prime editing guide RNAs in human cells. Nat. Biotechnol. *39*, 198–206.

44. Mathis, N., Allam, A., Kissling, L., Marquart, K.F., Schmidheini, L., Solari, C., Balázs, Z., Krauthammer, M., and Schwank, G. (2023). Predicting prime editing efficiency and product purity by deep learning. Nat. Biotechnol. *41*, 1151–1159.

45. Yu, G., Kim, H.K., Park, J., Kwak, H., Cheong, Y., Kim, D., Kim, J., Kim, J., and Kim, H.H. (2023). Prediction of efficiencies for diverse prime editing systems in multiple cell types. Cell *186*, 2256-2272.e23.

46. Koeppel, J., Weller, J., Peets, E.M., Pallaseni, A., Kuzmin, I., Raudvere, U., Peterson, H., Liberante, F.G., and Parts, L. (2023). Prediction of prime editing insertion efficiencies using sequence features and DNA repair determinants. Nat. Biotechnol. *41*, 1446–1456.

47. Mathis, N., Allam, A., Tálas, A., Kissling, L., Benvenuto, E., Schmidheini, L., Schep, R., Damodharan, T., Balázs, Z., Janjuha, S., et al. (2025). Machine learning prediction of prime editing efficiency across diverse chromatin contexts. Nat. Biotechnol. *43*, 712–719.

48. Menezes, M.R., Balzeau, J., and Hagan, J.P. (2018). 3' RNA uridylation in epitranscriptomics, gene regulation, and disease. Front. Mol. Biosci. *5*, 61.

49. Hendel, A., Bak, R.O., Clark, J.T., Kennedy, A.B., Ryan, D.E., Roy, S., Steinfeld, I., Lunstad, B.D., Kaiser, R.J., Wilkens, A.B., et al. (2015). Chemically modified guide RNAs enhance CRISPR-Cas genome editing in human primary cells. Nat. Biotechnol. *33*, 985–989.

50. Zhang, G., Liu, Y., Huang, S., Qu, S., Cheng, D., Yao, Y., Ji, Q., Wang, X., Huang, X., and Liu, J. (2022). Enhancement of prime editing via xrRNA motif-joined pegRNA. Nat. Commun. *13*, 1856.

51. Yan, J., Oyler-Castrillo, P., Ravisankar, P., Ward, C.C., Levesque, S., Jing, Y., Simpson, D., Zhao, A., Li, H., Yan, W., et al. (2024). Improving prime editing with an endogenous small RNA-binding protein. Nature *628*, 639–647.

52. Liu, B., Dong, X., Cheng, H., Zheng, C., Chen, Z., Rodríguez, T.C., Liang, S.-Q., Xue, W., and Sontheimer, E.J. (2022). A split prime editor with untethered reverse transcriptase and circular RNA template. Nat. Biotechnol. *40*, 1388–1393.

53. Doman, J.L., Pandey, S., Neugebauer, M.E., An, M., Davis, J.R., Randolph, P.B., McElroy, A., Gao, X.D., Raguram, A., Richter, M.F., et al. (2023). Phage-assisted

evolution and protein engineering yield compact, efficient prime editors. Cell *186*, 3983-4002.e26.

54. Liu, P., Liang, S.-Q., Zheng, C., Mintzer, E., Zhao, Y.G., Ponnienselvan, K., Mir, A., Sontheimer, E.J., Gao, G., Flotte, T.R., et al. (2021). Improved prime editors enable pathogenic allele correction and cancer modelling in adult mice. Nat. Commun. *12*, 2121.

55. Liang, R., He, Z., Zhao, K.T., Zhu, H., Hu, J., Liu, G., Gao, Q., Liu, M., Zhang, R., Qiu, J.-L., et al. (2024). Prime editing using CRISPR-Cas12a and circular RNAs in human cells. Nat. Biotechnol. https://doi.org/10.1038/s41587-023-02095-x.

56. Kweon, J., Yoon, J.-K., Jang, A.-H., Shin, H.R., See, J.-E., Jang, G., Kim, J.-I., and Kim, Y. (2021). Engineered prime editors with PAM flexibility. Mol. Ther. *29*, 2001–2007.

57. Davis, J.R., Banskota, S., Levy, J.M., Newby, G.A., Wang, X., Anzalone, A.V., Nelson, A.T., Chen, P.J., Hennes, A.D., An, M., et al. (2024). Efficient prime editing in mouse brain, liver and heart with dual AAVs. Nat. Biotechnol. *42*, 253–264.

58. Lan, T., Chen, H., Tang, C., Wei, Y., Liu, Y., Zhou, J., Zhuang, Z., Zhang, Q., Chen, M., Zhou, X., et al. (2023). Mini-PE, a prime editor with compact Cas9 and truncated reverse transcriptase. Mol. Ther. Nucleic Acids *33*, 890–897.

59. Grünewald, J., Miller, B.R., Szalay, R.N., Cabeceiras, P.K., Woodilla, C.J., Holtz, E.J.B., Petri, K., and Joung, J.K. (2023). Engineered CRISPR prime editors with compact, untethered reverse transcriptases. Nat. Biotechnol. *41*, 337–343.

60. Mu, S., Chen, H., Li, Q., Gou, S., Liu, X., Wang, J., Zheng, W., Chen, M., Jin, Q., Lai, L., et al. (2024). Enhancing prime editor flexibility with coiled-coil heterodimers. Genome Biol. *25*, 108.

61. Ono, Y., Peterka, M., Love, M., Bhandari, A., Gordon, E., Ball, J.S., Tyler, C.R., Rees, S., Bohlooly-Y, M., Maresca, M., et al. (2025). Optimised genome editing for precise DNA insertion and substitution using Prime Editors in zebrafish. bioRxiv. https://doi.org/10.1101/2025.04.23.650248.

62. Lin, Q., Jin, S., Zong, Y., Yu, H., Zhu, Z., Liu, G., Kou, L., Wang, Y., Qiu, J.-L., Li, J., et al. (2021). High-efficiency prime editing with optimized, paired pegRNAs in plants. Nat. Biotechnol. *39*, 923–927.

63. Anzalone, A.V., Gao, X.D., Podracky, C.J., Nelson, A.T., Koblan, L.W., Raguram, A., Levy, J.M., Mercer, J.A.M., and Liu, D.R. (2022). Programmable deletion, replacement, integration and inversion of large DNA sequences with twin prime editing. Nat. Biotechnol. *40*, 731–740.

64. Choi, J., Chen, W., Suiter, C.C., Lee, C., Chardon, F.M., Yang, W., Leith, A., Daza, R.M., Martin, B., and Shendure, J. (2022). Precise genomic deletions using paired prime editing. Nat. Biotechnol. *40*, 218–226.

65. Jiang, T., Zhang, X.-O., Weng, Z., and Xue, W. (2022). Deletion and replacement of long genomic sequences using prime editing. Nat. Biotechnol. *40*, 227–234.

66. Wang, J., He, Z., Wang, G., Zhang, R., Duan, J., Gao, P., Lei, X., Qiu, H., Zhang, C., Zhang, Y., et al. (2022). Efficient targeted insertion of large DNA fragments without DNA donors. Nat. Methods *19*, 331–340.

67. Zhuang, Y., Liu, J., Wu, H., Zhu, Q., Yan, Y., Meng, H., Chen, P.R., and Yi, C. (2022). Increasing the efficiency and precision of prime editing with guide RNA pairs. Nat. Chem. Biol. *18*, 29–37.

68. Tao, R., Wang, Y., Jiao, Y., Hu, Y., Li, L., Jiang, L., Zhou, L., Qu, J., Chen, Q., and Yao, S. (2022). Bi-PE: bi-directional priming improves CRISPR/Cas9 prime editing in mammalian cells. Nucleic Acids Res. *50*, 6423–6434.

69. Zheng, C., Liu, B., Dong, X., Gaston, N., Sontheimer, E.J., and Xue, W. (2023). Template-jumping prime editing enables large insertion and exon rewriting in vivo. Nat. Commun. *14*, 3369.

70. Yarnall, M.T.N., Ioannidi, E.I., Schmitt-Ulms, C., Krajeski, R.N., Lim, J., Villiger, L., Zhou, W., Jiang, K., Garushyants, S.K., Roberts, N., et al. (2023). Drag-and-drop genome insertion of large sequences without double-strand DNA cleavage using CRISPR-directed integrases. Nat. Biotechnol. *41*, 500–512.

71. Pandey, S., Gao, X.D., Krasnow, N.A., McElroy, A., Tao, Y.A., Duby, J.E., Steinbeck, B.J., McCreary, J., Pierce, S.E., Tolar, J., et al. (2025). Efficient site-specific integration of large genes in mammalian cells via continuously evolved recombinases and prime editing. Nat. Biomed. Eng. *9*, 22–39.

72. Levesque, S., Kawashima, N., Hwang, G., Becerra, B., Schoonenberg, V.A.C., Mannherz, W., Homfeldt, L., Pinello, L., Agarwal, S., and Bauer, D.E. (2025). *In cellulo*DNA assembly for targeted genomic integration and rearrangement in human cells. bioRxiv. https://doi.org/10.1101/2025.06.16.659926.

73. Liu, B., Petti, A., Zhou, X., Cheng, H., Zhou, L., Jiang, T., Sontheimer, E.J., and Xue, W. (2025). Prime assembly with linear DNA donors enables large genomic insertions. bioRxiv. https://doi.org/10.1101/2025.06.16.659978.

74. Xiong, Y., Su, Y., He, R., Han, X., Li, S., Liu, M., Xi, X., Liu, Z., Wang, H., Xie, S., et al. (2025). EXPERT expands prime editing efficiency and range of large fragment edits. Nat. Commun. *16*, 1592.

75. Doudna, J.A. (2020). The promise and challenge of therapeutic genome editing. Nature *578*, 229–236.

76. Abramson, J.S., Palomba, M.L., Gordon, L.I., Lunning, M.A., Wang, M., Arnason, J., Mehta, A., Purev, E., Maloney, D.G., Andreadis, C., et al. (2020). Lisocabtagene maraleucel for patients with relapsed or refractory large B-cell lymphomas (TRANSCEND NHL 001): a multicentre seamless design study. Lancet *396*, 839–852.

77. Russell, S., Bennett, J., Wellman, J.A., Chung, D.C., Yu, Z.-F., Tillman, A., Wittes, J., Pappas, J., Elci, O., McCague, S., et al. (2017). Efficacy and safety of voretigene neparvovec (AAV2-hRPE65v2) in patients with RPE65-mediated inherited retinal dystrophy: a randomised, controlled, open-label, phase 3 trial. Lancet *390*, 849–860.

78. Day, J.W., Finkel, R.S., Chiriboga, C.A., Connolly, A.M., Crawford, T.O., Darras, B.T., Iannaccone, S.T., Kuntz, N.L., Peña, L.D.M., Shieh, P.B., et al. (2021). Onasemnogene abeparvovec gene therapy for symptomatic infantile-onset spinal muscular atrophy in patients with two copies of SMN2 (STR1VE): an open-label, single-arm, multicentre, phase 3 trial. Lancet Neurol. *20*, 284–293.

79. Gillmore, J.D., Gane, E., Taubel, J., Kao, J., Fontana, M., Maitland, M.L., Seitzer, J., O'Connell, D., Walsh, K.R., Wood, K., et al. (2021). CRISPR-Cas9 in vivo gene editing for transthyretin amyloidosis. N. Engl. J. Med. *385*, 493–502.

80. Li, A., Lee, C.M., Hurley, A.E., Jarrett, K.E., De Giorgi, M., Lu, W., Balderrama, K.S., Doerfler, A.M., Deshmukh, H., Ray, A., et al. (2019). A self-deleting AAV-CRISPR system for in vivo genome editing. Mol. Ther. Methods Clin. Dev. *12*, 111–122.

81. Petris, G., Casini, A., Montagna, C., Lorenzin, F., Prandi, D., Romanel, A., Zasso, J., Conti, L., Demichelis, F., and Cereseto, A. (2017). Hit and go CAS9 delivered through a lentiviral based self-limiting circuit. Nat. Commun. *8*, 15334.

82. Chew, W.L., Tabebordbar, M., Cheng, J.K.W., Mali, P., Wu, E.Y., Ng, A.H.M., Zhu, K., Wagers, A.J., and Church, G.M. (2016). A multifunctional AAV-CRISPR-Cas9 and its host response. Nat. Methods *13*, 868–874.

83. Deyle, D.R., and Russell, D.W. (2009). Adeno-associated virus vector integration. Curr. Opin. Mol. Ther. *11*, 442–447.

84. Rosas, L.E., Grieves, J.L., Zaraspe, K., La Perle, K.M., Fu, H., and McCarty, D.M. (2012). Patterns of scAAV vector insertion associated with oncogenic events in a mouse model for genotoxicity. Mol. Ther. *20*, 2098–2110.

85. Nelson, C.E., Wu, Y., Gemberling, M.P., Oliver, M.L., Waller, M.A., Bohning, J.D., Robinson-Hamm, J.N., Bulaklak, K., Castellanos Rivera, R.M., Collier, J.H., et al. (2019). Long-term evaluation of AAV-CRISPR genome editing for Duchenne muscular dystrophy. Nat. Med. *25*, 427–432.

86. Nguyen, G.N., Everett, J.K., Kafle, S., Roche, A.M., Raymond, H.E., Leiby, J., Wood, C., Assenmacher, C.-A., Merricks, E.P., Long, C.T., et al. (2021). A long-term study of AAV gene therapy in dogs with hemophilia A identifies clonal expansions of transduced liver cells. Nat. Biotechnol. *39*, 47–55.

87. Fiumara, M., Ferrari, S., Omer-Javed, A., Beretta, S., Albano, L., Canarutto, D., Varesi, A., Gaddoni, C., Brombin, C., Cugnata, F., et al. (2024). Genotoxic effects of base and prime editing in human hematopoietic stem cells. Nat. Biotechnol. *42*, 877–891.

88. Zhang, S., Shen, J., Li, D., and Cheng, Y. (2021). Strategies in the delivery of Cas9 ribonucleoprotein for CRISPR/Cas9 genome editing. Theranostics *11*, 614–648.

89. Green, M., Ishino, M., and Loewenstein, P.M. (1989). Mutational analysis of HIV-1 Tat minimal domain peptides: identification of trans-dominant mutants that suppress HIV-LTR-driven gene expression. Cell *58*, 215–223.

90. Staahl, B.T., Benekareddy, M., Coulon-Bainier, C., Banfal, A.A., Floor, S.N., Sabo, J.K., Urnes, C., Munares, G.A., Ghosh, A., and Doudna, J.A. (2017). Efficient genome editing in the mouse brain by local delivery of engineered Cas9 ribonucleoprotein complexes. Nat. Biotechnol. *35*, 431–434.

91. Chen, K., Stahl, E.C., Kang, M.H., Xu, B., Allen, R., Trinidad, M., and Doudna, J.A. (2024). Engineering self-deliverable ribonucleoproteins for genome editing in the brain. Nat. Commun. *15*, 1727.

92. Murriel, C.L., and Dowdy, S.F. (2006). Influence of protein transduction domains on intracellular delivery of macromolecules. Expert Opin. Drug Deliv. *3*, 739–746.

93. Richard, J.P., Melikov, K., Vives, E., Ramos, C., Verbeure, B., Gait, M.J., Chernomordik, L.V., and Lebleu, B. (2003). Cell-penetrating peptides. A reevaluation of the mechanism of cellular uptake. J. Biol. Chem. *278*, 585–590.

94. Hołubowicz, R., Du, S.W., Felgner, J., Smidak, R., Choi, E.H., Palczewska, G., Menezes, C.R., Dong, Z., Gao, F., Medani, O., et al. (2025). Safer and efficient base editing and prime editing via ribonucleoproteins delivered through optimized lipid-nanoparticle formulations. Nat. Biomed. Eng. *9*, 57–78.

95. Thach, T.T., Bae, D.H., Kim, N.H., Kang, E.S., Lee, B.S., Han, K., Kwak, M., Choi, H., Nam, J., Bae, T., et al. (2019). Lipopeptide-based nanosome-mediated delivery of hyperaccurate CRISPR/Cas9 ribonucleoprotein for gene editing. Small *15*, e1903172.

96. Li, L., Song, L., Liu, X., Yang, X., Li, X., He, T., Wang, N., Yang, S., Yu, C., Yin, T., et al. (2017). Artificial virus delivers CRISPR-Cas9 system for genome editing of cells in mice. ACS Nano *11*, 95–111.

97. Rui, Y., Wilson, D.R., Choi, J., Varanasi, M., Sanders, K., Karlsson, J., Lim, M., and Green, J.J. (2019). Carboxylated branched poly(β-amino ester) nanoparticles enable robust cytosolic protein delivery and CRISPR-Cas9 gene editing. Sci. Adv. *5*, eaay3255.

98. Ding, F., Huang, X., Gao, X., Xie, M., Pan, G., Li, Q., Song, J., Zhu, X., and Zhang, C. (2019). A non-cationic nucleic acid nanogel for the delivery of the CRISPR/Cas9 gene editing tool. Nanoscale *11*, 17211–17215.

99. Taharabaru, T., Yokoyama, R., Higashi, T., Mohammed, A.F.A., Inoue, M., Maeda, Y., Niidome, T., Onodera, R., and Motoyama, K. (2020). Genome editing in a wide area of the brain using dendrimer-based ternary polyplexes of Cas9 ribonucleoprotein. ACS Appl. Mater. Interfaces *12*, 21386–21397.

100. Lee, K., Conboy, M., Park, H.M., Jiang, F., Kim, H.J., Dewitt, M.A., Mackley, V.A., Chang, K., Rao, A., Skinner, C., et al. (2017). Nanoparticle delivery of Cas9 ribonucleoprotein and donor DNA in vivo induces homology-directed DNA repair. Nat. Biomed. Eng. *1*, 889–901.

101. Lee, B., Lee, K., Panda, S., Gonzales-Rojas, R., Chong, A., Bugay, V., Park, H.M., Brenner, R., Murthy, N., and Lee, H.Y. (2018). Nanoparticle delivery of CRISPR into the brain rescues a mouse model of fragile X syndrome from exaggerated repetitive behaviours. Nat. Biomed. Eng. *2*, 497–507.

102. Eweje, F., Ibrahim, V., Shajii, A., Walsh, M.L., Ahmad, K., Alrefai, A., Miyasato, D., Davis, J.R., Ham, H., Li, K., et al. (2025). Self-assembling protein nanoparticles for cytosolic delivery of nucleic acids and proteins. Nat. Biotechnol., 1–14.

103. Liang, X., Potter, J., Kumar, S., Zou, Y., Quintanilla, R., Sridharan, M., Carte, J., Chen, W., Roark, N., Ranganathan, S., et al. (2015). Rapid and highly efficient mammalian cell engineering via Cas9 protein transfection. J. Biotechnol. *208*, 44–53.

104. Gao, X., Tao, Y., Lamas, V., Huang, M., Yeh, W.-H., Pan, B., Hu, Y.-J., Hu, J.H., Thompson, D.B., Shu, Y., et al. (2018). Treatment of autosomal dominant hearing loss by in vivo delivery of genome editing agents. Nature *553*, 217–221.

105. Dass, C.R. (2004). Lipoplex-mediated delivery of nucleic acids: factors affecting in vivo transfection. J. Mol. Med. *82*, 579–591.

106. Gandek, T.B., van der Koog, L., and Nagelkerke, A. (2023). A comparison of cellular uptake mechanisms, delivery efficacy, and intracellular fate between liposomes and extracellular vesicles. Adv. Healthc. Mater. *12*, e2300319.

107. Yin, X., Harmancey, R., McPherson, D.D., Kim, H., and Huang, S.-L. (2023). Liposome-based carriers for CRISPR genome editing. Int. J. Mol. Sci. *24*. https://doi.org/10.3390/ijms241612844.

108. Polack, F.P., Thomas, S.J., Kitchin, N., Absalon, J., Gurtman, A., Lockhart, S., Perez, J.L., Pérez Marc, G., Moreira, E.D., Zerbini, C., et al. (2020). Safety and efficacy of the BNT162b2 mRNA Covid-19 vaccine. N. Engl. J. Med. *383*, 2603–2615.

109. Kazemian, P., Yu, S.-Y., Thomson, S.B., Birkenshaw, A., Leavitt, B.R., and Ross, C.J.D. (2022). Lipid-nanoparticle-based delivery of CRISPR/Cas9 genome-editing components. Mol. Pharm. *19*, 1669–1686.

110. Miller, J.B., Zhang, S., Kos, P., Xiong, H., Zhou, K., Perelman, S.S., Zhu, H., and Siegwart, D.J. (2017). Non-viral CRISPR/Cas gene editing in vitro and in vivo enabled by synthetic nanoparticle co-delivery of Cas9 mRNA and sgRNA. Angew. Chem. Int. Ed Engl. *56*, 1059–1063.

111. Finn, J.D., Smith, A.R., Patel, M.C., Shaw, L., Youniss, M.R., van Heteren, J., Dirstine, T., Ciullo, C., Lescarbeau, R., Seitzer, J., et al. (2018). A single administration of CRISPR/Cas9 lipid nanoparticles achieves robust and persistent in vivo genome editing. Cell Rep. *22*, 2227–2235.

112. Qiu, M., Glass, Z., Chen, J., Haas, M., Jin, X., Zhao, X., Rui, X., Ye, Z., Li, Y., Zhang, F., et al. (2021). Lipid nanoparticle-mediated codelivery of Cas9 mRNA and single-guide RNA achieves liver-specific in vivo genome editing of Angptl3. Proc. Natl. Acad. Sci. U. S. A. *118*. https://doi.org/10.1073/pnas.2020401118.

113. Kenjo, E., Hozumi, H., Makita, Y., Iwabuchi, K.A., Fujimoto, N., Matsumoto, S., Kimura, M., Amano, Y., Ifuku, M., Naoe, Y., et al. (2021). Low immunogenicity of LNP allows repeated administrations of CRISPR-Cas9 mRNA into skeletal muscle in mice. Nat. Commun. *12*, 7101.

114. Herrera-Barrera, M., Gautam, M., Lokras, A., Vlasova, K., Foged, C., and Sahay, G. (2023). Lipid nanoparticle-enabled intracellular delivery of prime editors. AAPS J. *25*, 65.

115. Hou, X., Zaks, T., Langer, R., and Dong, Y. (2021). Lipid nanoparticles for mRNA delivery. Nat. Rev. Mater. *6*, 1078–1094.

116. Wang, M., Alberti, K., Sun, S., Arellano, C.L., and Xu, Q. (2014). Combinatorially designed lipid-like nanoparticles for intracellular delivery of cytotoxic protein for cancer therapy. Angew. Chem. Int. Ed Engl. *53*, 2893–2898.

117. Wei, T., Cheng, Q., Min, Y.-L., Olson, E.N., and Siegwart, D.J. (2020). Systemic nanoparticle delivery of CRISPR-Cas9 ribonucleoproteins for effective tissue specific genome editing. Nat. Commun. *11*, 3232.

118. Zuris, J.A., Thompson, D.B., Shu, Y., Guilinger, J.P., Bessen, J.L., Hu, J.H., Maeder, M.L., Joung, J.K., Chen, Z.-Y., and Liu, D.R. (2015). Cationic lipid-mediated delivery of proteins enables efficient protein-based genome editing in vitro and in vivo. Nat. Biotechnol. *33*, 73–80.

119. Wang, M., Zuris, J.A., Meng, F., Rees, H., Sun, S., Deng, P., Han, Y., Gao, X., Pouli, D., Wu, Q., et al. (2016). Efficient delivery of genome-editing proteins using bioreducible lipid nanoparticles. Proc. Natl. Acad. Sci. U. S. A. *113*, 2868–2873.

120. Onuma, H., Sato, Y., and Harashima, H. (2023). Lipid nanoparticle-based ribonucleoprotein delivery for in vivo genome editing. J. Control. Release *355*, 406–416.

121. Chen, K., Han, H., Zhao, S., Xu, B., Yin, B., Lawanprasert, A., Trinidad, M., Burgstone, B.W., Murthy, N., and Doudna, J.A. (2024). Lung and liver editing by lipid nanoparticle delivery of a stable CRISPR-Cas9 ribonucleoprotein. Nat. Biotechnol., 1–13.

122. Dipalo, L.L., Mikkelsen, J.G., Gijsbers, R., and Carlon, M.S. (2025). Trojan horse-like vehicles for CRISPR-Cas delivery: Engineering extracellular vesicles and virus-like particles for precision gene editing in cystic fibrosis. Hum. Gene Ther. https://doi.org/10.1089/hum.2024.258.

123. Valadi, H., Ekström, K., Bossios, A., Sjöstrand, M., Lee, J.J., and Lötvall, J.O. (2007). Exosome-mediated transfer of mRNAs and microRNAs is a novel mechanism of genetic exchange between cells. Nat. Cell Biol. *9*, 654–659.

124. Kim, H.I., Park, J., Zhu, Y., Wang, X., Han, Y., and Zhang, D. (2024). Recent advances in extracellular vesicles for therapeutic cargo delivery. Exp. Mol. Med. *56*, 836–849.

125. Mangeot, P.-E., Dollet, S., Girard, M., Ciancia, C., Joly, S., Peschanski, M., and Lotteau, V. (2011). Protein transfer into human cells by VSV-G-induced nanovesicles. Mol. Ther. *19*, 1656–1666.

126. Montagna, C., Petris, G., Casini, A., Maule, G., Franceschini, G.M., Zanella, I., Conti, L., Arnoldi, F., Burrone, O.R., Zentilin, L., et al. (2018). VSV-G-enveloped vesicles for traceless delivery of CRISPR-Cas9. Mol. Ther. Nucleic Acids *12*, 453–462.

127. Campbell, L.A., Coke, L.M., Richie, C.T., Fortuno, L.V., Park, A.Y., and Harvey, B.K. (2019). Gesicle-mediated delivery of CRISPR/Cas9 ribonucleoprotein complex for inactivating the HIV provirus. Mol. Ther. *27*, 151–163.

128. Gee, P., Lung, M.S.Y., Okuzaki, Y., Sasakawa, N., Iguchi, T., Makita, Y., Hozumi, H., Miura, Y., Yang, L.F., Iwasaki, M., et al. (2020). Extracellular nanovesicles for packaging of CRISPR-Cas9 protein and sgRNA to induce therapeutic exon skipping. Nat. Commun. *11*, 1334.

129. Zhang, X., Xu, Q., Zi, Z., Liu, Z., Wan, C., Crisman, L., Shen, J., and Liu, X. (2020). Programmable extracellular vesicles for macromolecule delivery and genome modifications. Dev. Cell *55*, 784-801.e9.

130. Stranford, D.M., Simons, L.M., Berman, K.E., Cheng, L., DiBiase, B.N., Hung, M.E., Lucks, J.B., Hultquist, J.F., and Leonard, J.N. (2024). Genetically encoding multiple functionalities into extracellular vesicles for the targeted delivery of biologics to T cells. Nat. Biomed. Eng. *8*, 397–414.

131. Whitley, J.A., Kim, S., Lou, L., Ye, C., Alsaidan, O.A., Sulejmani, E., Cai, J., Desrochers, E.G., Beharry, Z., Rickman, C.B., et al. (2022). Encapsulating Cas9 into extracellular vesicles by protein myristoylation. J. Extracell. Vesicles *11*, e12196.

132. Zeng, W., Zheng, L., Li, Y., Yang, J., Mao, T., Zhang, J., Liu, Y., Ning, J., Zhang, T., Huang, H., et al. (2024). Engineered extracellular vesicles for delivering functional

Cas9/gRNA to eliminate hepatitis B virus cccDNA and integration. Emerg. Microbes Infect. *13*, 2284286.

133. Nabhan, J.F., Hu, R., Oh, R.S., Cohen, S.N., and Lu, Q. (2012). Formation and release of arrestin domain-containing protein 1-mediated microvesicles (ARMMs) at plasma membrane by recruitment of TSG101 protein. Proc. Natl. Acad. Sci. U. S. A. *109*, 4146–4151.

134. Chen, Z., Wang, Q., and Lu, Q. (2025). Engineering ARMMs for improved intracellular delivery of CRISPR-Cas9. Extracell. Vesicle *5*, 100082.

135. Hung, M.E., and Leonard, J.N. (2016). A platform for actively loading cargo RNA to elucidate limiting steps in EV-mediated delivery. J. Extracell. Vesicles *5*, 31027.

136. Kojima, R., Bojar, D., Rizzi, G., Hamri, G.C.-E., El-Baba, M.D., Saxena, P., Ausländer, S., Tan, K.R., and Fussenegger, M. (2018). Designer exosomes produced by implanted cells intracerebrally deliver therapeutic cargo for Parkinson's disease treatment. Nat. Commun. *9*, 1305.

137. Yao, X., Lyu, P., Yoo, K., Yadav, M.K., Singh, R., Atala, A., and Lu, B. (2021). Engineered extracellular vesicles as versatile ribonucleoprotein delivery vehicles for efficient and safe CRISPR genome editing. J. Extracell. Vesicles *10*, e12076.

138. Ye, Y., Zhang, X., Xie, F., Xu, B., Xie, P., Yang, T., Shi, Q., Zhang, C.-Y., Zhang, Y., Chen, J., et al. (2020). An engineered exosome for delivering sgRNA:Cas9 ribonucleoprotein complex and genome editing in recipient cells. Biomater. Sci. *8*, 2966–2976.

139. Osteikoetxea, X., Silva, A., Lázaro-Ibáñez, E., Salmond, N., Shatnyeva, O., Stein, J., Schick, J., Wren, S., Lindgren, J., Firth, M., et al. (2022). Engineered Cas9 extracellular vesicles as a novel gene editing tool. J. Extracell. Vesicles *11*, e12225.

140. Liang, X., Gupta, D., Xie, J., Van Wonterghem, E., Van Hoecke, L., Hean, J., Niu, Z., Ghaeidamini, M., Wiklander, O.P.B., Zheng, W., et al. (2025). Engineering of extracellular vesicles for efficient intracellular delivery of multimodal therapeutics including genome editors. Nat. Commun. *16*, 4028.

141. Niu, Z., Zhou, H., Zheng, W., Hayes, O.G., Hou, V.W.Q., Görgens, A., Roudi, S., Zhou, G., Wiklander, R.J., Sych, T., et al. (2025). Screening scaffold proteins for improved functional delivery of luminal proteins using engineered extracellular vesicles. J. Control. Release *384*, 113882.

142. Pan, Y., Yang, X., Zeng, Z., Liu, F., Luo, J., Shen, M., Zhou, W., Li, J., Jiang, G., Sun, L., et al. (2025). 124I-labelled BMSC-derived extracellular vesicles deliver CRISPR/Cas9 ribonucleoproteins with a GFP-reporter system to inhibit osteosarcoma proliferation and metastasis. J. Extracell. Vesicles *14*, e70130.

143. Lindel, F., Dodt, C.R., Weidner, N., Noll, M., Bergemann, F., Behrendt, R., Fischer, S., Dietrich, J., Cartellieri, M., Hamann, M.V., et al. (2019). TraFo-CRISPR: Enhanced genome engineering by transient foamy virus vector-mediated delivery of CRISPR/Cas9 components. Mol. Ther. Nucleic Acids *18*, 708–726.

144. Liu, Q., Zhao, C., Sun, K., Deng, Y., and Li, Z. (2023). Engineered biocontainable RNA virus vectors for non-transgenic genome editing across crop species and genotypes. Mol. Plant *16*, 616–631.

145. Freed, E.O. (1998). HIV-1 gag proteins: diverse functions in the virus life cycle. Virology *251*, 1–15.

146. Aoki, T., Miyauchi, K., Urano, E., Ichikawa, R., and Komano, J. (2011). Protein transduction by pseudotyped lentivirus-like nanoparticles. Gene Ther. *18*, 936–941.

147. Cai, Y., Bak, R.O., Krogh, L.B., Staunstrup, N.H., Moldt, B., Corydon, T.J., Schrøder, L.D., and Mikkelsen, J.G. (2014). DNA transposition by protein transduction of the piggyBac transposase from lentiviral Gag precursors. Nucleic Acids Res. *42*, e28.

148. Skipper, K.A., Nielsen, M.G., Andersen, S., Ryø, L.B., Bak, R.O., and Mikkelsen, J.G. (2018). Time-restricted PiggyBac DNA transposition by transposase protein delivery using Lentivirus-derived nanoparticles. Mol. Ther. Nucleic Acids *11*, 253–262.

149. Cai, Y., Bak, R.O., and Mikkelsen, J.G. (2014). Targeted genome editing by lentiviral protein transduction of zinc-finger and TAL-effector nucleases. Elife *3*, e01911.

150. Choi, J.G., Dang, Y., Abraham, S., Ma, H., Zhang, J., Guo, H., Cai, Y., Mikkelsen, J.G., Wu, H., Shankar, P., et al. (2016). Lentivirus pre-packed with Cas9 protein for safer gene editing. Gene Ther. *23*, 627–633.

151. Urano, E., Aoki, T., Futahashi, Y., Murakami, T., Morikawa, Y., Yamamoto, N., and Komano, J. (2008). Substitution of the myristoylation signal of human immunodeficiency virus type 1 Pr55Gag with the phospholipase C-δ1 pleckstrin homology domain results in infectious pseudovirion production. J. Gen. Virol. *89*, 3144–3149.

152. Sato, A., Isaka, Y., Kodama, M., Yoshimoto, J., Kawauchi, S., Kuwata, T., Adachi, A., Hayami, M., Yoshi, O., and Fujiwara, T. (1995). Targeting of chrolamphenicol acetyltransferase to human immunodeficiency virus particles via Vpr and Vpx. Microbiol. Immunol. *39*, 1015–1019.

153. Wu, X., Liu, H., Xiao, H., Kim, J., Seshaiah, P., Natsoulis, G., Boeke, J.D., Hahn, B.H., and Kappes, J.C. (1995). Targeting foreign proteins to human immunodeficiency virus particles via fusion with Vpr and Vpx. J. Virol. *69*, 3389–3398.

154. Link, N., Aubel, C., Kelm, J.M., Marty, R.R., Greber, D., Djonov, V., Bourhis, J., Weber, W., and Fussenegger, M. (2006). Therapeutic protein transduction of mammalian cells and mice by nucleic acid-free lentiviral nanoparticles. Nucleic Acids Res. *34*, e16.

155. Indikova, I., and Indik, S. (2020). Highly efficient “hit-and-run” genome editing with unconcentrated lentivectors carrying Vpr.Prot.Cas9 protein produced from RRE-containing transcripts. Nucleic Acids Res. *48*, 8178–8187.

156. Uchida, N., Drysdale, C.M., Nassehi, T., Gamer, J., Yapundich, M., DiNicola, J., Shibata, Y., Hinds, M., Gudmundsdottir, B., Haro-Mora, J.J., et al. (2021). Cas9 protein delivery non-integrating lentiviral vectors for gene correction in sickle cell disease. Mol. Ther. Methods Clin. Dev. *21*, 121–132.

157. Colgan, J., Yuan, H.E., Franke, E.K., and Luban, J. (1996). Binding of the human immunodeficiency virus type 1 Gag polyprotein to cyclophilin A is mediated by the central region of capsid and requires Gag dimerization. J. Virol. *70*, 4299–4310.

158. Kaczmarczyk, S.J., Sitaraman, K., Young, H.A., Hughes, S.H., and Chatterjee, D.K. (2011). Protein delivery using engineered virus-like particles. Proc. Natl. Acad. Sci. U. S. A. *108*, 16998–17003.

159. Mangeot, P.E., Risson, V., Fusil, F., Marnef, A., Laurent, E., Blin, J., Mournetas, V., Massouridès, E., Sohier, T.J.M., Corbin, A., et al. (2019). Genome editing in primary cells and in vivo using viral-derived Nanoblades loaded with Cas9-sgRNA ribonucleoproteins. Nat. Commun. *10*, 45.

160. Gutierrez-Guerrero, A., Abrey Recalde, M.J., Mangeot, P.E., Costa, C., Bernadin, O., Périan, S., Fusil, F., Froment, G., Martinez-Turtos, A., Krug, A., et al. (2021). Baboon envelope pseudotyped “nanoblades” carrying Cas9/gRNA complexes allow efficient genome editing in human T, B, and CD34+ cells and knock-in of AAV6-encoded donor DNA in CD34+ cells. Front. Genome Ed. *3*, 604371.

161. Tiroille, V., Krug, A., Bokobza, E., Kahi, M., Bulcaen, M., Ensinck, M.M., Geurts, M.H., Hendriks, D., Vermeulen, F., Larbret, F., et al. (2023). Nanoblades allow high-level genome editing in murine and human organoids. Mol. Ther. Nucleic Acids *33*, 57–74.

162. Singsuksawat, E., Onnome, S., Posiri, P., Suphatrakul, A., Srisuk, N., Nantachokchawapan, R., Praneechit, H., Sae-Kow, C., Chidpratum, P., Sa-Ngiamsuntorn, K., et al. (2021). Potent programmable antiviral against dengue virus in primary human cells by Cas13b RNP with short spacer and delivery by VLP. Mol. Ther. Methods Clin. Dev. *21*, 729–740.

163. Banskota, S., Raguram, A., Suh, S., Du, S.W., Davis, J.R., Choi, E.H., Wang, X., Nielsen, S.C., Newby, G.A., Randolph, P.B., et al. (2022). Engineered virus-like particles for efficient in vivo delivery of therapeutic proteins. Cell *185*, 250-265.e16.

164. Nicosia, L., Pranke, I., Latorre, R.V., Murray, J.B., Lonetti, L., Cavusoglu-Doran, K., Dreano, E., Costello, J.P., Carroll, M., Melotti, P., et al. (2025). Adenine base editing with engineered virus-like particles rescues the CFTR mutation G542X in patient-derived intestinal organoids. iScience *28*, 111979.

165. Jeong, T.Y., Yoon, D.E., Kim, S.P., Yang, J., Lim, S.-Y., Ok, S., Ju, S., Park, J., Lee, S.B., Park, S.-J., et al. (2025). An innovative approach using CRISPR-ribonucleoprotein packaged in virus-like particles to generate genetically engineered mouse models. Nat. Commun. *16*, 3451.

166. Xu, D., Besselink, S., Ramadoss, G.N., Dierks, P.H., Lubin, J.P., Pattali, R.K., Brim, J.I., Christenson, A.E., Colias, P.J., Ornelas, I.J., et al. (2024). Programmable epigenome editing by transient delivery of CRISPR epigenome editor ribonucleoproteins. bioRxivorg. https://doi.org/10.1101/2024.11.26.625496.

167. Raguram, A., An, M., Chen, P.Z., and Liu, D.R. (2024). Directed evolution of engineered virus-like particles with improved production and transduction efficiencies. Nat. Biotechnol., 1–13.

168. Halegua, T., Risson, V., Carras, J., Rouyer, M., Coudert, L., Jacquier, A., Schaeffer, L., Ohlmann, T., and Mangeot, P.E. (2025). Delivery of Prime editing in human stem cells using pseudoviral NanoScribes particles. Nat. Commun. *16*, 397.

169. An, M., Raguram, A., Du, S.W., Banskota, S., Davis, J.R., Newby, G.A., Chen, P.Z., Palczewski, K., and Liu, D.R. (2024). Engineered virus-like particles for transient delivery of prime editor ribonucleoprotein complexes in vivo. Nat. Biotechnol. https://doi.org/10.1038/s41587-023-02078-y.

170. Hamilton, J.R., Tsuchida, C.A., Nguyen, D.N., Shy, B.R., McGarrigle, E.R., Sandoval Espinoza, C.R., Carr, D., Blaeschke, F., Marson, A., and Doudna, J.A. (2021). Targeted

delivery of CRISPR-Cas9 and transgenes enables complex immune cell engineering. Cell Rep. *35*, 109207.

171. Zila, V., Margiotta, E., Turoňová, B., Müller, T.G., Zimmerli, C.E., Mattei, S., Allegretti, M., Börner, K., Rada, J., Müller, B., et al. (2021). Cone-shaped HIV-1 capsids are transported through intact nuclear pores. Cell *184*, 1032-1046.e18.

172. Hamilton, J.R., Chen, E., Perez, B.S., Sandoval Espinoza, C.R., Kang, M.H., Trinidad, M., Ngo, W., and Doudna, J.A. (2024). In vivo human T cell engineering with enveloped delivery vehicles. Nat. Biotechnol. https://doi.org/10.1038/s41587-023-02085-z.

173. Ngo, W., Peukes, J., Baldwin, A., Xue, Z.W., Hwang, S., Stickels, R.R., Lin, Z., Satpathy, A.T., Wells, J.A., Schekman, R., et al. (2025). Mechanism-guided engineering of a minimal biological particle for genome editing. Proc. Natl. Acad. Sci. U. S. A. *122*, e2413519121.

174. Haldrup, J., Andersen, S., Labial, A.R.L., Wolff, J.H., Frandsen, F.P., Skov, T.W., Rovsing, A.B., Nielsen, I., Jakobsen, T.S., Askou, A.L., et al. (2023). Engineered lentivirus-derived nanoparticles (LVNPs) for delivery of CRISPR/Cas ribonucleoprotein complexes supporting base editing, prime editing and *in vivo* gene modification. Nucleic Acids Res. *51*, 10059–10074.

175. Prel, A., Caval, V., Gayon, R., Ravassard, P., Duthoit, C., Payen, E., Maouche-Chretien, L., Creneguy, A., Nguyen, T.H., Martin, N., et al. (2015). Highly efficient in vitro and in vivo delivery of functional RNAs using new versatile MS2-chimeric retrovirus-like particles. Molecular Therapy - Methods and Clinical Development *2*, 15039.

176. Ling, S., Yang, S., Hu, X., Yin, D., Dai, Y., Qian, X., Wang, D., Pan, X., Hong, J., Sun, X., et al. (2021). Lentiviral delivery of co-packaged Cas9 mRNA and a Vegfa-targeting guide RNA prevents wet age-related macular degeneration in mice. Nat. Biomed. Eng. *5*, 144–156.

177. Yin, D., Ling, S., Wang, D., Dai, Y., Jiang, H., Zhou, X., Paludan, S.R., Hong, J., and Cai, Y. (2021). Targeting herpes simplex virus with CRISPR-Cas9 cures herpetic stromal keratitis in mice. Nat. Biotechnol. *39*, 567–577.

178. Lu, B., Javidi-Parsijani, P., Makani, V., Mehraein-Ghomi, F., Sarhan, W.M., Sun, D., Yoo, K.W., Atala, Z.P., Lyu, P., and Atala, A. (2019). Delivering SaCas9 mRNA by lentivirus-like bionanoparticles for transient expression and efficient genome editing. Nucleic Acids Res. *47*, 1–13.

179. Knopp, Y., Geis, F.K., Heckl, D., Horn, S., Neumann, T., Kuehle, J., Meyer, J., Fehse, B., Baum, C., Morgan, M., et al. (2018). Transient retrovirus-based CRISPR/Cas9 all-in-one particles for efficient, targeted gene knockout. Mol. Ther. Nucleic Acids *13*, 256–274.

180. Baron, Y., Sens, J., Lange, L., Nassauer, L., Klatt, D., Hoffmann, D., Kleppa, M.-J., Barbosa, P.V., Keisker, M., Steinberg, V., et al. (2022). Improved alpharetrovirus-based Gag.MS2 particles for efficient and transient delivery of CRISPR-Cas9 into target cells. Mol. Ther. Nucleic Acids *27*, 810–823.

181. Lyu, P., Javidi-Parsijani, P., Atala, A., and Lu, B. (2019). Delivering Cas9/sgRNA ribonucleoprotein (RNP) by lentiviral capsid-based bionanoparticles for efficient “hit-and-run” genome editing. Nucleic Acids Res. *47*, e99.

182. Lu, Z., Yao, X., Lyu, P., Yadav, M., Yoo, K., Atala, A., and Lu, B. (2021). Lentiviral capsid-mediated Streptococcus pyogenes Cas9 ribonucleoprotein delivery for efficient and safe multiplex genome editing. CRISPR J. *4*, 914–928.

183. Lyu, P., Lu, Z., Cho, S.-I., Yadav, M., Yoo, K.W., Atala, A., Kim, J.-S., and Lu, B. (2021). Adenine base editor ribonucleoproteins delivered by Lentivirus-like particles show high on-target base editing and undetectable RNA off-target activities. CRISPR J. *4*, 69–81.

184. Yadav, M., Atala, A., and Lu, B. (2022). Developing all-in-one virus-like particles for Cas9 mRNA/single guide RNA co-delivery and aptamer-containing lentiviral vectors for improved gene expression. Int. J. Biol. Macromol. *209*, 1260–1270.

185. Ling, S., Zhang, X., Dai, Y., Jiang, Z., Zhou, X., Lu, S., Qian, X., Liu, J., Selfjord, N., Satir, T.M., et al. (2025). Customizable virus-like particles deliver CRISPR-Cas9 ribonucleoprotein for effective ocular neovascular and Huntington's disease gene therapy. Nat. Nanotechnol. *20*, 543–553.

186. Yin, D., Zhong, Y., Ling, S., Lu, S., Wang, X., Jiang, Z., Wang, J., Dai, Y., Tian, X., Huang, Q., et al. (2025). Dendritic-cell-targeting virus-like particles as potent mRNA vaccine carriers. Nat. Biomed. Eng. *9*, 185–200.

187. Sayers, J.R., and Eckstein, F. (1991). A single-strand specific endonuclease activity copurifies with overexpressed T5 D15 exonuclease. Nucleic Acids Res. *19*, 4127–4132.

188. Garforth, S.J., Ceska, T.A., Suck, D., and Sayers, J.R. (1999). Mutagenesis of conserved lysine residues in bacteriophage T5 5'-3' exonuclease suggests separate mechanisms of endo-and exonucleolytic cleavage. Proc. Natl. Acad. Sci. U. S. A. *96*, 38–43.

189. Liang, Z., Wu, Y., Guo, Y., and Wei, S. (2023). Addition of the T5 exonuclease increases the prime editing efficiency in plants. J. Genet. Genomics. https://doi.org/10.1016/j.jgg.2023.03.008.

190. Lu, C., Kuang, J., Shao, T., Xie, S., Li, M., Zhu, L., and Zhu, L. (2022). Prime editing: An all-rounder for genome editing. Int. J. Mol. Sci. *23*, 9862.

191. Zalatan, J.G., Lee, M.E., Almeida, R., Gilbert, L.A., Whitehead, E.H., La Russa, M., Tsai, J.C., Weissman, J.S., Dueber, J.E., Qi, L.S., et al. (2015). Engineering complex synthetic transcriptional programs with CRISPR RNA scaffolds. Cell *160*, 339–350.

192. Porreca, I., Blassberg, R., Harbottle, J., Joubert, B., Mielczarek, O., Stombaugh, J., Hemphill, K., Sumner, J., Pazeraitis, D., Touza, J.L., et al. (2024). An aptamer-mediated base editing platform for simultaneous knockin and multiple gene knockout for allogeneic CAR-T cells generation. Mol. Ther. *32*, 2692–2710.

193. Wu, Y., Zhong, A., Sidharta, M., Kim, T.W., Ramirez, B., Persily, B., Studer, L., and Zhou, T. (2024). Robust and inducible genome editing via an all-in-one prime editor in human pluripotent stem cells. Nat. Commun. *15*, 10824.

194. Durrant, M.G., Fanton, A., Tycko, J., Hinks, M., Chandrasekaran, S.S., Perry, N.T., Schaepe, J., Du, P.P., Lotfy, P., Bassik, M.C., et al. (2023). Systematic discovery of recombinases for efficient integration of large DNA sequences into the human genome. Nat. Biotechnol. *41*, 488–499.

195. Fanton, A., Bartie, L.J., Martins, J.Q., Tran, V.Q., Goudy, L., Durrant, M.G., Wei, J., Pawluk, A., Konermann, S., Marson, A., et al. (2024). Site-specific DNA insertion into the human genome with engineered recombinases. bioRxiv. https://doi.org/10.1101/2024.11.01.621560.

196. Hew, B.E., Gupta, S., Sato, R., Waller, D.F., Stoytchev, I., Short, J.E., Sharek, L., Tran, C.T., Badran, A.H., and Owens, J.B. (2024). Directed evolution of hyperactive integrases for site specific insertion of transgenes. Nucleic Acids Res. *52*, e64.

197. Cho, N.H., Cheveralls, K.C., Brunner, A.-D., Kim, K., Michaelis, A.C., Raghavan, P., Kobayashi, H., Savy, L., Li, J.Y., Canaj, H., et al. (2022). OpenCell: Endogenous tagging for the cartography of human cellular organization. Science *375*, eabi6983.

198. Choi, J., Chen, W., Minkina, A., Chardon, F.M., Suiter, C.C., Regalado, S.G., Domcke, S., Hamazaki, N., Lee, C., Martin, B., et al. (2022). A time-resolved, multi-symbol molecular recorder via sequential genome editing. Nature *608*, 98–107.

199. Loveless, T.B., Carlson, C.K., Dentzel Helmy, C.A., Hu, V.J., Ross, S.K., Demelo, M.C., Murtaza, A., Liang, G., Ficht, M., Singhai, A., et al. (2025). Open-ended molecular recording of sequential cellular events into DNA. Nat. Chem. Biol. *21*, 512–521.

200. Musunuru, K., Grandinette, S.A., Wang, X., Hudson, T.R., Briseno, K., Berry, A.M., Hacker, J.L., Hsu, A., Silverstein, R.A., Hille, L.T., et al. (2025). Patient-specific in vivo gene editing to treat a rare genetic disease. N. Engl. J. Med. *392*, 2235–2243.

201. FDA clears prime editors for testing in humans (2024). Nat. Biotechnol. *42*, 691.

202. Zheng, C., Zhang, G., Dean, L.J., Sontheimer, E.J., and Xue, W. (2025). The reverse transcriptase domain of prime editors contributes to DNA repair in mammalian cells. Nat. Biotechnol., 1–8.

203. Habib, O., Habib, G., Hwang, G.-H., and Bae, S. (2022). Comprehensive analysis of prime editing outcomes in human embryonic stem cells. Nucleic Acids Res. *50*, 1187–1197.

204. Hu, J.H., Miller, S.M., Geurts, M.H., Tang, W., Chen, L., Sun, N., Zeina, C.M., Gao, X., Rees, H.A., Lin, Z., et al. (2018). Evolved Cas9 variants with broad PAM compatibility and high DNA specificity. Nature *556*, 57–63.

205. Walton, R.T., Christie, K.A., Whittaker, M.N., and Kleinstiver, B.P. (2020). Unconstrained genome targeting with near-PAMless engineered CRISPR-Cas9 variants. Science *368*, 290–296.

206. Zhao, L., Koseki, S.R.T., Silverstein, R.A., Amrani, N., Peng, C., Kramme, C., Savic, N., Pacesa, M., Rodríguez, T.C., Stan, T., et al. (2023). PAM-flexible genome editing with an engineered chimeric Cas9. Nat. Commun. *14*, 6175.

207. Eggers, A.R., Chen, K., Soczek, K.M., Tuck, O.T., Doherty, E.E., Xu, B., Trinidad, M.I., Thornton, B.W., Yoon, P.H., and Doudna, J.A. (2024). Rapid DNA unwinding accelerates genome editing by engineered CRISPR-Cas9. Cell *187*, 3249-3261.e14.

208. Nayfach, S., Bhatnagar, A., Novichkov, A., Estevam, G.O., Kim, N., Hill, E., Ruffolo, J.A., Silverstein, R., Gallagher, J., Kleinstiver, B., et al. (2025). Engineering of CRISPR-Cas PAM recognition using deep learning of vast evolutionary data. bioRxivorg. https://doi.org/10.1101/2025.01.06.631536.

209. Silverstein, R.A., Kim, N., Kroell, A.-S., Walton, R.T., Delano, J., Butcher, R.M., Pacesa, M., Smith, B.K., Christie, K.A., Ha, L.L., et al. (2025). Custom CRISPR-Cas9 PAM variants via scalable engineering and machine learning. Nature. https://doi.org/10.1038/s41586-025-09021-y.

210. Alves, C.R.R., Das, S., Krishnan, V., Ha, L.L., Fox, L.R., Stutzman, H.E., Shamber, C.E., Kalailingam, P., McCarthy, S., Lino Cardenas, C.L., et al. (2024). In vivo treatment of a severe vascular disease via a bespoke CRISPR-Cas9 base editor. bioRxivorg. https://doi.org/10.1101/2024.11.11.621817.

211. Raghavan, R., Friedrich, M., King, I., Killian, M., Platten, M., Macrae, R., Song, Y., Nivon, L., and Zhang, F. (2023). Rational engineering of minimally immunogenic nucleases for gene therapy. Blood *142*, 7126–7126.

212. Ruffolo, J.A., Nayfach, S., Gallagher, J., Bhatnagar, A., Beazer, J., Hussain, R., Russ, J., Yip, J., Hill, E., Pacesa, M., et al. (2024). Design of highly functional genome editors by modeling the universe of CRISPR-Cas sequences. bioRxiv. https://doi.org/10.1101/2024.04.22.590591.

213. Tou, C.J., and Kleinstiver, B.P. (2023). Recent advances in double-strand break-free kilobase-scale genome editing technologies. Biochemistry *62*, 3493–3499.

214. Klompe, S.E., Vo, P.L.H., Halpin-Healy, T.S., and Sternberg, S.H. (2019). Transposon-encoded CRISPR-Cas systems direct RNA-guided DNA integration. Nature *571*, 219–225.

215. Strecker, J., Ladha, A., Gardner, Z., Schmid-Burgk, J.L., Makarova, K.S., Koonin, E.V., and Zhang, F. (2019). RNA-guided DNA insertion with CRISPR-associated transposases. Science *364*, 48–53.

216. Tou, C.J., Orr, B., and Kleinstiver, B.P. (2023). Precise cut-and-paste DNA insertion using engineered type V-K CRISPR-associated transposases. Nat. Biotechnol. *41*, 968–979.

217. Witte, I.P., Lampe, G.D., Eitzinger, S., Miller, S.M., Berríos, K.N., McElroy, A.N., King, R.T., Stringham, O.G., Gelsinger, D.R., Vo, P.L.H., et al. (2025). Programmable gene insertion in human cells with a laboratory-evolved CRISPR-associated transposase. Science *388*, eadt5199.

218. Fell, C.W., Villiger, L., Lim, J., Hiraizumi, M., Tagliaferri, D., Yarnall, M.T.N., Lee, A., Jiang, K., Kayabolen, A., Krajeski, R.N., et al. (2025). Reprogramming site-specific retrotransposon activity to new DNA sites. Nature, 1–10.

219. Akopian, A., He, J., Boocock, M.R., and Stark, W.M. (2003). Chimeric recombinases with designed DNA sequence recognition. Proc. Natl. Acad. Sci. U. S. A. *100*, 8688–8691.

220. Zhang, M., Yang, C., Tasan, I., and Zhao, H. (2021). Expanding the potential of mammalian genome engineering via targeted DNA integration. ACS Synth. Biol. *10*, 429–446.

221. Mukhametzyanova, L., Schmitt, L.T., Torres-Rivera, J., Rojo-Romanos, T., Lansing, F., Paszkowski-Rogacz, M., Hollak, H., Brux, M., Augsburg, M., Schneider, P.M., et al. (2024). Activation of recombinases at specific DNA loci by zinc-finger domain insertions. Nat. Biotechnol. *42*, 1844–1854.

222. Durrant, M.G., Perry, N.T., Pai, J.J., Jangid, A.R., Athukoralage, J.S., Hiraizumi, M., McSpedon, J.P., Pawluk, A., Nishimasu, H., Konermann, S., et al. (2024). Bridge RNAs direct programmable recombination of target and donor DNA. Nature *630*, 984–993.

223. Truong, D.-J.J., Armbrust, N., Geilenkeuser, J., Lederer, E.-M., Santl, T.H., Beyer, M., Ittermann, S., Steinmaßl, E., Dyka, M., Raffl, G., et al. (2022). Intron-encoded cistronic transcripts for minimally invasive monitoring of coding and non-coding RNAs. Nat. Cell Biol. *24*, 1666–1676.

224. Hess, G.T., Frésard, L., Han, K., Lee, C.H., Li, A., Cimprich, K.A., Montgomery, S.B., and Bassik, M.C. (2016). Directed evolution using dCas9-targeted somatic hypermutation in mammalian cells. Nat. Methods *13*, 1036–1042.

225. Borer, R.A., Lehner, C.F., Eppenberger, H.M., and Nigg, E.A. (1989). Major nucleolar proteins shuttle between nucleus and cytoplasm. Cell *56*, 379–390.

226. Inman, G.J., Nicolás, F.J., and Hill, C.S. (2002). Nucleocytoplasmic shuttling of Smads 2, 3, and 4 permits sensing of TGF-beta receptor activity. Mol. Cell *10*, 283–294.

227. Gruber, C., Krautner, L., Bergant, V., Grass, V., Ma, Z., Rheinemann, L., Krus, A., Reinhardt, F., Mazneykova, L., Rocha-Hasler, M., et al. (2024). Engineered, nucleocytoplasmic shuttling Cas13d enables highly efficient cytosolic RNA targeting. Cell Discov. *10*, 42.

228. Haurwitz, R.E., Jinek, M., Wiedenheft, B., Zhou, K., and Doudna, J.A. (2010). Sequence- and structure-specific RNA processing by a CRISPR endonuclease. Science *329*, 1355–1358.

229. Sternberg, S.H., Haurwitz, R.E., and Doudna, J.A. (2012). Mechanism of substrate selection by a highly specific CRISPR endoribonuclease. RNA *18*, 661–672.

230. Nissim, L., Perli, S.D., Fridkin, A., Perez-Pinera, P., and Lu, T.K. (2014). Multiplexed and programmable regulation of gene networks with an integrated RNA and CRISPR/Cas toolkit in human cells. Mol. Cell *54*, 698–710.

231. Haurwitz, R.E., Sternberg, S.H., and Doudna, J.A. (2012). Csy4 relies on an unusual catalytic dyad to position and cleave CRISPR RNA. EMBO J. *31*, 2824–2832.

232. Borchardt, E.K., Vandoros, L.A., Huang, M., Lackey, P.E., Marzluff, W.F., and Asokan, A. (2015). Controlling mRNA stability and translation with the CRISPR endoribonuclease Csy4. RNA *21*, 1921–1930.

233. Borchardt, E.K., Meganck, R.M., Vincent, H.A., Ball, C.B., Ramos, S.B.V., Moorman, N.J., Marzluff, W.F., and Asokan, A. (2017). Inducing circular RNA formation using the CRISPR endoribonuclease Csy4. RNA *23*, 619–627.

234. Huang, S., Zhang, Z., Tao, W., Liu, Y., Li, X., Wang, X., Harati, J., Wang, P.-Y., Huang, X., and Lin, C.-P. (2022). Broadening prime editing toolkits using RNA-Pol-II-driven engineered pegRNA. Mol. Ther. *30*, 2923–2932.

235. Zhang, L., Qiu, X., Zhou, Y., Luo, Z., Zhu, L., Shao, J., Xie, M., and Wang, H. (2025). A trigger-inducible split-Csy4 architecture for programmable RNA modulation. Nucleic Acids Res. *53*. https://doi.org/10.1093/nar/gkae1319.

236. Cai, Y., Laustsen, A., Zhou, Y., Sun, C., Anderson, M.V., Li, S., Uldbjerg, N., Luo, Y., Jakobsen, M.R., and Mikkelsen, J.G. (2016). Targeted, homology-driven gene insertion in stem cells by ZFN-loaded “all-in-one” lentiviral vectors. Elife *5*, e12213.

237. Deshpande, A., Bryer, A.J., Andino-Moncada, J.R., Shi, J., Hong, J., Torres, C., Harel, S., Francis, A.C., Perilla, J.R., Aiken, C., et al. (2024). Elasticity of the HIV-1 core facilitates nuclear entry and infection. PLoS Pathog. *20*, e1012537.

238. Kreysing, J.P., Heidari, M., Zila, V., Cruz-León, S., Obarska-Kosinska, A., Laketa, V., Rohleder, L., Welsch, S., Köfinger, J., Turoňová, B., et al. (2025). Passage of the HIV capsid cracks the nuclear pore. Cell *188*, 930-943.e21.

239. Patinios, C., Gupta, D., Bassett, H.V., Collins, S.P., Kamm, C., Kibe, A., Wang, Y., Zhao, C., Vollen, K., Toussaint, C., et al. (2024). Targeted DNA ADP-ribosylation triggers templated repair in bacteria and base mutagenesis in eukaryotes. bioRxivorg. https://doi.org/10.1101/2024.11.17.623984.

240. Accola, M.A., Strack, B., and Göttlinger, H.G. (2000). Efficient Particle Production by Minimal Gag Constructs Which Retain the Carboxy-Terminal Domain of Human Immunodeficiency Virus Type 1 Capsid-p2 and a Late Assembly Domain. Preprint, https://doi.org/10.1128/jvi.74.12.5395-5402.2000 https://doi.org/10.1128/jvi.74.12.5395-5402.2000.

241. Wurst, W., Schuhmacher, M., Gruber, C., Lang, C., Ruijpers, R., Mazneykova, L., Krus, A., Tremmel, B., Reinhardt, F., Kadletz, K., et al. (2024). Creating bottom-up RNA transfer vehicles from synthetic protein assemblies. Research Square. https://doi.org/10.21203/rs.3.rs-5123765/v1.

242. Banerjee, A., Berzhkovskii, A., and Nossal, R. (2014). Efficiency of cellular uptake of nanoparticles via receptor-mediated endocytosis. arXiv [q-bio.SC].

243. Li, S.-D., and Huang, L. (2008). Pharmacokinetics and biodistribution of nanoparticles. Mol. Pharm. *5*, 496–504.

244. Pavlou, M., Schön, C., Occelli, L.M., Rossi, A., Meumann, N., Boyd, R.F., Bartoe, J.T., Siedlecki, J., Gerhardt, M.J., Babutzka, S., et al. (2021). Novel AAV capsids for intravitreal gene therapy of photoreceptor disorders. EMBO Mol. Med. *13*, e13392.

245. Weinmann, J., Weis, S., Sippel, J., Tulalamba, W., Remes, A., El Andari, J., Herrmann, A.-K., Pham, Q.H., Borowski, C., Hille, S., et al. (2020). Identification of a myotropic AAV by massively parallel in vivo evaluation of barcoded capsid variants. Nat. Commun. *11*, 5432.

246. Münch, R.C., Janicki, H., Völker, I., Rasbach, A., Hallek, M., Büning, H., and Buchholz, C.J. (2013). Displaying high-affinity ligands on adeno-associated viral vectors enables tumor cell-specific and safe gene transfer. Mol. Ther. *21*, 109–118.

247. Hosseini-Kharat, M., Bremmell, K.E., and Prestidge, C.A. (2025). Why do lipid nanoparticles target the liver? Understanding of biodistribution and liver-specific tropism. Mol. Ther. Methods Clin. Dev. *33*, 101436.

248. Masarwy, R., Stotsky-Oterin, L., Elisha, A., Hazan-Halevy, I., and Peer, D. (2024). Delivery of nucleic acid based genome editing platforms via lipid nanoparticles: Clinical applications. Adv. Drug Deliv. Rev. *211*, 115359.

249. Wang, S., Wang, H., Drabek, A., Smith, W.S., Liang, F., and Huang, Z.R. (2024). Unleashing the potential: Designing antibody-targeted lipid nanoparticles for industrial applications with CMC considerations and clinical outlook. Mol. Pharm. *21*, 4–17.

250. Kedmi, R., Veiga, N., Ramishetti, S., Goldsmith, M., Rosenblum, D., Dammes, N., Hazan-Halevy, I., Nahary, L., Leviatan-Ben-Arye, S., Harlev, M., et al. (2018). A modular platform for targeted RNAi therapeutics. Nat. Nanotechnol. *13*, 214–219.

251. Cheng, Q., Wei, T., Farbiak, L., Johnson, L.T., Dilliard, S.A., and Siegwart, D.J. (2020). Selective organ targeting (SORT) nanoparticles for tissue-specific mRNA delivery and CRISPR-Cas gene editing. Nat. Nanotechnol. *15*, 313–320.

252. Kim, M., Song, E.S., Chen, J.C., Chatterjee, S., Sun, Y., Lee, S.M., Wu, S., Patel, P., Tian, Z., Kantor, A., et al. (2025). Dual SORT LNPs for multi-organ base editing. Nat. Biotechnol., 1–9.

253. Brown, D.W., Wee, P., Bhandari, P., Bukhari, A., Grin, L., Vega, H., Hejazi, M., Sosnowski, D., Ablack, J., Clancy, E.K., et al. (2024). Safe and effective in vivo delivery of DNA and RNA using proteolipid vehicles. Cell *187*, 5357-5375.e24.

254. Yang, Y., Vanin, E.F., Whitt, M.A., Fornerod, M., Zwart, R., Schneiderman, R.D., Grosveld, G., and Nienhuis, A.W. (1995). Inducible, high-level production of infectious murine leukemia retroviral vector particles pseudotyped with vesicular stomatitis virus G envelope protein. Hum. Gene Ther. *6*, 1203–1213.

255. Naldini, L., Blömer, U., Gallay, P., Ory, D., Mulligan, R., Gage, F.H., Verma, I.M., and Trono, D. (1996). In vivo gene delivery and stable transduction of nondividing cells by a lentiviral vector. Science *272*, 263–267.

256. Nikolic, J., Belot, L., Raux, H., Legrand, P., Gaudin, Y., and A Albertini, A. (2018). Structural basis for the recognition of LDL-receptor family members by VSV glycoprotein. Nat. Commun. *9*, 1029.

257. Finkelshtein, D., Werman, A., Novick, D., Barak, S., and Rubinstein, M. (2013). LDL receptor and its family members serve as the cellular receptors for vesicular stomatitis virus. Proc. Natl. Acad. Sci. U. S. A. *110*, 7306–7311.

258. Burns, J.C., Friedmann, T., Driever, W., Burrascano, M., and Yee, J.K. (1993). Vesicular stomatitis virus G glycoprotein pseudotyped retroviral vectors: concentration to very high titer and efficient gene transfer into mammalian and nonmammalian cells. Proc. Natl. Acad. Sci. U. S. A. *90*, 8033–8037.

259. Ferlin, A., Raux, H., Baquero, E., Lepault, J., and Gaudin, Y. (2014). Characterization of pH-sensitive molecular switches that trigger the structural transition of vesicular stomatitis virus glycoprotein from the postfusion state toward the prefusion state. J. Virol. *88*, 13396–13409.

260. Amirache, F., Lévy, C., Costa, C., Mangeot, P.-E., Torbett, B.E., Wang, C.X., Nègre, D., Cosset, F.-L., and Verhoeyen, E. (2014). Mystery solved: VSV-G-LVs do not allow efficient gene transfer into unstimulated T cells, B cells, and HSCs because they lack the LDL receptor. Blood *123*, 1422–1424.

261. Humbert, O., Gisch, D.W., Wohlfahrt, M.E., Adams, A.B., Greenberg, P.D., Schmitt, T.M., Trobridge, G.D., and Kiem, H.-P. (2016). Development of third-generation cocal

envelope producer cell lines for robust Lentiviral gene transfer into hematopoietic stem cells and T-cells. Mol. Ther. *24*, 1237–1246.

262. Trobridge, G.D., Wu, R.A., Hansen, M., Ironside, C., Watts, K.L., Olsen, P., Beard, B.C., and Kiem, H.-P. (2010). Cocal-pseudotyped lentiviral vectors resist inactivation by human serum and efficiently transduce primate hematopoietic repopulating cells. Mol. Ther. *18*, 725–733.

263. Spindler, M.J., Amezquita, A., Byrne, E.F.X., Edgar, R., Ravi, S., Sandhu, S., Weller, T., and Johnson, D.S. (2025). Discovery and validation of alternatives to VSV-G for pseudotyping of Lentiviral vectors for in vivo delivery of anti-tumor transgenes. bioRxiv. https://doi.org/10.1101/2025.03.03.641199.

264. Girard-Gagnepain, A., Amirache, F., Costa, C., Lévy, C., Frecha, C., Fusil, F., Nègre, D., Lavillette, D., Cosset, F.-L., and Verhoeyen, E. (2014). Baboon envelope pseudotyped LVs outperform VSV-G-LVs for gene transfer into early-cytokine-stimulated and resting HSCs. Blood *124*, 1221–1231.

265. Bernadin, O., Amirache, F., Girard-Gagnepain, A., Moirangthem, R.D., Lévy, C., Ma, K., Costa, C., Nègre, D., Reimann, C., Fenard, D., et al. (2019). Baboon envelope LVs efficiently transduced human adult, fetal, and progenitor T cells and corrected SCID-X1 T-cell deficiency. Blood Adv. *3*, 461–475.

266. Mirow, M., Schwarze, L.I., Fehse, B., and Riecken, K. (2021). Efficient pseudotyping of different Retroviral vectors using a novel, Codon-optimized gene for chimeric GALV envelope. Viruses *13*, 1471.

267. Renner, A., Stahringer, A., Ruppel, K.E., Fricke, S., Koehl, U., and Schmiedel, D. (2024). Development of KoRV-pseudotyped lentiviral vectors for efficient gene transfer into freshly isolated immune cells. Gene Ther. *31*, 378–390.

268. Sandrin, V., Boson, B., Salmon, P., Gay, W., Nègre, D., Le Grand, R., Trono, D., and Cosset, F.-L. (2002). Lentiviral vectors pseudotyped with a modified RD114 envelope glycoprotein show increased stability in sera and augmented transduction of primary lymphocytes and CD34+ cells derived from human and nonhuman primates. Blood *100*, 823–832.

269. Le, T.A., Chu, V.T., Lino, A.C., Schrezenmeier, E., Kressler, C., Hamo, D., Rajewsky, K., Dörner, T., and Dang, V.D. (2022). Efficient CRISPR-Cas9-mediated mutagenesis in primary human B cells for identifying plasma cell regulators. Mol. Ther. Nucleic Acids *30*, 621–632.

270. Jargalsaikhan, B.-E., Muto, M., Been, Y., Matsumoto, S., Okamura, E., Takahashi, T., Narimichi, Y., Kurebayashi, Y., Takeuchi, H., Shinohara, T., et al. (2024). The dual-pseudotyped Lentiviral vector with VSV-G and Sendai virus HN enhances infection efficiency through the synergistic effect of the envelope proteins. Viruses *16*, 827.

271. Kato, S., Inoue, K.-I., Kobayashi, K., Yasoshima, Y., Miyachi, S., Inoue, S., Hanawa, H., Shimada, T., Takada, M., and Kobayashi, K. (2007). Efficient gene transfer via retrograde transport in rodent and primate brains using a human immunodeficiency virus type 1-based vector pseudotyped with rabies virus glycoprotein. Hum. Gene Ther. *18*, 1141–1151.

272. Kato, S., Kobayashi, K., Inoue, K.-I., Kuramochi, M., Okada, T., Yaginuma, H., Morimoto, K., Shimada, T., Takada, M., and Kobayashi, K. (2011). A lentiviral strategy

for highly efficient retrograde gene transfer by pseudotyping with fusion envelope glycoprotein. Hum. Gene Ther. *22*, 197–206.

273. Kayman, S.C., Park, H., Saxon, M., and Pinter, A. (1999). The hypervariable domain of the murine leukemia virus surface protein tolerates large insertions and deletions, enabling development of a retroviral particle display system. J. Virol. *73*, 1802–1808.

274. Beilstein, F., Abou Hamdan, A., Raux, H., Belot, L., Ouldali, M., Albertini, A.A., and Gaudin, Y. (2020). Identification of a pH-sensitive switch in VSV-G and a crystal structure of the G pre-fusion state highlight the VSV-G structural transition pathway. Cell Rep. *32*, 108042.

275. Schlehuber, L.D., and Rose, J.K. (2004). Prediction and identification of a permissive epitope insertion site in the vesicular stomatitis virus glycoprotein. J. Virol. *78*, 5079–5087.

276. Duquénois, I., Stéphanie Thébault, Johari, S., Raux, H., Lagaudrière-Gesbert, C., Perez, F., Albertini, A.A., and Gaudin, Y. (2024). Optimization of the VSV G backbone for amino terminal fusion with nanobodies allowing its retargeting to receptors of therapeutic interest. bioRxiv, 2024.11.14.623577. https://doi.org/10.1101/2024.11.14.623577.

277. Dreja, H., and Piechaczyk, M. (2006). The effects of N-terminal insertion into VSV-G of an scFv peptide. Virol. J. *3*, 69.

278. Vamva, E., Ozog, S., Verhoeyen, E., James, R.G., Rawlings, D.J., and Torbett, B.E. (2022). An optimized measles virus glycoprotein-pseudotyped lentiviral vector production system to promote efficient transduction of human primary B cells. STAR Protoc. *3*, 101228.

279. Negrete, O.A., Levroney, E.L., Aguilar, H.C., Bertolotti-Ciarlet, A., Nazarian, R., Tajyar, S., and Lee, B. (2005). EphrinB2 is the entry receptor for Nipah virus, an emergent deadly paramyxovirus. Nature *436*, 401–405.

280. Bender, R.R., Muth, A., Schneider, I.C., Friedel, T., Hartmann, J., Plückthun, A., Maisner, A., and Buchholz, C.J. (2016). Receptor-targeted Nipah virus glycoproteins improve cell-type selective gene delivery and reveal a preference for membrane-proximal cell attachment. PLoS Pathog. *12*, e1005641.

281. Hammond, A.L., Plemper, R.K., Zhang, J., Schneider, U., Russell, S.J., and Cattaneo, R. (2001). Single-chain antibody displayed on a recombinant measles virus confers entry through the tumor-associated carcinoembryonic antigen. J. Virol. *75*, 2087–2096.

282. Anliker, B., Abel, T., Kneissl, S., Hlavaty, J., Caputi, A., Brynza, J., Schneider, I.C., Münch, R.C., Petznek, H., Kontermann, R.E., et al. (2010). Specific gene transfer to neurons, endothelial cells and hematopoietic progenitors with lentiviral vectors. Nat. Methods *7*, 929–935.

283. Zhou, Q., Schneider, I.C., Edes, I., Honegger, A., Bach, P., Schönfeld, K., Schambach, A., Wels, W.S., Kneissl, S., Uckert, W., et al. (2012). T-cell receptor gene transfer exclusively to human CD8(+) cells enhances tumor cell killing. Blood *120*, 4334–4342.

284. Frank, A.M., Braun, A.H., Scheib, L., Agarwal, S., Schneider, I.C., Fusil, F., Perian, S., Sahin, U., Thalheimer, F.B., Verhoeyen, E., et al. (2020). Combining T-cell-specific

activation and in vivo gene delivery through CD3-targeted lentiviral vectors. Blood Adv. *4*, 5702–5715.

285. Münch, R.C., Mühlebach, M.D., Schaser, T., Kneissl, S., Jost, C., Plückthun, A., Cichutek, K., and Buchholz, C.J. (2011). DARPins: an efficient targeting domain for lentiviral vectors. Mol. Ther. *19*, 686–693.

286. Weidner, T., Agarwal, S., Perian, S., Fusil, F., Braun, G., Hartmann, J., Verhoeyen, E., and Buchholz, C.J. (2021). Genetic in vivo engineering of human T lymphocytes in mouse models. Nat. Protoc. *16*, 3210–3240.

287. Buchholz, C.J., Friedel, T., and Büning, H. (2015). Surface-engineered viral vectors for selective and cell type-specific gene delivery. Trends Biotechnol. *33*, 777–790.

288. Michels, K.R., Sheih, A., Hernandez, S.A., Brandes, A.H., Parrilla, D., Irwin, B., Perez, A.M., Ting, H.-A., Nicolai, C.J., Gervascio, T., et al. (2023). Preclinical proof of concept for VivoVec, a lentiviral-based platform for in vivo CAR T-cell engineering. J. Immunother. Cancer *11*, e006292.

289. Dobson, C.S., Reich, A.N., Gaglione, S., Smith, B.E., Kim, E.J., Dong, J., Ronsard, L., Okonkwo, V., Lingwood, D., Dougan, M., et al. (2022). Antigen identification and high-throughput interaction mapping by reprogramming viral entry. Nat. Methods *19*, 449–460.

290. Yu, B., Shi, Q., Belk, J.A., Yost, K.E., Parker, K.R., Li, R., Liu, B.B., Huang, H., Lingwood, D., Greenleaf, W.J., et al. (2022). Engineered cell entry links receptor biology with single-cell genomics. Cell *185*, 4904-4920.e22.

291. Strebinger, D., Frangieh, C.J., Friedrich, M.J., Faure, G., Macrae, R.K., and Zhang, F. (2023). Cell type-specific delivery by modular envelope design. Nat. Commun. *14*, 5141.

292. Wagner, D.L., Koehl, U., Chmielewski, M., Scheid, C., and Stripecke, R. (2022). Review: Sustainable clinical development of CAR-T cells – switching from viral transduction towards CRISPR-Cas gene editing. Front. Immunol. *13*. https://doi.org/10.3389/fimmu.2022.865424.

293. Conti, A., Giannetti, K., Midena, F., Beretta, S., Gualandi, N., De Marco, R., Carsana, E., Varesi, A., Tavella, T., Alessandrini, L., et al. (2025). Senescence and inflammation are unintended adverse consequences of CRISPR-Cas9/AAV6-mediated gene editing in hematopoietic stem cells. Cell Rep. Med., 102157.

294. Ferrari, S., Jacob, A., Cesana, D., Laugel, M., Beretta, S., Varesi, A., Unali, G., Conti, A., Canarutto, D., Albano, L., et al. (2022). Choice of template delivery mitigates the genotoxic risk and adverse impact of editing in human hematopoietic stem cells. Cell Stem Cell *29*, 1428-1444.e9.

295. Shy, B.R., Vykunta, V.S., Ha, A., Talbot, A., Roth, T.L., Nguyen, D.N., Pfeifer, W.G., Chen, Y.Y., Blaeschke, F., Shifrut, E., et al. (2023). High-yield genome engineering in primary cells using a hybrid ssDNA repair template and small-molecule cocktails. Nat. Biotechnol. *41*, 521–531.

296. Nitulescu, A.-M., Du, W., Glaser, V., Kath, J., Aird, E.J., Cullot, G., Greensmith, R., Mikkelsen, N.S., Stein, M., Bak, R.O., et al. (2025). Single-stranded HDR templates with truncated Cas12a-binding sequences improve knock-in efficiencies in primary human T cells. Mol. Ther. Nucleic Acids *36*, 102568.

297. Letort, G., Duclert, A., Le Clerre, D., Chion-Sotinel, I., Salvatori, R., Dessez, E., Sevin, M., Rotondi, M., Ducani, C., Duchateau, P., et al. (2025). Circularization of single-stranded DNA donor template unleashes the power of non-viral gene delivery for long-term HSCs editing. bioRxiv. https://doi.org/10.1101/2025.02.19.638978.

298. Palfi, S., Gurruchaga, J.M., Lepetit, H., Howard, K., Ralph, G.S., Mason, S., Gouello, G., Domenech, P., Buttery, P.C., Hantraye, P., et al. (2018). Long-term follow-up of a Phase I/II study of ProSavin, a Lentiviral vector gene therapy for Parkinson's disease. Hum. Gene Ther. Clin. Dev. *29*, 148–155.

299. Rurik, J.G., Tombácz, I., Yadegari, A., Méndez Fernández, P.O., Shewale, S.V., Li, L., Kimura, T., Soliman, O.Y., Papp, T.E., Tam, Y.K., et al. (2022). CAR T cells produced in vivo to treat cardiac injury. Science *375*, 91–96.

300. Hunter, T.L., Bao, Y., Zhang, Y., Matsuda, D., Riener, R., Wang, A., Li, J.J., Soldevila, F., Chu, D.S.H., Nguyen, D.P., et al. (2025). In vivo CAR T cell generation to treat cancer and autoimmune disease. Science *388*, 1311–1317.

301. Schiroli, G., Conti, A., Ferrari, S., Della Volpe, L., Jacob, A., Albano, L., Beretta, S., Calabria, A., Vavassori, V., Gasparini, P., et al. (2019). Precise gene editing preserves hematopoietic stem cell function following transient p53-mediated DNA damage response. Cell Stem Cell *24*, 551-565.e8.

302. Truong, D.-J.J., Kühner, K., Kühn, R., Werfel, S., Engelhardt, S., Wurst, W., and Ortiz, O. (2015). Development of an intein-mediated split-Cas9 system for gene therapy. Nucleic Acids Res. *43*, 6450–6458.

303. Villiger, L., Grisch-Chan, H.M., Lindsay, H., Ringnalda, F., Pogliano, C.B., Allegri, G., Fingerhut, R., Häberle, J., Matos, J., Robinson, M.D., et al. (2018). Treatment of a metabolic liver disease by in vivo genome base editing in adult mice. Nat. Med. *24*, 1519–1525.

304. Levy, J.M., Yeh, W.-H., Pendse, N., Davis, J.R., Hennessey, E., Butcher, R., Koblan, L.W., Comander, J., Liu, Q., and Liu, D.R. (2020). Cytosine and adenine base editing of the brain, liver, retina, heart and skeletal muscle of mice via adeno-associated viruses. Nat. Biomed. Eng. *4*, 97–110.

305. Wu, Y., Wan, X., Zhao, D., Chen, X., Wang, Y., Tang, X., Li, J., Li, S., Sun, X., Bi, C., et al. (2023). AAV-mediated base-editing therapy ameliorates the disease phenotypes in a mouse model of retinitis pigmentosa. Nat. Commun. *14*, 4923.

306. Gao, Z., Ravendran, S., Mikkelsen, N.S., Haldrup, J., Cai, H., Ding, X., Paludan, S.R., Thomsen, M.K., Mikkelsen, J.G., and Bak, R.O. (2022). A truncated reverse transcriptase enhances prime editing by split AAV vectors. Mol. Ther. *30*, 2942–2951.

307. Bae, S., Park, J., and Kim, J.-S. (2014). Cas-OFFinder: a fast and versatile algorithm that searches for potential off-target sites of Cas9 RNA-guided endonucleases. Bioinformatics *30*, 1473–1475.

308. Tsai, S.Q., Zheng, Z., Nguyen, N.T., Liebers, M., Topkar, V.V., Thapar, V., Wyvekens, N., Khayter, C., Iafrate, A.J., Le, L.P., et al. (2015). GUIDE-seq enables genome-wide profiling of off-target cleavage by CRISPR-Cas nucleases. Nat. Biotechnol. *33*, 187–197.

309. Tsai, S.Q., Nguyen, N.T., Malagon-Lopez, J., Topkar, V.V., Aryee, M.J., and Joung, J.K. (2017). CIRCLE-seq: a highly sensitive in vitro screen for genome-wide CRISPR-Cas9 nuclease off-targets. Nat. Methods *14*, 607–614.

310. Wienert, B., Wyman, S.K., Richardson, C.D., Yeh, C.D., Akcakaya, P., Porritt, M.J., Morlock, M., Vu, J.T., Kazane, K.R., Watry, H.L., et al. (2019). Unbiased detection of CRISPR off-targets in vivo using DISCOVER-Seq. Science *364*, 286–289.

311. Lazzarotto, C.R., Malinin, N.L., Li, Y., Zhang, R., Yang, Y., Lee, G., Cowley, E., He, Y., Lan, X., Jividen, K., et al. (2020). CHANGE-seq reveals genetic and epigenetic effects on CRISPR-Cas9 genome-wide activity. Nat. Biotechnol. *38*, 1317–1327.

312. Coroadinha, A.S. (2023). Host cell restriction factors blocking efficient vector transduction: Challenges in Lentiviral and adeno-associated vector based gene therapies. Cells *12*. https://doi.org/10.3390/cells12050732.

313. Segel, M., Lash, B., Song, J., Ladha, A., Liu, C.C., Jin, X., Mekhedov, S.L., Macrae, R.K., Koonin, E.V., and Zhang, F. (2021). Mammalian retrovirus-like protein PEG10 packages its own mRNA and can be pseudotyped for mRNA delivery. Science *373*, 882–889.

314. Ashley, J., Cordy, B., Lucia, D., Fradkin, L.G., Budnik, V., and Thomson, T. (2018). Retrovirus-like Gag Protein Arc1 Binds RNA and Traffics across Synaptic Boutons. Cell *172*, 262-274.e11.

315. Segura, M. de L.M., Kamen, A., and Garnier, A. (2006). Downstream processing of oncoretroviral and lentiviral gene therapy vectors. Biotechnol. Adv. *24*, 321–337.

316. Segura, M.M., Garnier, A., Di Falco, M.R., Whissell, G., Meneses-Acosta, A., Arcand, N., and Kamen, A. (2008). Identification of host proteins associated with Retroviral vector particles by proteomic analysis of highly purified vector preparations. J. Virol. *82*, 1107–1117.

317. Burnie, J., and Guzzo, C. (2019). The incorporation of host proteins into the external HIV-1 envelope. Viruses *11*, 85.

318. Milani, M., Annoni, A., Bartolaccini, S., Biffi, M., Russo, F., Di Tomaso, T., Raimondi, A., Lengler, J., Holmes, M.C., Scheiflinger, F., et al. (2017). Genome editing for scalable production of alloantigen-free lentiviral vectors for in vivo gene therapy. EMBO Mol. Med. *9*, 1558–1573.

319. Effio, C.L., and Hubbuch, J. (2015). Next generation vaccines and vectors: Designing downstream processes for recombinant protein-based virus-like particles. Biotechnol. J. *10*, 715–727.

320. Merten, O.-W., Hebben, M., and Bovolenta, C. (2016). Production of lentiviral vectors. Mol. Ther. Methods Clin. Dev. *3*, 16017.

321. Gándara, C., Affleck, V., and Stoll, E.A. (2018). Manufacture of third-generation Lentivirus for preclinical use, with process development considerations for translation to Good Manufacturing Practice. Hum. Gene Ther. Methods *29*, 1–15.

322. Ahn, S.-H., Ryu, S.-W., Choi, H., You, S., Park, J., and Choi, C. (2022). Manufacturing therapeutic exosomes: From bench to industry. Mol. Cells *45*, 284–290.

323. Holic, N., Frin, S., Seye, A.K., Galy, A., and Fenard, D. (2017). Improvement of DE Novo cholesterol biosynthesis efficiently promotes the production of human immunodeficiency virus type 1-derived Lentiviral vectors. Hum. Gene Ther. Methods *28*, 67–77.

324. Milani, M., Annoni, A., Moalli, F., Liu, T., Cesana, D., Calabria, A., Bartolaccini, S., Biffi, M., Russo, F., Visigalli, I., et al. (2019). Phagocytosis-shielded lentiviral vectors improve liver gene therapy in nonhuman primates. Sci. Transl. Med. *11*, eaav7325.

325. Klimpel, M., Obert, C., Terrao, M., Singh, P., Wei, H., Chen, C.-G., Gille, A., Wissing, S., and Laux, H. (2025). Challenges in lentiviral vector production: retro-transduction of producer cell lines. Front. Bioeng. Biotechnol. *13*, 1569298.

326. Lan, Y.-J., Nguyen, Q.V., Chao, T.-L., Yeh, K.-L., and Lin, S. (2024). A robust platform for BaEVRless-lentiviral synthesis and primary natural killer cell transduction. bioRxiv. https://doi.org/10.1101/2024.04.03.587896.

327. Segura, M.M., Kamen, A.A., and Garnier, A. (2011). Overview of current scalable methods for purification of viral vectors. Methods Mol. Biol. *737*, 89–116.

328. Zhou, Y., McNamara, R.P., and Dittmer, D.P. (2020). Purification methods and the presence of RNA in virus particles and extracellular vesicles. Viruses *12*, 917.

329. Valkama, A.J., Oruetxebarria, I., Lipponen, E.M., Leinonen, H.M., Käyhty, P., Hynynen, H., Turkki, V., Malinen, J., Miinalainen, T., Heikura, T., et al. (2020). Development of large-scale downstream processing for Lentiviral vectors. Mol. Ther. Methods Clin. Dev. *17*, 717–730.

330. Chen, Y., Zhu, Q., Cheng, L., Wang, Y., Li, M., Yang, Q., Hu, L., Lou, D., Li, J., Dong, X., et al. (2021). Exosome detection via the ultrafast-isolation system: EXODUS. Nat. Methods *18*, 212–218.

331. Minh, A.D., and Kamen, A.A. (2021). Critical assessment of purification and analytical technologies for enveloped viral vector and vaccine processing and their current limitations in resolving co-expressed extracellular vesicles. Vaccines (Basel) *9*, 823.

332. Soldi, M., Sergi Sergi, L., Unali, G., Kerzel, T., Cuccovillo, I., Capasso, P., Annoni, A., Biffi, M., Rancoita, P.M.V., Cantore, A., et al. (2020). Laboratory-scale Lentiviral vector production and purification for enhanced ex vivo and in vivo genetic engineering. Mol. Ther. Methods Clin. Dev. *19*, 411–425.

333. Steppert, P., Burgstaller, D., Klausberger, M., Berger, E., Aguilar, P.P., Schneider, T.A., Kramberger, P., Tover, A., Nöbauer, K., Razzazi-Fazeli, E., et al. (2016). Purification of HIV-1 gag virus-like particles and separation of other extracellular particles. J. Chromatogr. A *1455*, 93–101.

334. Steppert, P., Burgstaller, D., Klausberger, M., Tover, A., Berger, E., and Jungbauer, A. (2017). Quantification and characterization of virus-like particles by size-exclusion chromatography and nanoparticle tracking analysis. J. Chromatogr. A *1487*, 89–99.

335. Dissanayake, K., Midekessa, G., Lättekivi, F., and Fazeli, A. (2021). Measurement of the size and concentration and zeta potential of extracellular vesicles using nanoparticle tracking analyzer. Methods Mol. Biol. *2273*, 207–218.

336. González-Domínguez, I., Puente-Massaguer, E., Cervera, L., and Gòdia, F. (2020). Quality assessment of virus-like particles at single particle level: A comparative study. Viruses *12*, 223.

337. Monopoli, M.P., Aberg, C., Salvati, A., and Dawson, K.A. (2012). Biomolecular coronas provide the biological identity of nanosized materials. Nat. Nanotechnol. *7*, 779–786.

338. Kim, E.-Y., Stanton, J., Korber, B.T.M., Krebs, K., Bogdan, D., Kunstman, K., Wu, S., Phair, J.P., Mirkin, C.A., and Wolinsky, S.M. (2008). Detection of HIV-1 p24 Gag in plasma by a nanoparticle-based bio-barcode-amplification method. Nanomedicine (Lond.) *3*, 293–303.

339. Renner, T.M., Tang, V.A., Burger, D., and Langlois, M.-A. (2020). Intact viral particle counts measured by flow virometry provide insight into the infectivity and genome packaging efficiency of Moloney Murine leukemia virus. J. Virol. *94*. https://doi.org/10.1128/JVI.01600-19.